U.S. Department
of Transportation
**Federal Railroad
Administration**

Wheelclimb Derailment Processes and Derailment Criteria

Office of Research and
Development
Washington DC 20590

Larry M. Sweet
Amir Karmel

Department of Mechanical and
Aerospace Engineering
Princeton University
Princeton NJ 08544

DOT/FRA/ORD-84/05
DOT-TSC-FRA-83-6

June 1984
Final Report

NOTICE

This document is disseminated under the sponsorship of the Department of Transportation in the interest of information exchange. The United States Government assumes no liability for its contents or use thereof.

NOTICE

The United States Government does not endorse products or manufacturers. Trade or manufacturers' names appear herein solely because they are considered essential to the object of this report.

Technical Report Documentation Page

1. Report No.	2. Government Accession No.	3. Recipient's Catalog No.
DOT/FRA/ORD-84/05	PB85 149367/AS	

4. Title and Subtitle	5. Report Date
WHEELCLIMB DERAILMENT PROCESSES AND DERAILMENT CRITERIA	June 1984
	6. Performing Organization Code: DTS-73

7. Author(s)	8. Performing Organization Report No.
Larry M. Sweet and Amir Karmel	DOT-TSC-FRA-83-6

9. Performing Organization Name and Address	10. Work Unit No. (TRAIS)
Department of Mechanical and Aerospace Engineering* Princeton University Princeton NJ 08544	RR319/R3304
	11. Contract or Grant No.: DOT-TSC-1603
	13. Type of Report and Period Covered: Final Report August 1982-August 1983
12. Sponsoring Agency Name and Address U.S. Department of Transportation Federal Railroad Administration Office of Research and Development Washington DC 20590	14. Sponsoring Agency Code: RRD-10

15. Supplementary Notes

*Under contract to: U.S. Department of Transportation
Research and Special Programs Administration
Transportation Systems Center
Cambridge MA 02142

16. Abstract

The most widely accepted criterion for wheelclimb derailment defines an upper limit for safe operation on wheel/rail contact forces on the climbing wheel, with the limit varying with time duration of the forces. For dynamic wheelclimb processes with significant lateral velocities, lateral forces may be measured for short time durations that are larger than those that may be sustained without derailment in steady state. To study wheelclimb derailment processes and evaluate derailment criteria, a series of derailment experiments was conducted using a one-fifth scale model of a single wheelset on tangent track subjected to static and dynamic loading conditions. The results of these experiments were compared to simulations based on a nonlinear theory developed to represent the important phenomena associated with dynamic wheelclimb.

This study shows that the Japanese National Railways (JNR) and other time-duration dependent criteria based on wheel load measurements alone are unsuccessful in predicting derailment safety for dynamic wheelclimb. For wheelclimb processes involving negligible lateral velocities, the derailment limit can be estimated from quasi-steady analysis of wheel/rail forces. Evidence has been found that derailment criteria employing variables measured in addition to wheel loads may be successful in predicting derailment safety, and that diagnostic criteria may be developed for warning of impending derailment.

17. Key Words	18. Distribution Statement
Derailment, Derailment Criteria, Scale Model Testing, Track/Train Dynamics, Wheelset Dynamics	DOCUMENT IS AVAILABLE TO THE PUBLIC THROUGH THE NATIONAL TECHNICAL INFORMATION SERVICE, SPRINGFIELD, VIRGINIA 22161

19. Security Classif. (of this report)	20. Security Classif. (of this page)	21. No. of Pages	22. Price
UNCLASSIFIED	UNCLASSIFIED	198	

Form DOT F 1700.7 (8-72) Reproduction of completed page authorized

METRIC CONVERSION FACTORS

Approximate Conversions to Metric Measures

Symbol	When You Know	Multiply by	To Find	Symbol
		LENGTH		
in	inches	2.5	centimeters	cm
ft	feet	30	centimeters	cm
yd	yards	0.9	meters	m
mi	miles	1.6	kilometers	km
		AREA		
in^2	square inches	6.5	square centimeters	cm^2
ft^2	square feet	0.09	square meters	m^2
yd^2	square yards	0.8	square meters	m^2
mi^2	square miles	2.6	square kilometers	km^2
	acres	0.4	hectares	ha
		MASS (weight)		
oz	ounces	28	grams	g
lb	pounds	0.45	kilograms	kg
	short tons (2000 lb)	0.9	tonnes	t
		VOLUME		
tsp	teaspoons	5	milliliters	ml
Tbsp	tablespoons	15	milliliters	ml
fl oz	fluid ounces	30	milliliters	ml
c	cups	0.24	liters	l
pt	pints	0.47	liters	l
qt	quarts	0.95	liters	l
gal	gallons	3.8	liters	l
ft^3	cubic feet	0.03	cubic meters	m^3
yd^3	cubic yards	0.76	cubic meters	m^3
		TEMPERATURE (exact)		
°F	Fahrenheit temperature	5/9 (after subtracting 32)	Celsius temperature	°C

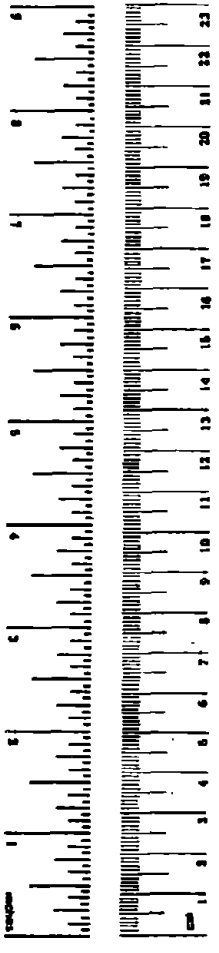

Approximate Conversions from Metric Measures

Symbol	When You Know	Multiply by	To Find	Symbol
		LENGTH		
mm	millimeters	0.04	inches	in
cm	centimeters	0.4	inches	in
m	meters	3.3	feet	ft
m	meters	1.1	yards	yd
km	kilometers	0.6	miles	mi
		AREA		
cm^2	square centimeters	0.16	square inches	in^2
m^2	square meters	1.2	square yards	yd^2
km^2	square kilometers	0.4	square miles	mi^2
ha	hectares (10,000 m^2)	2.5	acres	
		MASS (weight)		
g	grams	0.035	ounces	oz
kg	kilograms	2.2	pounds	lb
t	tonnes (1000 kg)	1.1	short tons	
		VOLUME		
ml	milliliters	0.03	fluid ounces	fl oz
l	liters	2.1	pints	pt
l	liters	1.06	quarts	qt
l	liters	0.26	gallons	gal
m^3	cubic meters	35	cubic feet	ft^3
m^3	cubic meters	1.3	cubic yards	yd^3
		TEMPERATURE (exact)		
°C	Celsius temperature	9/5 (then add 32)	Fahrenheit temperature	°F

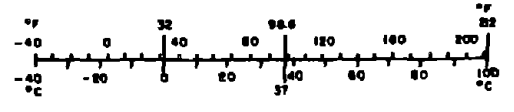

NOTICE

THIS DOCUMENT HAS BEEN REPRODUCED FROM THE BEST COPY FURNISHED US BY THE SPONSORING AGENCY. ALTHOUGH IT IS RECOGNIZED THAT CERTAIN PORTIONS ARE ILLEGIBLE, IT IS BEING RELEASED IN THE INTEREST OF MAKING AVAILABLE AS MUCH INFORMATION AS POSSIBLE.

PREFACE AND ACKNOWLEDGEMENTS

In support of the Improved Track Structures Research Program of the Office of Research and Development of the Federal Railroad Administration (FRA), the Transportation Systems Center (TSC) is conducting analytical and experimental studies of the relationship between track design and maintenance parameters and the safety and performance of trains, resulting from the dynamic interaction of the track and train. The objectives of this effort are directed towards the development of a technological data base that can be used by Government and industry to:

a. Establish safe operating regimes based on the dynamics of track/train interaction.

b. Evaluate the safety and economics of various types of train operation and track maintenance practices.

c. Formulate recommendations for reducing derailments due to track/train interaction.

The approach being employed in the conduct of these studies and in development of engineering guidelines to meet the above objectives includes the following:

a. Definition of performance indices which are related to the likelihood of vehicle derailment, lading damage, passenger ride quality, and operational efficiency.

b. Compilation of analysis tools and development of a methodology for relating track, rail car, locomotive, and train parameters to the performance indices.

c. Parametric studies relating the performance indices to track construction and maintenance parameters for the range of in-service train configurations, equipment parameters and speeds.

d. Development of techniques and methods for track/train dynamics, laboratory and full-scale test design, and rail vehicle model validation, by which the performance indices can be quantitatively evaluated and adjusted as required to provide their proper threshold values.

The principal safety-related problem currently facing the railroads is derailment. Derailments result in direct loss due to damage to rolling stock, track, lading and facilities, and in injury to passengers, and operators, and liability for release of hazardous materials. Less well-publicized, but of great significance, is the indirect economic loss due to decreased operating speeds and other factors affecting system performance that are found necessary because of the probability of derailments occurring. Advances in understanding of derailment phenomena would then have the dual benefit of (1) improving the technology to be more resistant to derailment, and (2) provide a rational basis for formulating economically sound safety standards for maintenance and operation that are designed to reduce derailment probability.

Because of the compelling importance of derailment as a problem both to the railroads and to our national transportation system, and the relatively undeveloped state-of-the-art in understanding the problem, the FRA has initiated a major research program in this area. This multifaced program, coordinated by TSC, involves the characterization of vehicles and trackage previously described, as well as formulation of appropriate models for quantifying derailment phenomena

and estimating resultant derailment probabilities. It is essential, however, that data be made available on the important derailment phenomena, so that the quantitative models used are soundly based. Until recently, experiments required to meet this requirement were prohibitively costly, time-consuming, hazardous, and potentially inaccurate due to the difficulty in controlling test conditions. Recently techniques and apparatus have been developed to perform meaningful experiments on derailment through the use of dynamically scaled models. In this study many of the requirements for quantification of derailment phenomena essential to the TSC program have been met by an experimental program which utilizes these techniques and apparatus.

The overall objective of this research program is to provide validation of analytical models of wheel/rail interaction and of performance indices that can be used to predict derailment. The experimental results from the scale model testing will be used as follows:

1. In confirming or improving analytical models of the mechanics of wheel/rail interaction, especially under extreme conditions of load or geometry.
2. In generating critical threshold values of performance indices which will accurately signal impending derailment.
3. In developing empirical models of wheel/rail interaction, which can be used without recourse to the detailed theory, and which may therefore provide a more efficient approach to analysis and simulation.

During the progress of this study many useful technical comments and suggestions have been contributed by staff at the U.S. Department of Transportation, Transportation Systems Center, Cambridge, Massachusetts. Particularly significant were the contributions of Mr. H.S.H. Lee, the Technical Monitor of the contract, Dr. Russel Brantman, and Mr. William Thompson, III. The authors acknowledge the contributions of Princeton University technical staff W.F. Putman, E. Griffith, and J. Grieb, and undergraduate students J. Karohl and P. Moy. The report manuscript was prepared by D. Grieb.

TABLE OF CONTENTS

LIST OF FIGURES

[ ] indicates references

LIST OF TABLES

LIST OF ABBREVIATIONS AND SYMBOLS

A_i, B_i	geometric parameters used in calculating contact ellipse
a_i, b_i	semi-axes of contact ellipse
$a(\theta), b(\theta)$	elliptic integrals used in calculating contact ellipse
$\bar{a}$	$a/\sqrt{ab}$
A	area (time integral) of L/V pulse
A/D	analog/digital converter
AMP	amplifier
$\bar{b}$	$b/\sqrt{ab}$
C	degrees, centigrade
cm	centimeter
D	width (time duration) of base of L/V pulse
DC	direct current
DCDT	direct current displacement transducer
DMUX	demultiplexer
E	modulus of elasticity
$F_{j,i}$	forces along $C_{j,i}$ axes
$f_{j,i}$	non-dimensional creep forces = $F_{j,i}/F_{3,i}$
$\tilde{F}_s$	primary suspension forces
F_{YO}	lateral force applied to truck frame along the Y axis
F_{ZO}	axle load
FM	frequency modulation
ft	foot
I_{xx}, I_{yy}, I_{zz}	wheelset moments of inertia about xyz axes
in	inch
JNR	Japanese National Railways
K_y, K_z, K_ψ, K_ϕ	primary suspension stiffnesses
L_i	distance from z-axis to wheel/rail contact points

LIST OF ABBREVIATIONS AND SYMBOLS (continued)

L/V	derailment quotient, ratio of lateral to vertical forces on axle or climbing wheel
m	meter
mm	millimeter
MUX	multiplexer
$\tilde{M}_s$	primary suspension moments
m_t	truck frame mass
m_w	wheelset mass
n	newton
$(Q/P)_i$	derailment quotient, ratio of lateral to vertical forces at wheel/rail contact point
$R_{1,i}, R'_{1,i}$	longitudinal and lateral radii of curvature of the wheel at wheel/rail contact points
$R'_{2,i}$	lateral radius of curvature of the rail at wheel/rail contact points
$r_{v,i}$	rolling radius of the wheel
r_o	rolling radius of wheels when wheelset is centered
s	seconds
S	shape factor for L/V pulse, increasing with p-lse sharpness
t	time
t_1	duration of L/V pulse
TACH	tachometer
TAT	time L/V pulse is above threshold value
TAZ	time L/V pulse is above zero
TNP	time L/V pulse is within N percent of peak value

LIST OF ABBREVIATIONS AND SYMBOLS (continued)

V	forward velocity of wheelset
$V_{2,i}$	velocity of wheel/rail contact point along $C_{2,i}$ axis
XYZ	reference system fixed with respect to rails
xyz	wheelset reference system (y axis always coincides with the axle and z axis lies in a vertical plane passing through the axle)
Y_t, Z_t	truck c.m.* lateral and vertical displacements along Y and Z axes
Y_w, Z_w	wheelset c.m.* lateral and vertical displacements along Y and Z axes
$\bar{\alpha}$	arctan (ν_y/ν_x)
α_i	wheel/rail contact angle with respect to XY plane
Γ_1, Γ_2	wheel L/V ratios on left and right wheels, respectively
δ_1, δ_2	lateral displacements of left and right rails, respectively
η	nondimensional roll moment applied to wheelset
η_d	nondimensional effective roll moment due to wheelset dynamics
μ	coefficient of friction
μm	microns $(10^{-6} m)$
ϵ	Poisson's ratio
Φ_t, Ψ_t	truck roll and yaw angles (positive clockwise looking forward)
Φ_w, Ψ_w	wheelset roll and yaw angles (positive clockwise looking forward)
Ω	axle rolling rotational velocity (about y-axis)
ξ, η, χ	Kalker creepage parameters [Equations (3.13) to (3.15)]

*Center of Mass

LIST OF ABBREVIATIONS AND SYMBOLS (continued)

ν_x	nondimensional longitudinal creepage
ν_y	nondimensional lateral creepage
$\bar{\nu}$	$\sqrt{\nu_x^2 + \nu_y^2}$
$\gamma_{j,i}$	creepages in $C_{j,i}$ directions
ρ_i	geometric parameter used in calculating the contact ellipse (Equation (12))
$\omega_{3,1}$	spin creepage

Subscripts

i	index used for wheel identification - i=1 for right wheel and i=2 for left
j	axis of contact zone coordinate - j=1 for longitudinal, j=2 for lateral, j=3 for normal direction
t	truck frame variable
w	wheelset variable

EXECUTIVE SUMMARY

Introduction

Statement of Problem:

The most widely accepted criterion for wheelclimb derailment defines an upper limit on wheel/rail contact forces on the climbing wheel, the limit varying with the time duration of the forces. The reliability of this criterion in predicting derailment is of major importance, since it is used to evaluate the derailment safety of railroad vehicles, operating conditions, and track structures. This report presents an analytical and experimental evaluation of time-dependent wheel load derailment criteria for wheelclimb, which shows that this type of criterion alone is inadequate for derailment prediction.

Main Objectives of Current Research:

The central goal of this program was to develop a fundamental understanding of the wheelclimb derailment process. Specific objectives undertaken to meet this goal were:

a. Establishment of an experimental data base of derailment events, using a dynamically scaled model of a single wheelset, for use in evaluating the validity of derailment criteria. Evaluation of specific candidate time-duration dependent wheel load criteria, such as that proposed by the Japanese National Railways (JNR).

b. Formulation of analytical models for predicting wheelclimb under quasisteady and dynamic loading conditions.

c. Experimental validation of the analytical models using scale model experimental data.

Technical Approach:

Derailment may occur as a result of several distinct processes, including wheelclimb, wheel lift, rail rollover, gauge spreading, and component failure, each requiring specification of allowable wheel/rail forces or other measures. This report concerns the first of these processes, which is directly related to the dynamics of the vehicle on curved and tangent track, and to the track misalignments that excite the vehicle. Wheelclimb is a derailment process in which large lateral forces acting on the wheelset cause on wheel to climb up and over the rail. When this wheel is in flange contact, large restoring forces resisting wheelclimb result from the large contact angle at the wheel/rail interface. Frictional effects, known as creep forces, aid or inhibit the process, depending on the angle of attack of the wheel relative to the rail.

The vector sum of the contact forces may be measured by an instrumented wheelset. Since the maximum allowable lateral force generally scales with vertical load on the derailing wheel, a derailment quotient, or L/V ratio, is often used as a measure of safety (L and V are the lateral and vertical force components, respectively). Under dynamic conditions, significantly larger derailment quotients may occur without derailment than would be expected under quasisteady operating conditions. The JNR derailment criterion was developed to account for this time-duration dependency.

To study the wheelclimb process in detail, three distinct processes were identified (Table EXEC.1):

a. Quasisteady wheelclimb, in which lateral velocity is negligible and the yaw angle remains essentially constant. This process applies to derailment during steady state curving.

b. Single degree-of-freedom (DOF) wheelclimb, in which lateral velocity effects are important, but the yaw angle remains essentially constant.

This condition describes steady state curving plus train action, discrete changes in track geometry, or truck hunting with relatively stiff primary yaw suspensions for the wheelset.

c. Two degree-of-freedom wheelclimb, which includes lateral velocity and changing yaw angle effects. This process describes dynamic curving, wheelset hunting, and truck hunting with relatively compliant yaw primary suspensions.

In this study the three derailment processes have been analyzed theoretically in detail. Experiments using a scale model wheelset on tangent track was used to validate the theoretical analysis. A computer program was developed for simulation of the wheelset, including coupling to the truck frame, which permits it to be integrated readily into complete vehicle simulations.

A comprehensive series of experiments was performed to evaluate existing and proposed derailment criteria for quasisteady and single DOF dynamic wheelclimb, and to validate theoretical models for all three processes.

Conclusions

The experimental and analytical studies of wheelclimb derailment presented in this report result in the following conclusions regarding derailment criteria:

1) Wheelclimb derailment criteria based on quasisteady theory are adequate for derailment prediction under conditions of negligible lateral incident velocity and constant positive yaw angle. At negative yaw angles derailment occurs at L/V ratios somewhat below the theoretical limits (Figure EXEC.1).

2) Application of the JNR and other time-duration dependent derailment criterion for nonderailment, marginal derailment, and complete

derailment cases are each spread over an order of magnitude in L/V ratio amplitude and time duration. None of the criteria tested could distinguish between safe and unsafe conditions. Defining a safety criterion below the derailment data would be overly conservative, possibly excluding vehicles, operating conditions, and track maintenance standards that could be demonstrated to be safe with a more discriminating criterion. Furthermore, the data provided do not necessarily establish a lower bound for derailment, since lower points possibly could be measured (Figure EXEC.2).

3) The analytical models for dynamic wheelclimb yield accurate predictions of wheelset response to external force inputs, in terms of wheelset motions during derailment and wheel/rail interaction forces (i.e. L/V ratios) (Figure EXEC.3).

4) Evidence has been found that derailment criteria employing variables measured in addition to wheel loads may be successful in predicting derailment safety, and that diagnostic criteria may be developed for warning of impending derailment (Figure EXEC.4).

Recommendation for Future Research

To achieve the objective of defining a reliable measure of derailment safety, the following would be useful as topics of future research:

a) New wheelclimb derailment criteria should be developed and validated that include variables in addition to wheel loads, such as lateral velocity and yaw angle, that are readily measured under full scale test conditions. Such multivariable criteria should be better indicators of derailment safety.

b) Criteria for the wheelclimb process should be combined with criteria for other derailments modes, such as gauge spreading and rail rollover, to yield a comprehensive safety measure. Track stiffness parameters would be key variables in the comprehensive criteria formulated.

c) The results of analytical and experimental studies of derailment of single wheelsets should be extended to complete trucks and vehicles. It is very important to establish the degree to which single wheelset criteria may be applied directly to complete vehicle configurations.

In addition to the above, the concept developed in this study of derailment diagnostics should be pursued. This technique provides a means for detecting marginally safe conditions in full scale tests, so that safety-related phenomena may be measured without actual derailments being required in the test plan. Scale model experiments will continue to be useful to the study of fundamental derailment processes, due to the greater control of test conditions possible and the relative ease of study of the full range of derailment conditions.

TABLE EXEC.1. COMPARISON OF WHEELCLIMB DERAILMENT PROCESSES

PROCESS IDENTIFICATION	NAME	LATERAL VELOCITY	YAW ANGLE	DESCRIPTION
A	Quasisteady wheelclimb	Negligible	Constant	Steady state curving
B	Single DOF wheelclimb	Important	Constant	Steady State curving plus train action, discrete changes in track geometry, truck hunting with stiff primary yaw suspensions
C	Two DOF wheelclimb	Important	Changing	Dynamic curving, wheelset hunting, truck hunting with compliant yaw suspensions

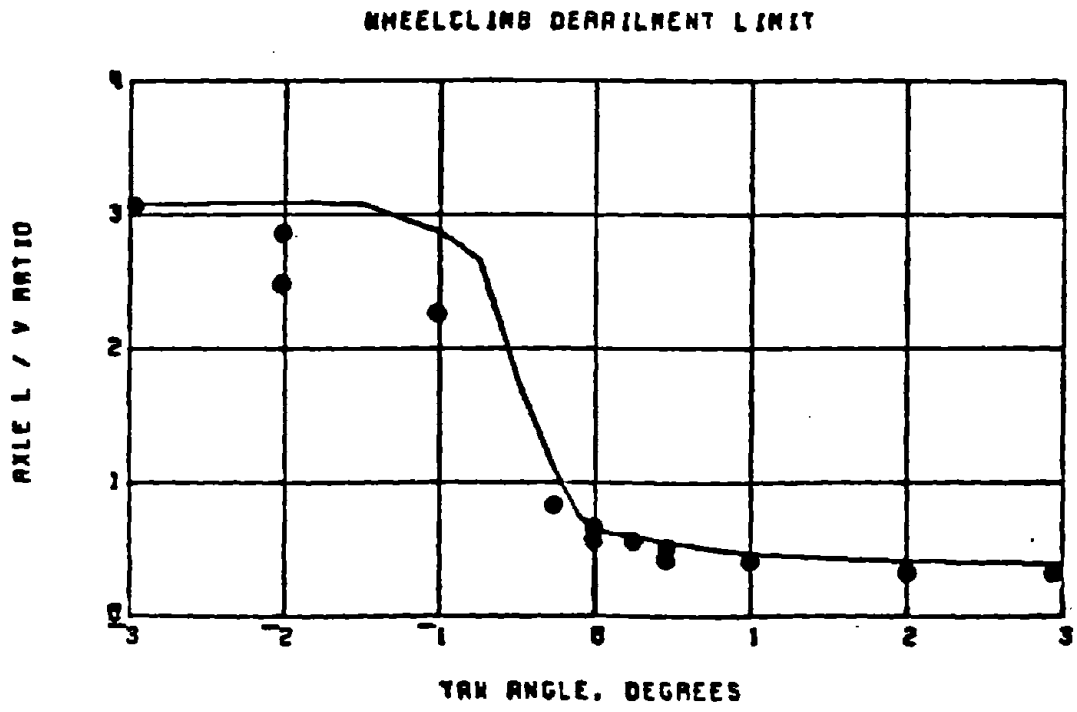

Figure EXEC.1 Comparison of Quasisteady Theory and Experiment for Wheelclimb Derailment Limit with Zero Roll Moment.

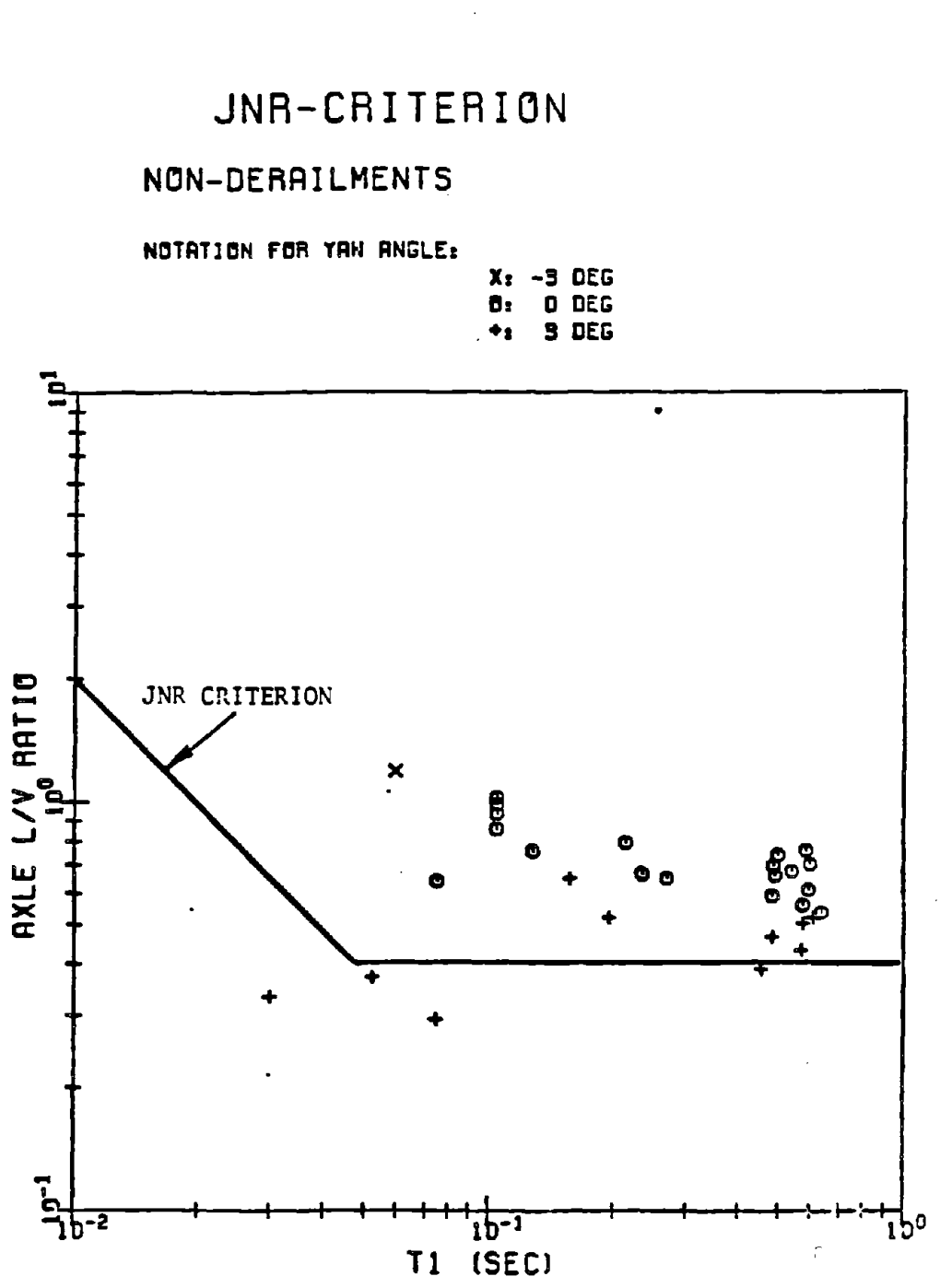

Figure EXEC.2a Comparison of Dynamic Wheelclimb Experimental Data with JNR Criterion for Nonderailment Cases.

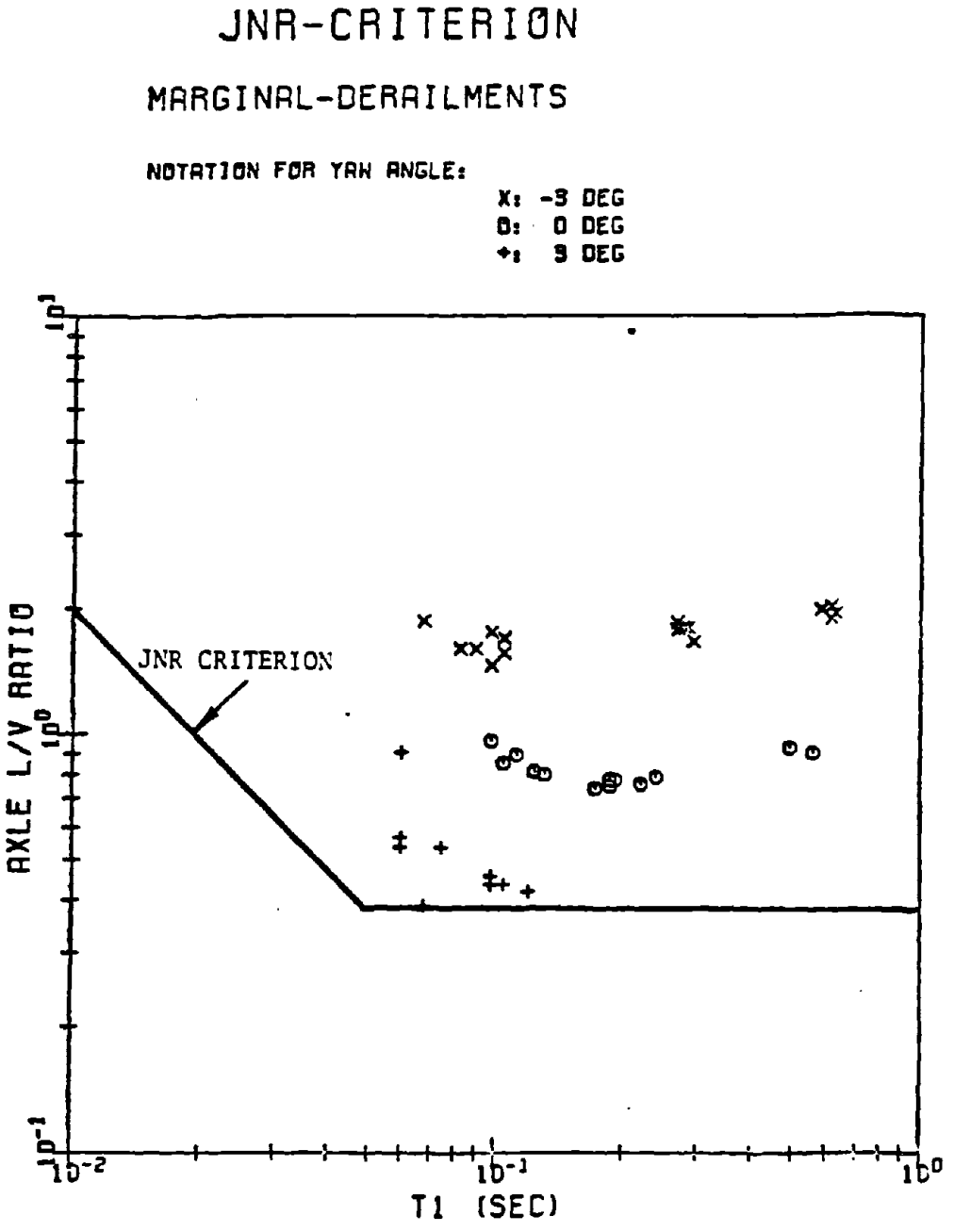

Figure EXEC.2b Comparison of Dynamic Wheelclimb Experimental Data with JNR Criterion for Marginal Derailment Cases.

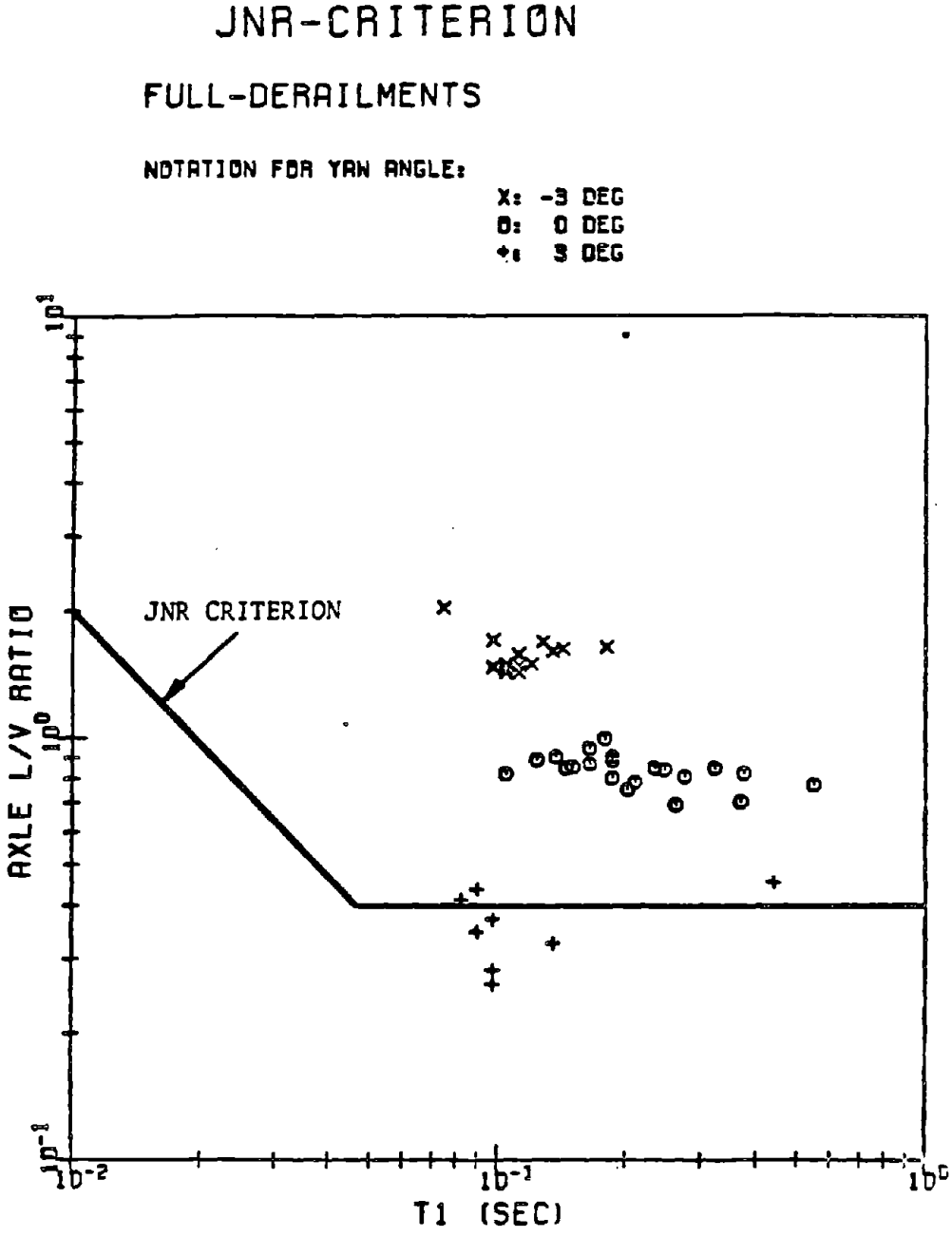

Figure EXEC.2c Comparison of Dynamic Wheelclimb Experimental Data with JNR Criterion for Complete Derailment Cases.

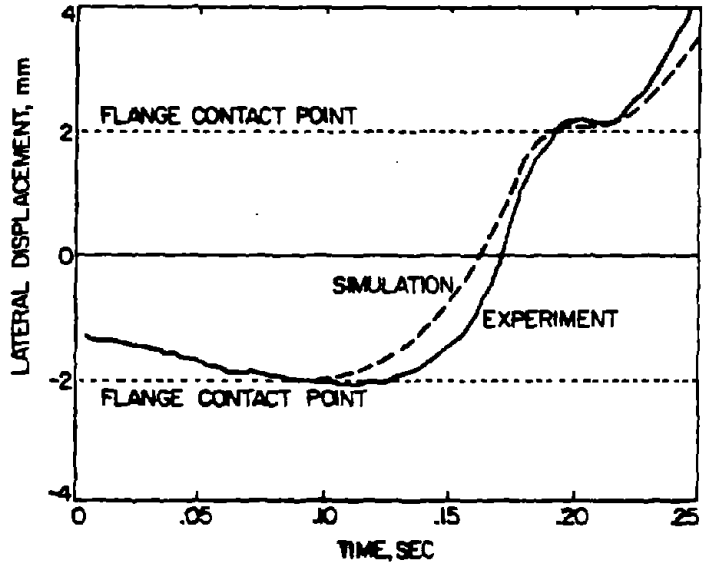

Figure EXEC.3 Measured and simulated wheelset lateral displacement.

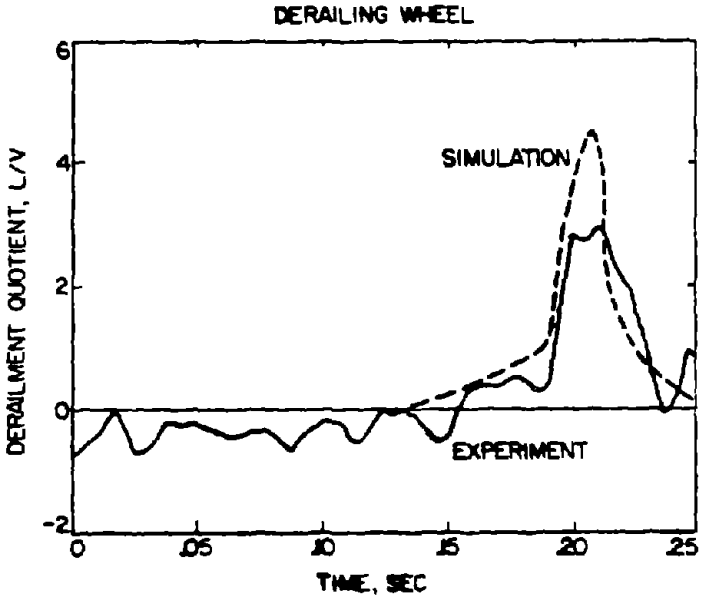

Figure EXEC.3 Measured and simulated derailment quotient (L/V ratio) on derailing wheel.

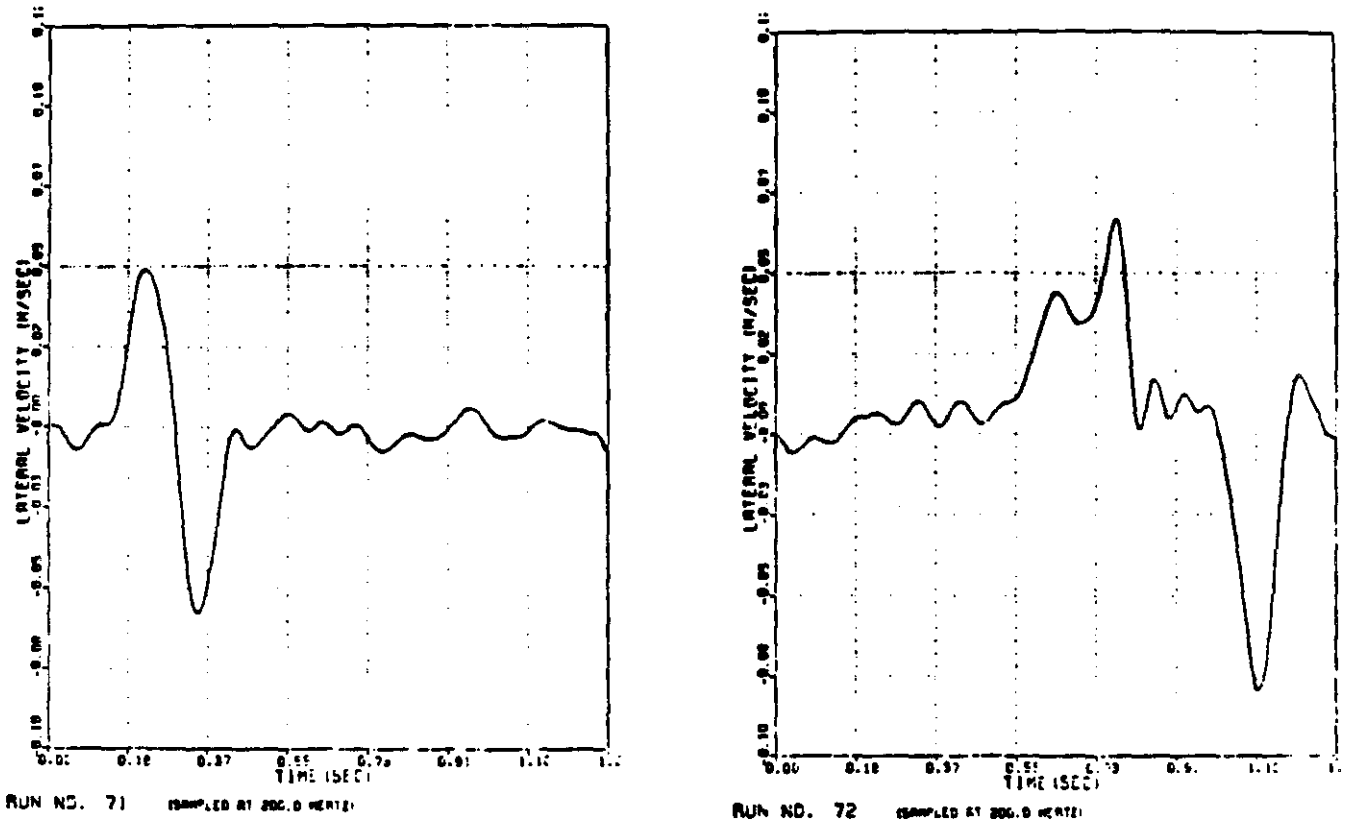

Figure EXEC.4 Generic Lateral Velocity Responses for Process B Dynamic Wheelclimb Tests. Double Peak Indicates Marginal Derailment Condition.

1. INTRODUCTION

The most widely accepted criterion for wheelclimb derailment defines an upper limit on wheel/rail contact forces on the climbing wheel, the limit varying with time duration of the forces. The reliability of this criterion in predicting derailment is of major importance, since it is used to evaluate the derailment safety of railroad vehicles, operating conditions, and track structures. This report presents an analytical and experimental evaluation of time-dependent wheel load derailment criteria for wheelclimb, which shows that this type of criterion alone is inadequate for derailment prediction. To study wheelclimb derailment processes and evaluate derailment criteria, a series of derailment experiments was conducted using a one-fifth scale model of a single wheelset on tangent track subjected to static and dynamic loading conditions. The results of these experiments were compared to simulations based on a nonlinear theory developed to represent the important phenomena associated with dynamic wheelclimb.

This study shows that the JNR and other time-duration dependent criteria based on wheel load measurements alone are unsuccessful in predicting derailment safety for dynamic wheelclimb. For wheelclimb processes involving negligible lateral velocities, the derailment limit can be estimated from quasisteady analysis of wheel/rail forces. Evidence has been found that derailment criteria employing variables measured in addition to wheel loads may be successful in predicting derailment safety, and that diagnostic criteria may be developed for warning of impending derailment.

There is a strong motivation for using wheel load measurements for derailment prediction. The mechanics of derailment for a complete truck are complex and highly nonlinear. At present no analytical model for complete trucks has been developed and validated that can relate measured variables other than wheel loads to derailment occurrence. The hope that wheel loads would be useful to derailment research has led to the development of instrumented wheelsets as major experimental research tools, which are also employed to study problems associated with failure, wear, and large deformation of wheels and track [22-24].*

The need for accurate and reliable methods for derailment prediction has intensified recently as efforts increase to relate vehicle characteristics, train operation, and track maintenance standards to system safety. With increasing success the relationships between vehicle and track descriptors and the resulting wheel/rail reaction forces have been quantified using analytical or empirical means [24-28]. The critical missing links are definitive specificatic relating these forces to safety.

Derailment may occur as a result of several distinct processes, including wheelclimb, wheel lift, rail rollover, gauge spreading, and component failure, each requiring specification of allowable wheel/rail forces or other measures [28 This report concerns the first of these processes, which is directly related to the dynamics of the vehicle on curved and tangent track, and to the track misalignments that excite the vehicle. Wheelclimb is a derailment process in which large lateral forces acting on the wheelset cause one wheel to climb up and over the rail (see Figure 1.1). When this wheel is in flange contact, large restoring forces resisting wheelclimb result from the large contact angle at the wheel/rail interface. Frictional effects, known as creep forces, aid or inhibit the

*Numbers in brackets refer to the list of References.

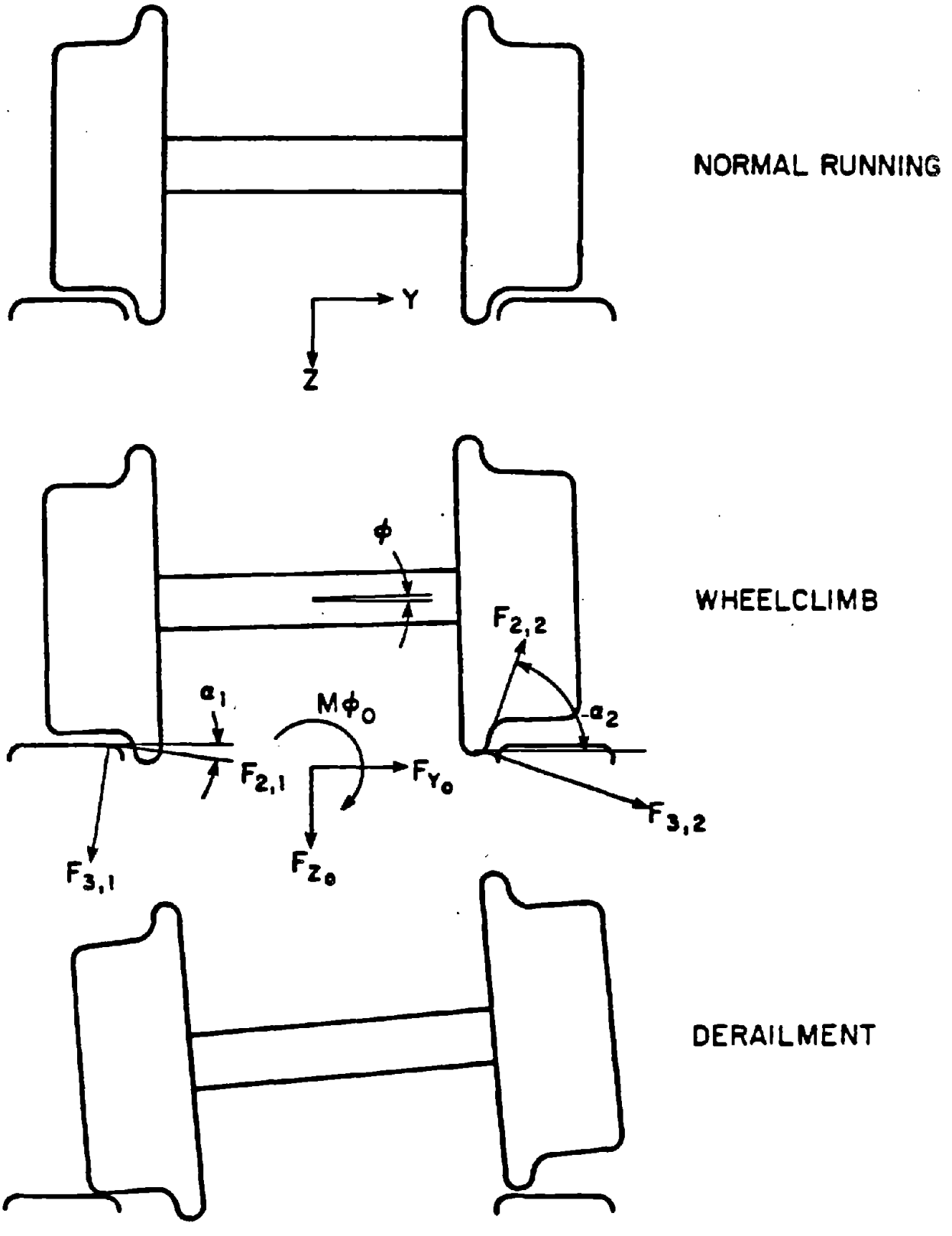

Figure 1.1 Definition of Forces Acting During Wheelclimb Derailment.

process depending on the angle of attack of the wheel relative to the rail. The vector sum of the contact forces are measured by an instrumented wheelset, and are distinct from the forces applied to the wheelset through its bearings.

Wheelclimb may occur at low forward and lateral velocities, with the resultant wheel/rail forces predicted using a quasisteady approach [5,8] , and have been confirmed experimentally in [8,30,31]. Since the limit on lateral forces F_{y_o} scales with vertical axle load F_{z_o} a derailment quotient, or L/V ratio, is often used, where L and V are the lateral and vertical components of the wheel/rail reaction forces. When significant lateral velocities occur during the wheelclimb process, lateral forces exceeding the quasisteady derailment limit generally occur, but only for relatively short time durations [24-26]. A criterion developed by the Japanese National Railways (JNR) attempts to account for the large contact forces by increasing the limit on allowed L/V ratios proportionally with $1/t_1$, where t_1 is the duration of the force pulse when it is less than 50 msec. [32].

The objective of the analytical and experimental research summarized in this report is the evaluation of the validity of wheelclimb criteria based on wheel load measurements. In order to systematically treat this objective, three distinct wheelclimb derailment processes may be identified, which become the basis for detailed analysis:

- Process A - Quasisteady wheelclimb, in which lateral velocity is negligible and the yaw angle remains essentially constant. This process applies to derailment during steady state curving.
- Process B - Single degree-of-freedom wheelclimb, in which lateral velocit effects are important, but yaw angle remains essentially constant. This condition describes steady state curving plus train action, discrete changes in track geometry, or truck hunting with relatively stiff primary yaw suspensions for the wheelset.

- Process C - Two degree-of-freedom wheelclimb, which includes lateral velocity and changing yaw angle effects. This process describes dynamic curving, wheelset hunting, and truck hunting with relatively compliant yaw primary suspensions.

In this study the three derailment processes described above are analyzed theoretically in detail. Experiments using a scale model wheelset on tangent track are used to validate the theoretical analysis. A computer program is developed for simulation of the wheelset, including coupling to the truck frame, which permits it to be integrated readily into complete vehicle simulations. A comprehensive series of experiments is described which are used to evaluate existing and proposed derailment criteria for quasisteady and single degree of freedom dynamic wheelclimb (Processes A and B).

Section 1 describes the motivation for this study, and reviews present knowledge in the field. Section 2 presents the analytical development of criteria for quasisteady wheelclimb. The experimental data presented agrees well with the derived criterion. In Section 3, a nonlinear model is validated for wheelset displacement responses to pulses in applied lateral forces. Simulations using the dynamic model indicate that the magnitude and duration of L/V ratios that would be measured during dynamic wheelclimb are not related in a functional way to derailment occurence.

In Section 4 time-duration dependent wheel load criteria for dynamic wheelclimb are evaluated. A variety of wheel load criteria, including the widely recognized JNR criterion, are applied to wheel load measurements taken from 112 derailment events, with none found to be successful in predicting derailment safety.

Appendix A summarizes the results of application of the variety of time-duration dependent wheel load criteria to the 112 derailment events recorded during the experiments. Appendix B describes in detail the apparatus used during Phase One of the research program, with the Phase Two apparatus described in Appendix C. The computer simulation program used to model wheelclimb derailment is listed in Appendix D.

2. QUASISTEADY WHEELCLIMB

2.1 Analytical Development

The steady rolling of a wheelset under load is a quasistatic process in which an equilibrium condition exists for all applied forces and moments due to vehicle and track loading. If for a given set of applied axle loads and wheelset yaw angle an equilibrium condition exists, characterized by a certain wheelset lateral position, wheelclimb derailment will not occur. If no stable equilibrium exists, wheelclimb derailment results. Yaw angle is defined to be positive when the derailing wheel is steered into the rail. For convenience, derailment is assumed to occur on the right rail, viewed in the direction of travel.

Since wheelset yaw angles are generally small, force and moment equilibrium conditions may be applied in a vertical plane passing through the axle. In this report the effect of translation of the wheel/rail contact points longitudinally along the rails is not considered. Analysis of the wheelset equilibrium conditions requires calculation of the forces at the contact points due to longitudinal, lateral and spin creep, each of which varies with wheelset lateral displacement, yaw angle, and axle angular velocity. The procedure for calculating the highly nonlinear wheel/rail contact forces in flange contact is presented in detail in [6], and is summarized schematically in Figure 2.1. The approach is similar to that presented in [5] and [13], and includes the Kalker creep force theory and iterative solutions for axle velocity and normal forces at the wheel/rail contact points. Numerical results are produced for specific wheel/rail contact geometries, computed for given wheel and rail profiles using algorithms developed in [17]. Creep

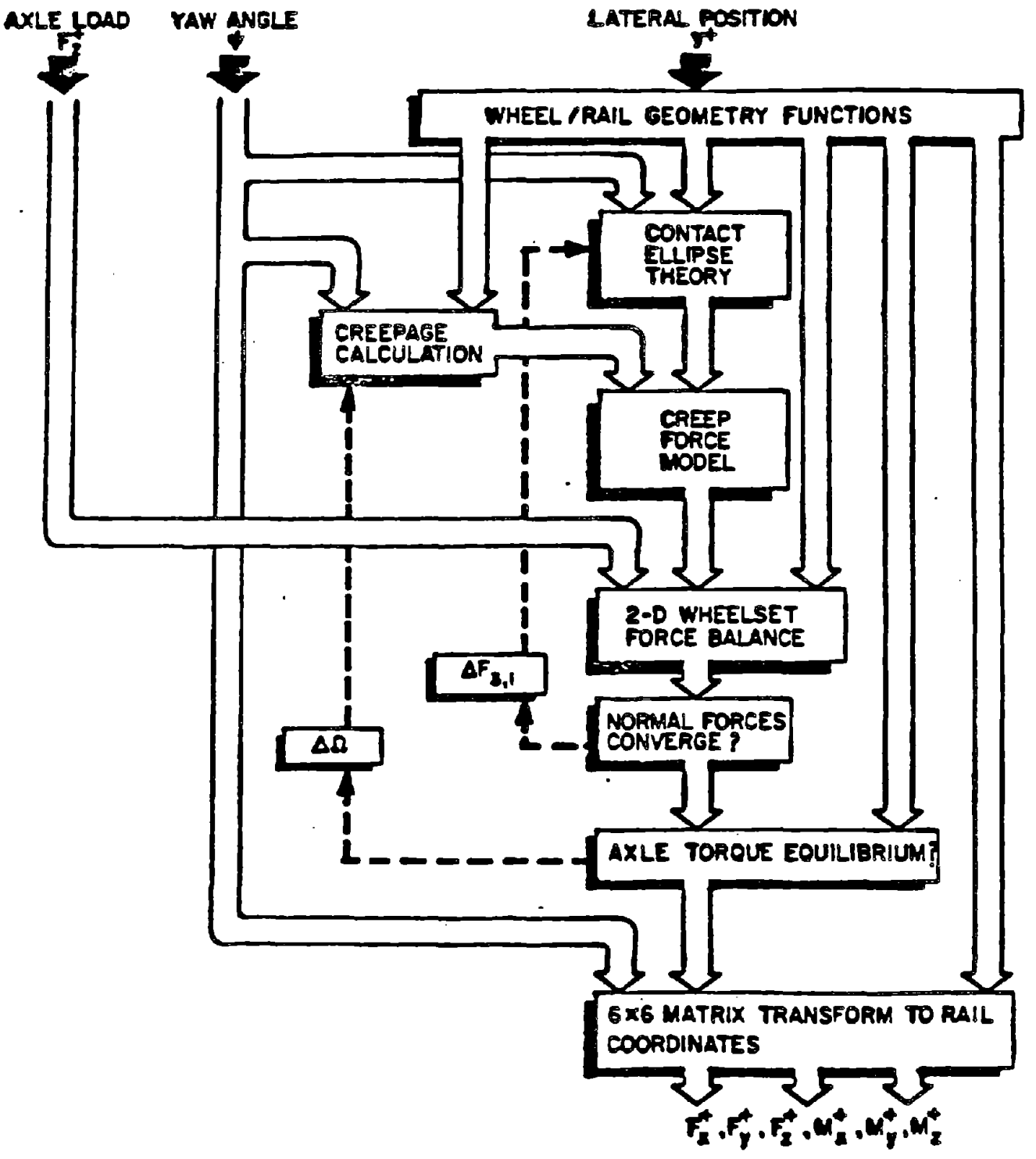

Figure 2.1 Algorithm Used to Evaluate Wheel/rail Contact Forces Acting on a Wheelset in Steady State.

forces at each contact point are determined through interpolation of numerical results from Kalker's Simplified Theory, tabulated for appropriate combinations of nondimensional creepages and contact ellipse geometry [14].

The quasisteady derailment limit (Process A) is derived by calculating the maximum applied lateral force that may be sustained for a given vertical force and roll moment applied to the wheelset. The net wheel/rail reaction forces and moments acting on the wheelset in steady state as shown in Figure 2.1 are balanced by applied forces F_{y_o}, F_{z_o}, and moment M_{ϕ_o}

Lateral force:

$$0 = F_{y_o} + \sum_{i=1}^{2} F_{3,i} \left(\mu f_{2,i} \cos\alpha_i + \sin\alpha_i\right) \tag{2.1}$$

Vertical force:

$$0 = F_{z_o} + \sum_{i=1}^{2} F_{3,i} \left(-\mu f_{2,i} \sin\alpha_i + \cos\alpha_i\right) \tag{2.2}$$

Roll Moment:

$$0 = M_{\phi_o} - \sum_{i=1}^{2} (-1)^i L_i F_{3,i} \left(-\mu f_{2,i} \sin\alpha_i + \cos\alpha_i\right) \tag{2.3}$$

The normal forces $F_{3,i}$ at the contact points may be eliminated to yield the vertical and lateral forces acting on each wheel. The wheel/rail reaction forces are then combined to give L/V ratios for the wheelset axle (both wheels) or for the climbing wheel only.

$$\left.\frac{L}{V}\right|_{axle} = [\ell_2\Gamma_1 + \ell_1\Gamma_2] + \frac{1}{2}\eta[-\Gamma_1 + \Gamma_2]$$

where $$\Gamma_1 = \frac{\tan(\alpha_1+\phi) + \mu f_{2,1}}{1 - \mu f_{2,1}\tan(\alpha_1+\phi)}$$

$$\Gamma_2 = \frac{\tan(\alpha_2+\phi) + \mu f_{2,2}}{1 - \mu f_{2,2}\tan(\alpha_2+\phi)} \qquad (2.4)$$

$$\eta = -\frac{2M_{\phi_o}}{(L_1 + L_2)F_{z_o}}$$

$$\ell_1 = \frac{L_1}{L_1 + L_2}$$

$$\ell_2 = \frac{L_2}{L_1 + L_2}$$

Parameters Γ_1 and Γ_2 are the individual wheel L/V ratios for the left and right wheels, respectively. Parameter η is the dimensionless roll moment, representing the degree of asymmetry in axle load between the extremes of wheel lift (with a practical range of ± 1). In the above equations $f_{2,1}$ and $f_{2,2}$ are the dimensionless lateral creep coefficients (including spin) on the left and right wheels, ϕ the wheelset roll angle, and α_1 and α_2 the associated contact angles, defined to be positive counterclockwise. The nomenclature and coordinate system is developed in [5,6]. For the quasisteady process, parameters Γ_1 and Γ_2 are functions of lateral position y and yaw angle ψ; for each value of ψ a maximum for L/V exists, usually close to the value for y which yields the maximum contact angle on the climbing wheel.

The L/V ratio for the climbing wheel is often used itself as a derailment criterion, and is defined using the above parameters as*

$$\left.\frac{L}{V}\right|_{\text{climbing wheel}} = \Gamma_2 = \frac{\tan(\alpha_2+\phi) + \mu f_{2,2}}{1 - \mu f_{2,2} \tan(\alpha_2+\phi)} \tag{2.5}$$

For large yaw angles Eq. (2.5) approaches the classical limit of Nadal [8], but for the range of conditions $-3^\circ < \psi < +3^\circ$ the nondimensional creep $f_{2,2}$ may vary considerably with wheelset loading, wheel/rail profiles, and yaw angle, over the range $-1 < f_{2,2} < 1$. Under quasisteady conditions, the creepages are functions only of the wheel and rail profiles, wheelset displacement, and yaw angle relative to the rail, so that Eqs. (2.1) through (2.5) are independent of forward velocity V.

2.2 Method of Computation

The method used for computing the quasisteady derailment limit is the same as that described in detail in [6], with the exception of the procedure used to calculate creep forces. In [6] creep forces are approximated by calculating initially the forces due to longitudinal, lateral, and spin creepages separately, then added vectorially with approximate adhesion limits imposed. Further study has shown that at negative yaw angles and large spin creepage (i.e. flange contact) significant errors accrue using this approximation, yielding derailment limits at large negative angles that do not agree with Nadal's limit.

The new procedure uses creep force calculations based on Kalker's Simplified Theory, so that creep forces in the lateral and longitudinal directions are computed directly from the three creepage components [18].

*For simplicity assume right wheel is climbing.

To make the computation efficient, nondimensional creep forces are precomputed and stored using the following procedure:

1) The lateral displacement at which the contact angle is maximum is determined. This point is very close to the point of maximum lateral force (i.e. derailment limit) and eliminates the need to search over the y-direction.

2) The non-dimensional contact ellipse geometry factors $\bar{a} = a/\sqrt{ab}$ and $\bar{b} = b/\sqrt{ab}$ are computed for this lateral displacement. These factors are independent of wheel loads. The effect of ψ on these parameters is neglected, also the nondimensional spin creep χ is computed.

3) For the above values of $\bar{a}$, $\bar{b}$, χ and Poisson's ratio the Kalker program is run repeatedly to generate a table of lateral and longitudinal nondimensional creep forces for all possible values of lateral and longitudinal creepages ν_y and ν_y, respectively. The table is expressed in coordinates $\bar{\nu}$ and $\bar{\alpha}$, which are the polar transformations of ν_y and ν_x.

4) For each value of ν_x and ν_y desired, the creep forces are calculated from the table using interpolation based on the Lagrange polynomial method.

The resulting calculations yield a limit for large negative yaw angles of L/V_{axle} equal to 3.1, which agrees with Nadal's limit, in contrast to a value of 2.0 computed in [29]. At large positive yaw angles both the above and previously used methods yield the correct Nadal limit.

2.3 Comparison of Axle and Wheel L/V Ratio Criteria

Due to the nonlinearity of the creep force phenomenon, wheelclimb derailment limits based on both axle and wheel forces vary with axle

loading. Using numerical results for wheels and rails with new profiles extended from [6] to cases with non-zero roll moments, the degree to which each criterion may be applied universally is demonstrated. In Figure 2.2 wheel and axle L/V ratios are shown for varying axle vertical load. Both criteria are insensitve to vertical load, with minor variation evident only in the range $-1.4^{o} < \psi < 0^{o}$. The two criteria are related for all vertical axle loads by a single function shown in Figure 2.3. Figure 2.4 shows the effect of roll moment parameter η on the two criteria. A positive roll moment, increasing the vertical force on the wheel in flange contact, produces a larger axle L/V ratio for wheelclimb derailment for all yaw angles. The scaling of the derailment limit with roll moment is reflected in the relative insensitivity in the wheel L/V ratio. Although the roll moment parameter η does not appear explicitly in Eq. 2.5, it does affect the solution for wheelset force equilibrium, causing variations in $f_{2,2}$ over the range $-1.0^{o} < \psi < 1.0^{o}$. The relations between the two criteria for varying roll moment is shown in Figure 2.3.

Table 2.1 summarizes the relative advantages of use of criteria of each type. For situations in which axle loads including roll moments are known, from simulation or vehicle measurements, axle L/V ratios are better since the individual wheel forces are not required. If the roll moment is not known, as may be the case for field experiments on full scale vehicles, wheel L/V ratios are better when applied to data from instrumented wheelsets.

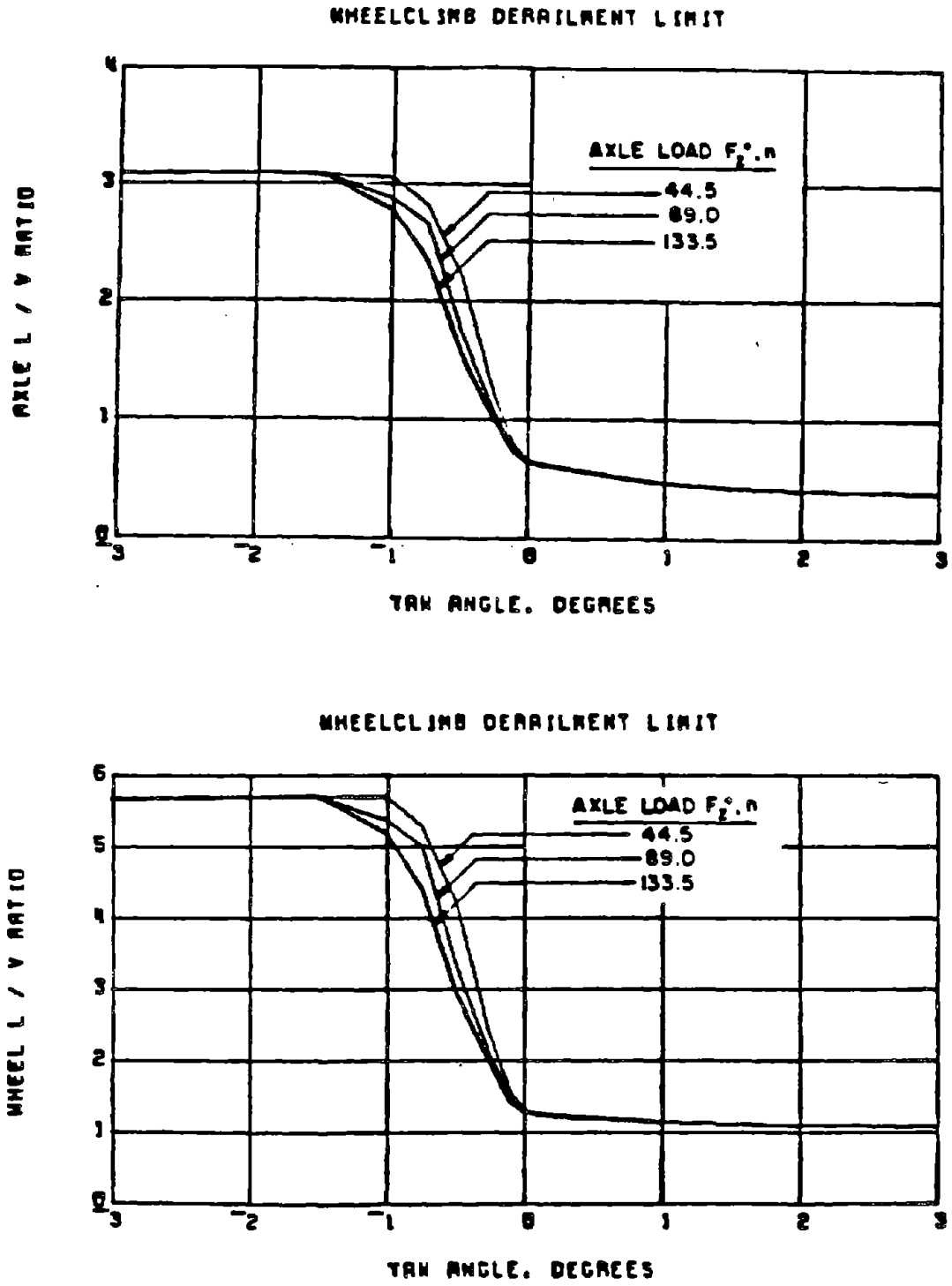

Figure 2.2 Effect of Axle Load F_z on Axle (above) and Wheel (below) L/V Ratio Derailment Limits.

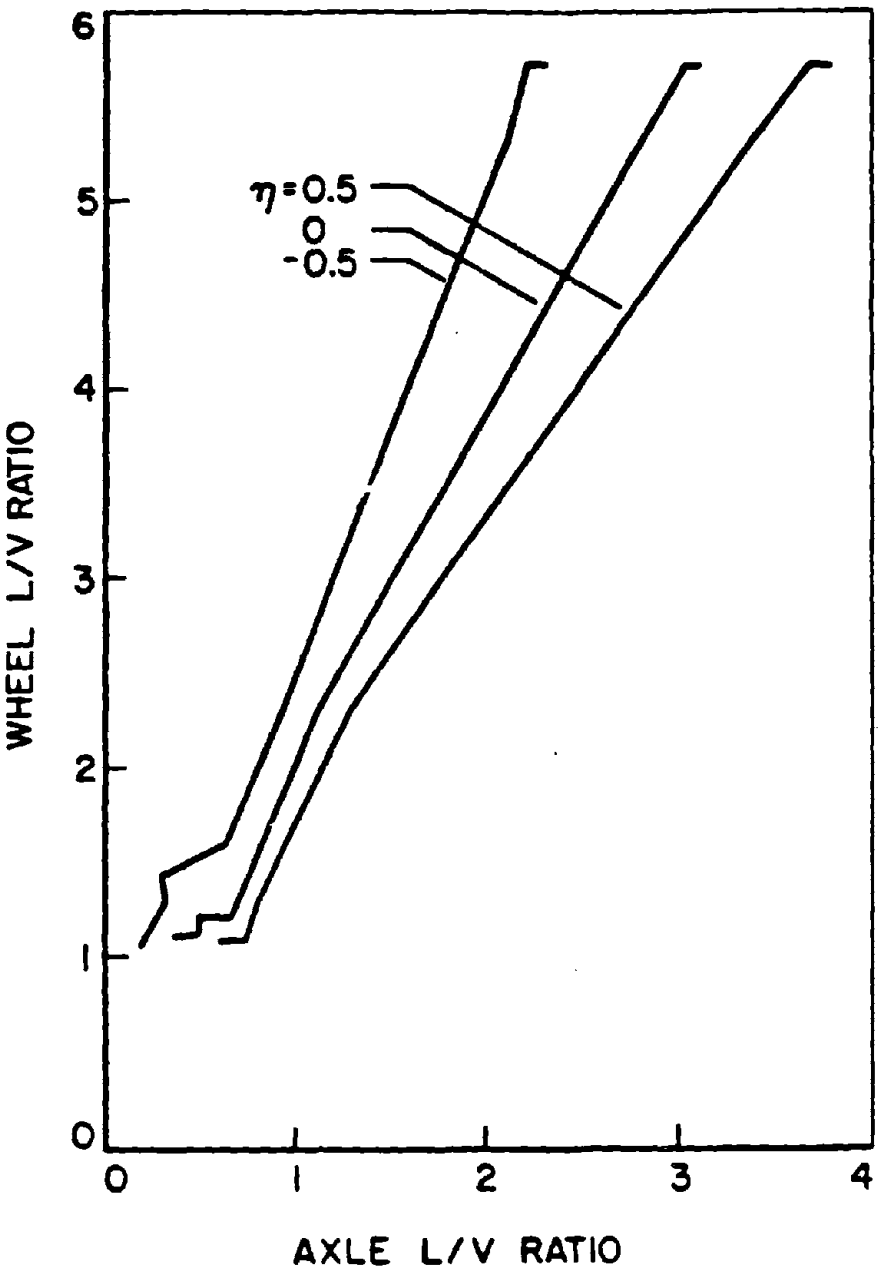

2.3 Comparison of Wheel and Axle L/V Ratio Quasisteady Derailment Limits

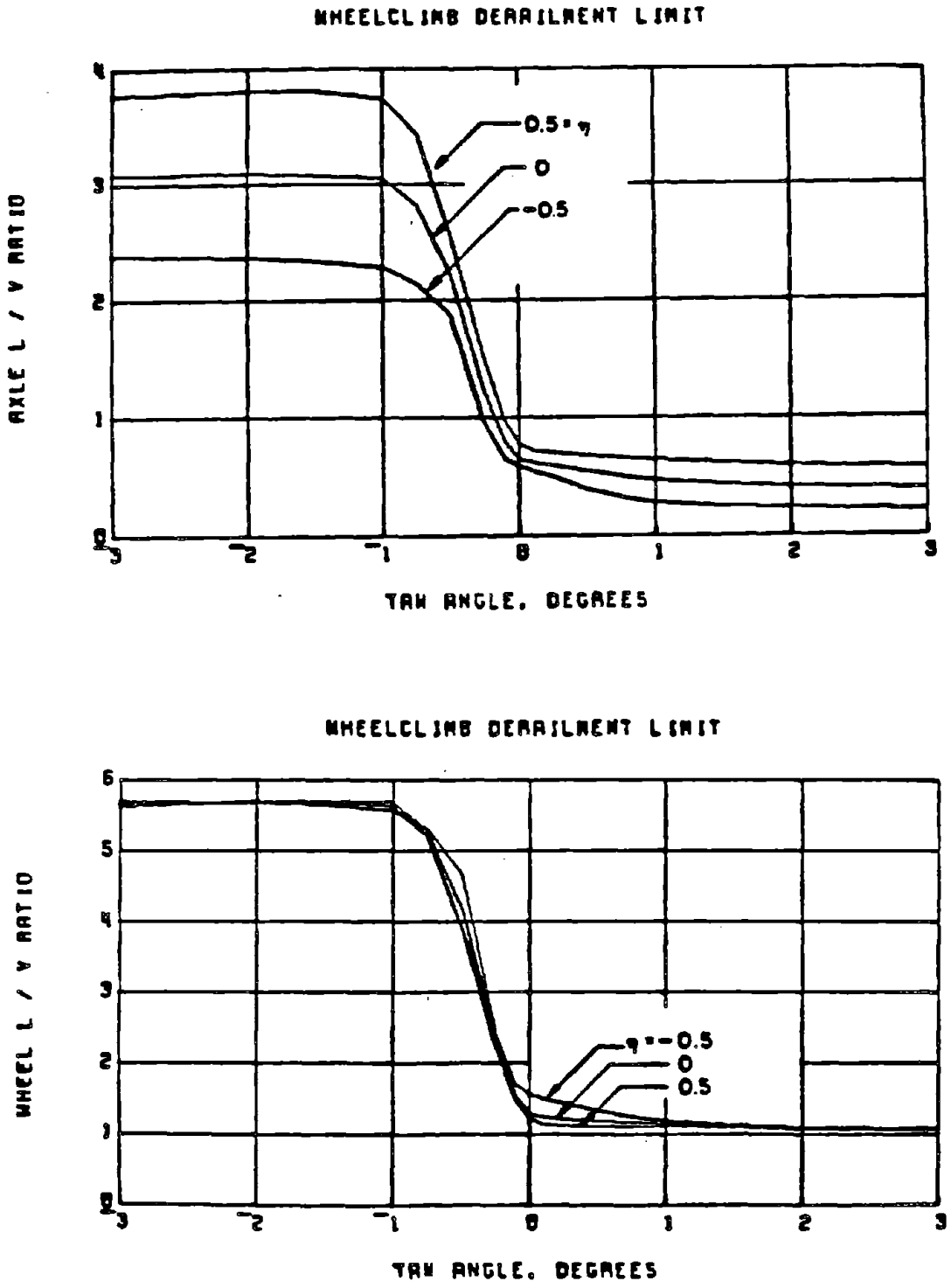

Figure 2.4 Effect of Nondimensional Roll Moment η on Axle (above) and Wheel (below) L/V Ratio Derailment Limits.

TABLE 2.1 COMPARISON OF AXLE AND WHEEL L/V RATIO CRITERIA

Advantage	Axle L/V	Wheel L/V
Insensitive to axle vertical load	yes	yes
Insensitive to axle roll moment	no	yes
Shows variation with yaw angle	yes	yes
Does not require simulation or measurement of individual wheel contact forces	yes	no

2.4 Experimental Validation and Usefulness of Model

The quasisteady wheelclimb experiments* consist of a lateral force ramp loading applied to the wheelset, with vertical axle load, yaw angle and forward velocity held fixed. The loading rate is held small to preserve quasisteady conditions. Typical time histories of axle L/V ratio and lateral displacement are shown in Figure 2.5.

The time histories indicate a very well-defined derailment limit. Fluctuations in the measured responses are due to variations in local track geometry; the "track signature" is quite repeatable when the experiment is duplicated at the same track location, even at different forward velocities. At other track locations, the fluctuations over the time history differ, but the L/V derailment limits are consistent within a range of $\pm 5\%$. The temporal frequencies of these fluctuations are sufficiently low to maintain quasisteady conditions. Since the variations in track alignment and rail profile in the scale model are less than that expected in full scale, the fluctuations in measured responses shown are probably smaller than would be expected in field testing.

Experiments such as that illustrated in Figure 2.5 were conducted for the range of yaw angles $-3^{\circ} \leq \psi \leq 3^{\circ}$. The maximum axle L/V ratio immediately before derailment for each yaw angle is recorded in Figure 2.6 for the case of zero applied roll moment. Agreement between theory and experiment is generally good, although the theory overestimates the derailment limit for negative angles in the transition region between -0.5° and -2.0°.

---

* Apparatus described in Appendix B.

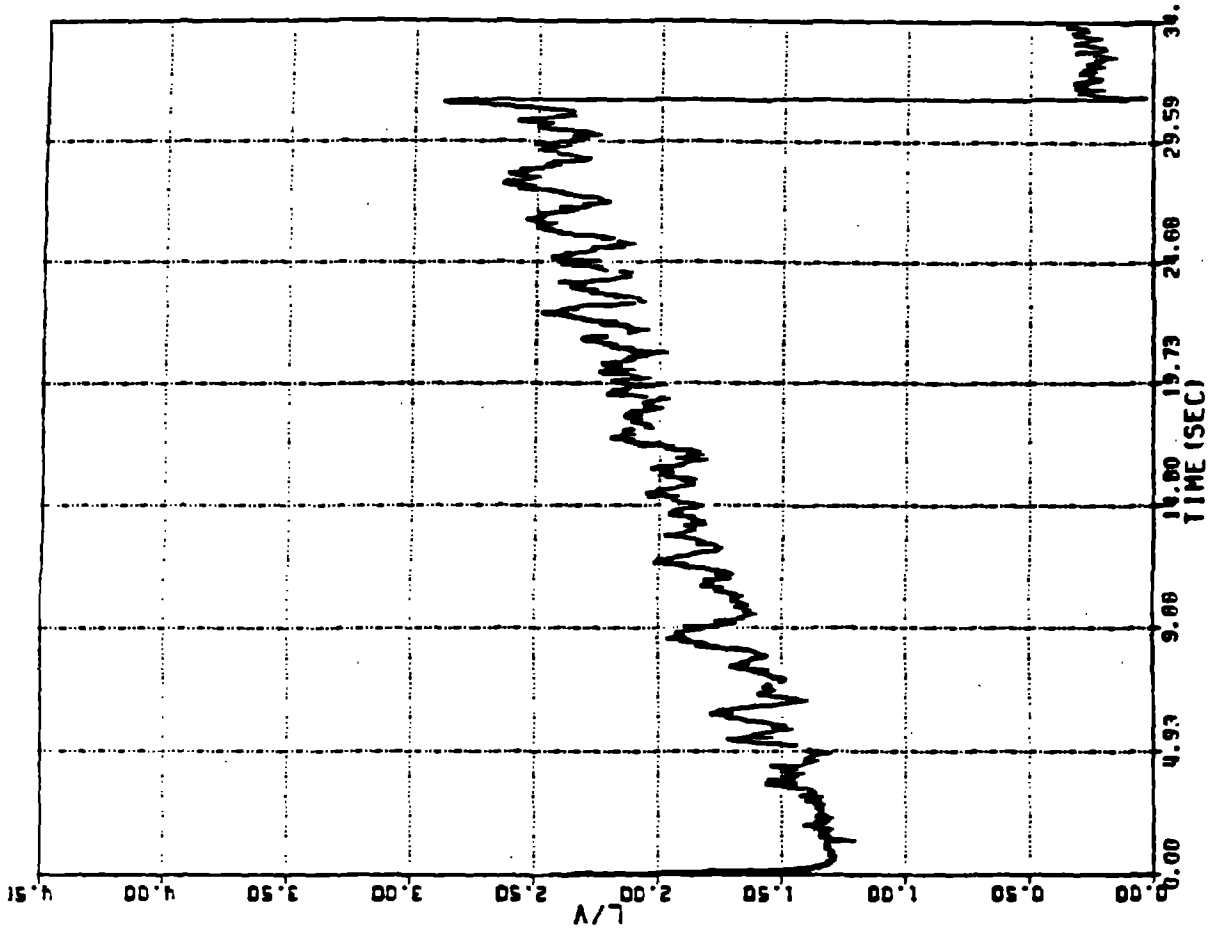

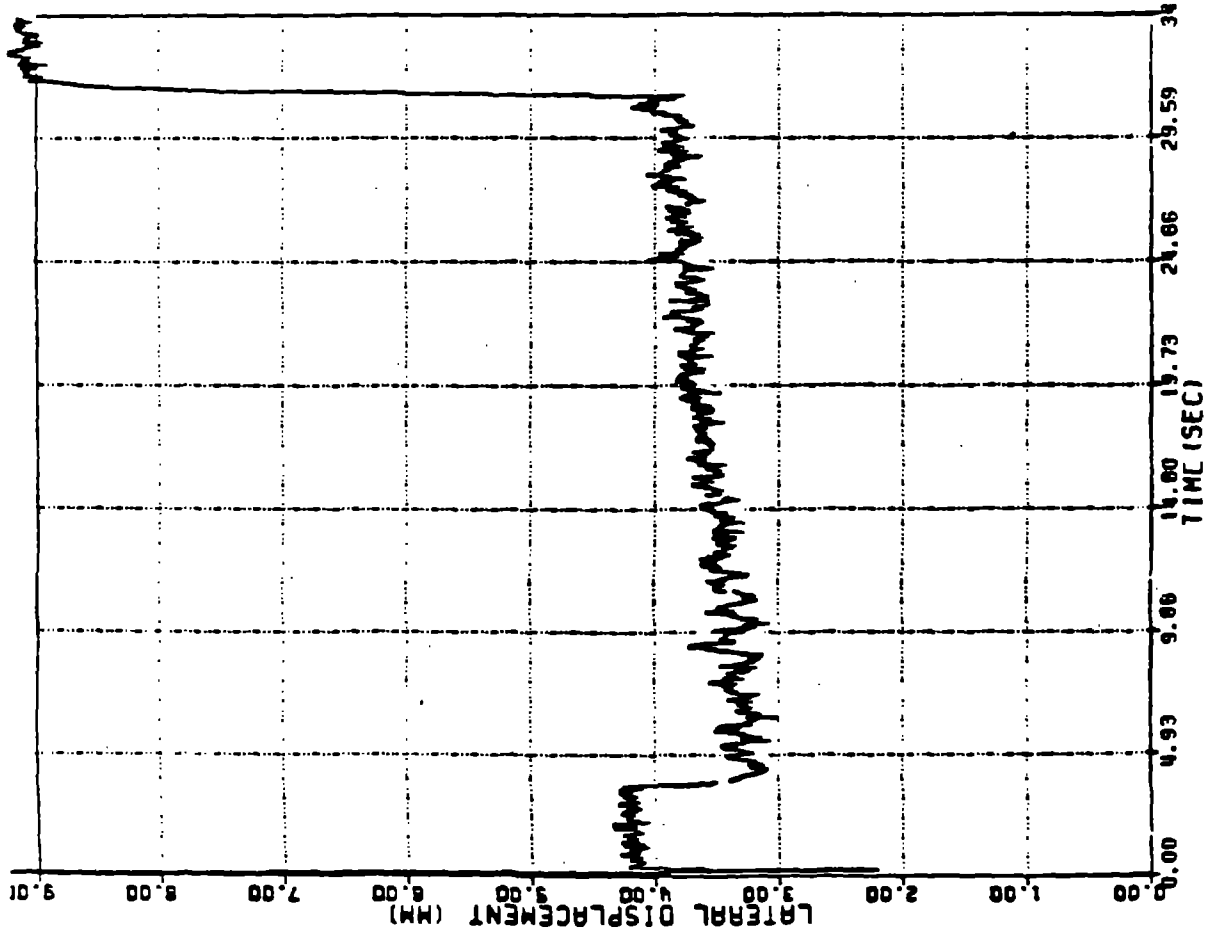

Figure 2.5 Typical Experimental Time Histories of Lateral Displacement and Axle L/V Ratio During Quasisteady Wheelclimb Derailment.

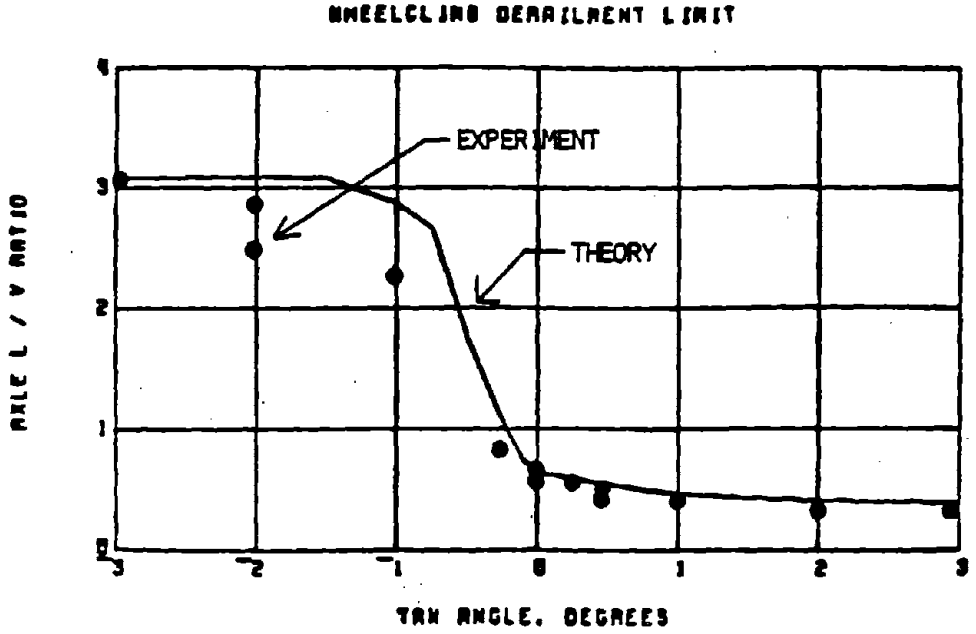

Figure 2.6 Comparison of Quasisteady Theory and Experiment for Wheelclimb Derailment Limit with Zero Roll Moment.

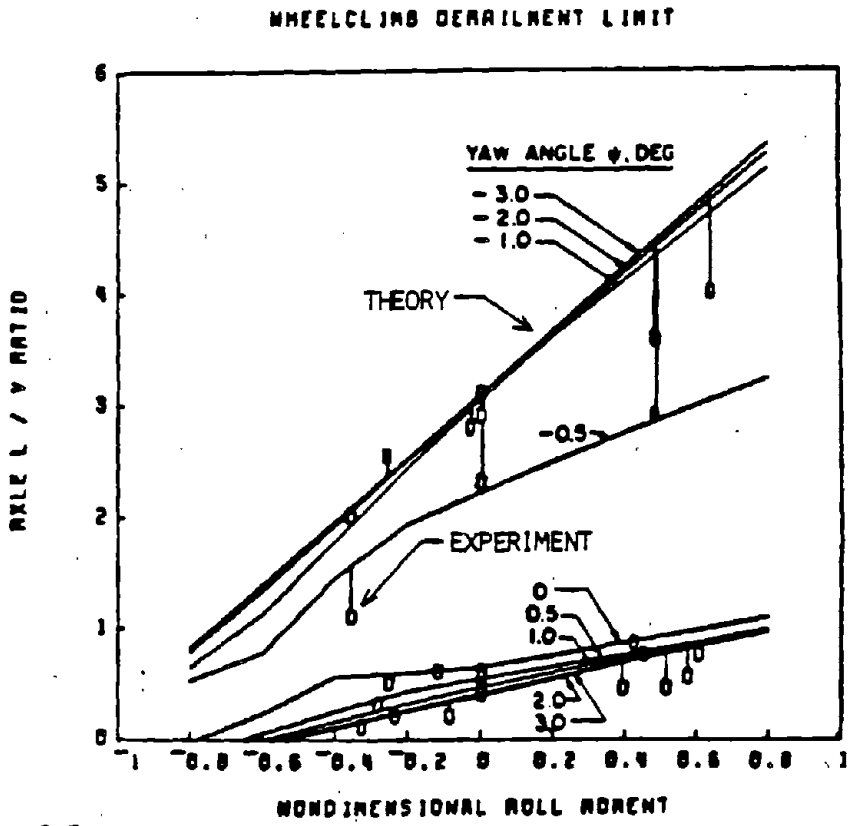

Figure 2.7 Comparison of Quasisteady Theory and Experiment for Wheelclimb Derailment Limit for Varying Yaw Angles and

The results for quasisteady wheelclimb are consistent with roller rig data in [7], where the theory also overpredicts the derailment limit for negative yaw angles (but with a smaller error). The source of the discrepancy in the present tests has not been positively identified, but may be due either to the presence of the lateral track dynamic input (not accounted for in theory) or to local variation in friction coefficient or contact angle. Since the data presented are the only published results for tangent track experiments, conservative safety criteria should be based on the lower measured values rather than the theory for negative yaw angles.

Three possible sources of error may account for this discrepancy, two experimental and one theoretical. In the vicinity of the derailment location on the track, local variation in rail profile curvature from nominal values may produce significant changes in nondimensional lateral creep coefficient $f_{2,2}$. Error in $f_{2,2}$ or friction coefficient μ would produce an error in the predicted derailment limit. The third possible source of error results from the high ratio of the semi-axes of the contact ellipse in flange contact. For the wheel and rail profiles used in the experiment the ratio a/b is 16, which is beyond the numerical range computed by Kalker and the experimental range measured by Brickle [5]. Therefore numerical error in the calculated creep forces is not excluded as an explanation for the difference between theory and experiment.

The effect of roll moment on the measured axle L/V derailment limit is shown in Figure 2.7. Data points shown without lines are touching

the predicted derailment limit at the associated yaw angle. Data points with lines indicate the differences between theory and experiment. The application of constant roll moments under rolling conditions on the track was difficult experimentally, resulting in some scatter in the data. The agreement between theory and experiment is good, with the same differences as discussed above for negative yaw angles.

3. DYNAMIC WHEELCLIMB

3.1 Analytical Development

3.1.1 Introduction

Numerous theoretical models for wheelset dynamics are available in the literature [1-4]. For large amplitude wheelset motions, the mechanics and dynamics become highly nonlinear, due to the effects of contact geometry and rolling friction creep forces. For motions during which tread contact is maintained on both wheels, whether the wheel profiles are conical or curved, the wheelset dynamic equations include many terms of approximately equal magnitude. Under conditions of severe flange contact leading to derailment, the relative magnitudes of these various dynamic terms differ considerably from their values in the tread contact case, leading to conclusions different in certain respects from those of the cited references.

Compared to the rather rigorous analytical models of the preceeding references, theories used for analysis of derailment mechanics have been simplified. Equilibrium models for wheels and rails in flange contact by Gilchrist and Brickle [5], Sweet [6], and Yokose and Arai [7] have successfully predicted quasisteady derailment limits. Dynamic wheelclimb models by Sweet [8] and Yokose [7,9,10] on the other hand, have all been based on certain assumptions which have not been fully verified by simulation or experiment.

In this study a detailed model for wheelset derailment has been developed. The wheelset motion includes three independent degrees of freedom; lateral displacement, yaw angle, and axle rolling angular velocity. The truck motion includes a single degree of freedom: the lateral displacement of the truck frame.

While nearly all analyses include the first two motions of the wheelset, only more recent papers by Clark [11] and Duffek [12] have accounted for the deviation of the rolling velocity from the nominal value of V/r_o expected when the wheelset is centered and rolls with zero slip. As shown in [6], during steady flange contact the axle speed drops by about 3%, which should have a significant effect on calculation of the longitudinal creepage.

If wheel/rail contact is maintained on both wheels, the wheelset vertical and roll degrees of freedom are not independent and may be expressed as a function of the lateral motion. Imposition of these kinematic constraints leads to generation of significant dynamic components in the equations of motion. A wheelset kinematic model is developed in this report to account for these dynamic effects, as well as for computation of lateral creepages in the contact zones as a function of the velocity of the wheelset center of mass.

A digital computer program for solving the resulting equations of motion is described. The program is compatible with published programs used for computation of contact geometry and creep force functions.

3.1.2 Kinematics of Wheelset Motion

Kinematic Model: Careful representation of the kinematics of wheelset motion is needed for determination of the creepages at the wheel/rail interfaces and the coupling of the vertical, lateral and roll motions. The kinematic analysis employs three sets of coordinate systems, as illustrated in Figure 3.1. The contact zone creepages depend on the relative velocities of the contact points of the wheels with respect to the rails. The wheelset kinematic model is used to determine these relative velocities in terms of the velocity of the wheelset center of mass, utilizing the geometrical constraints imposed by the rails on the wheelset motion. The model is also used to compute the

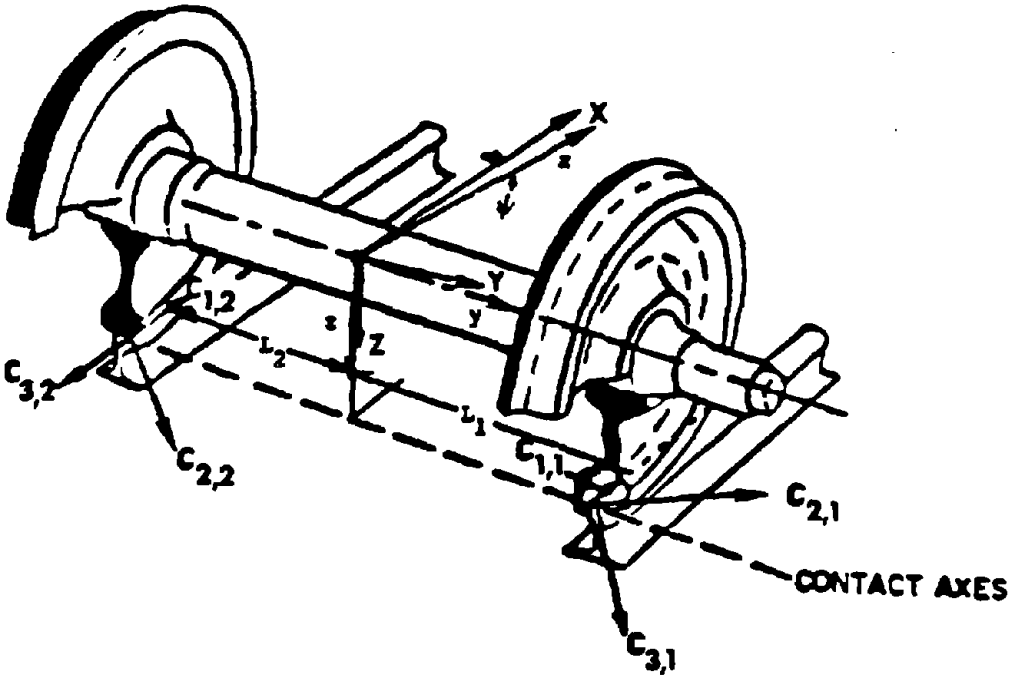

Figure 3.1 - Definition of Coordinate Systems for Wheelset and Contact Zones

wheelset vertical and roll accelerations, as functions of its lateral velocity and acceleration.

The wheelset kinematic model is illustrated in Figure 3.2. A two-dimensional, planar motion model is used to derive the relationships between lateral, vertical, and roll motions. The instantaneous center of rotation, point 0, is assumed to be in the YZ plane, with its location depending on the contact angles and contact points. The kinematic relationships are derived by first determining the position of the wheelset center of mass, point C, relative to the instantaneous center:

$$\overline{OC}^2 = \frac{L_2^2}{\cos^2\gamma_1} + \frac{(L_1+L_2)^2\cos^2\alpha_1}{\sin^2(|\alpha_1|+\alpha_2)} - \frac{2L_2(L_1+L_2)\cos\alpha_1\sin(\gamma_1+\alpha_2)}{\sin(|\alpha_1|+\alpha_2)\cos\gamma_1} \tag{3.1}$$

$$\text{where } \gamma_1 = \tan^{-1}(r_0/L_2) \tag{3.2}$$

$$\gamma_2 = \sin^{-1}[L_2\cos(\gamma_1+\alpha_2)/\overline{OC}\cos\gamma_1] \tag{3.3}$$

$$\beta = \gamma_2 - \alpha_2$$

From Equations 3.1 through 3.3 the instantaneous relationships between vertical, lateral, and roll motions are computed:

$$\frac{\partial Z_w}{\partial Y_w} = -\tan\beta \tag{3.4}$$

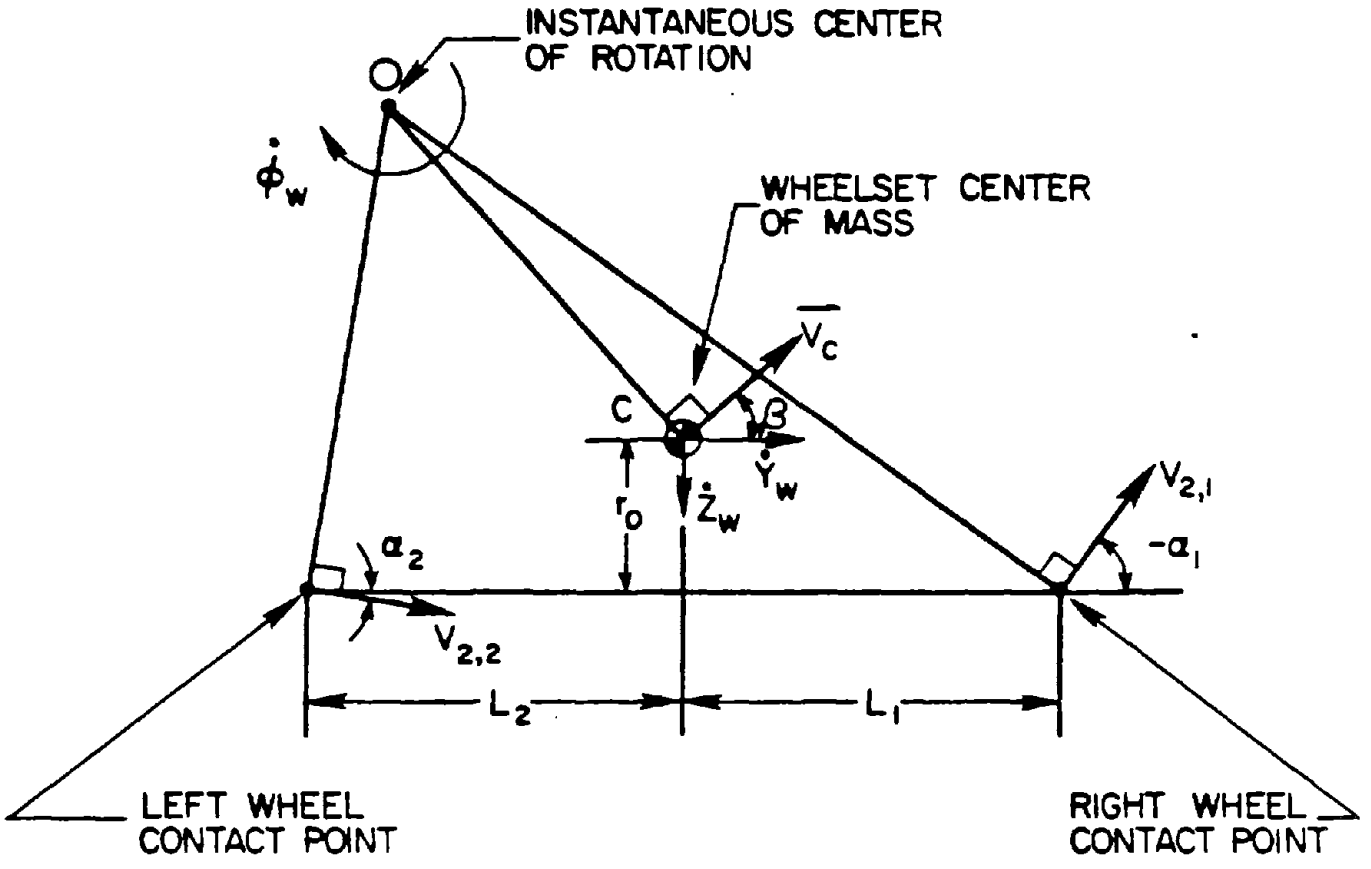

Figure 3.2 - Velocities Defined by Wheelset Kinematic Model

$$\frac{\partial \Phi_w}{\partial Y_w} = - \frac{1}{\overline{OC} \cos \beta} \tag{3.5}$$

Contact Zone Velocities

The lateral velocity in the contact plane at each contact point is determined by:

$$v_{2,1} = \frac{(L_1+L_2)\cos\alpha_2}{\sin(|\alpha_1|+\alpha_2)} \frac{\partial \Phi_w}{\partial Y_w} \dot{Y}_w \tag{3.6a}$$

$$v_{2,2} = \frac{(L_1+L_2)\cos\alpha_1}{\sin(|\alpha_1|+\alpha_2)} \frac{\partial \Phi_w}{\partial Y_w} \dot{Y}_w \tag{3.6b}$$

Creepages are defined using the model of Gilchrist and Brickle [5], with extensions to include dynamic effects. Sign conventions have been modified for consistency with Kalker theory.

For longitudinal creepage (non-dimensional):

$$\gamma_{1,i} = \frac{-\Omega r_{v,i} \cos\psi + V}{V} + (-1)^i \frac{\dot{\psi} L_i}{V} \tag{3.7}$$

For lateral creepage (non-dimensional):

$$\gamma_{2,i} = - \frac{\sin\psi}{\cos\alpha_i} + \frac{v_{2,i}}{V} \tag{3.8}$$

For spin creepage (dimensional):

$$\omega_{3,i} = \frac{\sin\alpha_i}{r_{v,i}} \tag{3.9}$$

Similar expressions were developed by Elkins and Gostling [13], although they used the wheelset c.m. lateral velocity Y_w instead of $V_{2,i}$. The spin creepage defined in Equation (3.9) is a function of contact geometry only, for a

given value of wheelset lateral displacement. The effects of yaw velocity and slip on spin creepage have been neglected. For non-zero values of yaw angle ψ_w the wheelset contact geometry and kinematics become three-dimensional, with the longitudinal displacements of the contact points probably being the most important three-dimensional effect. These effects have not been included in the present analysis.

Vertical and Roll Accelerations

The normal forces at the wheel/rail contact points depend on the vertical and roll velocities and accelerations of the wheelset. These quantities are found readily through application of the chain rule, which relates them to the wheelset lateral velocity and acceleration. For roll,

$$\dot{\Phi}_w = \frac{\partial \Phi_w}{\partial Y_w} \dot{Y}_w \tag{3.10}$$

$$\ddot{\Phi}_w = \frac{\partial \Phi_w}{\partial Y_w} \ddot{Y}_w + \frac{\partial^2 \Phi_w}{\partial Y_w^2} \dot{Y}_w^2 \tag{3.11}$$

Similar expressions hold for vertical displacement Z_w.

The first partial derivatives are given by Equations (3.4) and (3.5). Both the first and second derivatives are functions of contact geometry only, and may be pre-computed and stored as functions of wheelset lateral displacement.

3.1.3 Creep Forces Derived from Kalker Theory

Geometry of Contact Zone: The Kalker Simplified Theory of rolling contact is used to model the creepage forces at the wheel/rail interface. It is based on the Hertzian contact assumption [14], which expresses the contact zone shape and dimension in terms of the local geometry constraints of the wheel and rail. The contact ellipse semi-axes a_i and b_i are given by:

$$a_i = a(\theta_i)\sqrt[3]{\frac{F_{3,i}\rho_i}{n}} \qquad b_i = b(\theta_i)\sqrt[3]{\frac{F_{3,i}\rho_i}{n}}$$

where

$$\rho_i = \frac{4}{\frac{1}{R_{1,i}} + \frac{1}{R'_{2,i}} + \frac{1}{R'_{1,i}}} \qquad n = \frac{4E}{3(1-\epsilon^2)}$$

$$\cos\theta_i = \frac{B_i}{A_i} \qquad A_i = \frac{2}{\rho_i} \tag{3.12}$$

$$B_i = \frac{1}{2}\sqrt{(\frac{1}{R_{1,i}} - \frac{1}{R'_{1,i}})^2 + (\frac{1}{R'_{2,i}})^2 - 2(\frac{1}{R_{1,i}} - \frac{1}{R'_{1,i}})\frac{1}{R'_{2,i}}\cos 2\delta}$$

$$\delta = 90^\circ - \psi_w$$

Normalization of Creepages

Given the contact zone shape and dimension, and the associated creepages and spin, Kalker forms the non-dimensional creep parameters:

$$\xi_i = \gamma_{1,i}\frac{\rho_i}{\mu c_i} \tag{3.13}$$

$$\eta_i = \gamma_{2,i}\frac{\rho_i}{\mu c_i} \tag{3.14}$$

$$\chi_i = \omega_{3,i}\frac{\rho_i}{\mu} \tag{3.15}$$

where μ is the friction coefficient and $c_i = \sqrt{a_i b_i}$ (the geometrical mean of the contact ellipse semi-axes).

For any combination of a/b ratio and spin parameter χ, Kalker's Simplified Theory predicts the non-dimensional longitudinal and lateral creep forces $f_{1,i}$ and $f_{2,i}$. The dimensional creep forces applied by the rails on the rolling wheel along the contact zone system axes are:

$$F_{1,i} = -f_{1,i}\mu F_{3,i} \qquad F_{2,i} = -f_{2,i}\mu F_{3,i} \tag{3.16}$$

In addition to these forces, a pure moment is transmitted, but of negligible magnitude.

The angular velocity of the wheelset (moving forward) will produce positive spin on the left contact zone, and negative on the right. To account for negative spin, the following relationships are used, based on arguments of symmetry [14],

$$f_1(\xi,\eta,\chi)=-f_1(-\xi,\eta,\chi)=+f_1(\xi,-\eta,-\chi)=-f_1(-\xi,-\eta,-\chi) \tag{3.17}$$

$$f_2(\xi,\eta,\chi)=+f_2(-\xi,\eta,\chi)=-f_2(\xi,-\eta,-\chi)=-f_2(-\xi,-\eta,-\chi)$$

3.1.4 ANALYSIS OF WHEELSET DYNAMICS

Wheelset Equations of Motion

The following assumptions are employed in deriving the wheelset equations of motion. Roll and yaw angles are assumed to be small. Gravity and suspension forces are applied to the wheelset along the XYZ rail coordinates axes. The longitudinal and lateral axes of the contact ellipse are assumed to coincide with the X axis and the YZ plane, respectively. The equations of motion are derived using methods from [15] by Newtonian methods using Euler Angles for calculation of the gyroscopic terms.

The translational equations of motion are derived in the XYZ rail coordinate system (see Figure 3.3). Forces and moments transmitted to the wheelset from the truck frame through the primary suspension are represented by vectors $\bar{F}_s$ and $\bar{M}_s$, respectively.

In the Y-direction (lateral):

$$m_w\ddot{Y}_w = \sum_i F_{3,i}(\mu f_{2,i}\cos\alpha_i+\sin\alpha_i) + F_{SY} \tag{3.18}$$

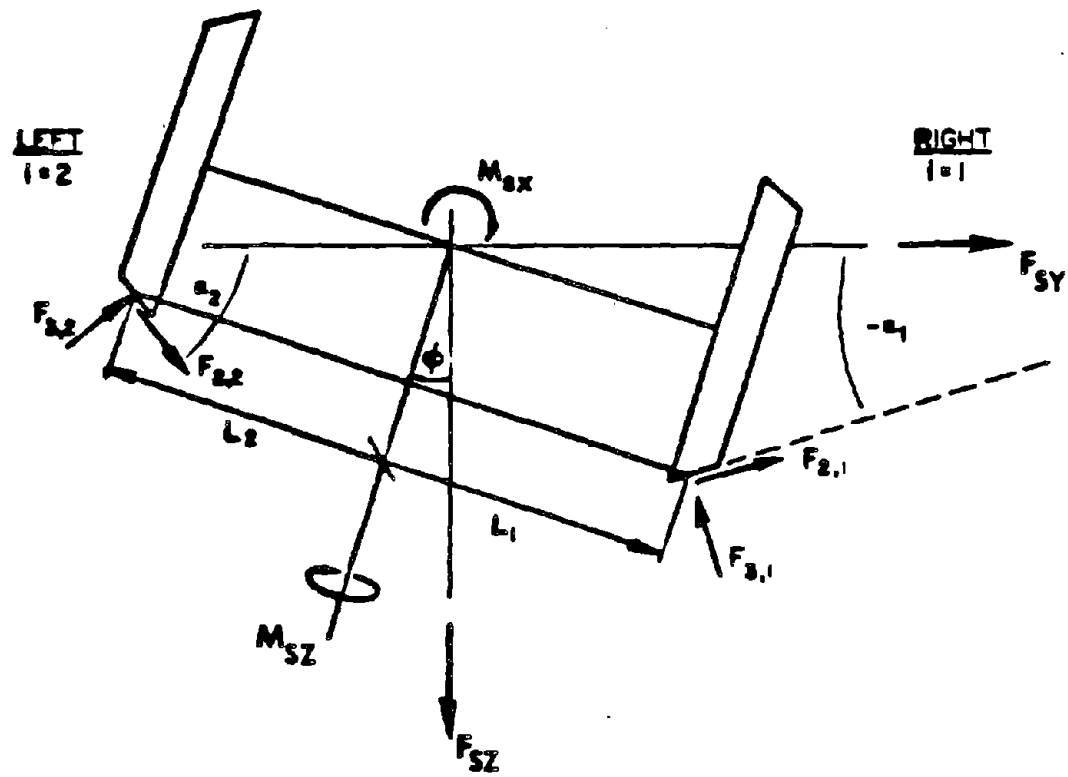

Figure 3.3 - External Forces and Moments Applied to the Wheelset

In the Z-direction (vertical):

$$m_w \ddot{Z}_w = \sum_i F_{3,i}(\mu f_{2,i} \sin\alpha_i - \cos\alpha_i) + F_{SZ} \tag{3.19}$$

The rotational equations of motion are derived in the rotating xyz system.

About the x axis (roll):

$$\sum_i F_{3,i}[(-1)^i(\cos\alpha_i - \mu f_{2,i}\sin\alpha_i)L_i - (\sin\alpha_i + \mu f_{2,i}\cos\alpha_i)r_{v,i}] + M_{sx} = \tag{3.20}$$

$$I_{xx}\ddot{\Phi}_w + (I_{zz} - I_{yy})\dot{\psi}^2_w \Phi_w + I_{yy}\Omega\dot{\psi}_w$$

About the y axis (pitch):

$$\mu \sum_i f_{1,i} F_{3,i} r_{v,i} = -I_{yy}\dot{\Omega} + I_{yy}(\bar{\dot{\psi}}_w \Phi_w + \dot{\psi}_w \dot{\Phi}_w) + \tag{3.21}$$

$$(I_{xx} - I_{zz})\,\dot{\Phi}_w \dot{\psi}_w - M_{sy}$$

About the z axis (yaw):

$$\mu \sum_i (-1)^i f_{1,i} F_{3,i} L_i = I_{zz}\ddot{\psi}_w + \dot{\psi}_w \dot{\Phi}_w \Phi_w (I_{yy} - I_{xx} - I_{zz}) - \tag{3.22}$$

$$\Omega \dot{\Phi}_w I_{yy} - M_{sz}$$

Application of the Geometrical Constraints

The geometrical constraints of the single point, continuous contact assumption can be used to express the normal forces at the contact zone by solving Equations (3.19) and (3.20).

Denote:

$$A = m_w \ddot{Z}_w - F_{SZ} \tag{3.23}$$

$$B = I_{xx}\ddot{\Phi}_w + (I_{zz}-I_{yy})\dot{\psi}_w^2\Phi_w + I_{yy}\Omega\dot{\psi}_w - M_{sx} \tag{3.24}$$

$$F_{3,1} = \frac{L_2A+B+\bar{r}(F_{SY}-m_w\ddot{Y}_w)}{(L_1+L_2)(\cos\alpha_1-\mu f_{2,1}\sin\alpha_1)} \tag{3.25}$$

$$F_{3,2} = \frac{}{(L_1+L_2)(\cos\alpha_2-\mu f_{2,2}\sin\alpha_2)} \tag{3.26}$$

where $\bar{r} = (r_{v,1}+r_{v,2})/2$

Coupling to Truck Frame

Loads from the truck frame are transmitted to the wheelset through the primary suspension (Figure 3.4). To obtain reasonable results for computed normal forces, the truck frame lateral displacement must be included in the simulation model. In this study, the truck yaw and roll angles and vertical displacement are treated as fixed, but these variables are included in the equations below for generality and ease of extension to future complete truck models.

For a passenger car, the primary suspension is linear so that

$$\begin{aligned} F_{SY} &= K_y(Y_t-Y_w) + B_y(\dot{Y}_t-\dot{Y}_w) \\ F_{SZ} &= K_z(Z_t-Z_w) + B_z(\dot{Z}_t-\dot{Z}_w) \\ M_{sz} &= K_\psi(\psi_t-\psi_w) + B_\psi(\dot{\psi}_t-\dot{\psi}_w) \\ M_{sx} &= K_\phi(\Phi_t-\Phi_w) + B_\phi(\dot{\Phi}_t-\dot{\Phi}_w) \end{aligned} \tag{3.27}$$

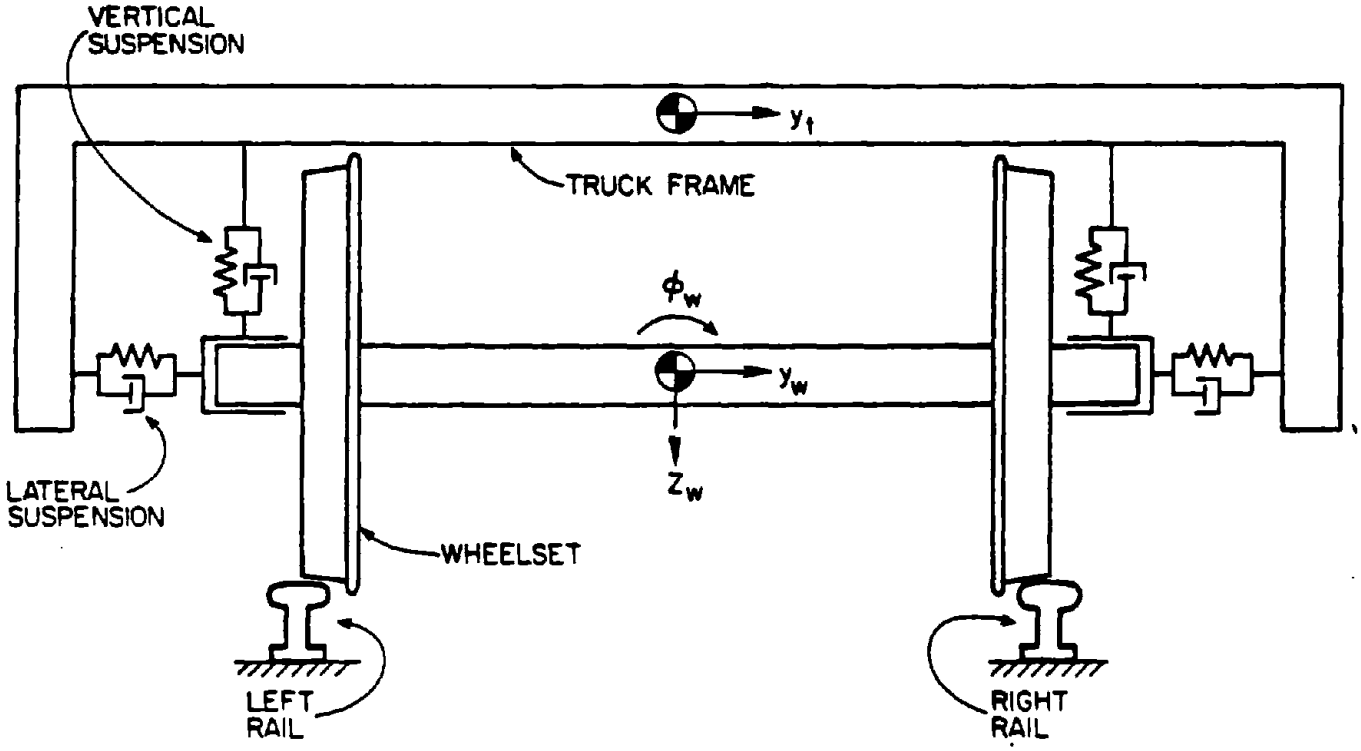

Figure 3.4 - Model used for single wheelset, primary suspension, and truck frame motion.

For fixed truck roll, yaw, and vertical displacements, the suspension forces reduce to:

$$\begin{aligned} F_{sz} &= -K_z Z_w - B_z \dot{Z}_w + F_{zo} \\ M_{sz} &= -K_\psi \psi_w - B_\psi \dot{\psi}_w + M_{zzo} \\ M_{sx} &= -K_\phi \Phi_w - B_\phi \dot{\Phi}_w + M_{xxo} \end{aligned} \tag{3.28}$$

where F_{zo}, M_{zzo}, and M_{xxo} are the steady axle load, steering moment, and roll moment, respectively.

Coupling between wheelset and truck dynamic motions is represented by the following equation for truck lateral displacement:

$$m_t \ddot{Y}_t = - F_{sy} + F_{yo} \tag{3.29}$$

where F_{yo} is an external force applied to the truck frame via the secondary suspension. For freight trucks the primary suspension is not linear. Equations (3.27) and (3.28) may be modified readily for this case.

Moments about the y-axis are produced by drag, traction, and braking forces. In this study these moments are set to zero, but for general safety assessments they should be considered, as pointed out by Gilchrist [5].

3.2 NUMERICAL SIMULATION METHOD

3.2.1 Program Description

The computer program that simulates the dynamic model is named WHSET. Figure 3.5 shows a flow chart for the computational model. WHSET and its associated subroutines compute the lateral, yaw, and axle rotational motions of a wheelset and the lateral displacement of a truck traveling at a constant forward speed on a track with or without irregularities. These motions are computed as functions of initial conditions and external excitations. The

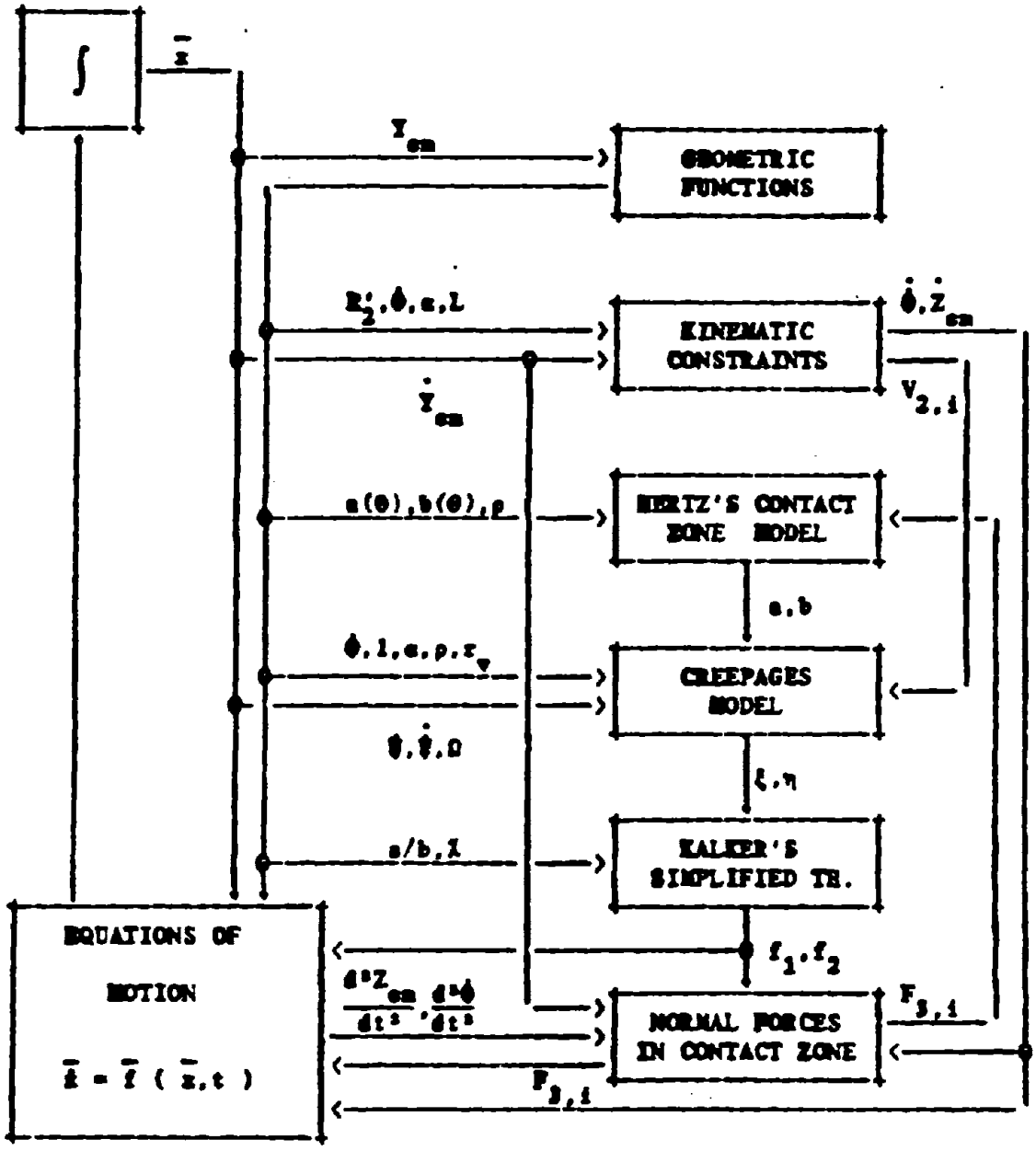

Figure 3.5 - Block Diagram of Dynamic Wheelclimb Computer Simulation Program (WHSET).

main program calls a number of subroutines that evaluate the first derivatives of a set of simultaneous nonlinear state equations, and then integrates them numerically. The program is written in FORTRAN (IBM extension to FORTRAN ANS), and is compatible with the IBM G and H compilers (see Appendix D for listing).

The numerical integration is performed using DERK, a program based on the sixth-order Runge Kutta method, which is included in the IBM library of scientific programs [16]. DERK finds approximations to the solution of a system of first-order ordinary differential equations of the form $\underline{x}'=f(\underline{x},t)$ with initial conditions.

The derivatives of the state variables depend on the contact geometry parameters (which are functions of the wheelset lateral displacement), the creep forces (which are functions of the wheelset velocities, the contact geometry and the normal forces), the wheel/rail contact normal forces, and the externally applied loads. To reduce computation time, the contact geometry functions and creep force/creepage relationships are pre-computed and stored as data files for use by WHSET. These data files are generated by computer programs previously developed under DOT sponsorship, known as WHRAILA and FORCES, and are widely available to researchers in the rail vehicle dynamics area.

Contact Geometry Functions

The program WHRAILA, developed by R. Heller and N. Cooperrider [17], solves for the following contact geometry parameters as functions of the wheelset lateral position: the wheel/rail contact angles α, the wheelset roll angle Φ_w, the wheelset c.m.* vertical displacement Z_w, the rolling radii of each wheel r_v, the distance between the wheelset c.m. and the contact points of the wheels L, and the lateral radii of curvature of the rails R_2'. WHRAILA

* In this study the wheelset center of mass (c.m.) is defined as the geometric center of the axle.

has been supplemented by additional routines which calculate the values of the elliptic integrals $a(\theta)$ and $b(\theta)$, the non-dimensional spin parameter χ, the geometric parameter ρ, the contact ellipse axes ratio a/b, and the partial derivatives defined in Equations (3.4) and (3.5) WHRAILA accepts as inputs specific wheel and rail profiles, gauge, flange clearance, cant angles and rail heights. The numerical results presented here are for new Association of American Railroads (AAR) profile wheels running on rails similar to 132 lb RE, CF and I unworn profile. The program assumes that single point contact is sustained on both wheels and that yaw angle effects may be neglected. Since these functions depend on lateral displacement alone, they do not have to be computed at each time step using WHRAILA. Instead, the values pre-computed at intervals of 0.51 mm are used as inputs to an interpolation routine. The program WHSET uses the IBM library program IVP, based on the Aiken's Lagrange method of interpolation [16].

Creep Force Calculation

The second data file represents the relationships between non-dimensional creep forces (f_1 and f_2) and non-dimensional creepages. The program FORCES [18] is used to pre-compute non-dimensional creep forces using the Kalker Simplified Theory. It takes as input the contact ellipse dimensions, non-dimensional spin and creep parameters, and Poisson's ratio. For every contact ellipse ratio a/b and non-dimensional spin parameter χ, a different table is generated for the creep coefficients as functions of the non-dimensional creep parameters in polar form.

The contact ellipse ratio and the non-dimensional spin parameter are determined by the contact geometry alone, the latter depending on the lateral displacement of the wheelset. Consequently, these two variables can be pre-computed for the full range of the lateral motion. A survey of numerical results

over the displacement range has been conducted, and 21 pairs have been distinguished so that the contact ellipse ratio and the non-dimensional spin parameter at any given displacement are within 10% tolerance of at least one of these 21 pairs. The program FORCES was run repeatedly for these pairs resulting in 21 table sets stored as data files.

At each lateral displacement, WHSET calls a subroutine to determine which of the 21 data files is to be used. It then interpolates the data in tables of this file, returning the lateral and longitudinal creep forces as functions of the creepages.

Program Outputs

The following output variables are generated by the simulation program:

1. Wheelset lateral displacement
2. Truck lateral displacement
3. Wheelset axle rolling velocity
4. Wheelset yaw angle
5. Normal force at each contact point
6. Derailment quotient for each wheel

The derailment quotient, the ratio of lateral to vertical wheel/rail forces, is the most frequently used measure of proneness to derailment [5-10,19]. In the literature it is designated by either (L/V) or (Q/P). Following the former convention:

$$\left(\frac{L}{V}\right)_i = \frac{\mu f_{2,i}\cos\alpha_i + \sin\alpha_i}{\mu f_{2,i}\sin\alpha_i - \cos\alpha_i} \tag{3.30}$$

3.3 SIMULATION RESULTS

3.3.1 Definition of Simulation Conditions

The parametric values for the simulation are selected for a typical high speed passenger car described in [20], and are summarized in Table 3.1.

TABLE 3.1

Simulation Parameters

Symbol	Value	Symbol	Value
m_w	1464 kg	K_z	2×10^6 n/m
m_t	2928 kg	K_ϕ	7.4×10^3 n-m/rad
I_{xx}, I_{zz}	680 kg-m^2	K_y	1.17×10^7 n/m
I_{yy}	136 kg-m^2	B_z	4×10^4 n-s/m
μ	0.3	B_y	5.84×10^4 n-s/m
ϵ	0.3	B_ϕ	1.5×10^2 n-m-s/rad
E	2×10^{11} n/m^2	K_ψ	5.43×10^4 n-m/rad
F_{ZO}	1.36×10^5 n	B_ψ	2.17×10^2 n-m-s/rad
ψ_t	0	M_{xxo}, M_{zzo}	0
V	50 m/s		

All other values for parameters in the equations of motion are provided by programs WHRAILA and FORCES, with extensions as described previously.

Some comments are needed regarding inclusion of the truck lateral degree of freedom. In many previous studies, and in the initial phases of this investigation, the dynamics of the wheelset alone were simulated. The dynamic fluctuations in normal force during derailment simulations that result from "wheelset-only" models are unrealistically large, due to high wheelset

accelerations. Adding the truck mass to the model yields much more natural behavior. Although the dynamics of a complete truck with secondary suspension, two axles, etc. are not modeled here, the present simulations do exhibit the important characteristics of wheelsets during derailment.

The simulation program accepts as inputs any combination of forces and moments applied to the truck frame and wheelset, plus track irregularities. For clarity in presentation, in the simulation results that follow the only input is lateral force applied to the truck frame.

3.3.2 Simulation Results

Representative simulation results are shown in Figures 3.6 and 3.7. Starting with the wheelset and truck frame in the track center position, the lateral force applied to the truck frame produces a damped sinusoidal truck lateral displacement. The wheelset lateral displacement lags, sharply decelerating after the initial flange contact.

In the derailment case, the wheelset first climbs the rail, falls slightly, then climbs again to complete derailment as the truck frame displacement reaches its second peak. Depending on initial conditions, the wheelset may derail on initial impact or later, emphasizing the importance of the dynamic coupling between wheelset and truck frame. Even though the derailment quotient exceeded the quasisteady limit (2.0 for ψ_w=0) for about 0.05 seconds (the JNR limit), the wheelset does not derail at this point.

After flange contact occurs, the axle speed drops, as expected from quasisteady theory. There is no fundamental difference between the derailment and non-derailment cases.

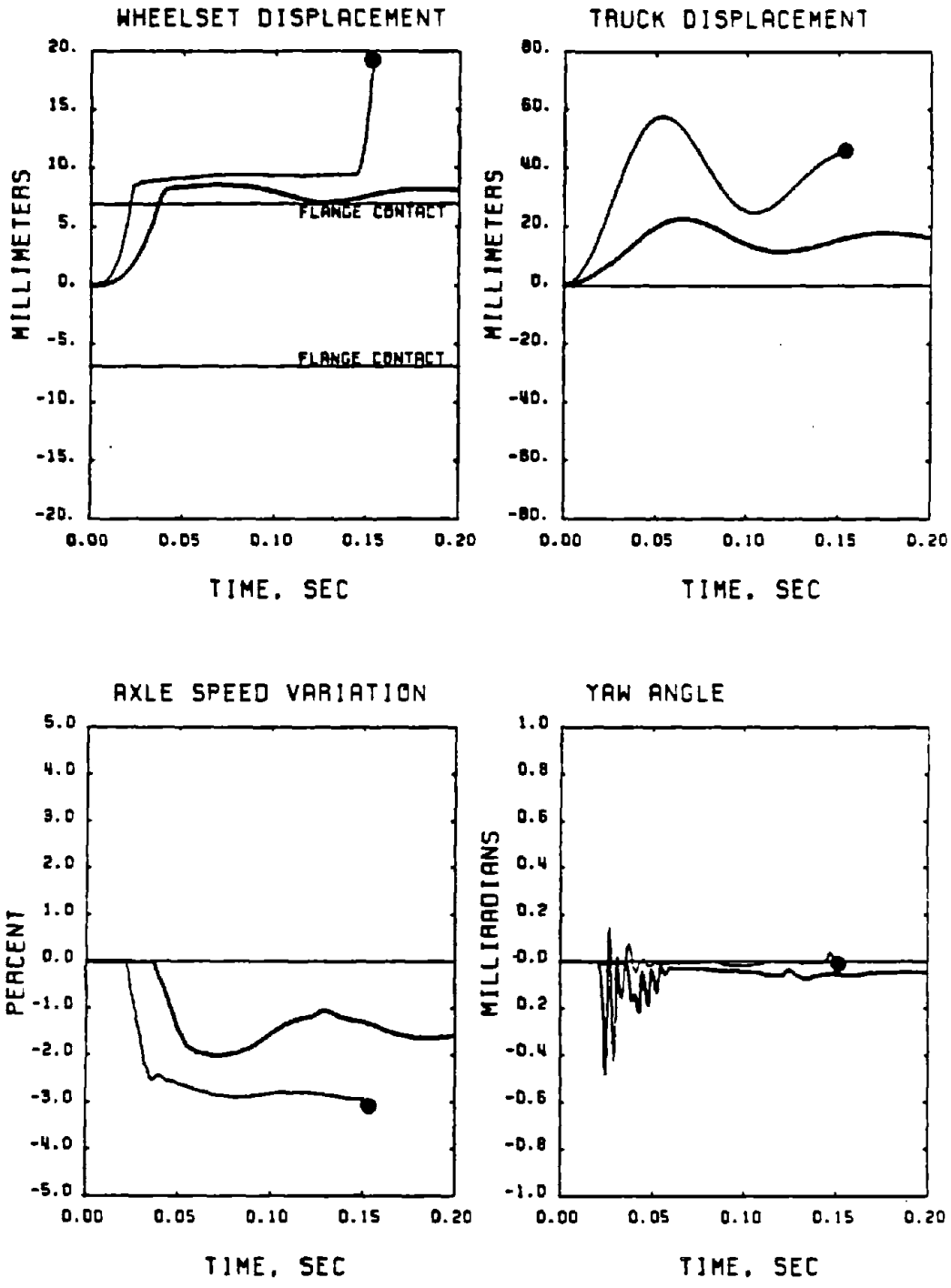

Figure 3.6 - Wheelset model simulations for non-derailing (dark line) and derailing (light line with dot) cases. Responses are to step input in lateral force applied to truck frame.

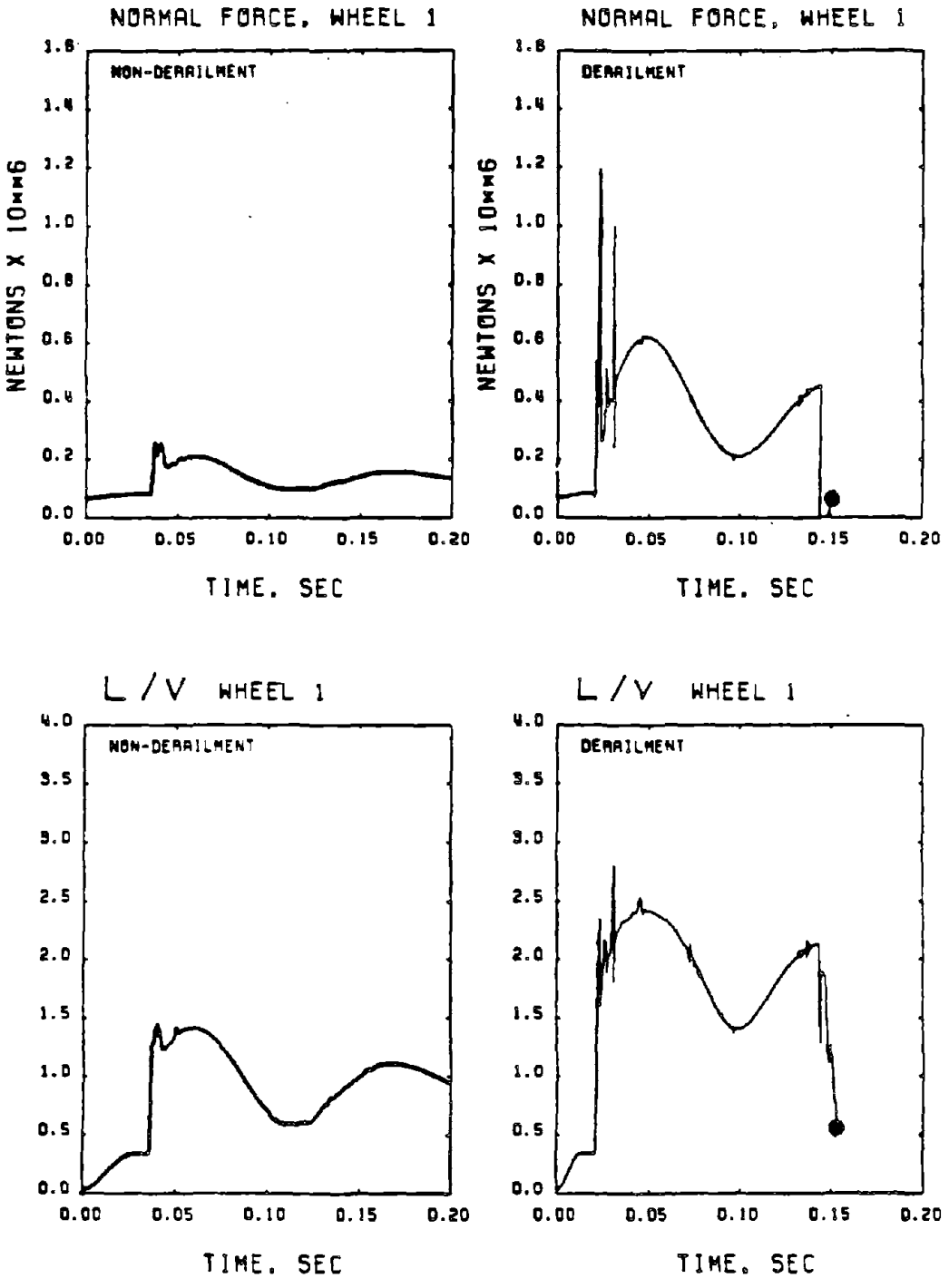

Figure 3.7 - Simulated wheel/rail normal force and derailment quotient on climbing wheel.

The drop in axle speed results in longitudinal creep forces imbalance and a yaw moment which steers the wheelset in the negative direction. Due to the rather stiff primary suspension, the magnitude of the resulting steering angles is quite small (less than 0.5 milliradians, or 0.03 deg). These small yaw angles considerably reduce the coupling between the longitudinal and lateral dynamics of the wheelset.

Figure 3.7 shows the normal force and derailment quotient for the climbing wheel. In the non-derailment case, the normal force starts at a level close to one-half the axle load. During flange contact, the normal force is much larger due to the increasing contact angle. The rapid deceleration of the wheelset results in a sharp peak in the normal force. Terms due to wheelset lateral, vertical, and roll accelerations all contribute to the increased normal force on the climbing wheel while decreasing it on the opposite wheel. The initial peak in normal force is also seen in the L/V response.

In the derailment case, the peaks in normal force and derailment quotient are much larger. These peaks may be unrealistically large, due to the assumption of rigid rails. They are not critical to the simulation, however, due to their extremely short duration. Peaks shown after initial flange contact are due to large values of partial derivative terms in Equations (3.10) and (3.11).

Just prior to derailment, the normal force goes to zero for a short time. Physically, the wheel is beginning to lose contact while the contact angles decreases. The large fluctuations in normal force and loss of contact prior to derailment have been confirmed experimentally in tests at JNR [10].

3.3.3 Discussion of Modeling Effects

The computer program was altered to study the effect of model complexity on the simulation results. The first simplification was to set the axle speed to V/r_o. Exclusion of this degree of freedom was found to have almost no effect on the simulation of the other dynamic variables as a result of the stiff suspension and the negligible steering effects. As a consequence, the value of the truck yaw angle ψ is very important to derailment safety, since the derailment limit falls from 2.0 to 0.8 as ψ_w increases from 0 to 50 milliradians. This result, predicted from quasisteady derailment theory, is verified by the dynamic simulation model. Passenger trucks with softer yaw suspensions and freight trucks may exhibit different behavior.

The acceleration terms in Equations (3.11) through (3.26) are significant in terms of their effects on wheelset motion, derailment quotient, and derailment proneness. In contrast, gyroscopic terms are not significant and may be omitted.

The simulation model presented in this report represents a successful extension of contemporary understanding on wheel/rail contact phenomena and wheelset dynamics to the wheelclimb derailment regime. Through the use of this detailed model, it has been determined that the following elements are necessary for simulation of wheelclimb derailment of a typical high speed passenger car with a stiff yaw suspension:

1. Wheelset and truck lateral displacement degrees of freedom.
2. Wheel/rail contact geometry parameters determined as functions of wheel and rail profiles.
3. Creep forces determined by Kalker Simplified Theory.

4. Wheel/rail normal forces computed from kinematic constraints resulting from continuous two-wheel, single-point contact, including acceleration effects.
5. Creepages determined by wheelset kinematics.
6. Truck yaw angle.

For freight trucks or passenger trucks with soft primary suspensions, wheelset yaw angle and axle rotational speed should be included as additional degrees of freedom. Gyroscopic terms are not critical to wheelclimb simulation.

The reduction in necessary degrees of freedom associated with stiff yaw suspension trucks results in significant reductions in computation time, which will be particularly important in multiple axle, complete vehicle simulations.

3.4 Experimental Validation and Usefulness of Model

3.4.1 Results of Phase One Experiments

To validate the theoretical analysis and simulation model, a series of experiments on dynamic wheelclimb was conducted during Phase One of this research program. The apparatus used is described in Appendix B, being identical to that used for study of quasisteady wheelclimb. Forces acting on the wheelset were measured with the six-component strain gauge balance, so that only axle L/V ratios could be measured. The only addition to the apparatus used in the quasisteady wheelclimb tests was a photocell actuated, pneumatic servo to apply step or pulse inputs in lateral load to the wheelset at designated locations along the track.

To simulate the mechanics of the wheelset test apparatus, it was necessary to modify the equations of motion derived in Section 3.1. These changes were required to properly represent the kinematics and dynamics of the rigid body elements that comprise the gimbel and linkage system described in Appendix B. Since the modified equations apply only to this unique apparatus and are not of general interest, they are not included in this report (for details, refer to [15]).

Representative simulated and measured responses for non-derailing and derailing cases are shown in Figures 3.8 and 3.9. The simulations include the dynamics of the pneumatic actuator used to apply the lateral force, which acts as a first-order lag with a time constant of 125 ms. The agreement between predicted and measured lateral displacements for non-derailing and derailing cases is good, although for the latter case the predicted derailment occurs more rapidly than that measured.

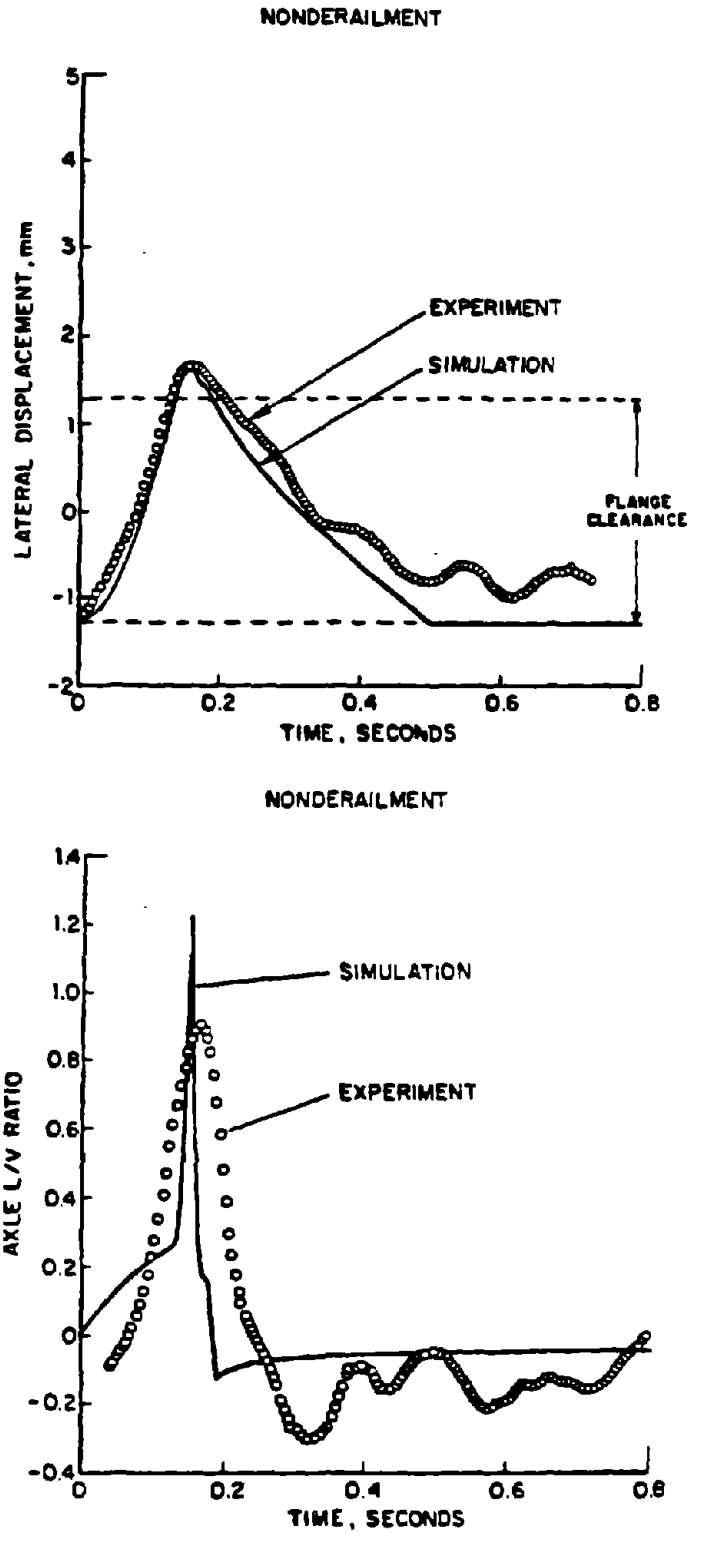

Figure 3.8 Simulated and Measured Dynamic Wheelclimb Lateral Displacement and Axle L/V Ratio Responses to Pulse Lateral Force Input (Non-derailing Case). Measurements from Phase One Experiments.

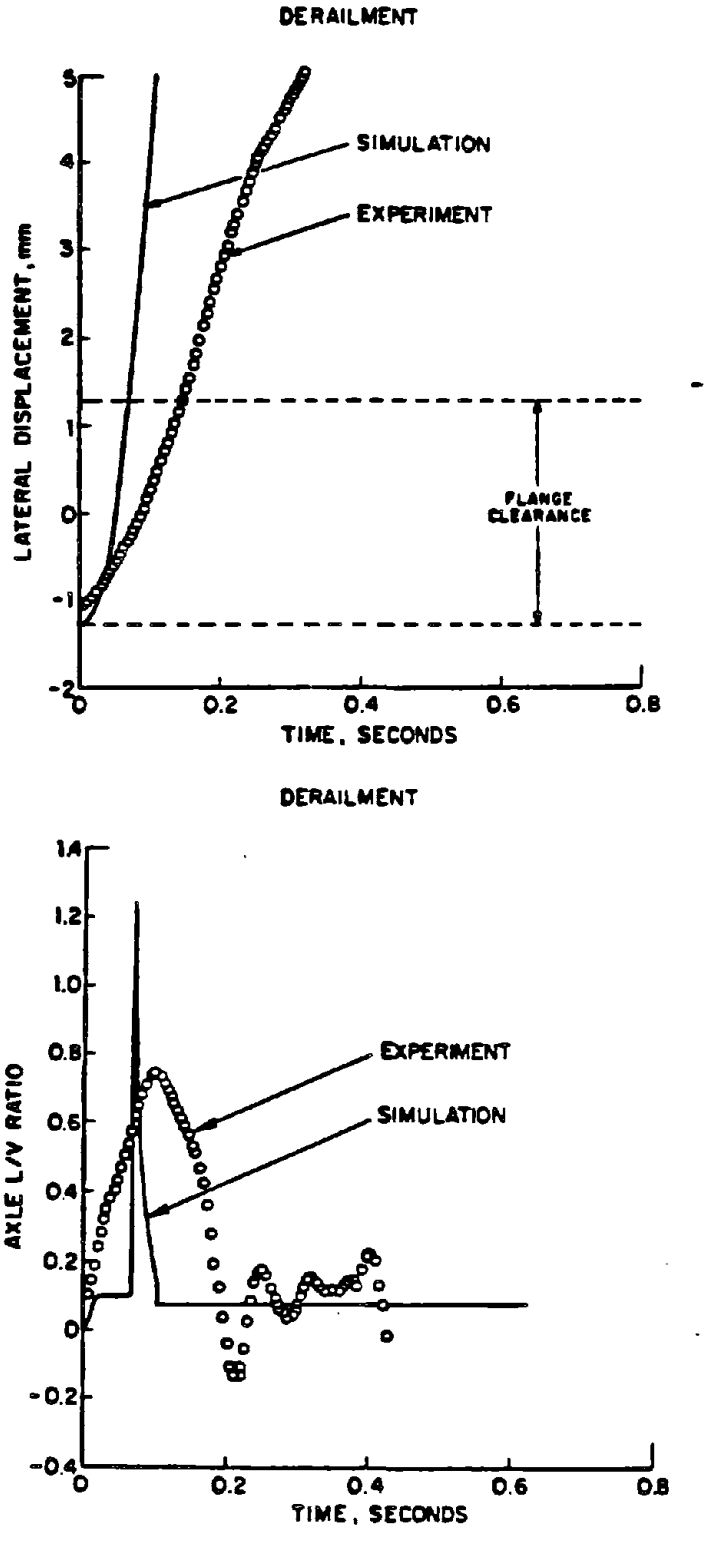

Figure 3.9 - Simulated and Measured Dynamic Wheelclimb Lateral Displacement and Axle L/V Ratio Responses to Pulse Lateral Force Input (Derailing Case). Measurements from Phase One Experiments.

Significant differences between predicted and measured time histories of the L/V ratio are evident in the figures shown. Specifically, the predicted responses characteristically exhibit higher maximum values and shorter time durations than those measured. To resolve this discrepancy, further research conducted under Phase Two of this study was directed towards refining the analytical model and improving the force measuring system used in the experiments. The results of Phase Two experiments are presented in the following section.

3.4.2 Results of Phase Two Experiments

At the onset of Phase Two, there were two principal factors considered as having the potential for influencing the measured wheel force signals:

1. The strain gauge balance signals measured in Phase One did not resolve, in an unambiguous manner, the various external and internal forces acting during the dynamic wheelclimb experiment. Under quasi-steady conditions, the external forces, in both vertical and lateral directions, approximately balance wheel/rail forces acting at the contact points. Since the strain gauge balance was mounted in series between the external and wheel/rail forces, the strain gauge balance was capable of sensing the desired variables under quasisteady conditions. Further, under quasisteady conditions, a simple functional relation exists relating axle and wheel L/V ratios, so that resolution of independent wheel ratios is not necessary. Under dynamic wheelclimb conditions, none of the above apply, so that it is desirable to have independent sensing of individual wheel loads, external forces, and inertial forces (i.e. accelerations).

2. The bandwidth of the instrumentation system used in Phase One was 25 Hz. The 25 Hz cutoff frequency was determined to be necessary to prevent aliasing of signals passed through the multiplexing circuits prior to recording on the FM tape recorder. The L/V ratio pulses predicted from the digital simulation contain significant high frequency content that would be attenuated by a 25 Hz lowpass filter.

To eliminate these limitations in the dynamic wheelclimb experiments, a new set of apparatus for force measurement was designed, fabricated, and carefully calibrated. Digital simulations were performed which passed the predicted wheel lateral and vertical force signals through lowpass filters, to determine the bandwidth necessary for recording of these signals in an unaltered state. The simulations clearly showed that the 25 Hz filter used in Phase One significantly attenuated and widened the L/V ratio pulse to qualitatively match that measured in Phase One. These simulations identified filter bandwidth as the principal cause of the Phase One discrepancy between theory and test. Further simulations showed that a cutoff frequency of 100 Hz was sufficient for recording wheel force signals without attenuation.

An instrumented wheelset was designed to measure lateral and vertical forces at each wheel/rail contact point. The ASEA/SJ configurations for lateral and vertical bridges were selected. Strain gauge locations were determined after mapping of the strain fields on the wheel plate surfaces, to maximize signal output with minimum ripple, load point sensitivity, and cross talk. External forces were measured separately with load cells, with the strain gauge balance used in Phase One installed to provide capability for Phase One/Phase Two data comparisons. Details

of the apparatus design and calibration are given in Appendix C.

Representative measurements of signals during derailment using the improved instrumentation system are presented in Figures 3.10 through 3.17. At the beginning of the test, the wheelset is positioned in tread contact near the opposite (left) rail using a special fixture. At a designated track location, a photocell senses a light, activating the lateral force actuator. The lateral force rises exponentially, as shown in Figure 3.10. The wheelset moved laterally in response to this input until it makes flange contact on the right rail, where it pauses for about 22 msec. After the wheel has climbed the rail, lateral displacement increases rapidly to complete derailment, as shown in Figure 3.11. As the wheelset approaches one rail, a strong yaw moment is produced by the longitudinal creep forces, causing a steering action in the negative direction, as shown in Figure 3.12. As demonstrated in both figures, the agreement with simulation is excellent.

Figures 3.13 through 3.15 show the forces acting at the wheel/rail interfaces. A large pulse in lateral force on the derailing wheel is produced during the period that the wheel is in flange contact (about 40 msec). This short duration is consistent with theory, and clearly shows that the long duration (order of 100 msec.) measured in Phase One resulted from the 25 Hz filters. The lateral forces measured on the non-derailing wheel result from creepage, and are consistent with a friction coefficient of 0.3. The vertical force on the derailing wheel (Figure 3.15) shows some fluctations from its nominal value of 22 N. The excursions at the flange contact point are consistent with model predictions, resulting from accelerations in the vertical direction caused by contact geometry constraints. Other fluctuations in vertical force result from track disturbances

in the vertical direction that were not included in the simulation model nor measured in the experiment.

The lateral acceleration of the wheelset is shown in Figure 3.16. The maximum deceleration is about -0.2 g, which corresponds to an inertial force of about -22 N. When compared to the lateral force measured at the derailing wheel (about 75 N. at the same time), the inertial force is significant. This indicates that measurement of wheel/rail loads at locations as close as possible to the contact points (i.e. using instrumented wheelsets) is superior to measurement at an interior point (i.e. using strain gage balance).

Finally, the predicted and measured L/V ratios are shown in Figure 3.17. The amplitude and duration of the primary and secondary peaks in the response are predicted well by the simulation. The first peak results from the large amplitude pulse in lateral force during flange contact; the second peak results from the dip in vertical force resulting from wheelset vertical acceleration.

The experiments performed in Phase Two demonstrate that the dynamic wheel-climb model presented in this report is capable of predicting both wheelset response to external force inputs and the resulting wheel/rail contact forces. This validated model should prove useful in the future in the evaluation of vehicle derailment safety and synthesis of new derailment criteria.

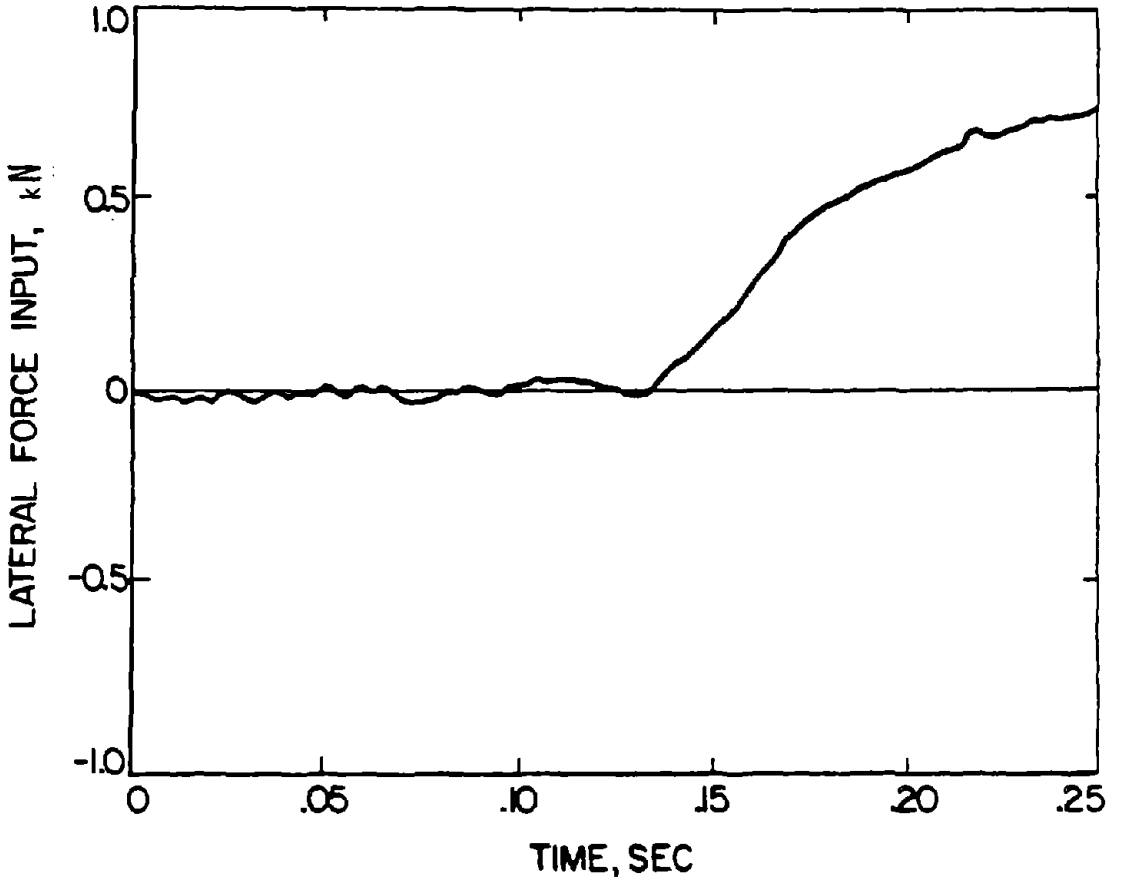

Figure 3.10 - Measured external lateral force applied to wheelset.

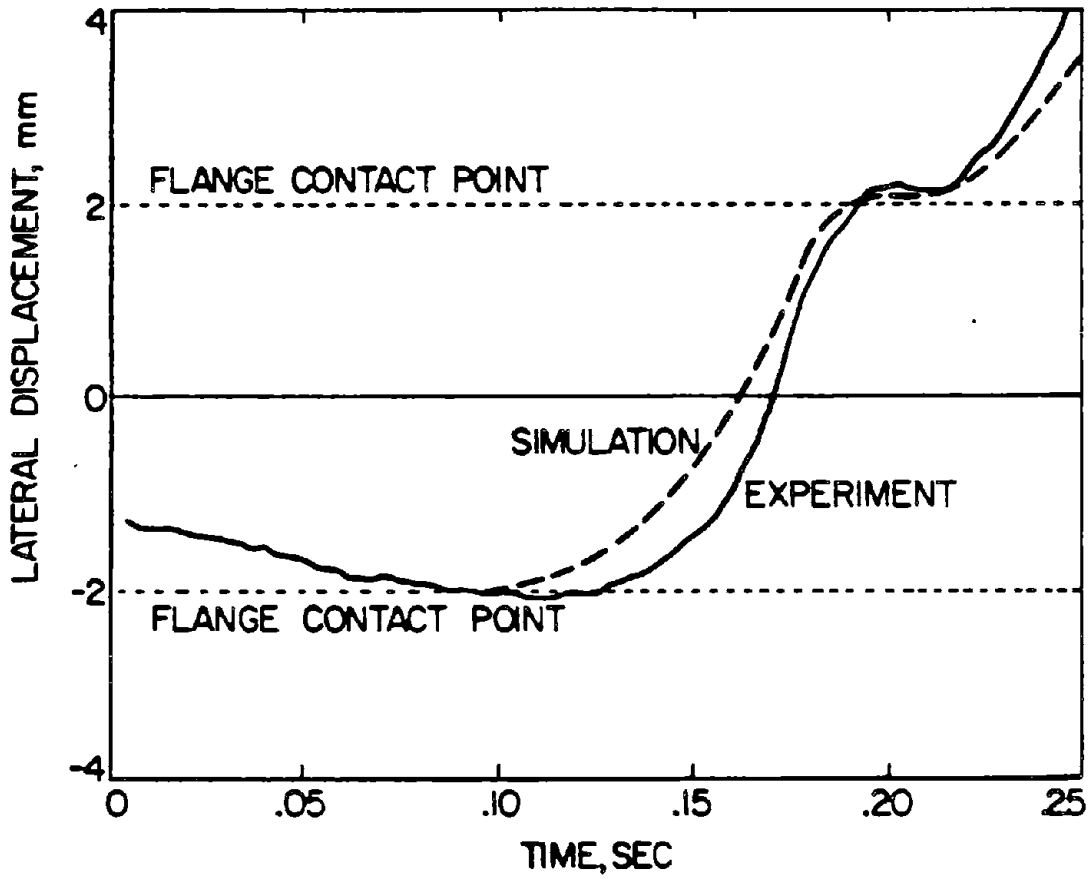

Figure 3.11 - Measured and simulated wheelset lateral displacement.

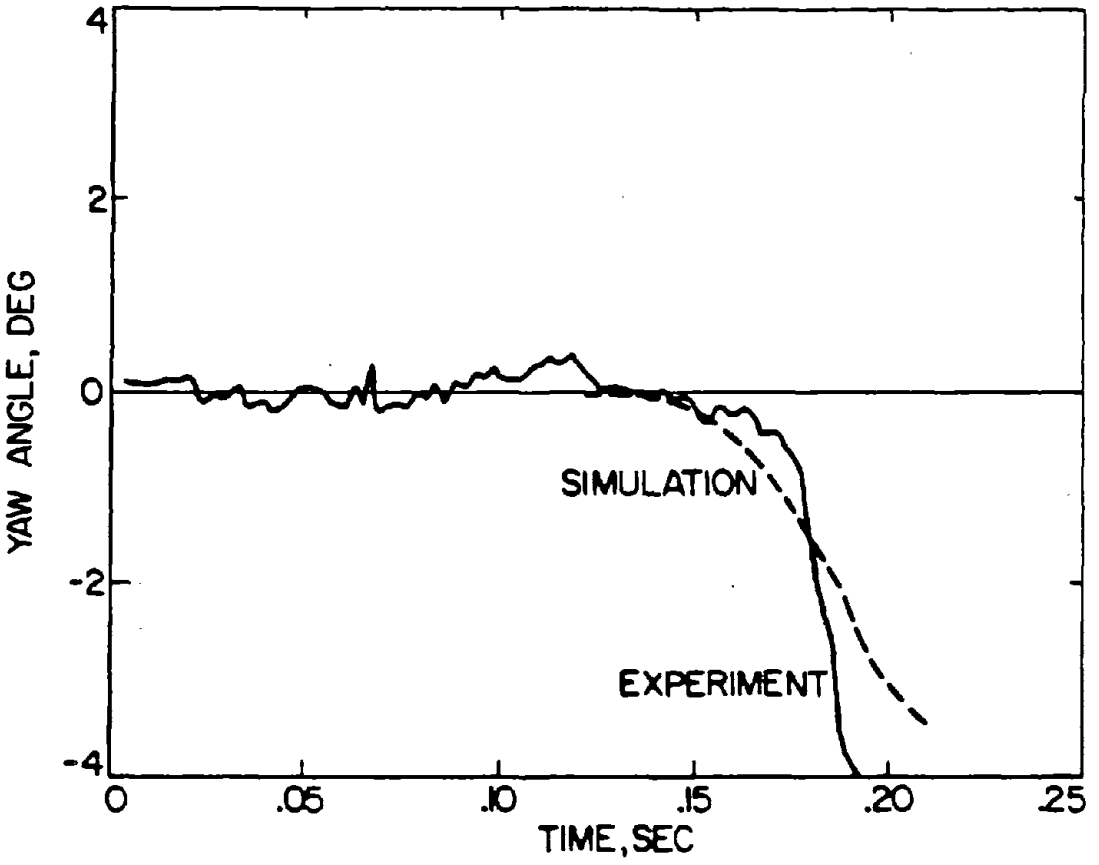

Figure 3.12 - Measured and simulated wheelset yaw angle.

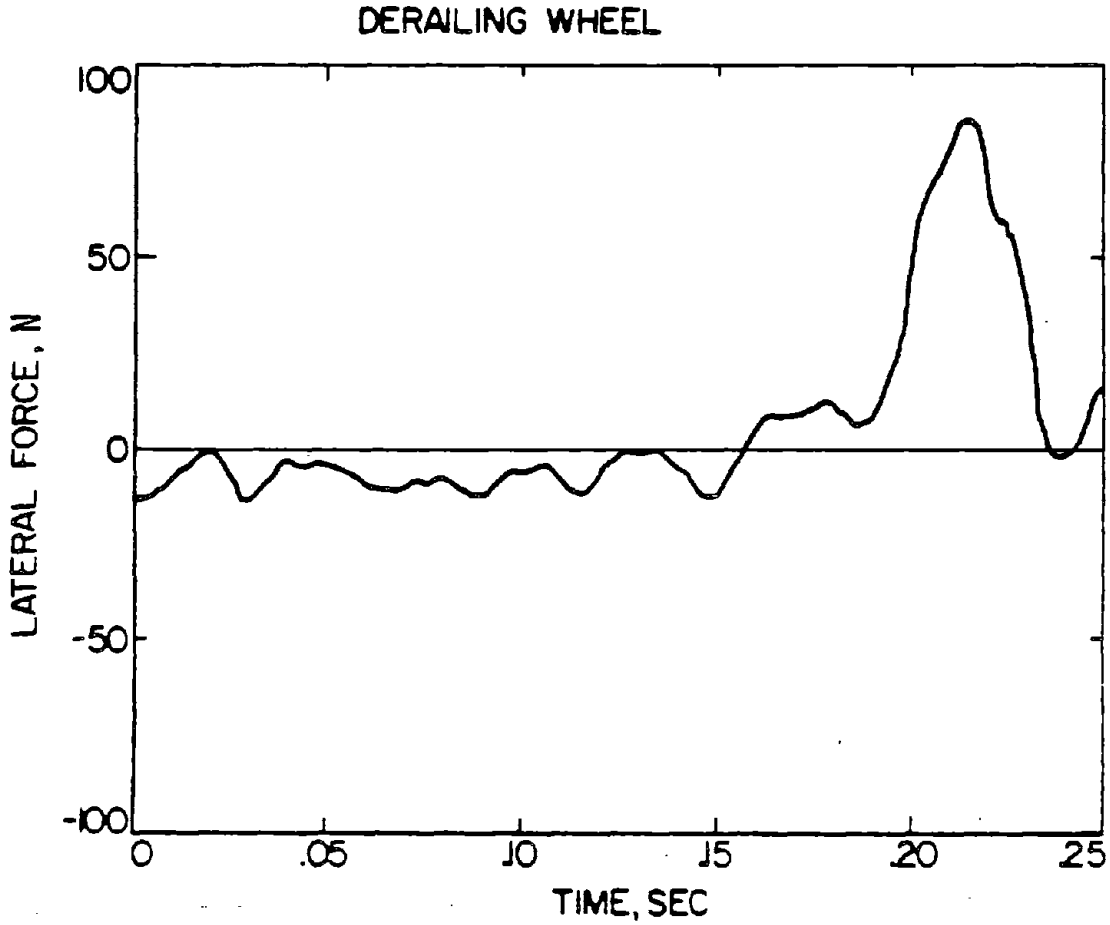

Figure 3.13 -- Measured lateral force on derailing wheel.

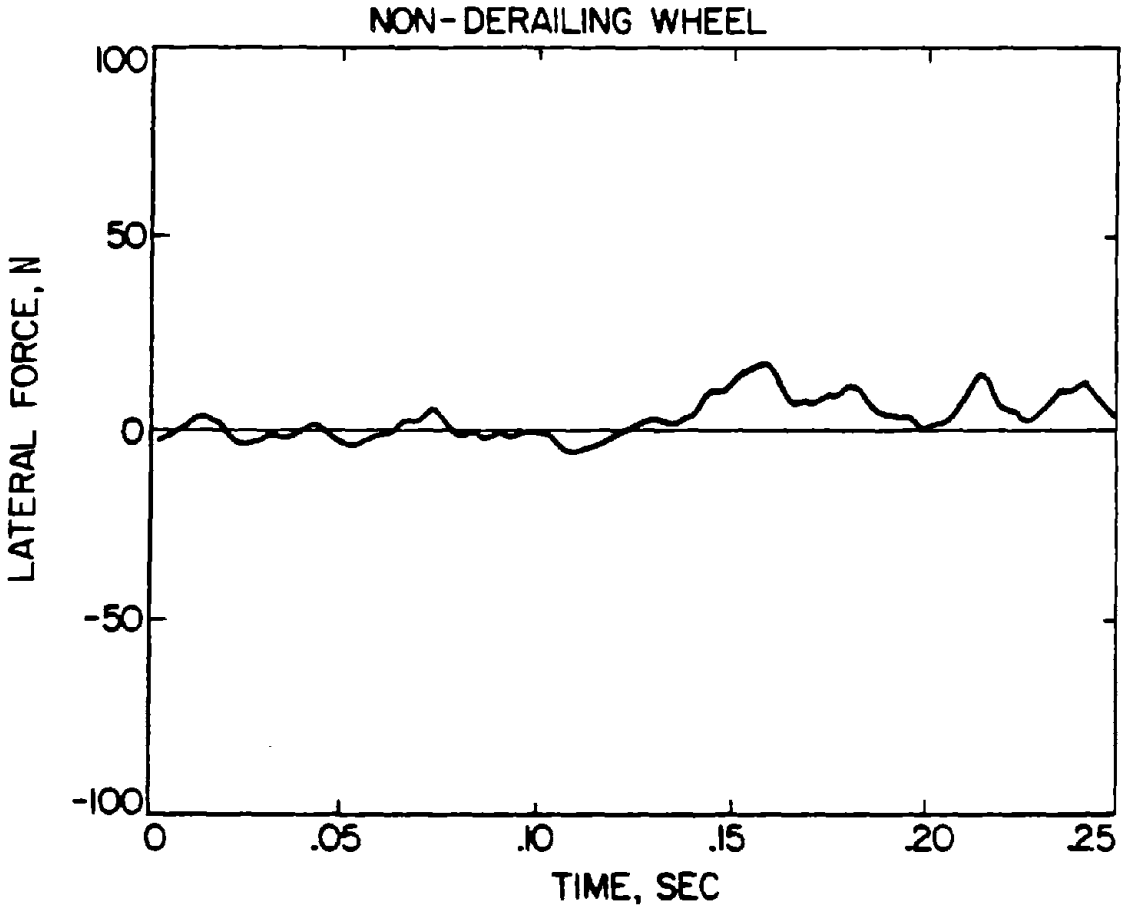

Figure 3.14 - Measured lateral force on non-derailing wheel.

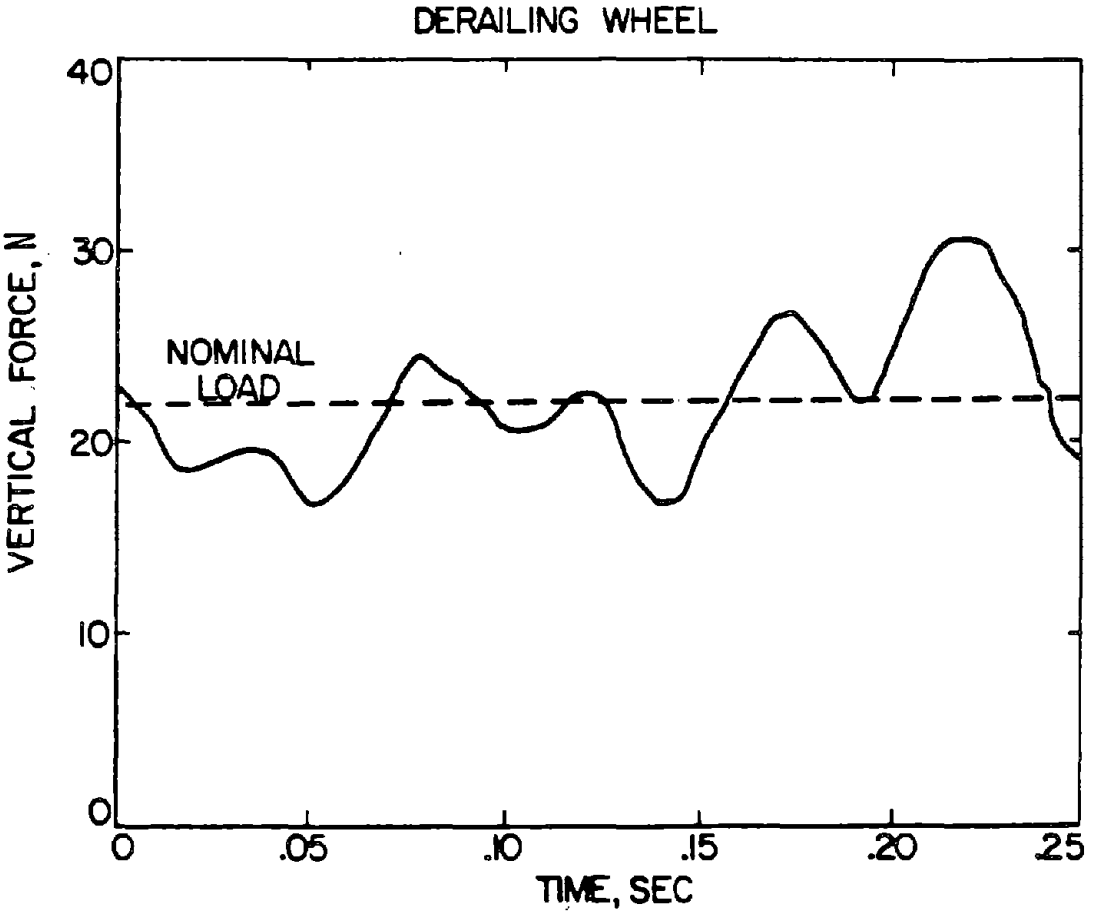

Figure 3.15 - Measured vertical force on derailing wheel.

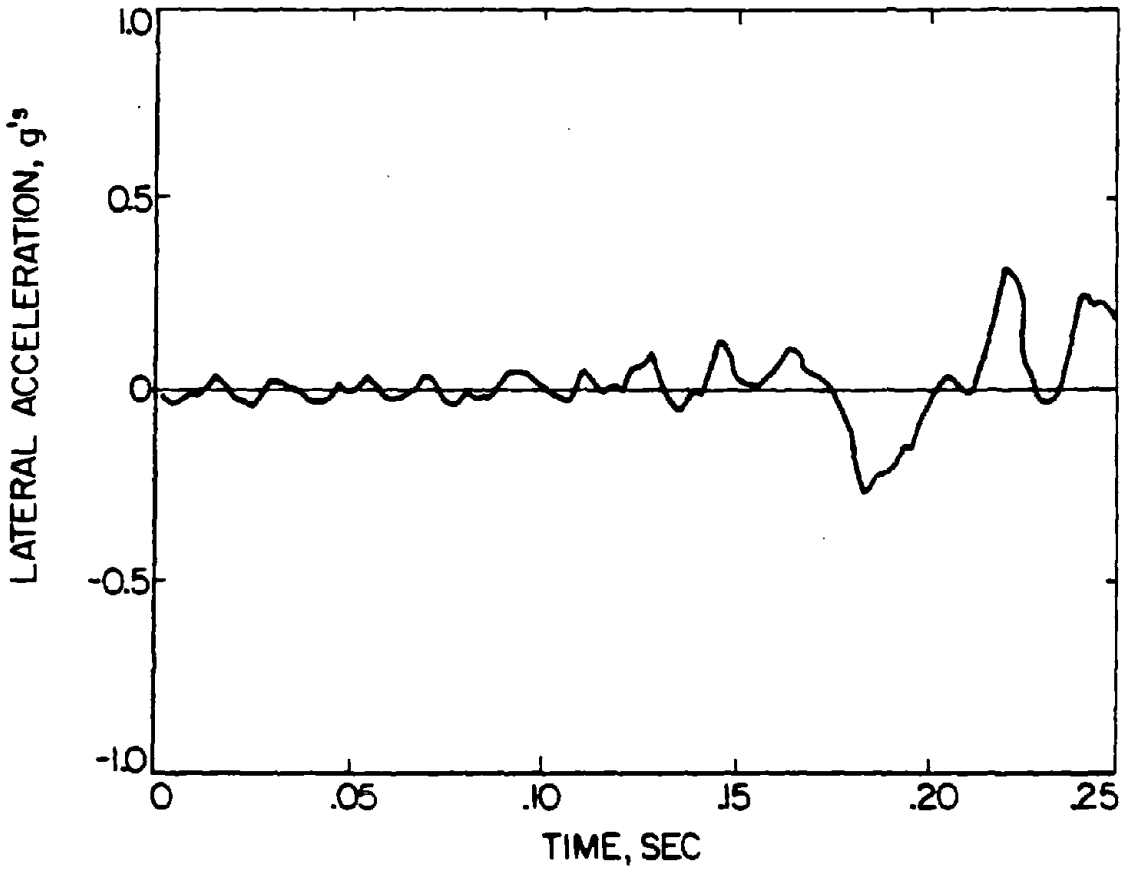

Figure 3.16 - Measured wheelset lateral acceleration.

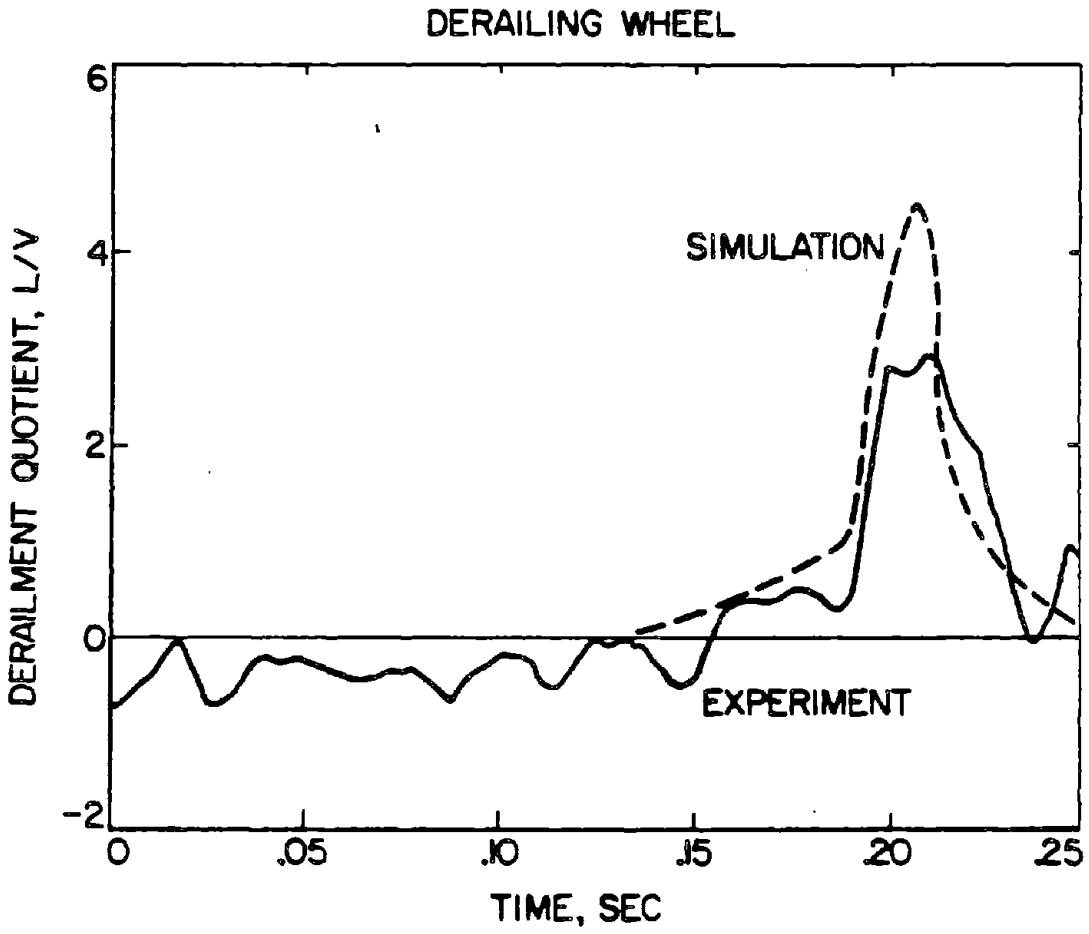

Figure 3.17 - Measured and simulated derailment quotient (L/V ratio) on derailing wheel.

4. EVALUATION OF DERAILMENT CRITERIA

4.1 Commonly Used Criteria

Although a larger set of variables are available from the experiments and simulations for use in synthesizing criteria for wheelclimb derailment, in this report attention is restricted to those criteria which make use of the time histories of wheel loads only. The objective here is to evaluate the hypothesis that sufficient information exists in the wheel load measurements alone to predict derailment safety reliably.

The basic information available in these pulselike signals may be distilled into the following quantities: peak value, integrated value, average value over pulse duration, pulse shape, duration above threshold, etc. Table 4.1 is a summary of candidate criteria which are of the general form of a load amplitude versus time duration. To test the hypothesis a wide selection of candidate criteria was explored. The widely used JNR Criterion is of Type 4 in the table; duration t_1 is defined to be 1.5 times the period during which the pulse exceeds 50% of its peak value [30].

Criteria 1 through 5 yield a single data point for each event; Criteria 6 yields a locus of points as the threshold value is swept from zero to the pulse peak. All criteria may be applied to either L/V ratios or lateral forces alone. Criteria involving peak values may lack physical significance and are vulnerable to erroneous conclusions drawn from noisy instrumentation or wheel loads resulting from high frequency vibration. Integrated lateral force has units of change in momentum, although it does not represent the time change in momentum since only the wheel/rail reaction

TABLE 4.1

CANDIDATE WHEELCLIMB DERAILMENT CRITERIA

TYPE	ORDINATE	ABSCISSA	SENSITIVITY*
1	PEAK VALUE	TIME ABOVE ZERO (TAZ)	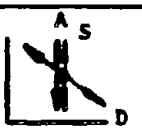
2	INTEGRATED VALUE	TAZ	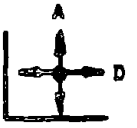
3	INTEGRATED VALUE/TAZ	TAZ	
4	PEAK VALUE	TIME WITHIN N% OF PEAK (TNP)	
5	INTEGRATED VALUE	TNP	
6	THRESHOLD VALUE	TIME PULSE EXCEEDS THRESHOLD (TAT)	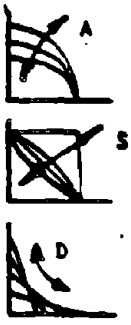

*SENSITIVITY TO PULSE AREA (A), SHAPE (S), AND DURATION ABOVE ZERO (D), EACH WITH OTHER PARAMETERS HELD CONSTANT. SHAPE VARIABLE S REPRESENTS TRANSITION THROUGH SHAPES

TO  TO  TO  TO  .

forces are being included. By dividing the integrated value by the time duration, the magnitude averaged over the pulse is obtained. Criteria 4 and 5 may be used to define pulse duration when the mean value of the signal before and after the pulse is above zero.

The sensitivity of each criterion to changes in pulse area, shape, and duration is shown in Table 4.1. In this context sensitivity refers to the ability of a criterion to discriminate between pulses on the basis of area, duration, or shape by yielding a different (x,y) value or locus in the graph. For example, if a criterion sensitive to area were found to be a good derailment predictor, then derailment could be correlated with momentum. Many additional criteria can be proposed, but they generally will perform in a manner very similar to those in Table 4.1.

4.2 Experimental Evaluation of the JNR Criterion

The recorded experimental wheel load and lateral displacement time histories were digitized and analyzed using computer subroutines which implemented the various criteria.

For Process B, 112 derailment events (occurrence of large L/V ratios or lateral displacements) were examined, distributed in the test matrix in Table 4.2. Cases were selected deliberately to be near the derailment limit, and do not reflect the distribution of their occurrence in the field. A special feature of these experiments is the large number of marginal and complete derailments, which would not generally be available from field tests.

TABLE 4.2

TEST MATRIX FOR DYNAMIC WHEELCLIMB EXPERIMENTS

TEST MATRIX

	Yaw Angle			
	3^{o}	0^{o}	-3^{o}	Total
No Derailment	10	19	1	30
Marginal Derailment	9	13	17	39
Complete Derailment	8	21	14	43
				112

Figure 4.1 illustrates the application of JNR criterion to a typical L/V ratio pulse using the algorithm shown in Figure 4.2, with the results of similar application to the events in the test matrix shown in Figure 4.3. The JNR Criterion is modified using Eqs. (2.4) and (2.5) to convert wheel L/V ratio to axle L/V ratio. It is clear from these results that not only does the JNR criterion not predict derailment, but that no criterion based solely on L/V ratio and time duration could separate the derailment, marginal derailment, and nonderailment regions. The data in Figure 4.3 includes measurements at all yaw angles; from the quasisteady derailment results strong influence of yaw angle could be expected by rescaling the data and JNR Criterion by the quasisteady limits shown in Figure 4.2 (0.4 at +3 deg., 0.6 at 0 deg., 3.1 at -3 deg.), a normalized version of the JNR Criterion results, given in Figure 4.4. The JNR Criterion is still an inadequate derailment predictor using this modification.

4.3 Experimental Evaluation of Alternative Wheel Load Criterion

The alternative wheelload derailment criteria are evaluated using the experimental data base by computing the following quantities:

TAT = time above threshold

PEAK = peak value of L/V ratio

AREA - L/V = $\int_{TAT} (\frac{L}{V})\, dt$

MOMENTUM = $\int_{TAT} L\, dt$

(AREA-L/V)/TAT = $\frac{1}{TAT} \int_{TAT} (\frac{L}{V})\, dt$

NORMALIZED MOMENTUM = $\frac{1}{TAT} \int_{TAT} L\, dt$

TJNR = t_1 in Figure 4.1

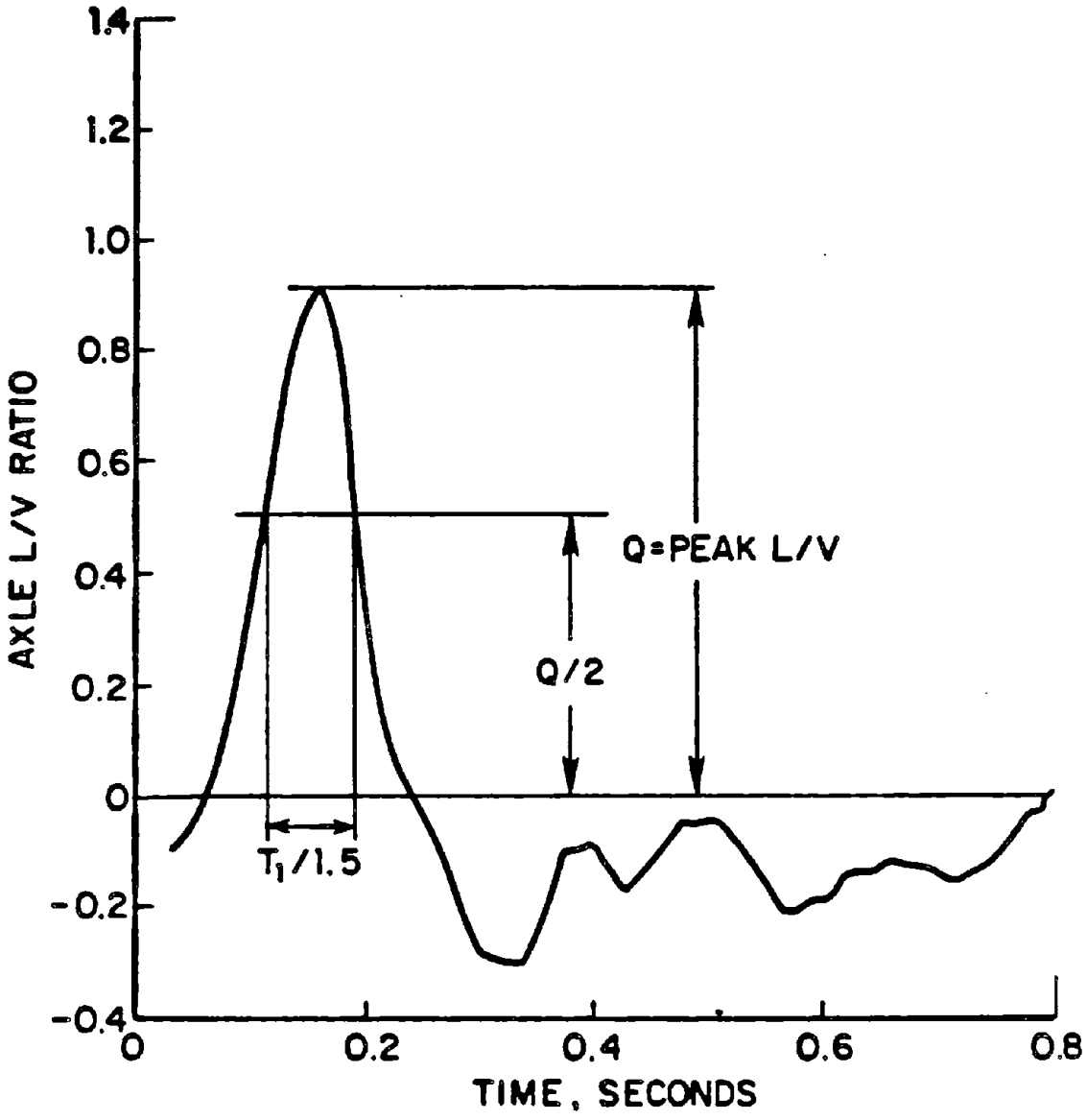

Figure 4.1 - Application of JNR Derailment Criterion to Typical L/V Pulse.

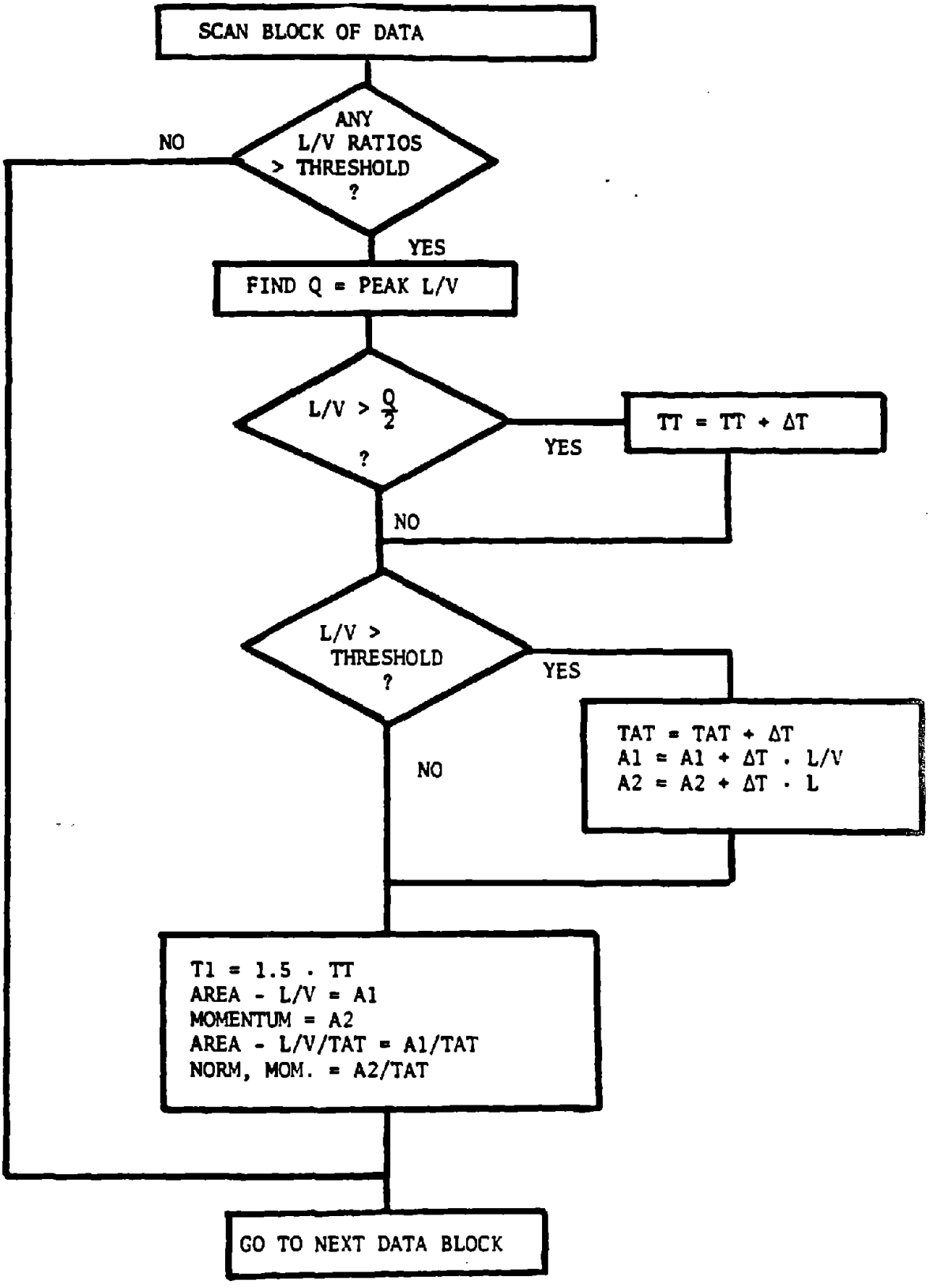

Figure 4.2 - Algorithm for Derailment Criteria Evaluation

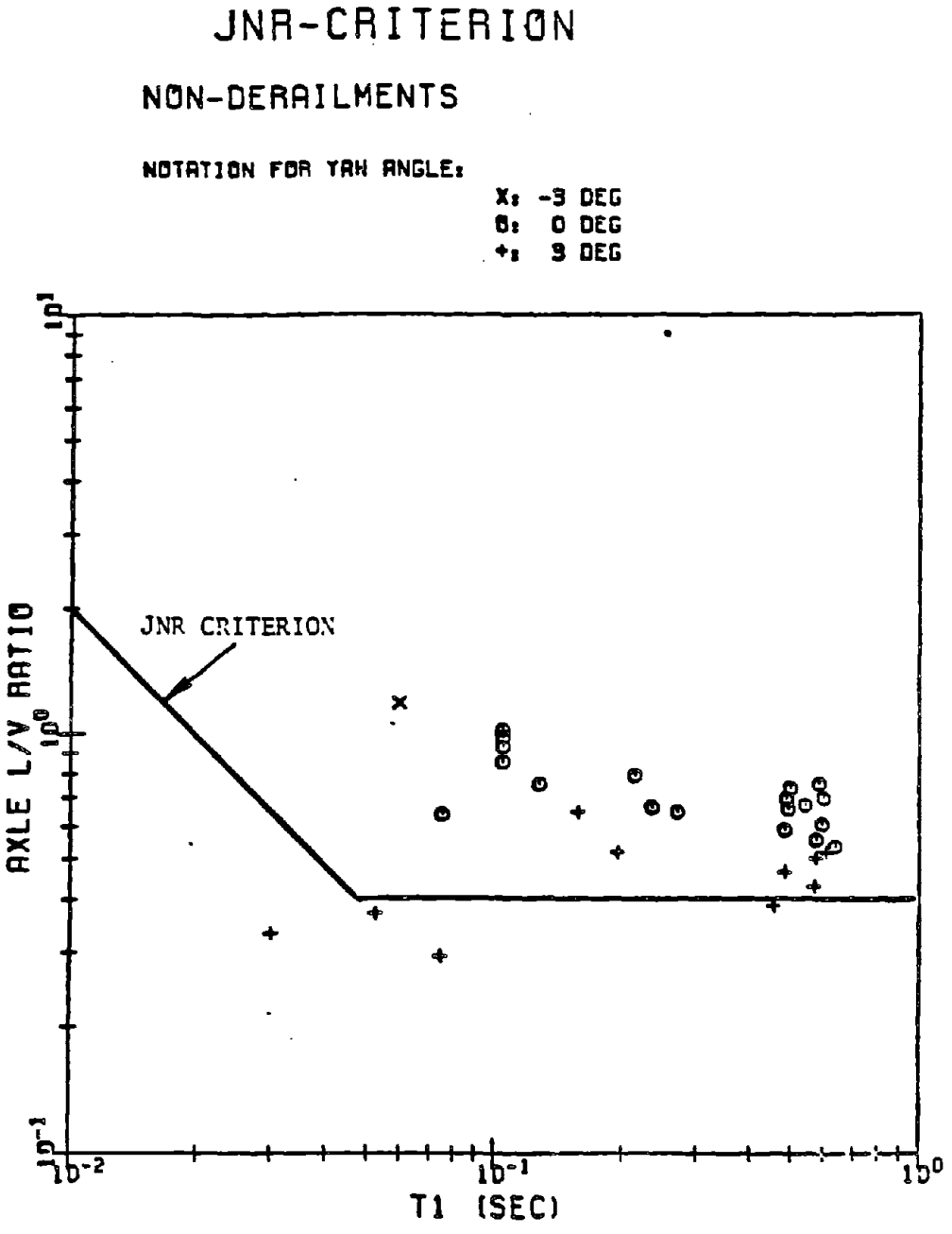

Figure 4.3 a. Comparison of Dynamic Wheelclimb Experimental Data with JNR Criterion for Nonderailment Cases.

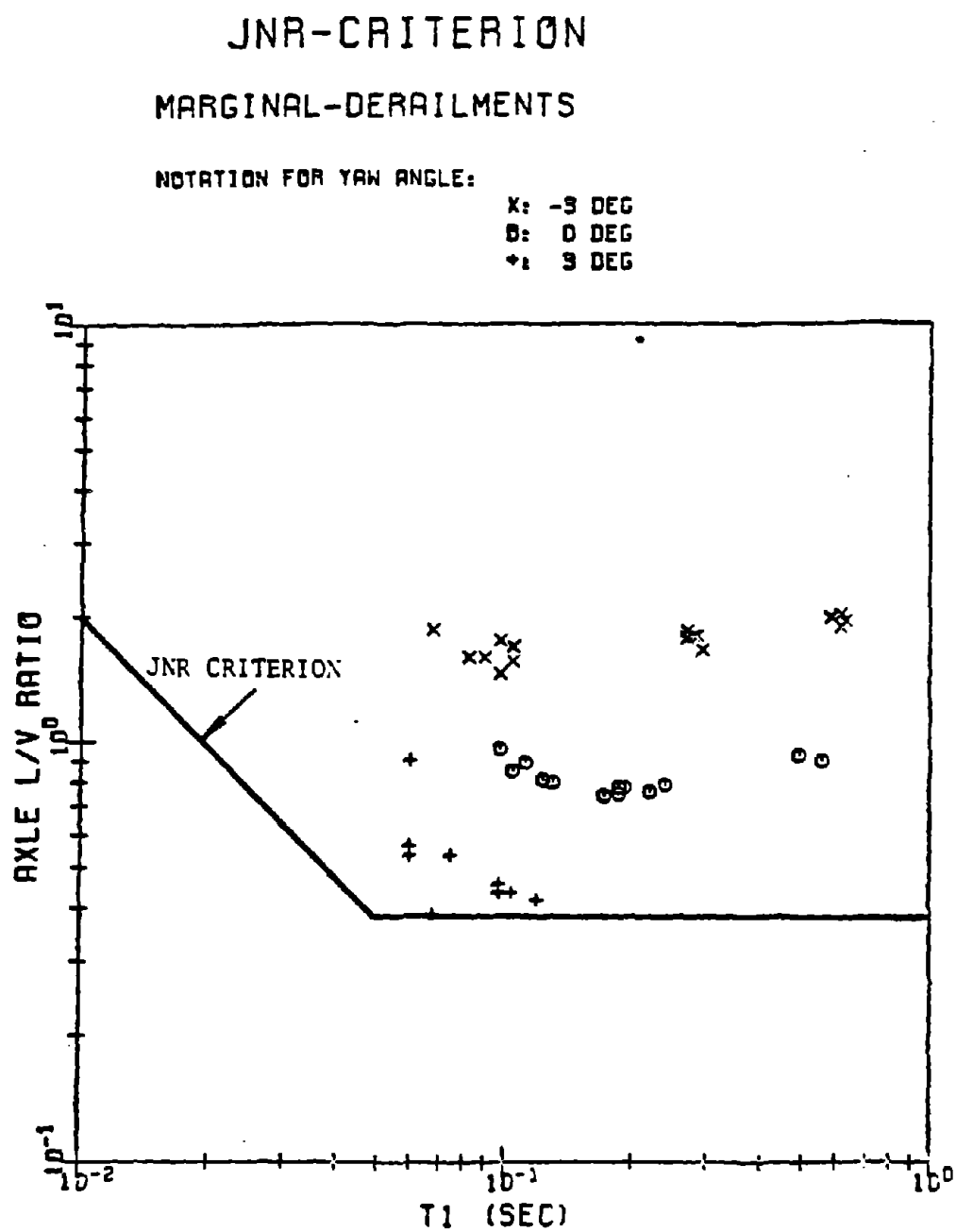

Figure 4.3.b. Comparison of Dynamic Wheelclimb Experimental Data with JNR Criterion for Marginal Derailment Cases.

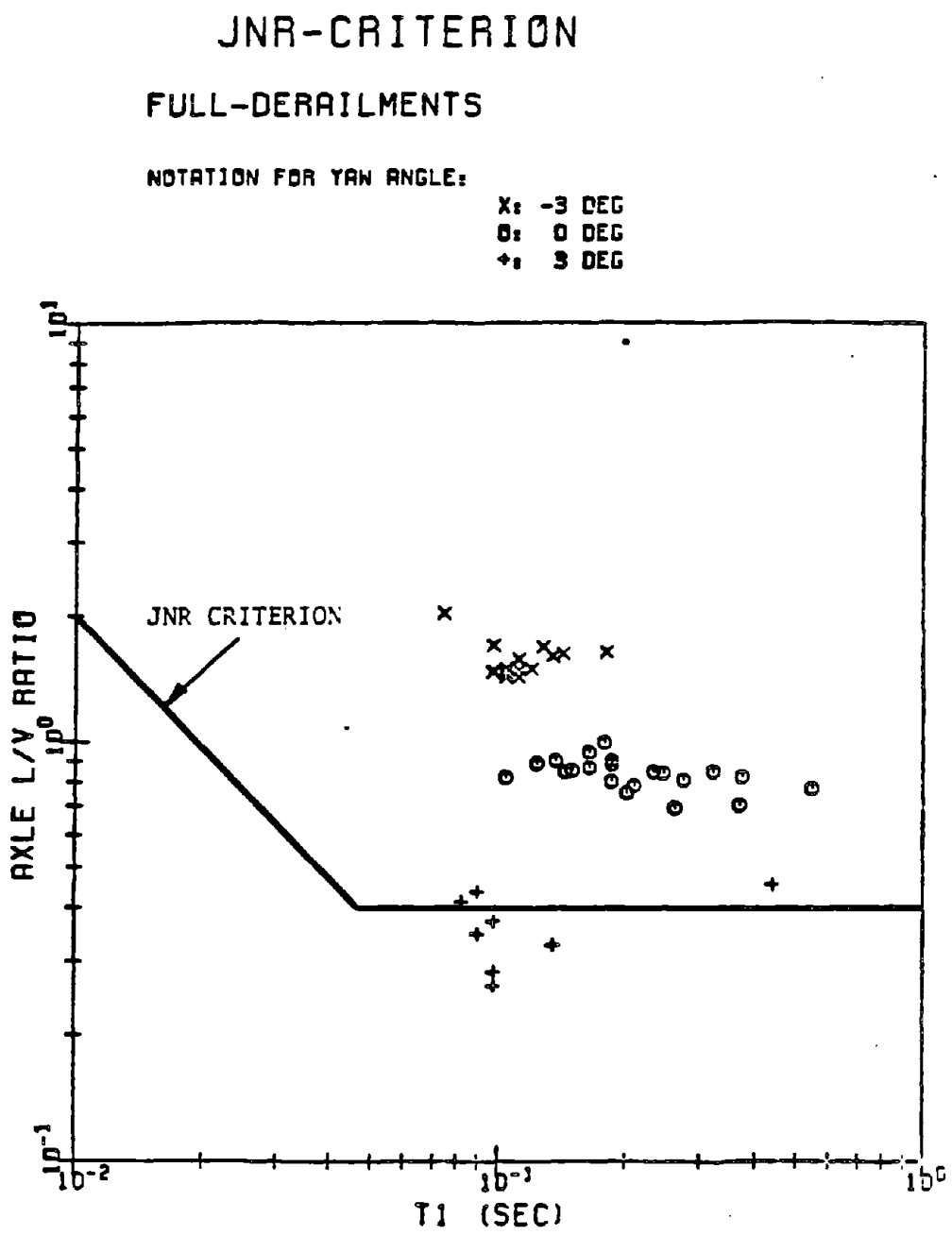

Figure 4.3.c. Comparison of Dynamic Wheelclimb Experimental Data with JNR Criterion for Complete Derailment Cases.

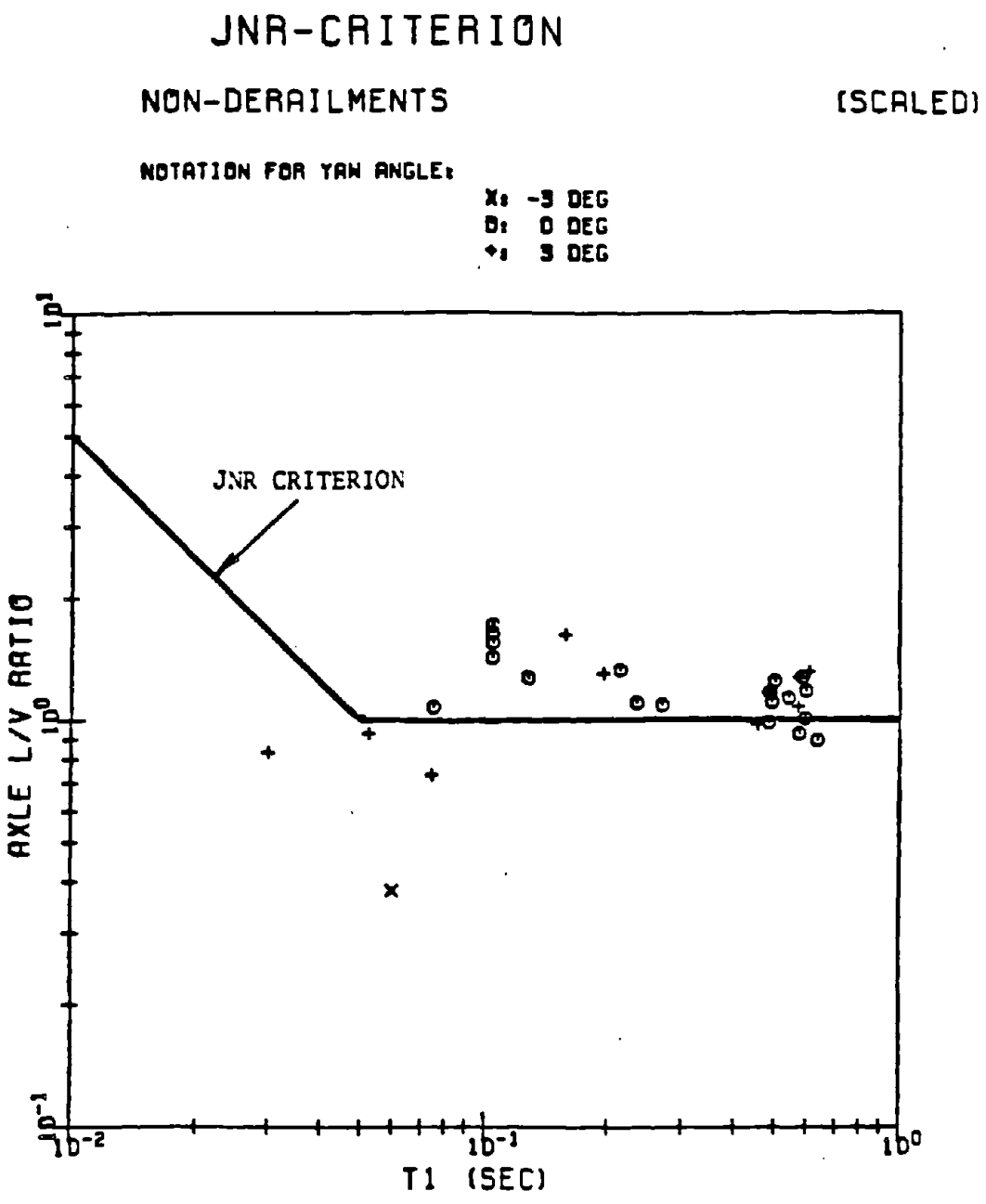

Figure 4.4.a. Comparison of Dynamic Wheelclimb Experimental Data with JNR Criterion with L/V Ratios Rescaled by the Quasisteady Derailment Limit at Each Yaw Angle for Nonderailment Cases.

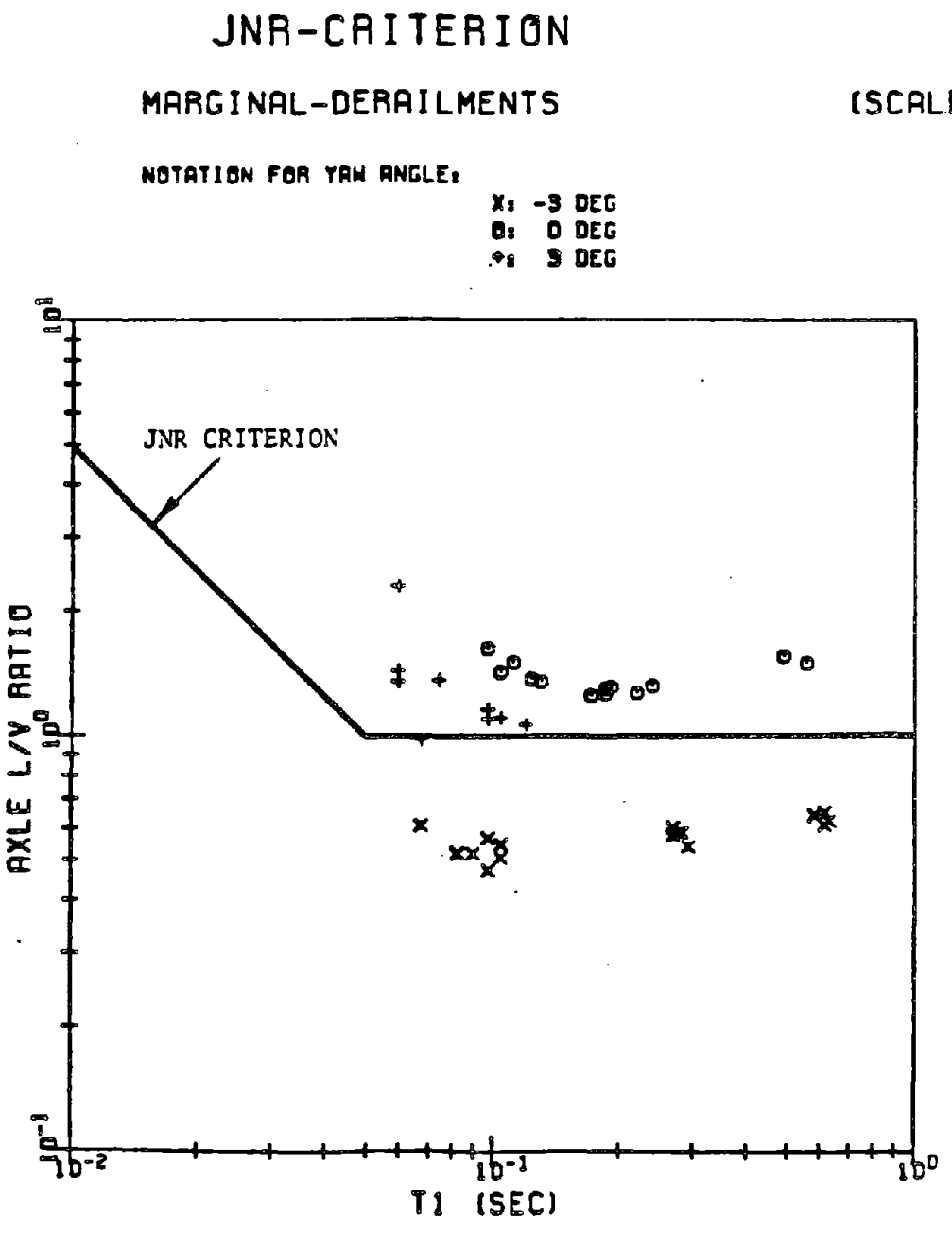

Figure 4.4.b. Comparison of Dynamic Wheelclimb Experimental Data with JNR Criterion with L/V Ratios Rescaled by the Quasisteady Derailment Limit at Each Yaw Angle for Marginal Derailment Cases.

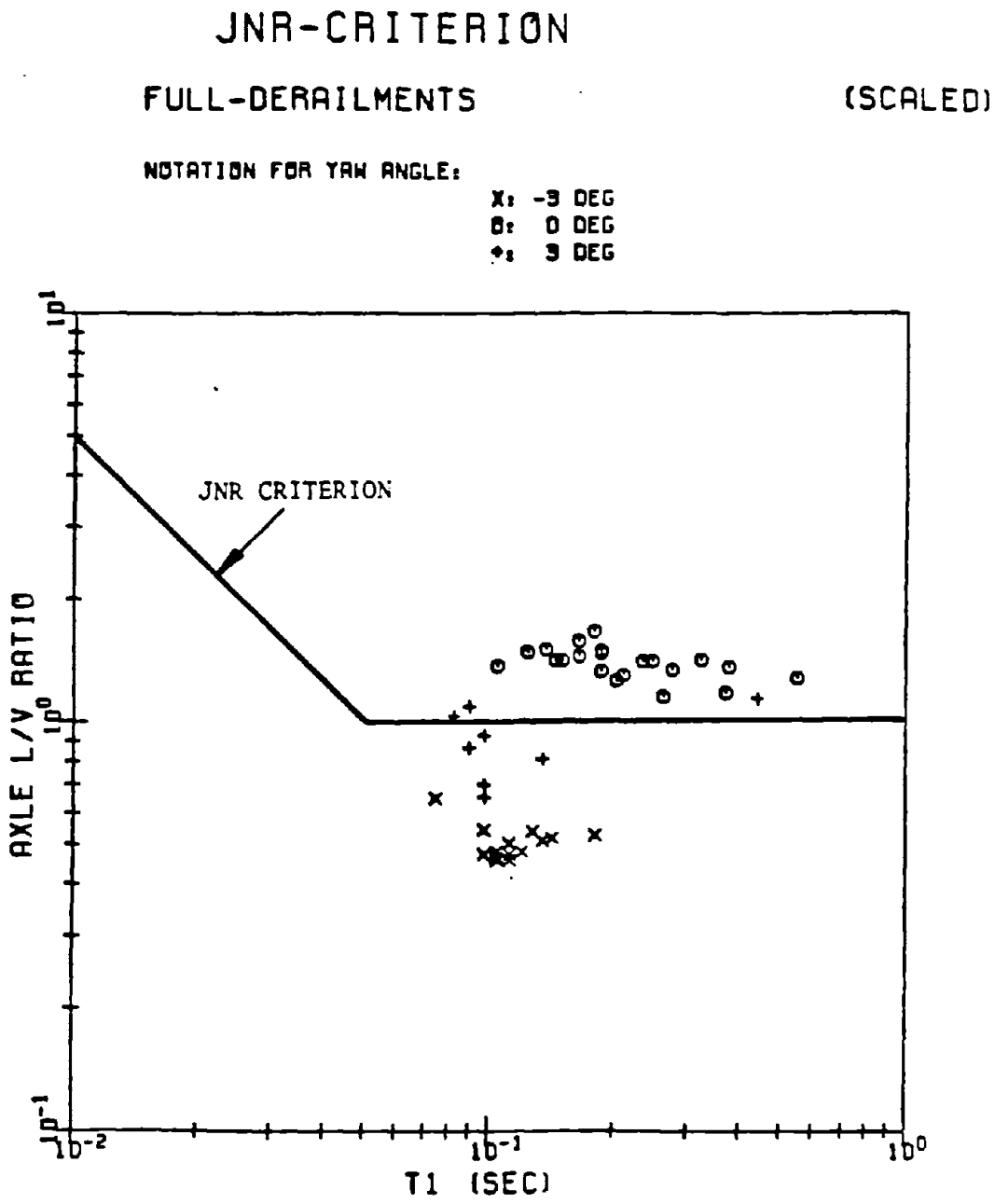

Figure 4.4.c. Comparison of Dynamic Wheelclimb Experimental Data with JNR Criterion with L/V Ratios Rescaled by the Quasisteady Derailment Limit at Each Yaw Angle for Complete Derailment Cases.

The results of these computations are tabulated in Appendix A. In the following paragraphs the results of application of the various criteria are plotted and discussed.

Type 1 - Peak value of L/V versus TAT

Figure 4.5 shows data for the three derailment conditions plotted in absolute and scaled formats (using L/V ratio scale factors for each yaw angle). As is the case using the JNR criterion, the spread of peak values for each derailment case covers almost a factor of ten in the absolute format and a factor of six in the scaled format. No significant time duration dependence is evident.

Type 2 - Integrated Values versus TAT

Figure 4.6 and 4.7 show data for L/V ratio and lateral force integrated over the pulse duration, the latter yielding a quantity with units of momentum. However, as previously discussed, the momentum quantity plotted here is not the momentum of the wheelset, but rather the change in momentum due to action of the contact forces alone. In both figures all data follow a distinct trend of increasing integrated values with increasing pulse durations. This result is consistent with the observation that the longer pulses are rather rectangular in shape. Neither criteria discriminates successfully among the three derailment conditions.

Type 3 - Normalized Integrated Values versus TAT

The proportionality between integrated values in Type 2 criteria and time duration is compensated by dividing the integrated value by the time duration. The resulting data are then the average values computed over the

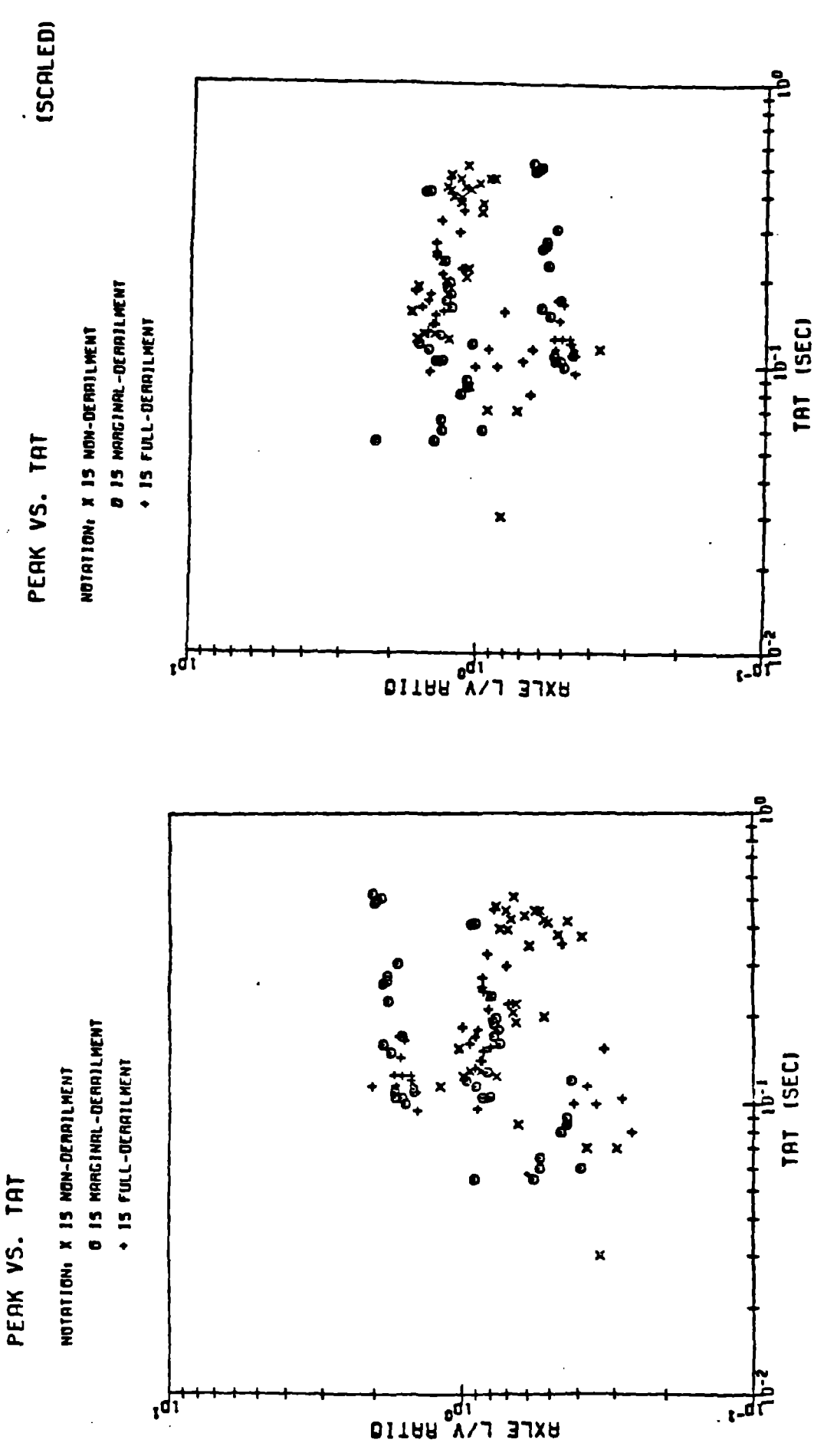

Figure 4.5 Absolute and Scaled Derailment Test Data: Peak L/V Ratio Versus Time Above Threshold.

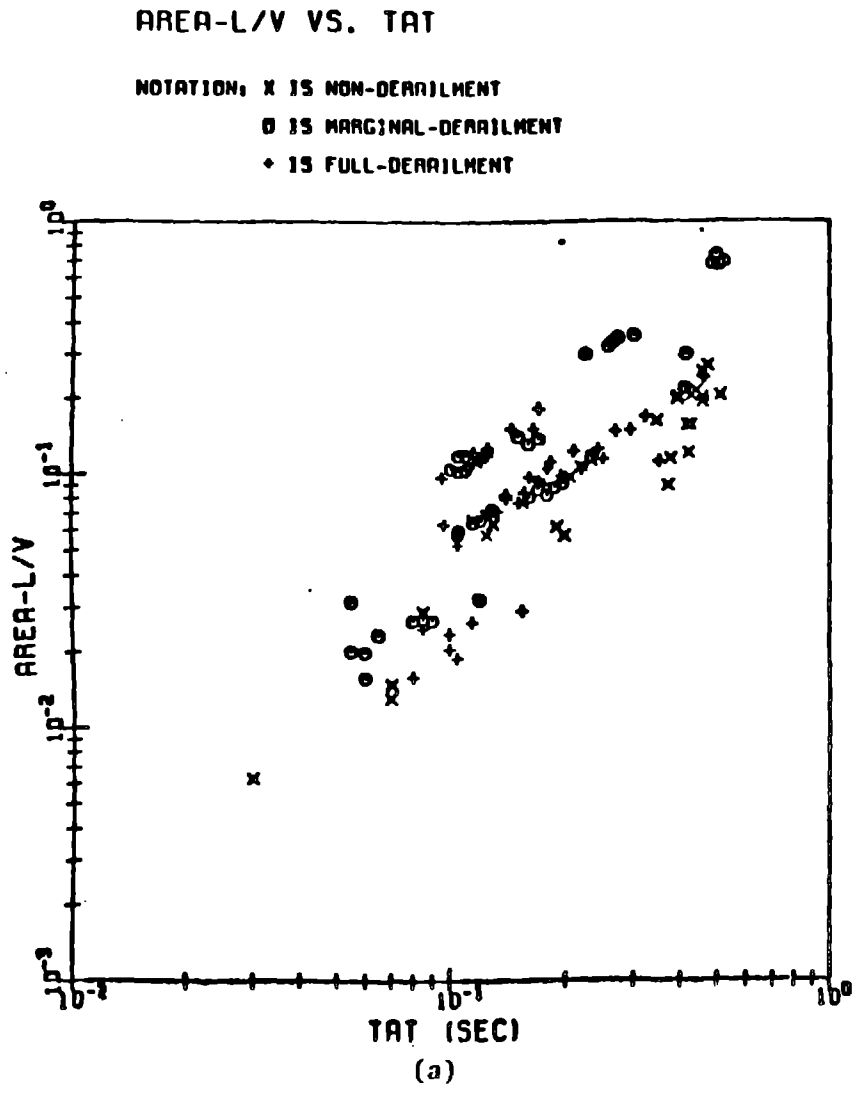

(a)

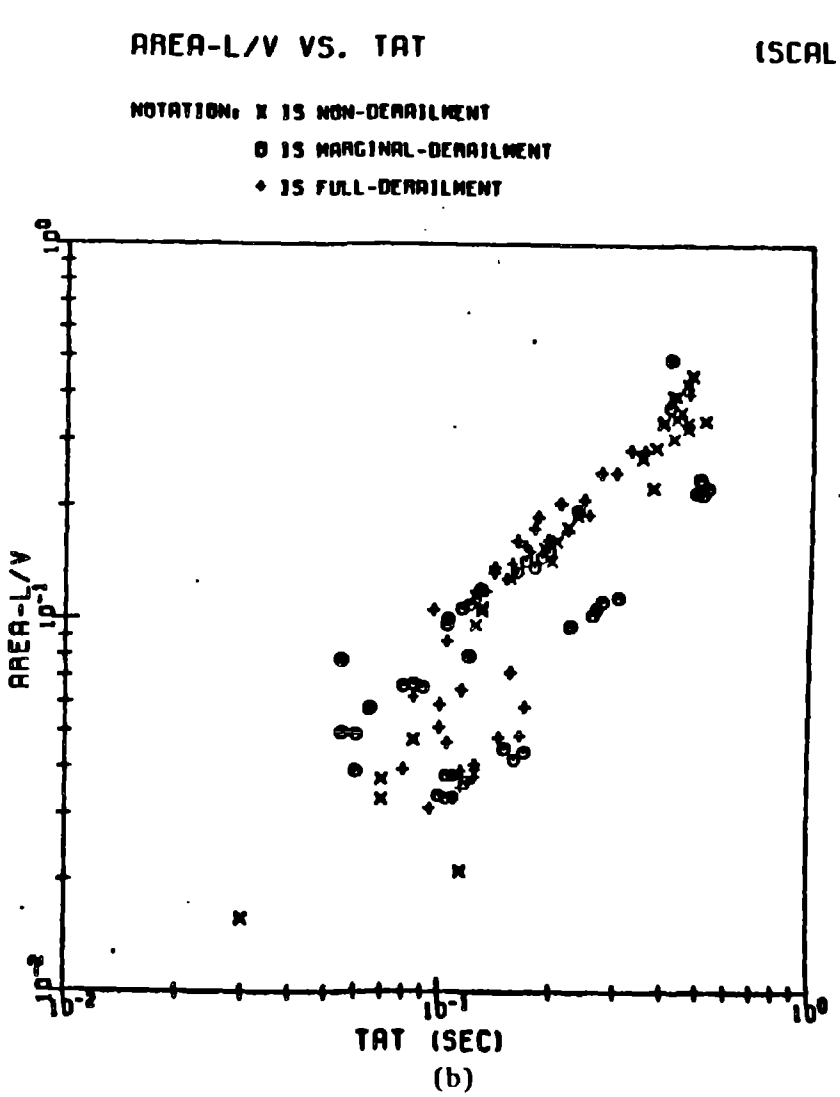

(b)

Figure 4.6 Absolute and Scaled Derailment Test Data: Integrated L/V Ratio Versus Time Above Threshold.

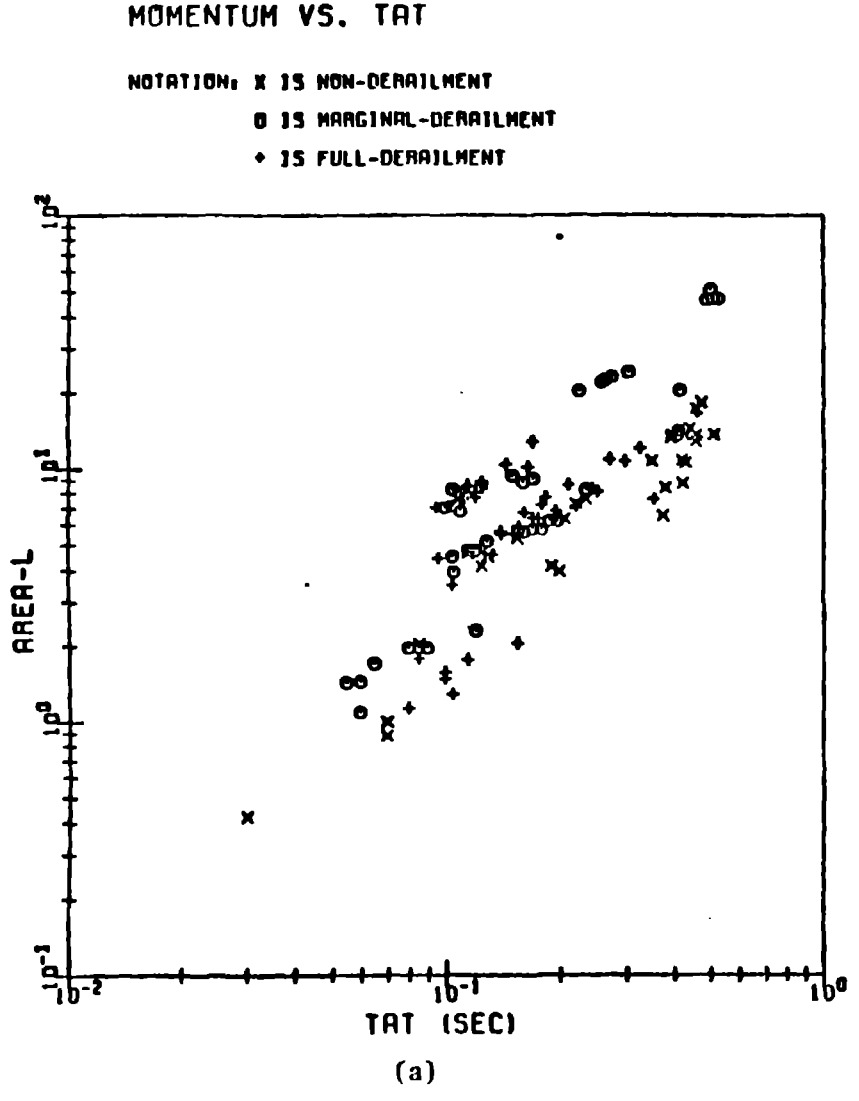

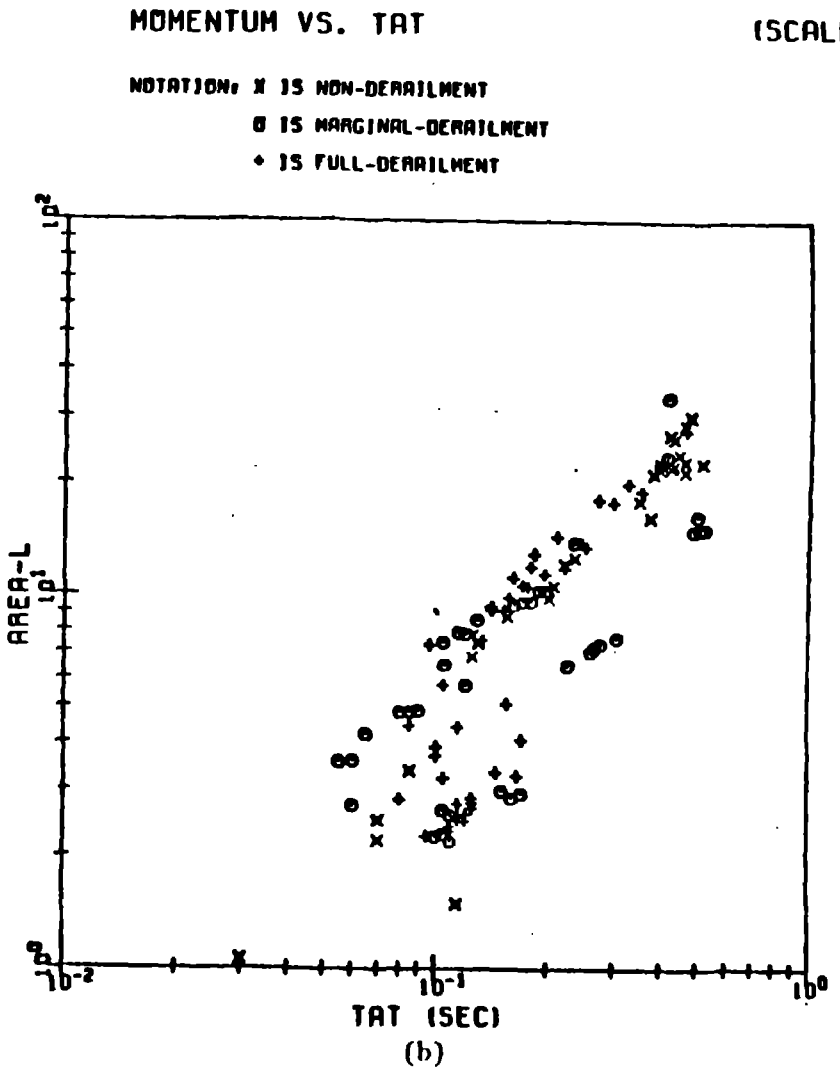

Figure 4.7 Absolute and Scaled Derailment Test Data: Integrated Lateral Force (momentum change) Versus Time Above Threshold.

duration of the pulse. Figures 4.8 and 4.9 show NORMALIZED AREA-L/V and MOMENTUM, respectively. The results are again very similar to those for the JNR and Type 1 criteria.

Type 4 - Peak Value versus TNP

The JNR Criterion is of this type, with results presented previously.

Type 5 - Integrated Value versus TNP

Same results as for Type 2, with data shifted to the left in each plot, since TNP is always less than TAT. Since no significant influence of time duration has been found in the test results, Types 2 and 3 criteria are equivalent.

Type 6 - Threshold Value versus Exceedance Time

This type of criterion is applied by sliding the threshold value, which is plotted as the ordinate, from zero to the peak value of the signal and computing the time that the pulse exceeds the threshold. In this manner, the pulse is mapped into the threshold - exceedance time plane as a continuous curve rather than a single point. Since the continuous curve retains much of the information content of the pulse, in contrast to criteria which reduce the pulse information to a single point, this procedure may have more potential for derailment condition discrimination. The exceedance curves plotted are for single pulses, and should not be confused with statistical plots for continuous running time histories including many pulses and intervening periods.

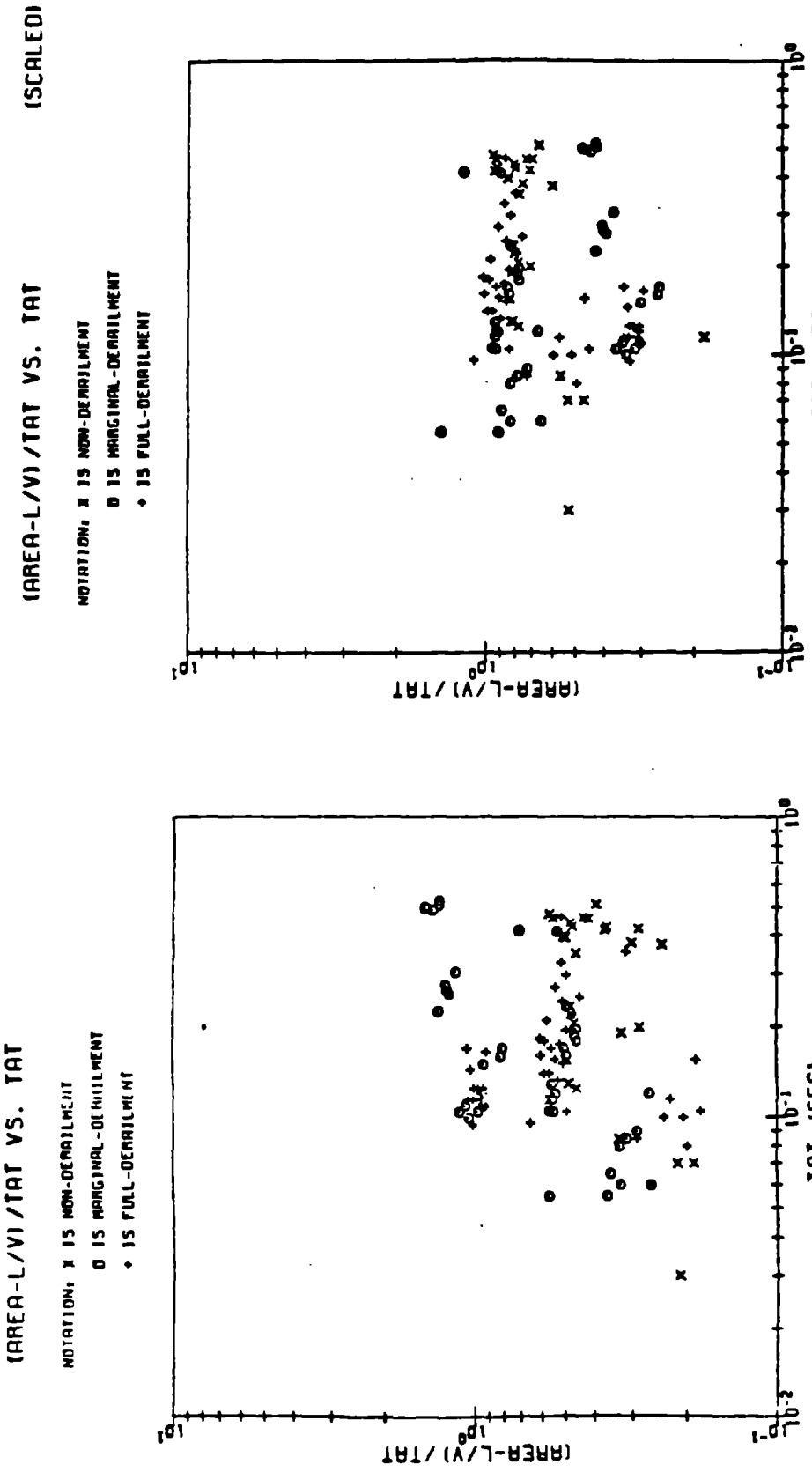

Figure 4.8 Absolute and Scaled Derailment Test Data: Average L/V Ratio During Pulse Versus Time Above Threshold.

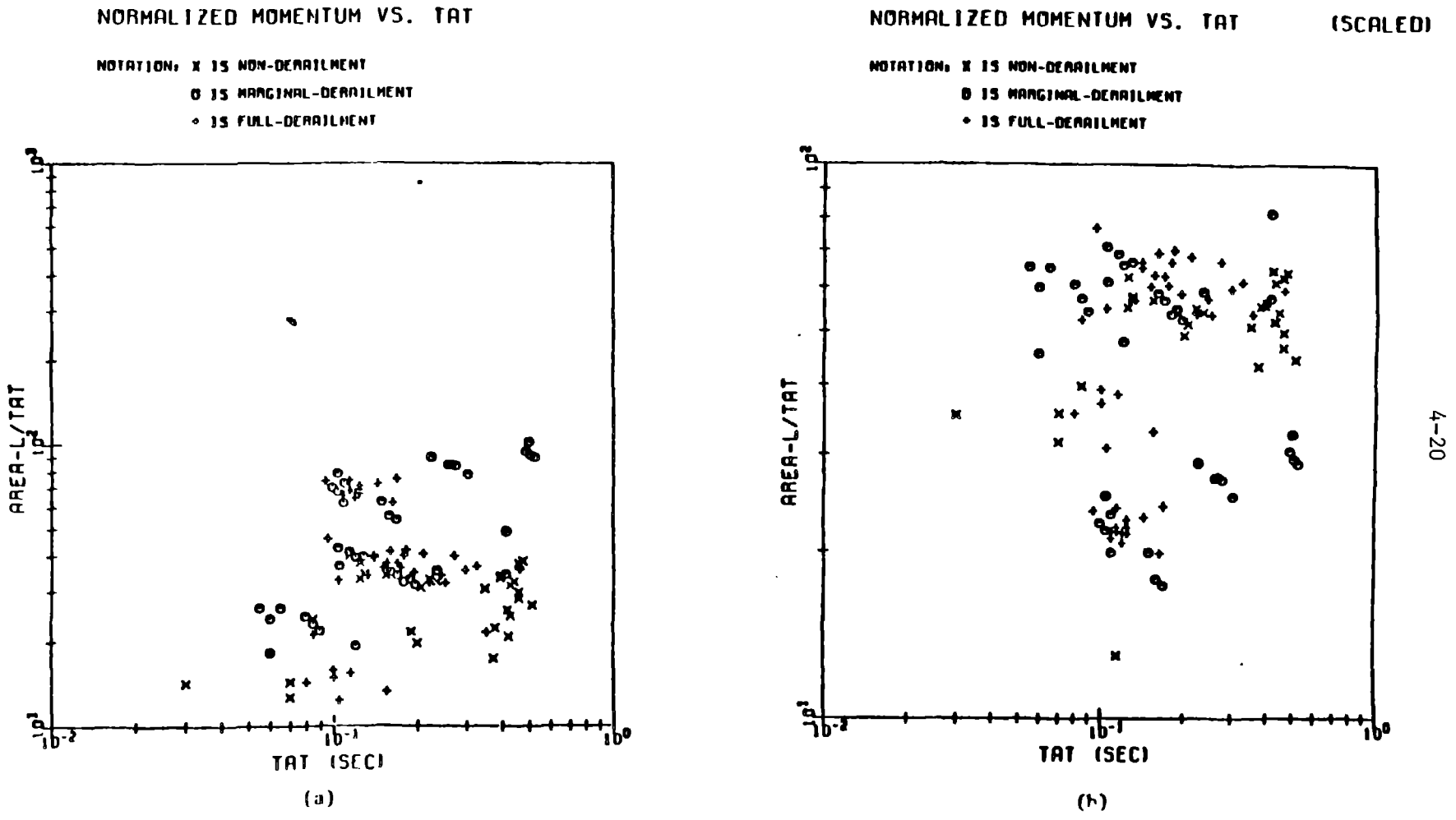

Figure 4.9 Absolute and Scaled Derailment Test Data: Average Lateral Force (momentum change) During Pulse Versus Time Above Threshold.

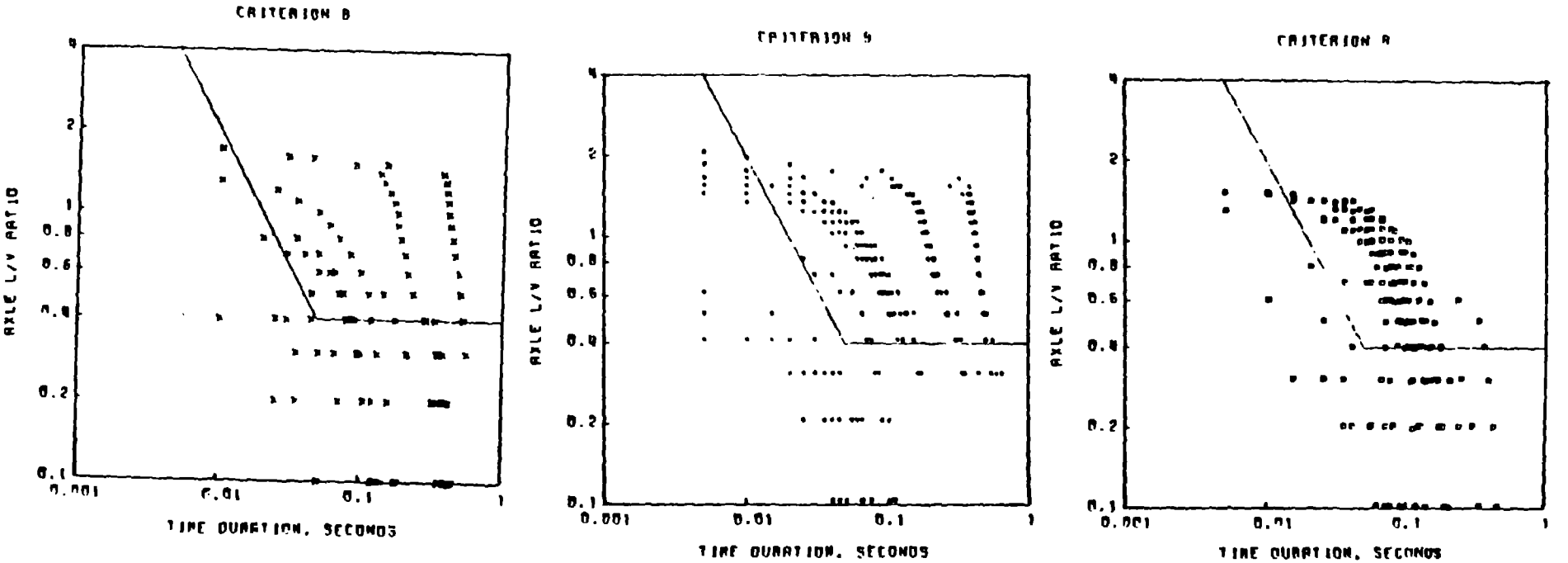

NONDERAILMENT

(a)

MARGINAL DERAILMENT

(b)

DERAILMENT

(c)

Figure 4.10 Threshold Level Versus Exceedance Time Plots for Derailment Test Pulses.

The results of this procedure applied to L/V ratio pulses are shown in Figure 4.10. The shapes of the curves plotted are generally similar to one another, indicative of pulse shapes ranging from half sine waves to rectangles. The curves for the three derailment conditions generally overlap in threshold values and exceedance times, with no apparent divisions among them.

4.4 Results from Variable Yaw Angle Tests

Tests were conducted with the yaw degree of freedom unlocked and a soft linear spring yaw suspension installed. These experiments for Process C permitted self steering by the wheelset under flange contact conditions and hunting phenomena at high speed. The data recorded were most interesting, but in retrospect the number of data points accumulated was too small to yield statistically meaningful results. The section that follows discusses the implications of the recorded observations as examples of the complexity of the dynamics of Process C, but at this time conclusions as definite as those for Processes A and B cannot be drawn.

The four generic types of responses recorded for the wheelset are shown in Figures 4.11 through 4.14. In Figure 4.11 the normal response of the wheelset at sub-critical velocities to track lateral random misalignments is shown. In the absence of flange contact axle L/V ratios are small (less than 0.05), lateral displacements relative to the track less than ±0.25 mm, and yaw angles less than ±0.50 mm. In Figure 4.12 limit cycle hunting of the wheelset is shown for velocities in excess of 6 m/s

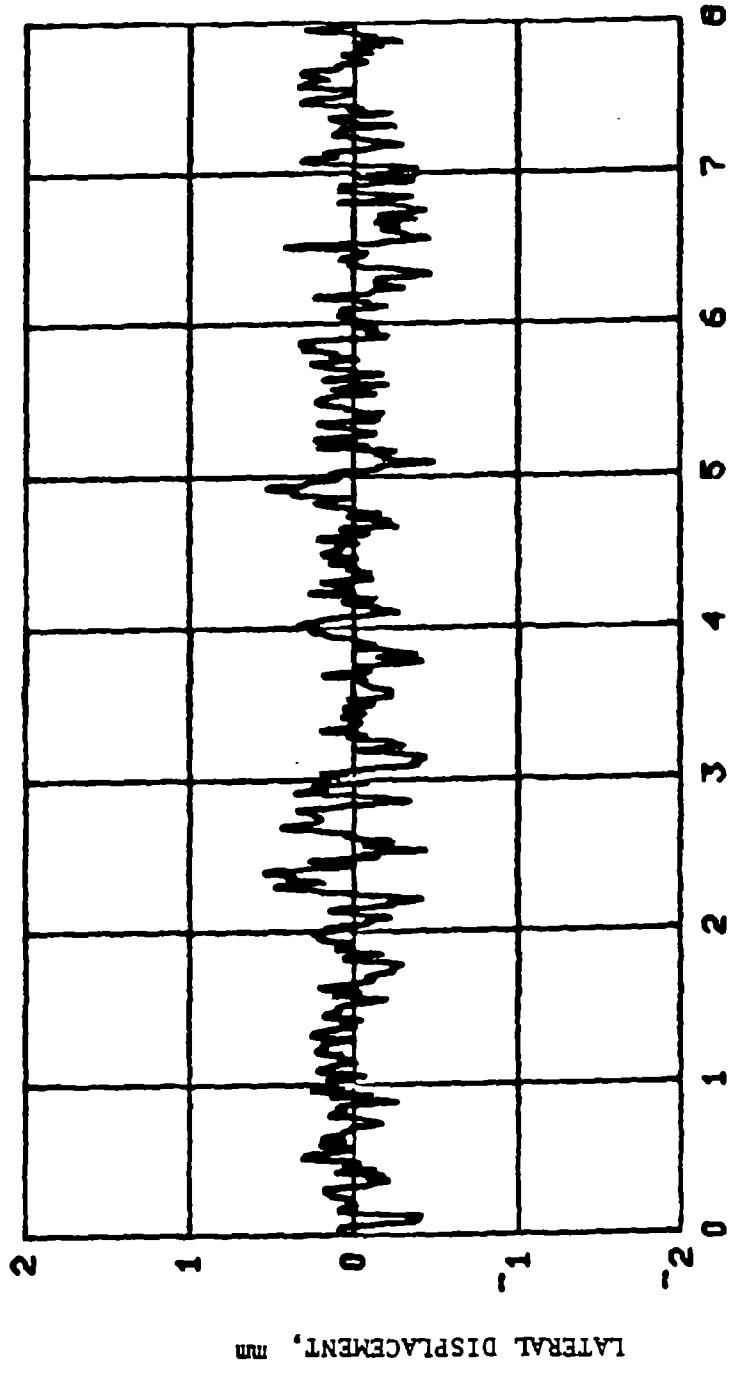

Figure 4.11 Two Degree of Freedom Response of Wheelset at Subcritical Velocities with No Flange Contact. Input Is Random Track Alignment, Model Speed is 3 m/s.

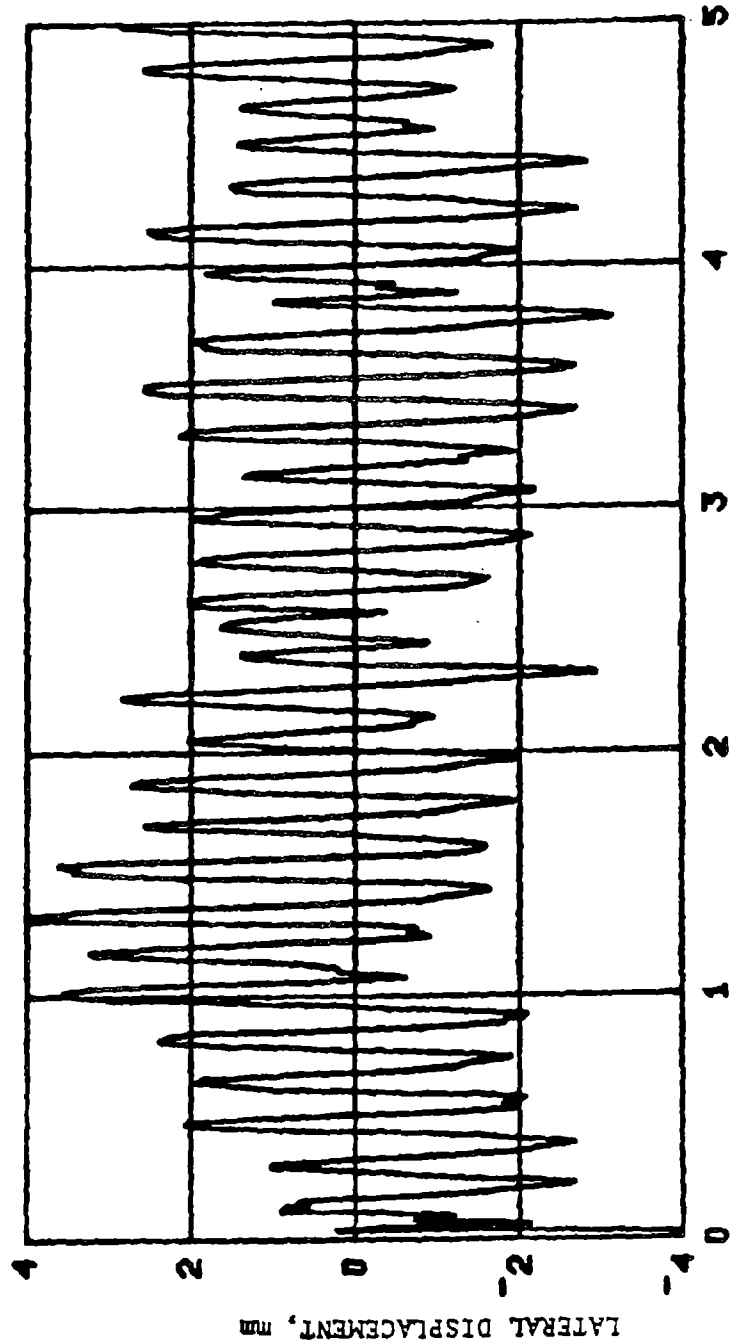

Figure 4.12 Limit Cycle Hunting of Wheelset Above Linear Critical Speed. Input is Random Track Alignment, Model Speed is 13 m/s.

model speed. The approximate ranges are ±0.4 for axle L/V ratios, ± 0.5 mm for lateral displacements relative to the track, and ± 1.5° for yaw angles. Derailments did not occur under these conditions.

In Figures 4.13 and 4.14 the responses to step inputs in lateral force are shown. The tests were conducted in the same manner as for Process B except that the rubber retaining wheels preventing derailment on the left rail were removed. Axle L/V ratios up to 1.2 were recorded, with yaw angles in the range of +2° to -6°, and lateral displacements including full derailment. This type of response occurred up to 3 m/s model speed. Above 3 m/s but below the apparent critical speed of 6 m/s a limit cycle hunting motion was initiated after release of the applied lateral force. This response is shown in Figure 4.14. The wheelset may or may not derail due to the initial application of the lateral force, but once the force was removed and hunting started no further derailments were observed. Detailed examination of this limit cycle showed that it is identical to the one found above 6 m/s in frequency and trajectory in the phase plane. The stability of the limit cycle behavior is shown in Figure 4.15, with a stable limit cycle existing for speeds below the critical velocity, contrary to limit cycle behavior predicted in several recent papers. The production of a limit cycle after a large lateral force is removed is of practical significance, since this could simulate conditions at the exit from a curve. Additional discussion of this behavior, known as a Hopf bifurcation is given in [2,4].

The most interesting results from a derailment prediction point of view are those typified by Figure 4.13. For the same applied lateral force both derailments and nonderailments occur.

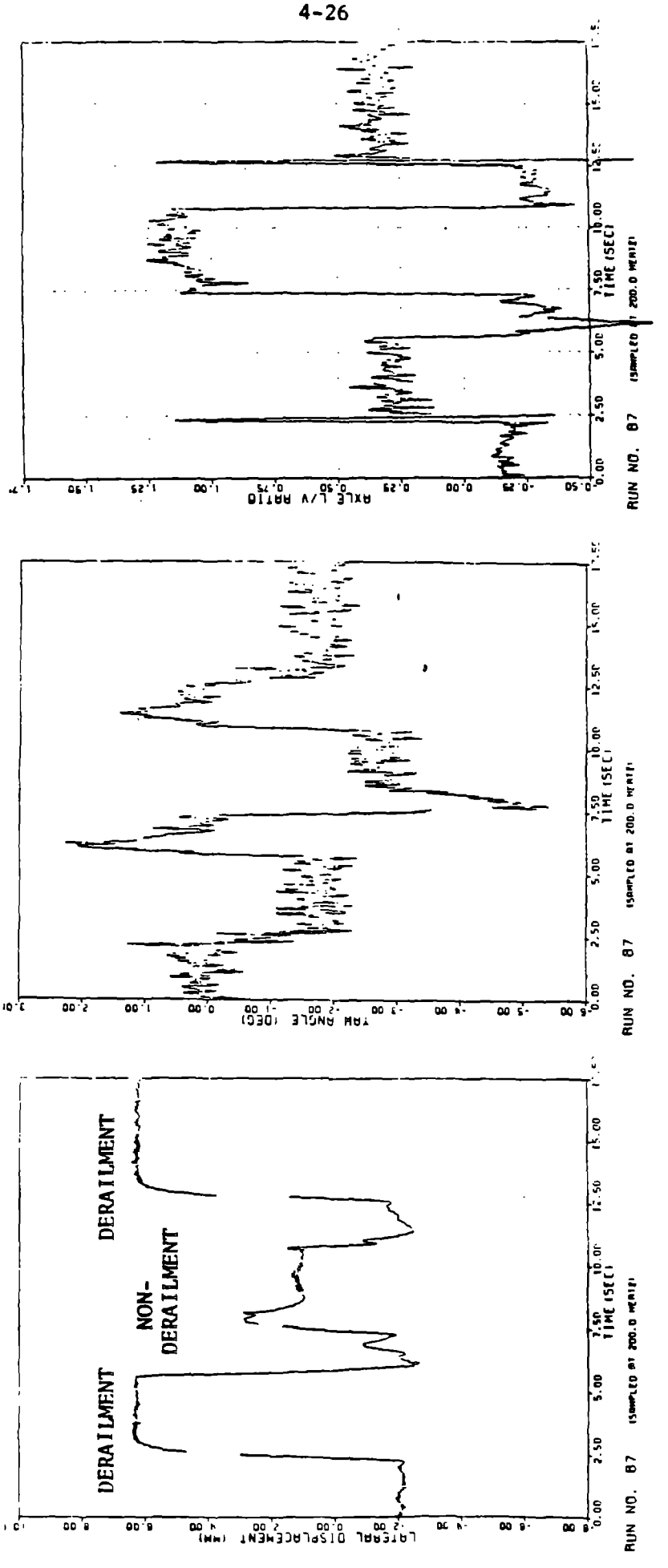

Figure 4.13 Two Degree of Freedom Wheelset Response to Step Lateral Force Inputs in Addition to Random Track Alignment.

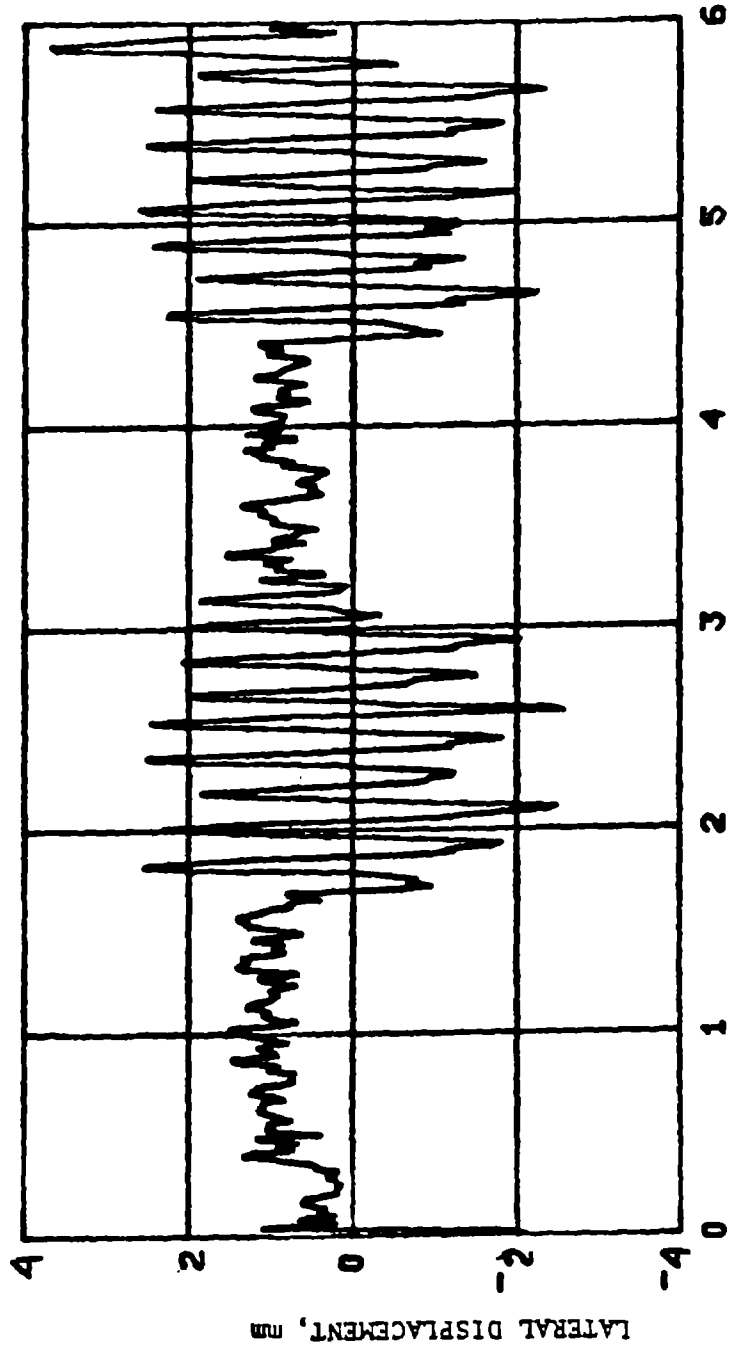

Figure 4.14 Limit Cycle Hunting Below Linear Critical Speed Initiated by Release of Applied Lateral Force, Model Speed is 6 m/s.

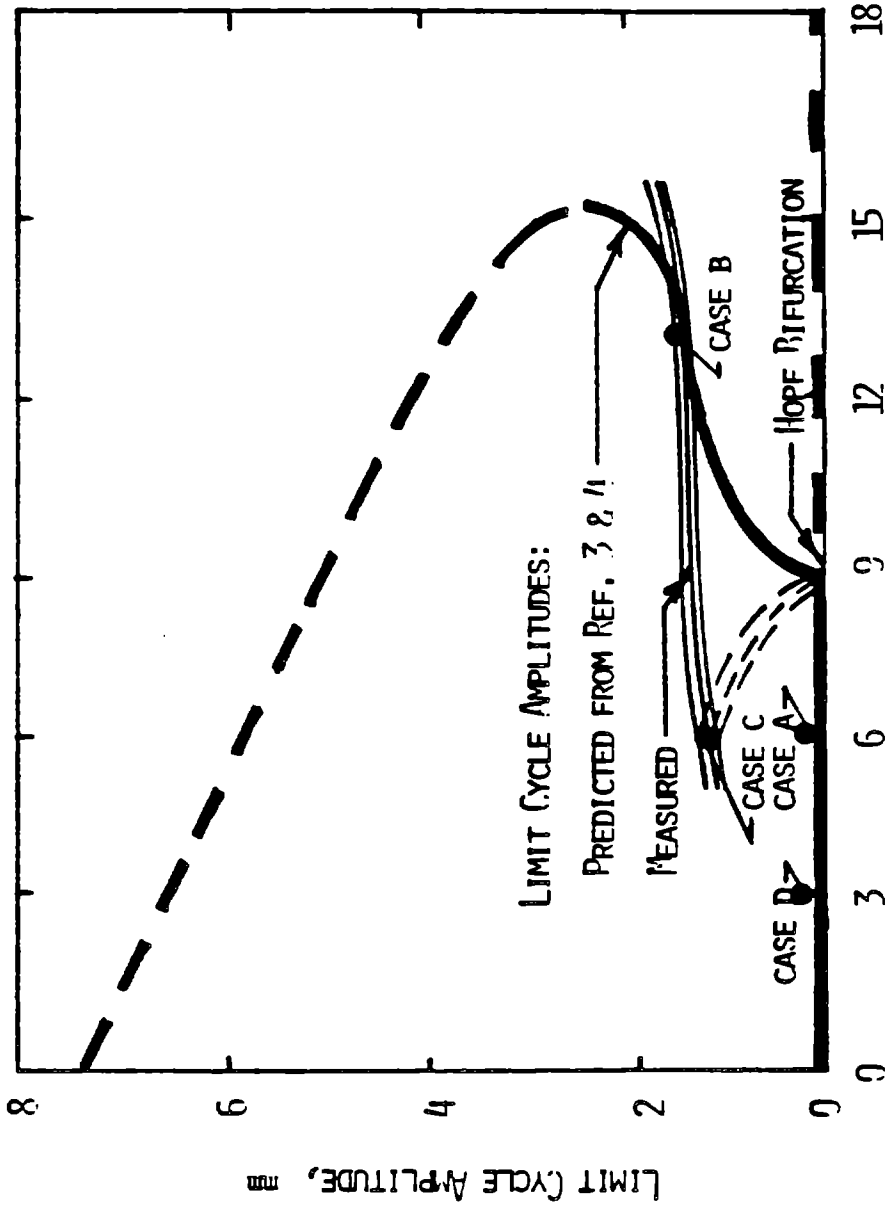

Figure 4.15 Stability of Limit Cycle Behavior as Function of Forward Speed and Limit Cycle Amplitude.

Close examination of the responses shows several key phenomena:

1) The yaw moment acting on the wheelset when in flange contact causes the axle to be steered towards the track center; i.e. a positive lateral displacement leads to a negative yaw rate. The yaw moment acts to inhibit the derailment process, since as the yaw angle becomes more negative, the lateral creep forces increase in the negative direction.

2) The key determinant of derailment is the yaw angle at the time of initial flange contact. In Figure 4.13, the yaw angles at contact for the derailing cases are about -1 degrees, while for the nonderailing case it is about -3 degrees. The value of the yaw angle at flange contact is a random variable, determined by the wheelset motion prior to application of the lateral force.

While insufficient data was obtained to evaluate derailment criteria quantitatively, the observations described above provide a qualitative indication that criteria which do not explictly or implictly account for yaw angle effects will not be successful predictors of derailment safety.

4.5 Discussion of Experimental Results for Dynamic Wheelclimb Processes

The experimental data presented in this section shows that a variety of time-duration dependent wheel load derailment criteria are unsuccessful in predicting derailment safety. The nonderailment, marginal derailment, and complete derailment cases are represented by these criteria with data points in overlapping regions spread generally over an order of magnitude. Defining derailment safety criteria below the minimum levels at which

derailment occurred would be overly conservative, possibly excluding vehicles, operating conditions, and track maintenance standards that could be demonstrated to be safe with more discriminating criteria. Even if these minimum levels were to be used, they do not establish a lower bound for derailment, since lower data points possibly could be measured.

The data presented do not indicate that a time-duration dependence should be included in derailment criteria. The time durations measured are in the range of 20 ms to 50 ms, somewhat above the range of durations in JNR data [7]. It is possible that under different experimental conditions impulsive wheel loads with very short (less than 10 ms) time durations and high amplitudes could be measured that would justify a time-duration dependence in wheel load.

4.6 Derailment Diagnostics

In the scale model test program reported here it was equally feasible to measure responses that did or did not involve derailment. In full scale tests of vehicle safety, in general it will not be feasible to derail vehicles. This presents a dilemna analagous to nondestructive material testing, being that if the test conditions are not severe enough, no data relevant to safety limits may be obtained. It is most desirable to be able to detect the approach to a derailment limit without exceeding it.

The measured responses shown in Figure 4.16 demonstrate such a diagnostic technique. By high-pass filtering and integrating the signal from an

accelerometer attached to the wheelset, the lateral velocity of the wheelset is obtained. The single peak shown in the left half of Figure 4.16 is generic to nonderailments, while the double peak on the right half is generic to marginal derailments. The physical explanations for these responses are straightforward. At initial flange contact, the rapid increase in contact angle rapidly decelerates the wheelset in the lateral direction, resulting in the first peak. In a nonderailment the velocity returns to zero, the derailment process stops with only a single peak.

In marginal and complete derailments the velocity does not return to zero after the first peak. In complete derailments after the deceleration associated with the first peak occurs, the wheelset again accelerates. In this case the velocity increases until the wheelset leaves the track. In marginal derailments the lateral forces applied to the wheelset reverse direction before the complete derailment, centering the wheelset on the track. This last second rescue causes the second peak.

This phenomenon may be readily exploited to achieve a simple diagnostic indicator of impending derailment conditions. Since the number of peaks, rather than absolute values of signals, are involved, simple logic circuits or microprocessor computer programs could test signals in real time. For example, the forward velocity of a locomotive under test could be increased on succeeding runs over a perturbed track section until double peaks are detected. At this point this test sequence could be terminated, with the knowledge that a derailment safety limit had been found.

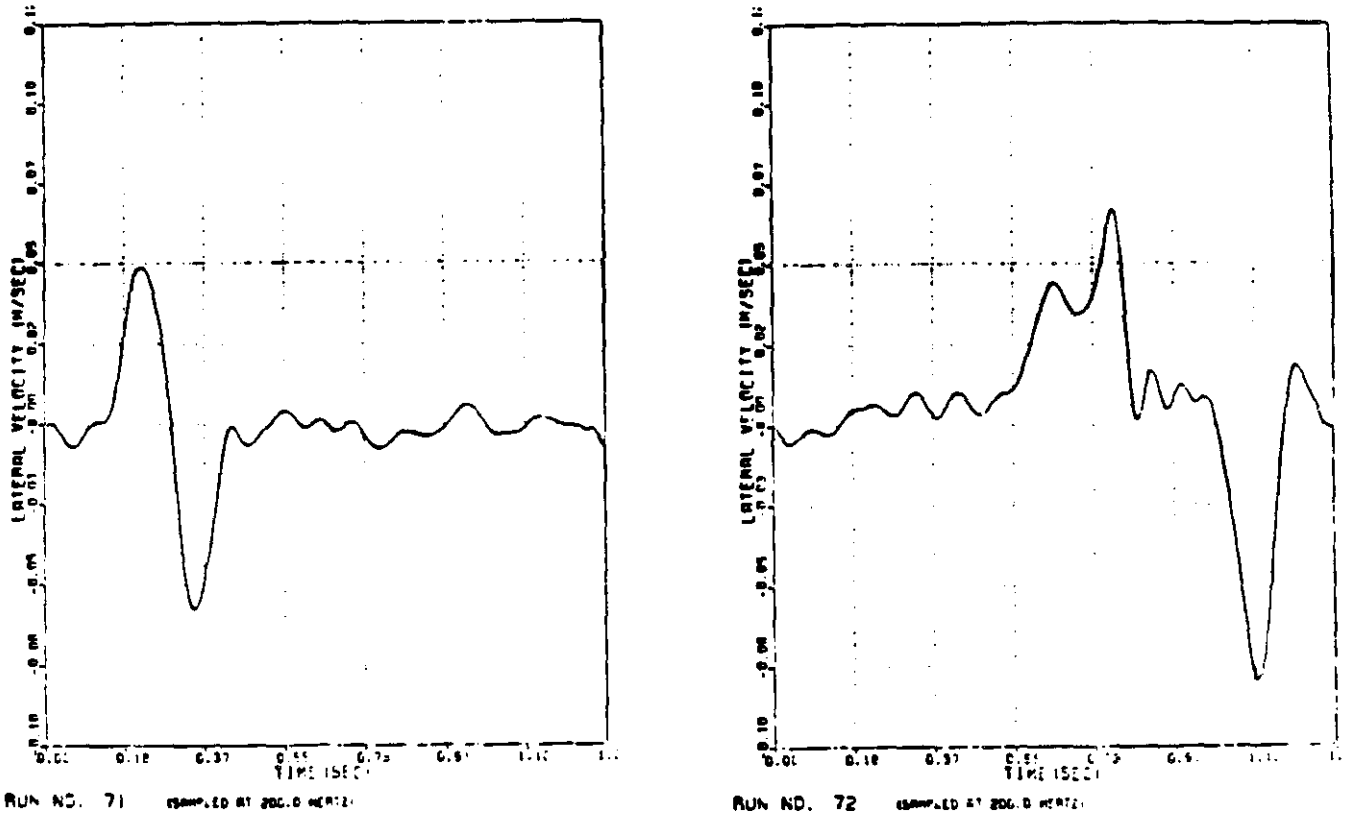

Figure 4.16 Generic Lateral Velocity Responses for Process B Dynamic Wheelclimb Tests. Double Peak Indicates Marginal Derailment Condition.

While more research is required to establish and validate diagnostic tools applicable to full scale vehicles, the initial success of this technique found from single wheelset experiments is most encouraging.

5. CONCLUSIONS

5.1 Conclusions

The experimental and analytical studies of wheelclimb derailment presented in this report result in the following conclusions regarding derailment criteria:

1) Wheelclimb derailment criteria based on quasisteady theory are adequate for derailment prediction under conditions of negligible lateral incident velocity and constant positive yaw angle. At negative yaw angles derailment occurs at L/V ratios somewhat below the predicted limits.

2) Application of the JNR and other time-duration dependent derailment criterion for nonderailment, marginal derailment, and complete derailment cases are each spread over an order of magnitude in L/V ratio amplitude and time duration. None of the criterion tested could distinguish between safe and unsafe conditions. Defining a safety criterion below the derailment data would be overly conservative, possibly excluding vehicles, operating conditions, and track and maintenance standards that could be demonstrated to be safe with a more discriminating criterion. Furthermore, the data provided do not necessarily establish a lower bound for derailment, since lower points possibly could be measured.

3) The analytical models for dynamic wheelclimb yield accurate predictions of wheelset response to external force inputs, in terms of wheelset motions during derailment and wheel/rail interaction forces (i.e. L/V ratios).

4) Evidence has been found that derailment criteria employing variables measured in addition to wheel loads may be successful in predicting derailment safety, and that diagnostic criteria may be developed for warning of impending derailment.

5.2 Recommendation for Future Research

To achieve the objective of defining a reliable measure of derailment safet the following would be useful as topics of future research:

a) New wheelclimb derailment criteria should be developed and validated that include variables in addition to wheel loads, such as lateral velocity and yaw angle, that are readily measured under full scale test conditions. Such multivariable criteria should be better indicators of derailment safety.

b) Criteria for the wheelclimb process should be combined with criteria for other derailment modes, such as gauge spreading and rail rollover, to yield a comprehensive safety measure. Track stiffness parameters would be key variables in the comprehensive criteria formulated.

c) The results of analytical and experimental studies of derailment of single wheelsets should be extended to complete trucks and vehicles. It is very important to establish the degree to which single wheelset criteria may be applied directly to complete vehicle configurations.

In addition to the above, the concept developed in this study of derailment diagnostics should be pursued. This technique provides a means for detecting marginally safe conditions in full scale tests, so that safety-related phenomena may be measured without actual derailments being required in the test plan. Scale model experiments will continue to be useful to the study of fundamental derailment processes, due to the greater control of test conditions possible and the relative ease of study of the full range of derailment conditions.

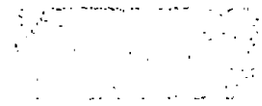

REFERENCES

1. Burton, T.D., "Influence of Wheel/Rail Contact Geometry on Large Amplitude Wheelset Equations of Motion," Trans. ASME, J. of Dynamic Systems, Measurement and Control, Vol. 103, No. 3, Sept. 1981.

2. Moelle, D., Steinborn, H., Gasch, R., "Computation of Limit Cycle of a Wheelset Using a Galerkin Method," The Dynamics of Vehicle on Roads and on Railway Tracks, Willumeit H.P. ed., Swets and Zeitlinger B. V., Lisse 1980.

3. Burton, T.D. and Whitman, A.M., "Nonlinear Kinematics of Wheel-Rail Contact," Trans. ASME, J. of Applied Mech., Vol. 45, No. 3, 1978, pp. 664-668.

4. Hauschild, W., The Application of Quasilinearization to the Limit Cycle Behavior of the Nonlinear Wheel-Rail System, Technical University of Berlin, Institut for Mechanik, 1980.

5. Gilchrist, A.O. and Brickle, B.V., "A Re-Examination of the Proneness to Derailment of a Railway Wheel-Set," J. Mech. Engr. Sci., Vol. 18, No. 3, 1976.

6. Sweet, L.M. and Sivak, J.A., "Nonlinear Wheelset Forces in Flange Contact-Part 1: Steady State Analysis and Numerical Results," ASME Journal of Dynamic Systems, Measurement and Control, Vol. 101, September 1979.

7. Arai, S. and Yokose, K., "Simulation of Lateral Motion of 2-Axle Railway Vehicle in Running," The Dynamics of Vehicles on Roads and Railway Tracks, Pacejka H. ed., Swets and Zeitlinger, B.V. Amsterdam, 1976.

8. Sweet. L.M., Karmel, A. and Moy, P., "Wheelclimb Derailment Criteria under Steady Rolling and Dynamic Loading Conditions," Dynamics of Vehicles on Roads and Railway Tracks, ed. Willumeit H.P., Swets and Zeitlinger B.V., Lisse, 1980.

9. Yokose, K., "A Theory of the Derailment of Wheelset," JNR Quart. Rep., Vol. 7, No. 3, pp. 30-34, 1966.

10. Matsudaira, T. and Yokose, K., "On The Derailment Induced by Lateral Impact of Wheelset," In Research on Tokaido Shinkansen, Vol. 3, JNR Rail. Tech. Res. Inst. Report, 1962 (in Japanese).

11. Clark, R.A., et al, "Prediction of the Dynamic Response of Vehicles to Lateral Track Irregularities," Proceedings of the Dynamics of Vehicles on Roads and Railway Track Conference, Cambridge, United Kingdom, 1981.

12. Duffek, W. and Jaschinski, A., "Efficient Implementation of Wheel Rail Contact Mechanics in Dynamic Curving," Proceedings of the Dynamics of Vehicles on Roads and Railway Track Conference, Cambridge, United Kingdom, 1981.

13. Elkins, J.A. and Gostling, R.J., "A General Quasisteady Curving Theory for Railway Vehicles," The Dynamics of Vehicles on Roads and on Tracks, Slibar A. and Springer H. eds., Swets and Zeitlinger B. V., 1978, pp. 388-406.

14. Kalker, J.J., "Simplified Theory of Rolling Contact," Delft Prog., Rep. Series C: Mechanical and Aeronautical Engineering and Shipbuilding 1, 1973, pp. 1-10.

15. Karmel, A., "Analytical and Experimental Studies of Derailment Processes of Railway Vehicles," Ph.D. Thesis, Princeton University, MAE Department, Princeton, New Jersey, September 1981.

16. IBM SL-Math Scientific Subroutine Package.

17. Heller, R. and Cooperrider, N.K., User's Manual for Asymmetric Wheel/Rail Contact Characterization Program, DOT Report FRA/ORD-78/05, Washington, D.C., December 1977.

18. Goree, J.G. and Law, E.H., User's Manual for Kalker's Simplified Theory, DOT Report FRA/ORD-78/06, Washington, D.C., December 1977.

19. Sweet, L.M. and Karmel, A., "Evaluation of Time-Duration Dependent Wheel Load Criteria for Wheelclimb Derailment," ASME Trans., J. of Dynamic Systems, Measurement, and Control, Vol. 103, No. 3, September 1981.

20. Hedrick, J.K., et al, Performance Limits of Rail Passenger Vehicles: Conventional, Radial and Innovative Trucks, Unpublished report prepared for U.S. DOT, September 1980.

21. Kalker, J.J. "Survey of Wheel-Rail Rolling Contact Theory". Vehicle System Dynamics, Vol. 8, No. 4, pp. 317-358, Sept. 1979.

22. Thompson, W.I., III, Plate Instrumented Wheelsets for the Measurement of Wheel/Rail Forces . Report No. FRA/ORD-80-58, Federal Railroad Administration, Washington, DC, October, 1980.

23. Pocklington, A.R. and Allen, R.A., "Improved Data from Load Measuring Wheels". Inst. Mech. Engr., Vol. 2, No. 4, pp. 37-43, July/August 1977.

24. Modransky, J., Donnelly, W.J., Novak, S.P., and Smith, K.R., "Instrumented Locomotive Wheels for Continuous Measurements of Vertical and Lateral Loads". ASME Paper 79-RT-8, Am. Soc. Mech. Engr., New York, February 1979.

25. Ikemori, M., "A Study of Track Maintenance for the Derailment Due to the Interaction Between Track and Vehicle." JNR Railway Tech. Res. Institute Quart. Rpts., Vol. 19, No. 1, 1978.

26. Tong, P., Brantman, R., and Greif, R., "Analysis and Measurement of Locomotive Dynamic Characteristics". ASME Paper 79-WA/RT-10, Am. Soc. Mech. Engr., New York, August 1979.

27. Dean, F.E. and Ahlbeck, D.R., "Criteria for High-Speed Curving of Rail Vehicles". ASME Paper 79-WA/RT-12, Am. Soc. Mech. Engr., New York, August 1979.

28. Brantman, R. Griffin, J.W., and Jeffcoat, R.L., "A Methodology for Estimating the Derailment Probability of a Fleet of Railway Vehicles". ASME Paper 79-WA/RT-6, Am. Soc. Mech. Engr., New York, August 1979.

29. Sweet, L.M., Sivak, J.A. and Putman, W.F., "Nonlinear Wheelset Forces in Flange Contact - Part II: Measurements Using Dynamically Scaled Models". ASME Trans., J. of Dyn. Sys., Meas., and Cont., Vol. 101, No. 3, pp. 247-255, September 1979.

30. Matsudaira, T., "Dynamics of High Speed Rolling Stock." JNR Railway Tech. Res. Institute Quart. Rpts., Special Issue, 1963.

31. Ensco, Inc. Test Run RG-145, April 1975. Reported in Ahlbeck, D.R. and Doyle, G.R., Comparative Analysis of Dynamics of Freight and Passenger Rail Vehicles, Battelle-Columbus Laboratories, NTIS No. PB-265-850, November 1976.

32. Kesler, K. Yang, T.-L., Mahone, G., and Boyd, P., "The Design and Application of Instrumented Wheelsets for Measuring Wheel/Rail Loads." Ensco, Inc., Alexandria, VA., presented at 1979 ASME Winter Annual Meeting, New York.

Appendix A

SUMMARY OF DERAILMENT TEST DATA AND COMPUTED INDICES

POINT NO.	RUN NO.	TAT	PEAK	AREA-L/V	AREA-L	TI
	NON-DERAILMENTS		YAW ANGLE= -3 DEGREES			
1	101	.115	1.103	.065	4.628	.060
	NON-DERAILMENTS		YAW ANGLE= 0 DEGREES			
2	57	.394	.699	.198	13.152	.488
3	57	.399	.742	.202	13.514	.502
4	57	.513	.661	.204	13.688	.495
5	61	.206	.664	.096	6.361	.234
6	61	.234	.795	.113	7.583	.213
7	61	.220	.653	.105	7.262	.268
8	62	.445	.606	.214	14.420	.591
9	62	.431	.676	.205	13.478	.543
10	69	.085	.642	.028	2.029	.075
11	69	.130	.857	.063	4.457	.105
12	69	.125	.760	.058	4.131	.127
13	71	.125	.983	.069	4.698	.105
14	71	.155	1.027	.077	5.286	.105
15	71	.130	.933	.064	4.508	.105
16	73	.350	.590	.162	10.718	.488
17	73	.460	.556	.193	12.922	.577
18	73	.460	.536	.201	13.714	.638
19	90	.475	.760	.269	18.163	.585
20	90	.460	.705	.254	17.229	.600
	NON-DERAILMENTS		YAW ANGLE= 3 DEGREES			
21	92	.420	.507	.156	10.881	.577
22	92	.430	.522	.157	10.541	.607
23	93	.425	.433	.121	8.838	.570
24	93	.300	.468	.115	8.456	.487
25	93	.375	.390	.090	6.507	.457
26	95	.190	.650	.062	4.104	.157
27	95	.200	.521	.057	3.926	.195
28	96	.070	.370	.015	.995	.052
29	96	.030	.333	.006	.422	.030
30	96	.070	.293	.013	.882	.075
	MARGINAL-DERAILMENTS		YAW ANGLE= -3 DEGREES			
31	104	.150	1.747	.140	9.285	.097
32	104	.110	1.460	.103	6.798	.097
33	104	.170	1.599	.137	9.156	.082
34	105	.100	1.563	.105	6.991	.105
35	105	.160	1.865	.131	8.858	.067
36	106	.110	1.692	.117	7.963	.105
37	106	.105	1.680	.110	8.212	.105
38	107	.265	1.747	.329	22.430	.285

39	107	.275	1.799	.344	23.029	.277
40	108	.305	1.663	.352	23.062	.292
41	109	.225	1.776	.296	20.226	.270
42	109	.260	1.849	.317	21.947	.270
43	112	.500	1.930	.732	50.621	.630
44	112	.490	1.906	.675	46.158	.585
45	112	.525	2.011	.694	47.012	.615
46	113	.510	1.878	.670	46.542	.615
47	115	.105	1.603	.102	7.108	.090

MARGINAL-DERAILMENTS YAW ANGLE= 0 DEGREES

48	58	.417	.897	.297	20.487	.557
49	60	.197	.750	.091	6.209	.220
50	60	.188	.776	.088	6.202	.186
51	60	.234	.788	.116	8.266	.241
52	62	.412	.927	.220	14.167	.495
53	65	.105	.803	.060	3.890	.131
54	65	.179	.748	.082	5.764	.186
55	65	.170	.776	.086	5.786	.192
56	66	.160	.743	.080	5.646	.172
57	67	.120	.813	.071	5.128	.124
58	70	.105	.849	.058	4.478	.105
59	70	.120	.962	.065	4.741	.097
60	70	.115	.894	.064	4.749	.113

MARGINAL-DERAILMENTS YAW ANGLE= 3 DEGREES

61	94	.120	.421	.032	2.296	.120
62	97	.090	.437	.026	1.958	.105
63	97	.055	.908	.031	1.435	.060
64	98	.085	.436	.027	1.950	.097
65	98	.030	.458	.026	1.945	.097
66	98	.060	.388	.016	1.091	.067
67	99	.060	.535	.020	1.441	.060
68	99	.065	.538	.023	1.693	.075
69	99	.055	.569	.020	1.434	.060

FULL-DERAILMENTS YAW ANGLE= -3 DEGREES

70	100	.125	1.696	.117	8.333	.097
71	105	.110	1.470	.102	7.200	.097
72	106	.115	1.451	.109	7.745	.105
73	107	.110	1.429	.104	7.437	.112
74	100	.095	1.426	.096	6.907	.105
75	108	.170	1.634	.179	12.723	.180
76	109	.120	1.495	.113	7.702	.105
77	113	.120	1.476	.114	8.035	.112
78	113	.145	1.619	.149	10.386	.142
79	114	.125	1.493	.122	8.580	.120
80	114	.125	1.593	.126	8.848	.135
81	114	.115	1.679	.122	8.539	.127
82	115	.115	2.819	.117	7.900	.075
83	115	.165	1.570	.150	10.152	.112

FULL-DERAILMENTS YAW ANGLE= 0 DEGREES

84	58	.179	.879	.104	7.152	.186
85	58	.211	.805	.121	8.607	.275
86	59	.290	.702	.148	10.679	.371
87	59	.325	.816	.169	11.995	.370
88	63	.183	.993	.111	7.711	.179
89	63	.160	.944	.097	6.662	.165
90	63	.170	.898	.094	6.396	.186
91	64	.252	.842	.114	8.087	.234
92	64	.243	.839	.124	8.308	.248
93	64	.270	.846	.147	10.833	.323
94	66	.151	.846	.077	5.471	.144
95	66	.156	.798	.004	5.898	.186
96	67	.133	.901	.071	4.545	.138
97	67	.096	.884	.063	4.429	.124
98	68	.105	.822	.052	3.463	.105
99	68	.140	.848	.000	5.470	.150
100	68	.140	.866	.002	5.601	.165
101	72	.220	.690	.103	7.088	.263
102	72	.195	.780	.097	6.825	.210
103	72	.175	.753	.091	6.350	.202
104	98	.465	.768	.248	16.577	.548

FULL-DERAILMENTS YAW ANGLE= 3 DEGREES

105	91	.115	.372	.026	1.768	.097
106	91	.105	.282	.019	1.294	.097
107	91	.100	.413	.024	1.569	.082
108	92	.355	.454	.112	7.620	.442
109	94	.100	.346	.020	1.481	.090
110	94	.080	.262	.016	1.134	.097
111	95	.155	.326	.029	2.046	.135
112	97	.085	.436	.025	1.783	.090

APPENDIX B

DESCRIPTION OF PHASE ONE APPARATUS AND WHEELCLIMB EXPERIMENTS

B.1 Description of Wheelset Apparatus

The development of validated derailment criteria has been inhibited previously by practical limitations in obtaining a comprehensive set of experimental measurements of critical variables under a range of conditions. The apparatus used in this research is designed to provide detailed measurements of wheelset motions and loading during the evolution of derailment events. It is also designed to provide sufficient control of test conditions so that the reproducibility of results may be established and the complete spectrum of phenomena necessary for derailment prediction be explored.

The apparatus used to study wheelclimb derailment is a one-fifth scale model wheelset described in detail in [29]. The wheels and rails are machined to unworn profiles from a polycarbonate resin material which assures proper scaling of the wheel/rail contact (creepage) forces in relation to the applied axle loading. The wheelset has lateral, vertical, yaw, and roll degrees of freedom, and is attached to a force measuring system with vertical and lateral freedoms, the latter simulating a generalized truck mass. The track structure is tangent track, rigid in bending and torsion to eliminate interactions between wheelset and track deflections, and maintained to Class 6+ geometry [31].

The apparatus consists of the following elements, shown in Figure B.1:

a) Wheelset or truck model, dynamically scaled from the full-scale prototype. Applied static and dynamic forces are scaled so that dynamic behavior of the prototype is reproduced.

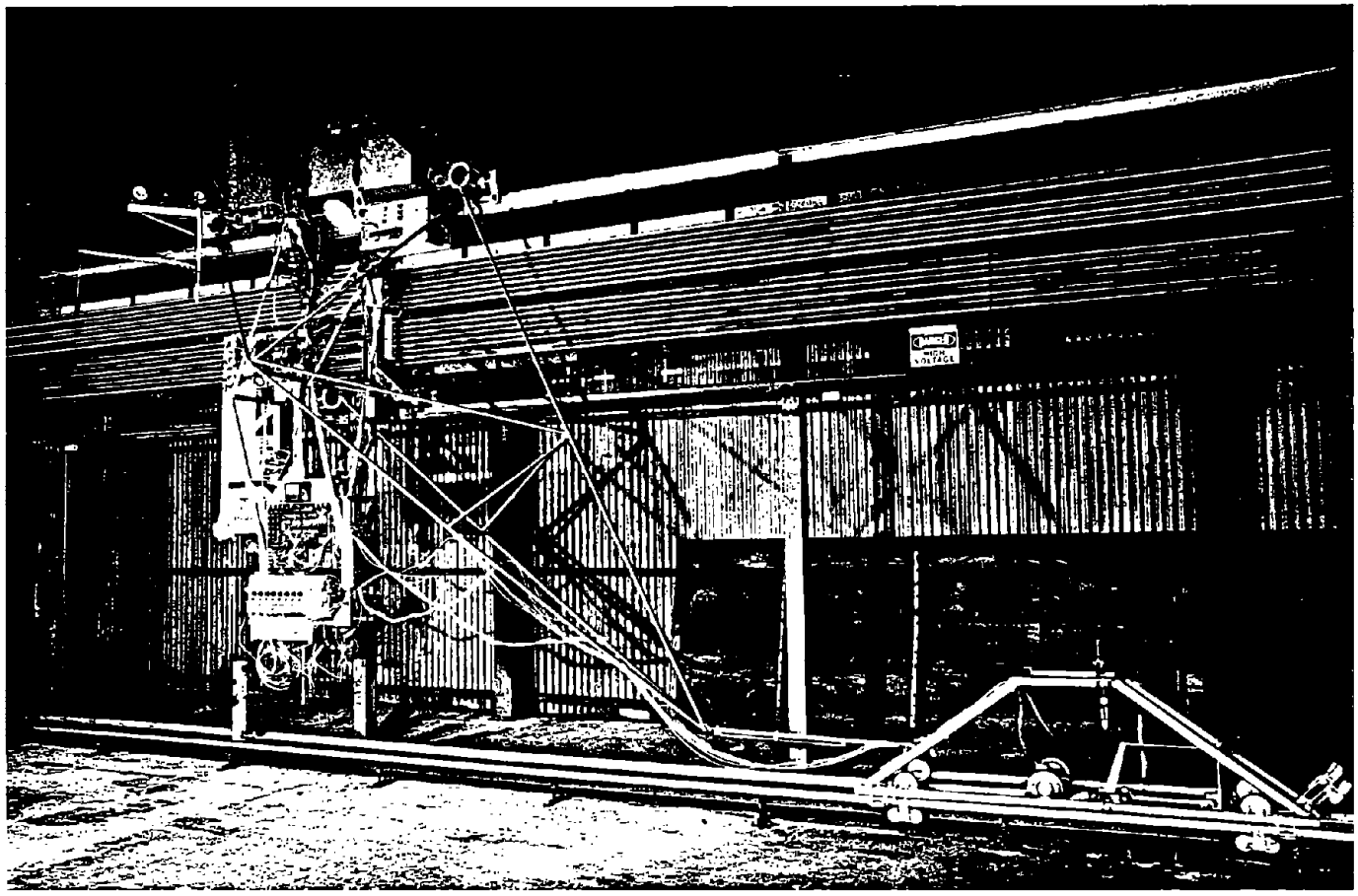

Figure B.1 Complete Scale Model Wheelset Experimental Apparatus, Showing Model Wheelset, Linkage and Gimbal System, Idler Carriage, and Powered Instrumented Test Carriage.

b) Linkage and gimbal systems providing the model with vertical and lateral displacement, yaw, roll, and pitch angular degrees-of-freedom. The sequence of freedoms provided is such that all possible body orientations and trajectories are obtainable, assuring normal wheel contact at all times.

c) Idler carriage traveling along the track with an independent suspension system to provide an attachment point for the linkage system. Running on well-aligned smooth rails, this rubber-tired carriage provides a reference for all force and displacement measurements. It also provides a platform for application of suspension forces, and is a mechanical link to external propulsion, power, data reduction, and data recording equipment.

d) Powered general purpose test carriage, providing velocity-controlled propulsion, instrumentation power, signal conditioning, and data recording. The powered carriage runs on an independent rail system.

In the following paragraphs the wheelset and support system are described in detail.

Wheelset Model and Gimbal System

The wheelset consists of two polycarbonate resin wheels machined by numerically-controlled lathe to the specified profile (Figure B.2), mounted on an instrumented axle. The gimbal system, shown in Figure B.3 and B.4, provides yaw, roll, and pitch angular degrees-of-freedom to the wheelset or truck body. Each rotation is supported by precision bearings mounted in close tolerance housings. The gimbal unit is designed to minimize deflections other than the desired rotations, yet be lightweight to reduce influence of gimbal inertia on wheelset dynamics.

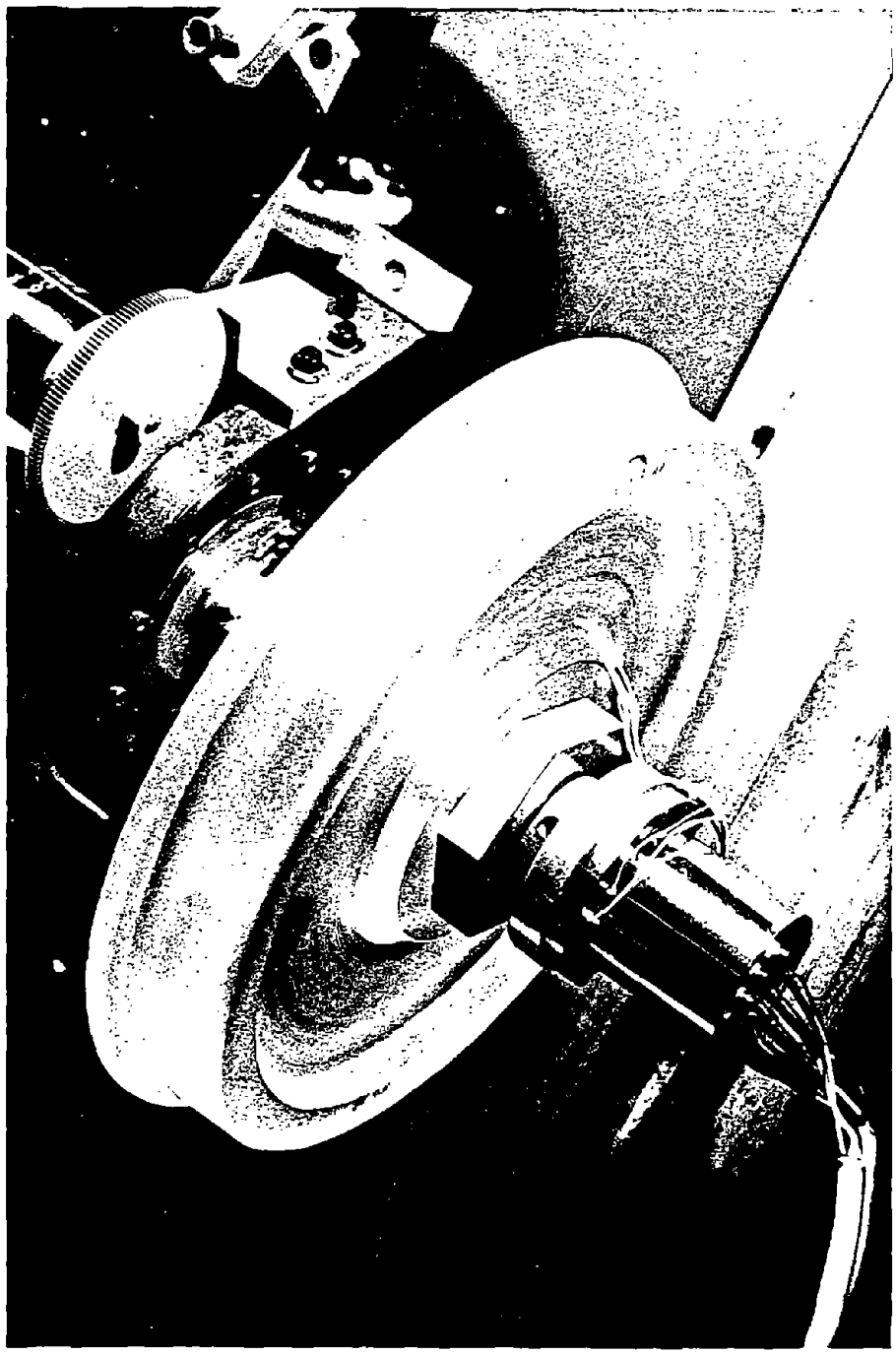

Figure B.2 Scaled Wheels Machined to Profile of New Full-Scale Wheels.

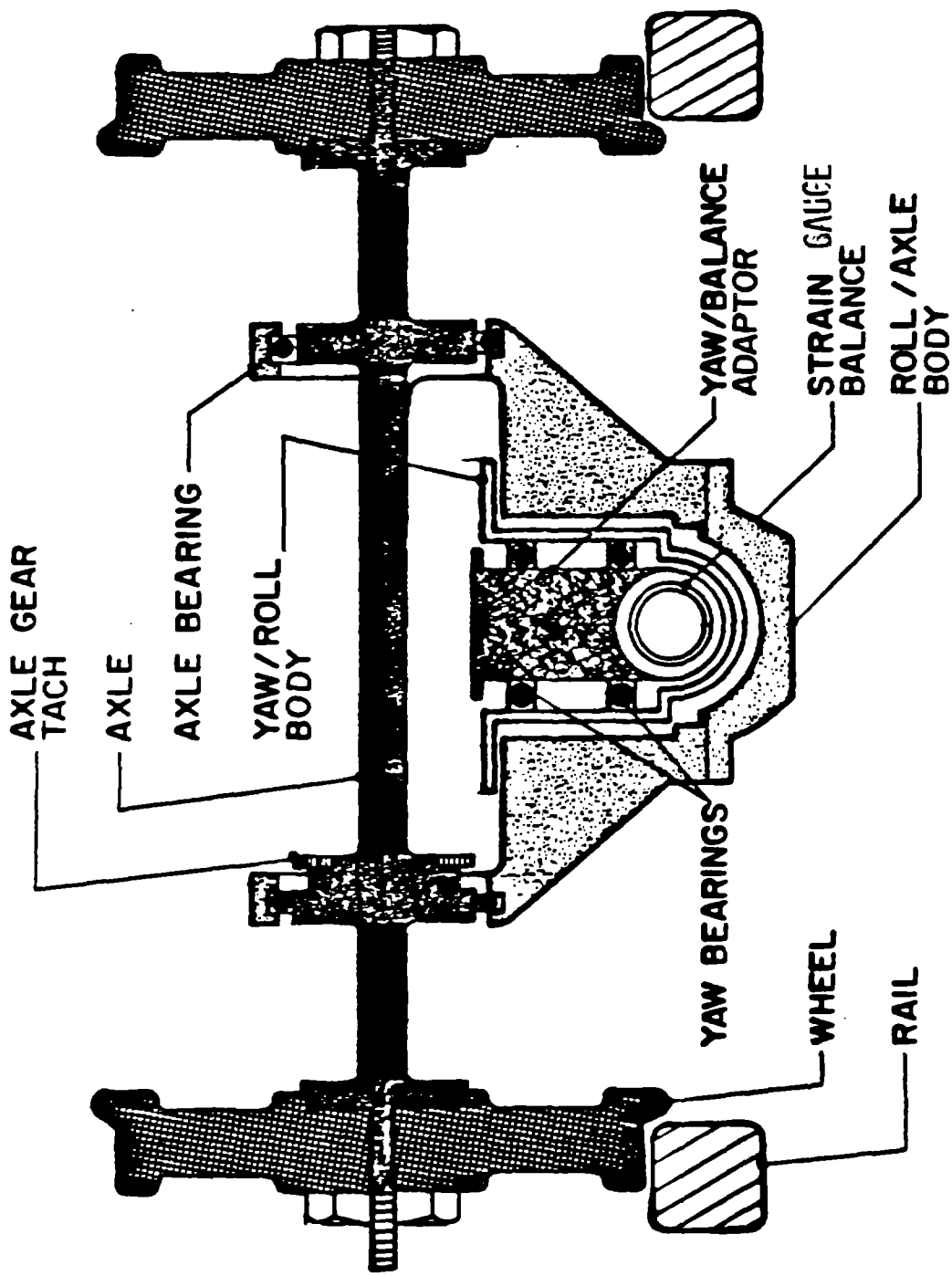

Figure B.3 Rear Section View of Wheelset Mounted in Gimbal System.

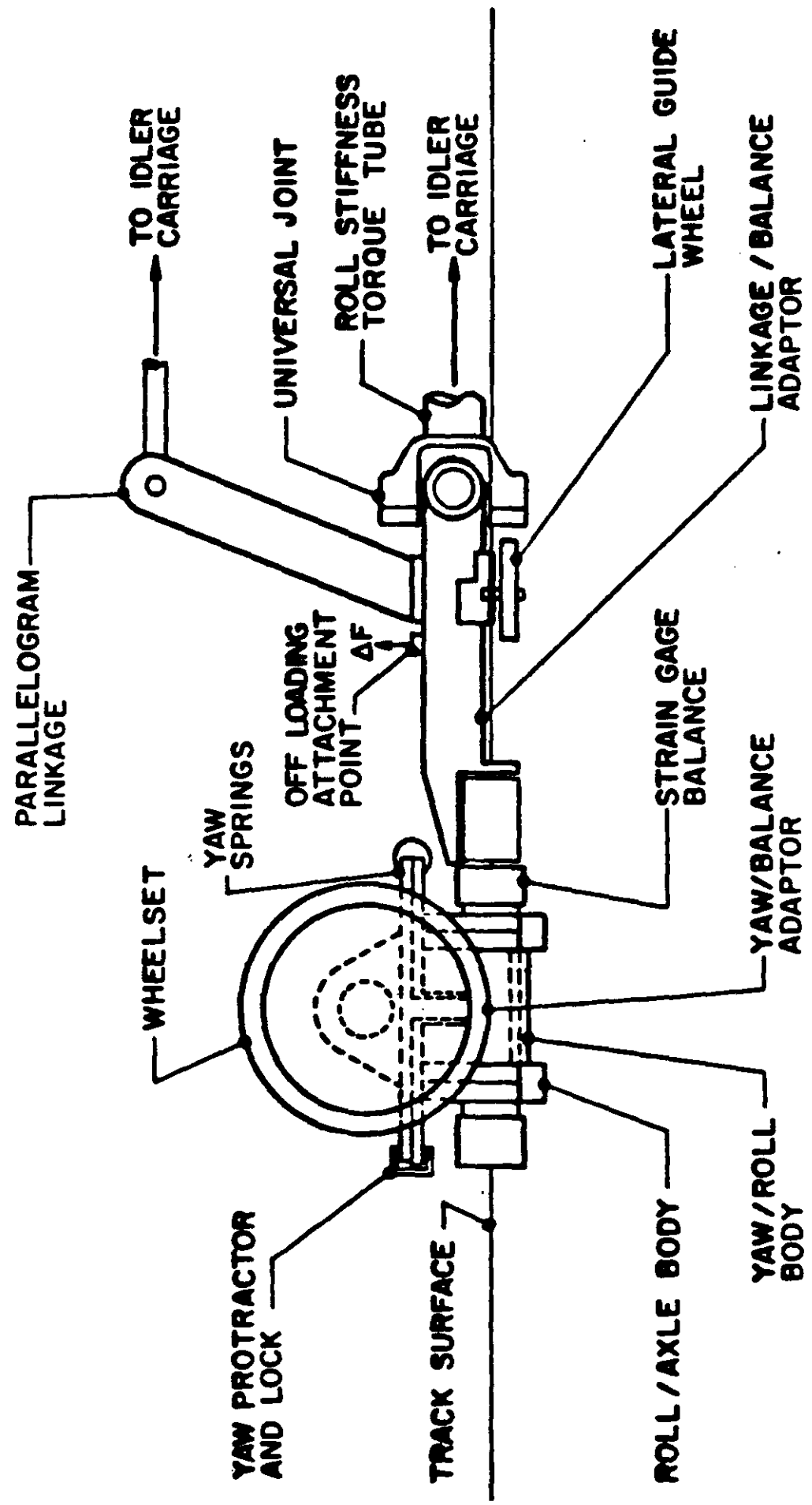

Figure B.4 Side View of Assembled Wheelset, Gimbal, and Linkage System

The base end of a six-component strain gauge balance is fixed to the linkage/balance adapter, constrained to move parallel to the track without roll, yaw, or pitch. By so doing, any forces or moments transmitted through the gauge to elements clamped to the metric end of the gauge are sensed in rail coordinates. The yaw/balance adapter is rigidly clamped around the gauge,with its other cylindrical axis oriented vertically.

The yaw/roll body adds the first rotational freedom. Its tee-section encloses that of the yaw/balance adapter; the yaw axis is supported by bearings, while the cylindrical section along the gauge allows clearance for ± 3 degrees yaw rotation. The lower cylinder of the yaw/roll body provides the axis of rotation for roll. On the top of the yaw/roll body is a yaw plate, parallel to a similar plate on the yaw/balance adapter. These plates are used for establishing the nature of the yaw freedom; at one end of the plates are locations for yaw springs, while at the other end are locking clamps to prevent yaw displacement as dictated by the experiment.

The roll/axle body allows the second rotational freedom. The lower bearing supports surround the cylindrical housing of the yaw/roll body, with bearings used for support. The yaw bearings pass through the center of the roll/axle body with clearance. The upper bearing supports are for the axle rotation freedom. In truck experiments, the axle is replaced by the truck center bolster.

The assembled gimbal system is shown in Figures B.5 and B.6. The strain gauge axis, coincident with the roll axis, is parallel to the track between the wheel/rail contact points (when wheelset is centered). The yaw rotation axis passes through the center of the wheelset.

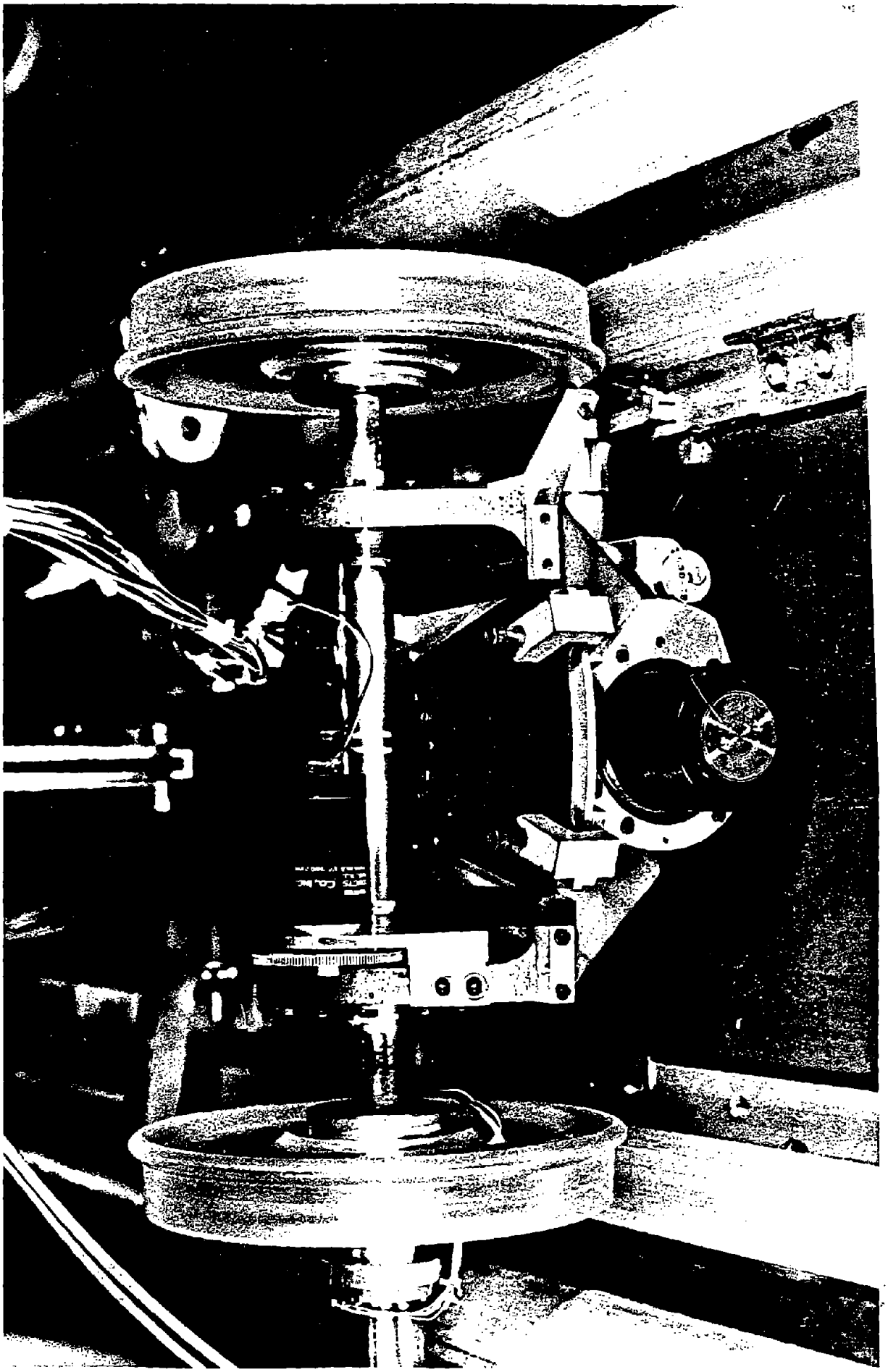

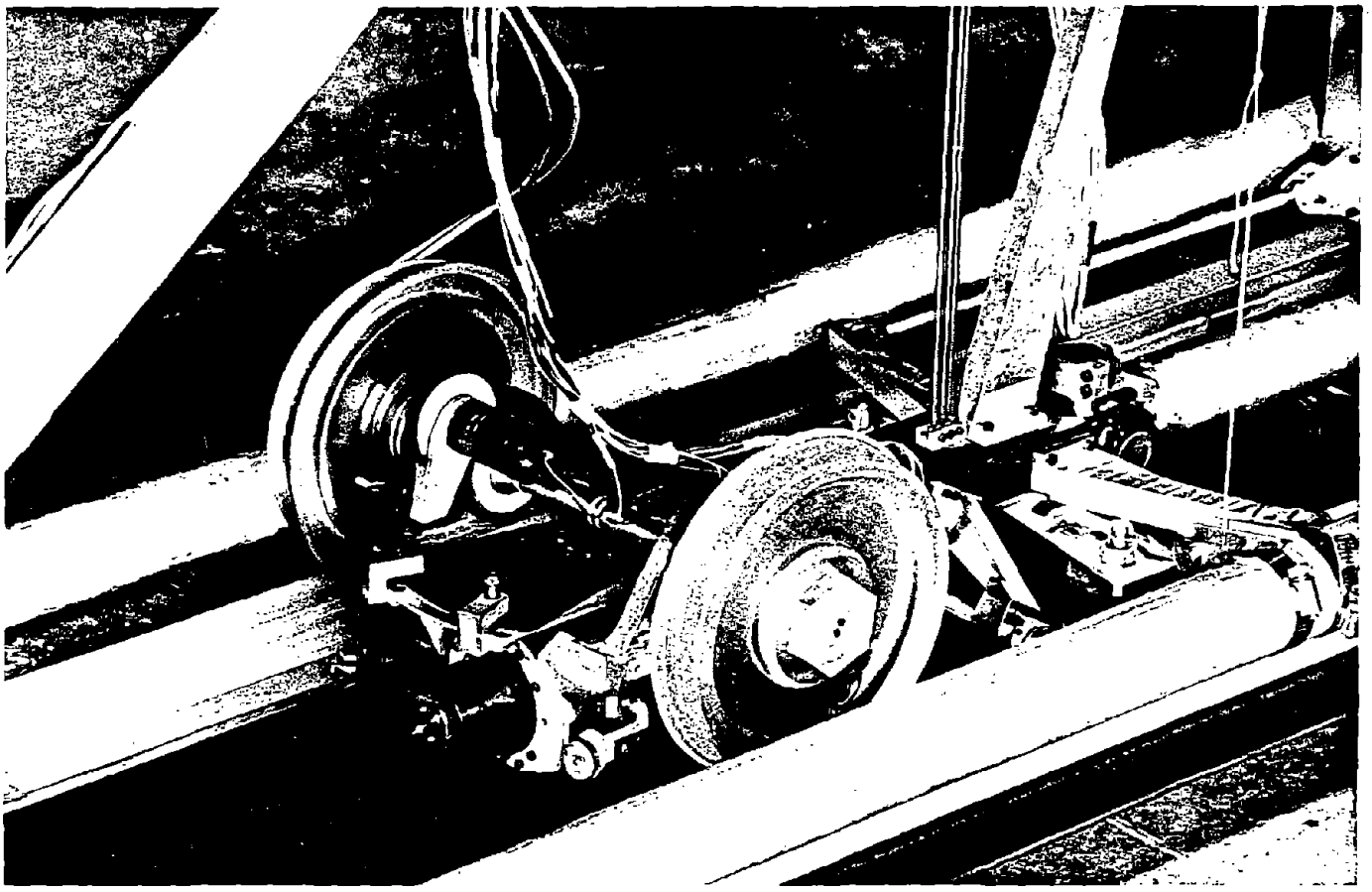

Figure B.6 Wheelset and Gimbal, Showing Yaw Protractor and Locking Device.

Lateral/Vertical Linkage System

The lateral/vertical linkage system, shown in Figures B.4 and B.7 connects the strain gauge balance to the idler carriage bulkhead in a manner that sustains its orientation parallel to the rails. The bulkhead is rigidly fixed to the idler carriage, so it is a fixed inertial plane normal to the rail x axis. Lateral and vertical freedoms with no yaw or pitch rotation are provided by the parallelogram linkages. The linkages by themselves do not provide adequate roll stiffness to the gauge balance base; this stiffness is provided by a torque tube connecting two automotive universal joints.

Idler and Powered Test Carriages

The track-mounted idler carriage with installed linkage/gimbal/wheelset assembly is shown in Figure B.8. The carriage serves three functions:

a) Provides a fixed reference for all force and displacement measurements.

b) Provides a platform for application of static and dynamic suspension vertical and lateral forces and moments to wheelsets and trucks.

c) Provides a link to main overhead carriage for propulsion, on-board power, data reduction, and data recording.

The carriage frame is fabricated of two-inch welded aluminum tubing for high strength to weight ratio. At each end of the carriage are three sets of pre-loaded opposing wheels that provide the carriage with its own independent suspension. Each wheel is aluminum with specially molded rubber tires. The rubber on the top and side wheels is hard to provide a stiff suspension as they roll on the smooth, aligned surfaces of the rail top and rail mounting bracket side surfaces. The rubber on the wheels riding on the rougher underside of the track support structure is softer. The pre-load is adjusted through cams built into offset wheel axles.

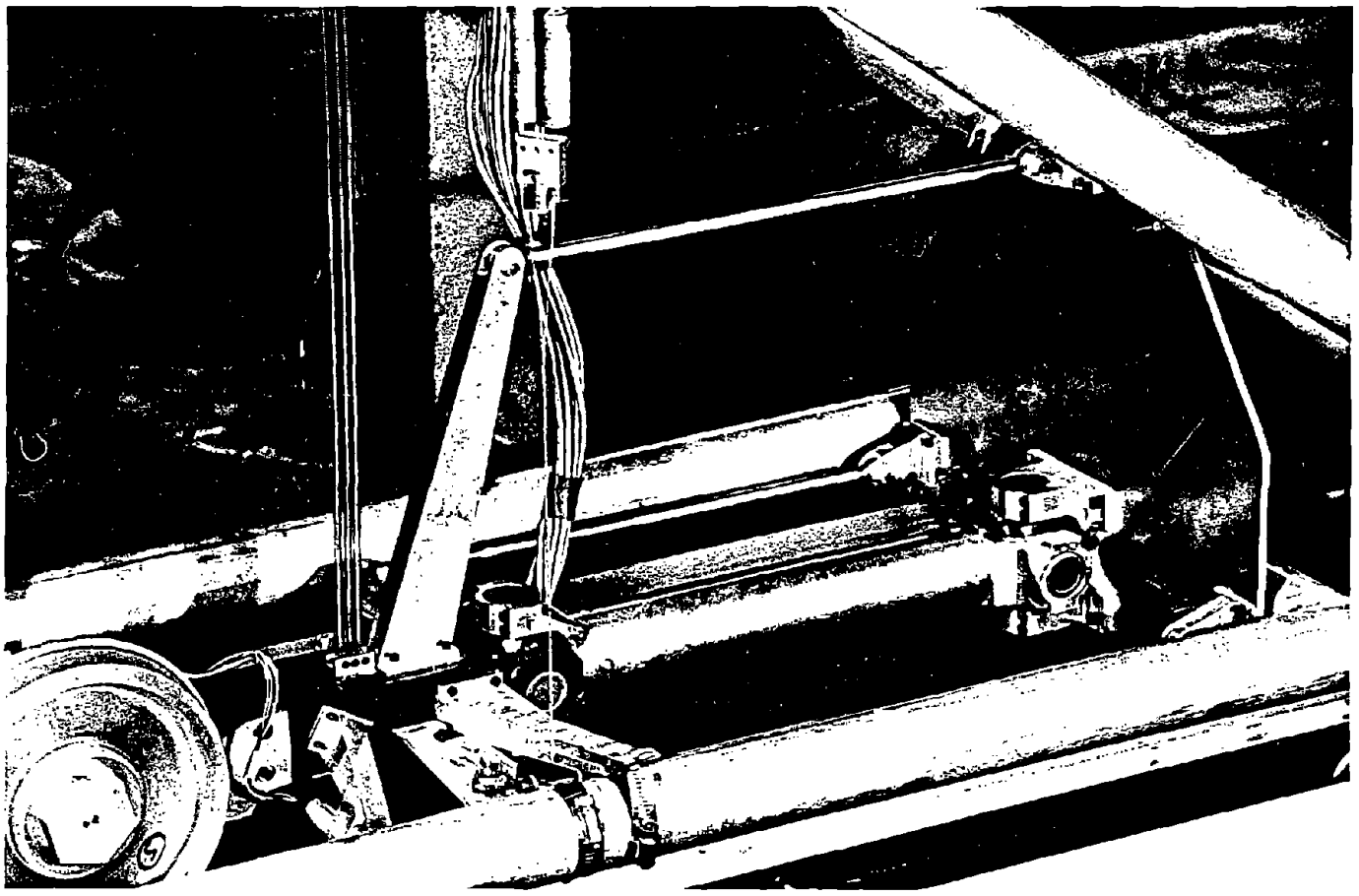

Figure B.7 Parallelogram Linkage and Torque Tube Preserving Rail Coordinate System Orientation of Gage Balance Through Connections to Bulkhead.

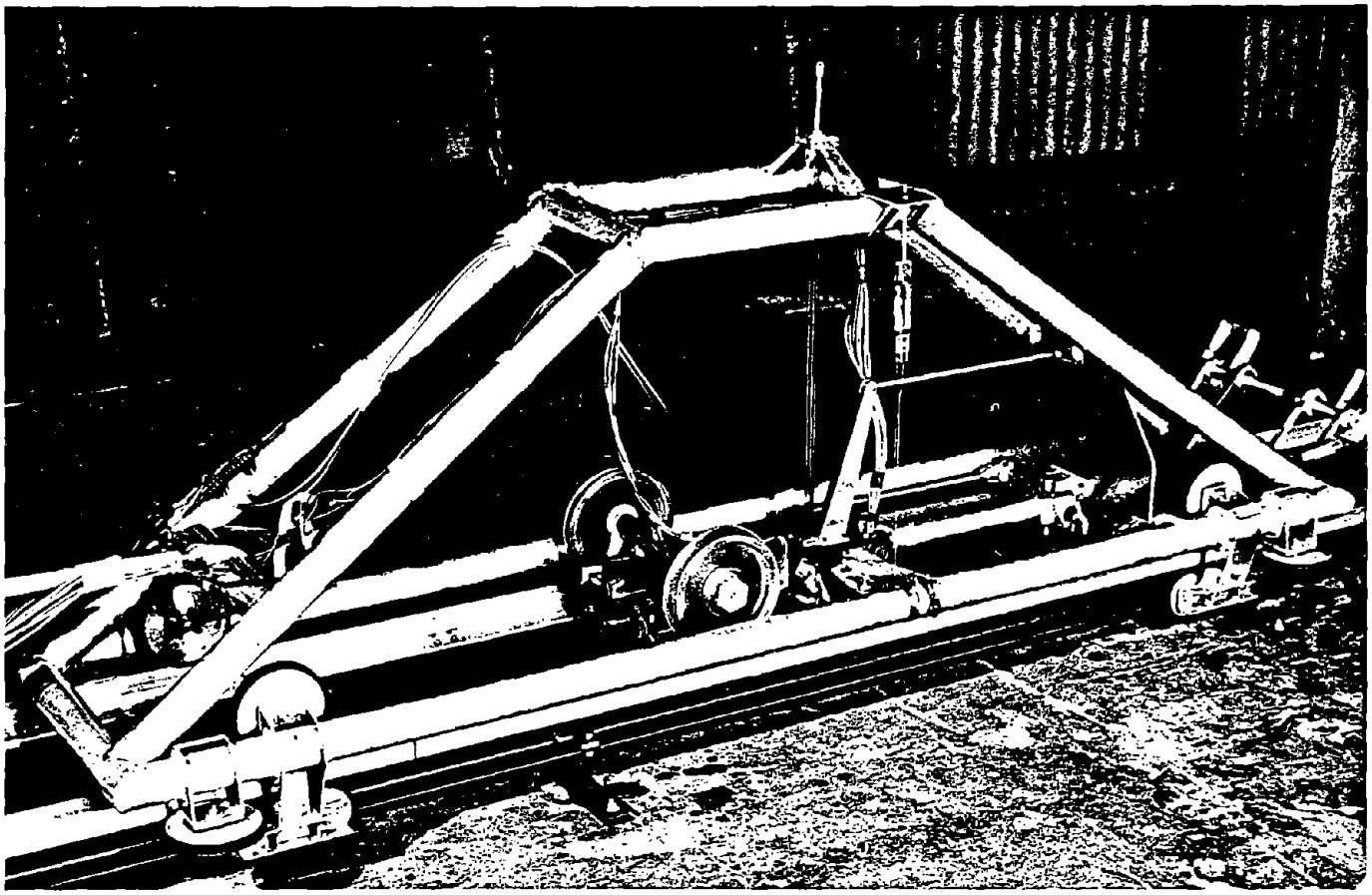

Figure B.8 Wheelset Apparatus Mounted in Idler Carriage.

The test carriage is powered by a variable displacement hydraulic pump with velocity feedback to provide precise velocity control (speed constant to 1%). The carriage maximum velocity is 12.2 m/sec. The complement of signal conditioning and recording equipment on-board is described in the following instrumentation section.

B.2 Instrumentation

The transducers employed in the wheelset experiments are listed in Table B.1. The principal force measurement device is a six-component internal strain gauge balance, shown in Figure B.9. This device measures all force and moment components transmitted from the base end to the gimbal-mounted model. Since the balance is maintained parallel to the track the forces and moments are measured in rail coordinates. When the wheelset is centered, the axis of the gauge is colinear with the contact points, as shown in Figure B.10.

Translational and angular displacements are measured by DCDT-type* linear transducers and geared potentiometers, positioned as shown in Figure B.10. The linear transducers measure track gauge and the lateral position of the balance, while the pots measure yaw and roll angles. Accelerometers measure wheelset and track lateral accelerations.

Axle speed is not constant, due to flanging, so that this variable is measured by DC tachometer (Figure B.10). This signal will also indicate abnormal test conditions such as gross wheel slippage.

---

* A Direct Current Displacement Transducer operates on the linear variable displacement transducer principle. An oscillator, rectifier, and low-pass filter built into the transducer housing provide a DC voltage output proportional to displacement.

TABLE B.1 INSTRUMENTATION USED IN SINGLE WHEELSET EXPERIMENTS

Transducer	Variable Measured	Symbol
Six-Component Strain Gauge Balance	Axial Force	F_x^+
	Lateral Force	F_y^+
	Vertical Force	F_2^+
	Yaw Moment	M_2^+
	Roll Moment	M_x^+
DC Generator (tachometer)	Wheelset Rolling Velocity	Ω
Geared Potentiometers (2)	Yaw Angle	ψ
	Roll Angle	ϕ
DCDT Displacement Transducers (2)	Lateral displacement of wheelset, relative to track	y
	Track Gauge	$\delta_1-\delta_2$
Servo Accelerometers (2)	Wheelset lateral acceleration	$\ddot{y}$
	Track lateral acceleration	$\ddot{\delta}$

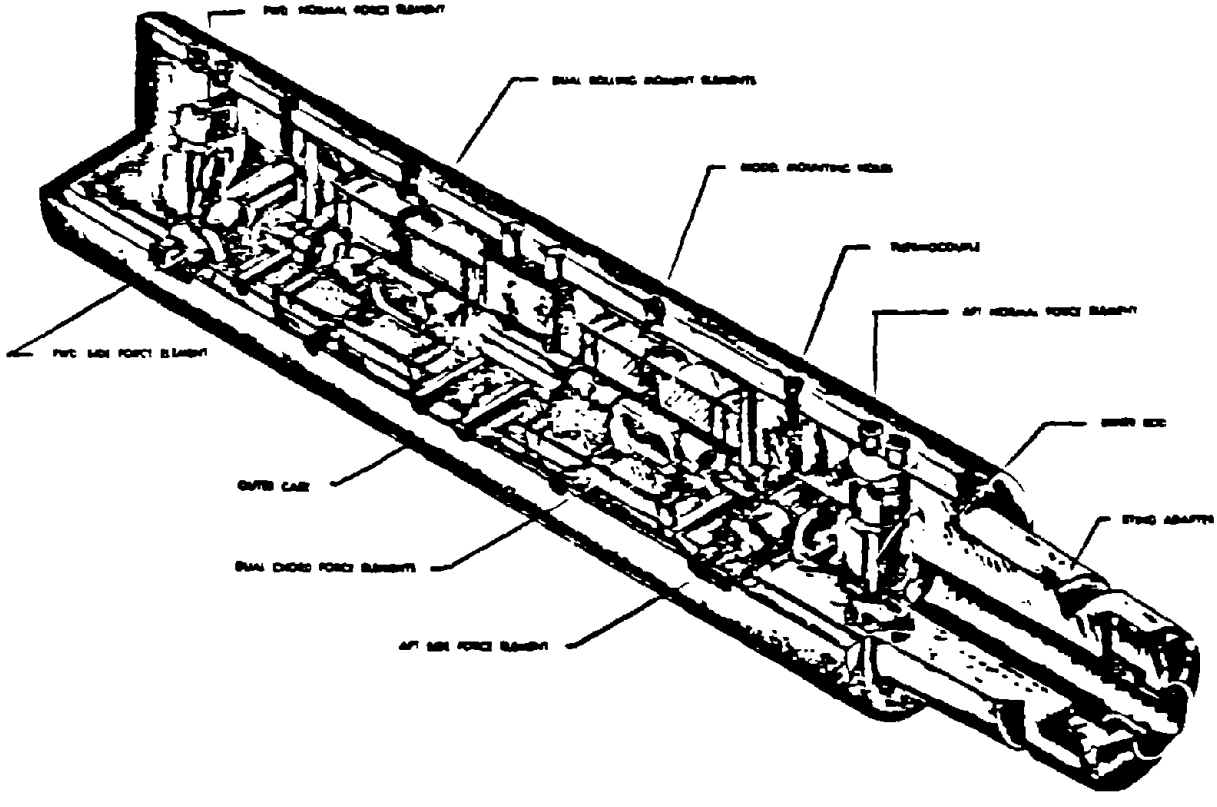

Figure B.9 Section View of Six-Component Internal Strain Gauge Balance.

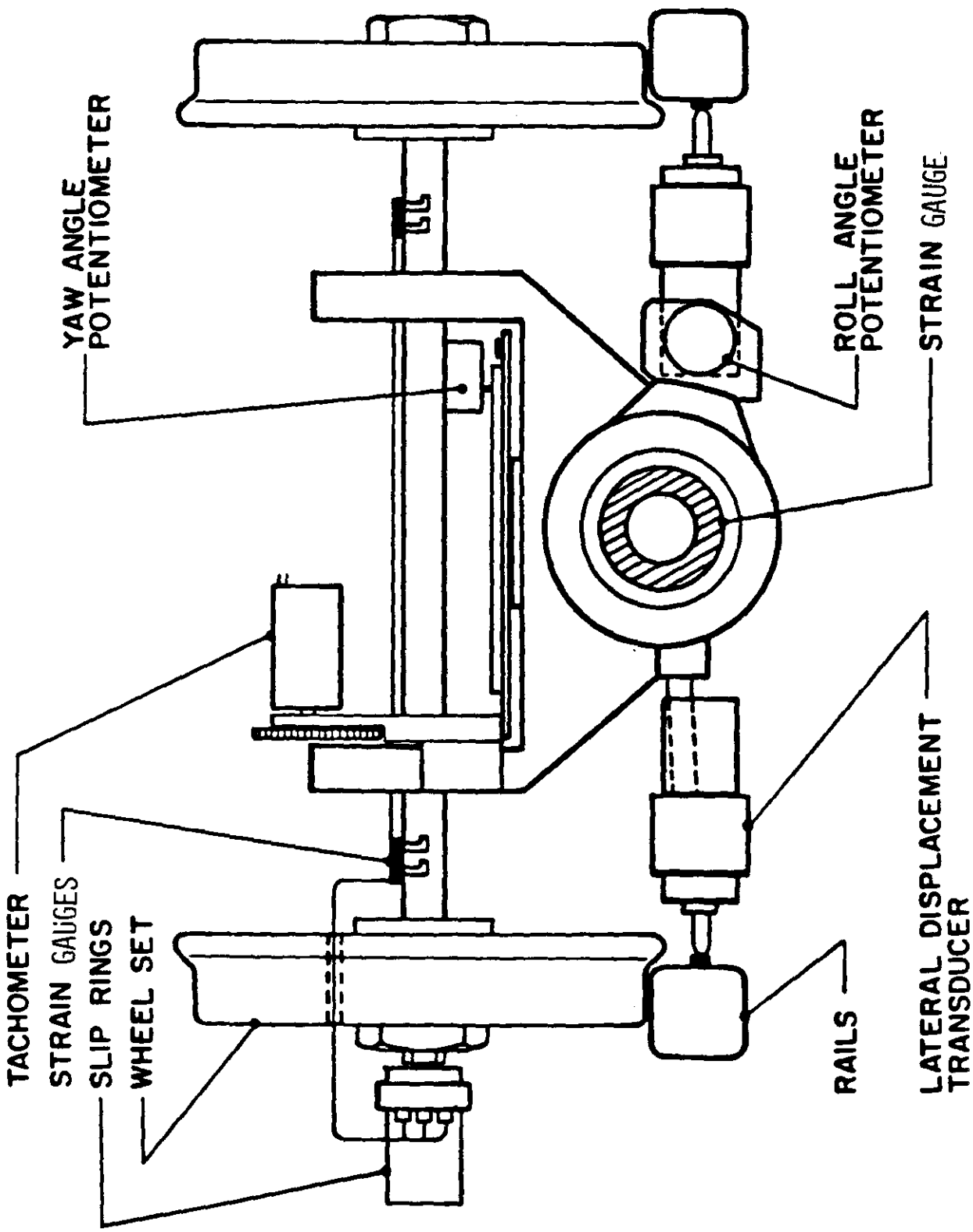

Figure B.10 Wheelset Instrumentation.

B.3 Data Acquisition and Reduction

The system used for data acquisition and reduction is shown schematically in Figure B.11. All data from the wheelset transducers is recorded on a four track frequency modulated (FM) cassette tape recorder. Eight channels are multiplexed onto each of two tracks, recording lower bandwidth signals. The higher bandwidth accelerometer signals are recorded directly on the remaining two tracks. Lowpass (25 Hz) analog filters are used between the transducers and multiplexer (100 samples/s) to minimize aliasing effects. One channel of the multiplexer is dedicated to recording an identification signal used to mark the locations of calibration data and running time records on the cassette tape.

After a series of test runs have been completed, the cassettes are played back for digitization of the signals. The multiplexed tracks are demultiplexed, and all signals are again lowpass filtered prior to digitization to minimizing aliasing. The sampling rate is 200 Hz. Data is stored on magnetic tape and reduced on an HP-1000 minicomputer system.

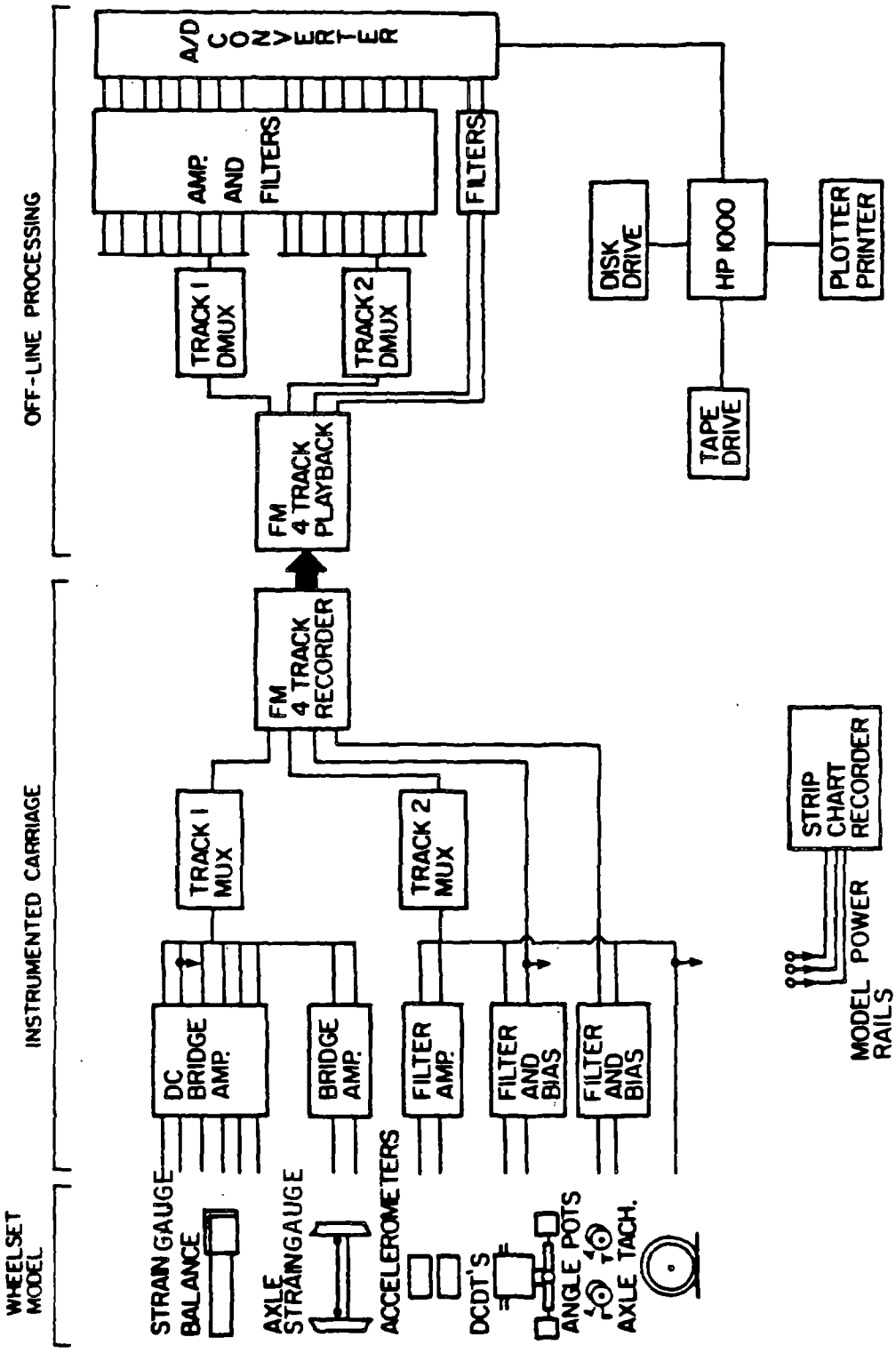
WHEELSET MODEL
INSTRUMENTED CARRIAGE
OFF-LINE PROCESSING
STRAIN GAUGE BALANCE
AXLE STRAIN GAUGE
ACCELEROMETERS
DCDT'S
ANGLE POTS
AXLE TACH.
DC BRIDGE AMP.
BRIDGE AMP.
FILTER AMP.
FILTER AND BIAS
FILTER AND BIAS
TRACK 1 MUX
TRACK 2 MUX
FM 4 TRACK RECORDER
FM 4 TRACK PLAYBACK
TRACK 1 DMUX
TRACK 2 DMUX
AMP. AND FILTERS
FILTERS
A/D CONVERTER
DISK DRIVE
HP 1000
TAPE DRIVE
PLOTTER PRINTER
STRIP CHART RECORDER
MODEL POWER RAILS

B.4 Track and Support Structure

Track Structure

To perform repeatable, systematic experiments on the dynamics of rail vehicles requires careful control and detailed knowledge of the track. Track irregularities provide the principal disturbance input to the truck, and coupling between vehicle and track support structures may be significant. Track in service is subjected to intermittent loadings, wear, extremes of temperature, and variations in other ambient conditions that lead to irregularities in track geometry, railhead profile, and rail surface condition that may vary with time and track location.

The objective of the track design in this program is to minimize the influence of these effects in order to isolate the important wheelset dynamic properties. It is emphasized that non-ideal track characteristics are extremely important to derailment in the field; in future experiments the importance of such effects may be explored by systematically introducing them into the model experiments.

Consistent test track conditions are maintained through the following:

a) The track structure is designed to provide sufficient static and dynamic stiffness so that changes in track geometry under load are negligible. Such high stiffness isolates the truck dynamics; in subsequent programs track flexibility may be incorporated in the experiments to quantify the importance of this effect.

b) Track geometry is specified using statistical models, calibrated with survey data taken at periodic time intervals. Adjustments are provided for vertical and lateral alignment, gauge, and cross elevation.

c) The railhead profile is machined to be invariant over the track length. Profiles from different track locations may be sampled over time to check wear through use of optical comparators and contact impression tape.

d) Uniform surface condition of the rails is maintained by its indoor location and periodic cleaning with methyl alcohol as standard test procedure.

e) Irregularities induced by temperature variations (range of 27°C yearly) are minimized by design; measurable effects are eliminated through realignment.

These design goals are quantified as specifications in Table B.2. The remainder of this section describes the design and measured characteristics of the track and support structure.

The support structure shown in Figures B.12 and B.13 is an elevated dual channel beam configuration with cross webs for increased torsional rigidity. The structure is supported on 1/2 in. (1.27 cm) threaded studs, permitting vertical alignment and cross elevation adjustment. The support studs are welded to steel cross ties, which are secured to the concrete floor wi thunderstud bolts. Rail lateral alignment and gauge adjustment are achieved through movement of rail mounting brackets along a steel plate bolted to

TABLE B.2 DESIGN GOALS FOR SCALE MODEL TRACK

Parameter	Goal
Track Stiffness:	
- Vertical	0.125 mm deflection for 445 N vertical load on both rails
- Lateral	0.125 mm deflection for 111 N lateral load on one rail
Alignment:	
- Vertical & Lateral	Spectral density, in scale, as good as or better than Class 6 track.
- Gauge	287 $\pm$ 0.25 mm
- Cross-elevation	$\pm$ 0.25 mm (0.08 percent slope)

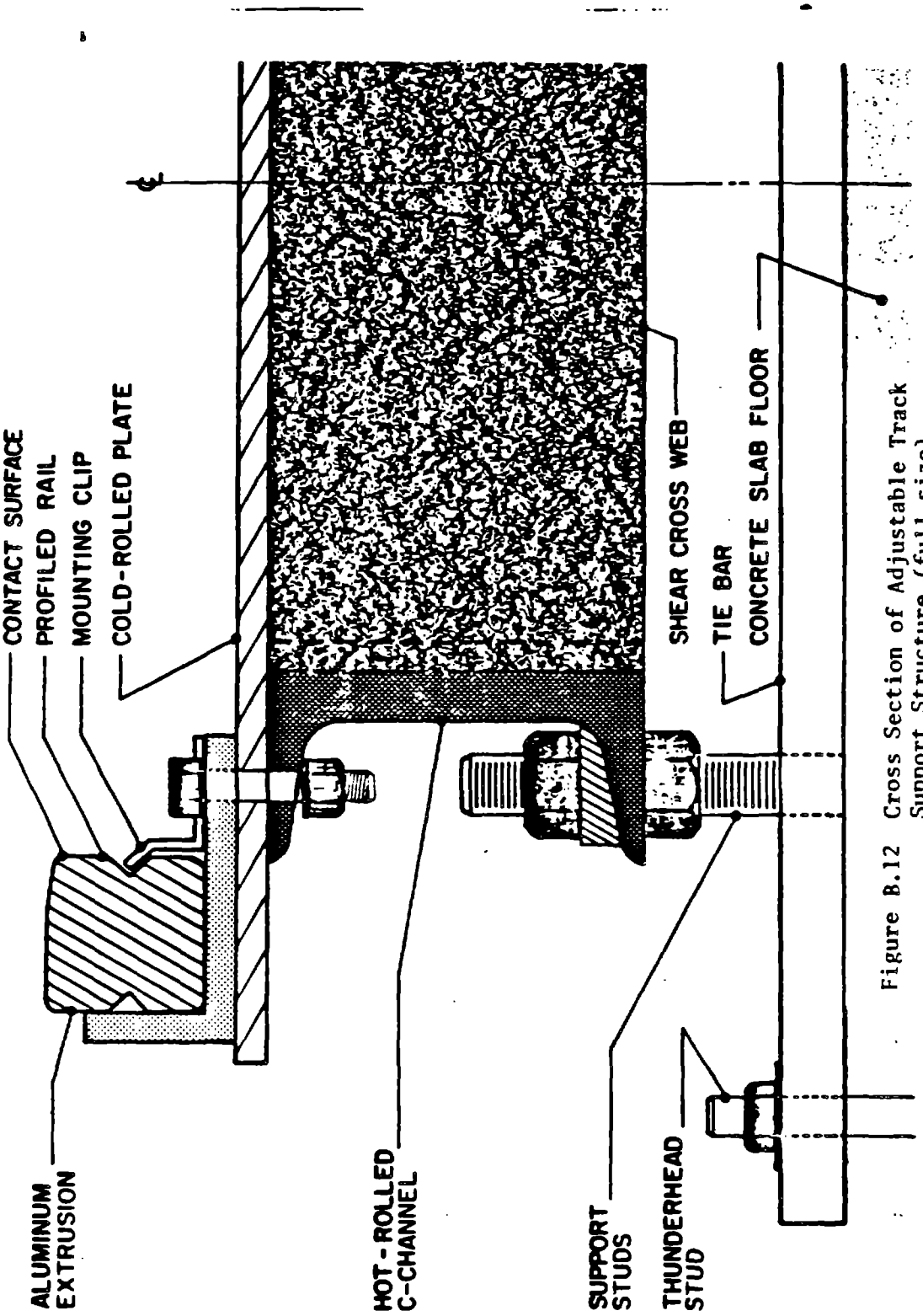

Figure B.12 Cross Section of Adjustable Track Support Structure (full size).

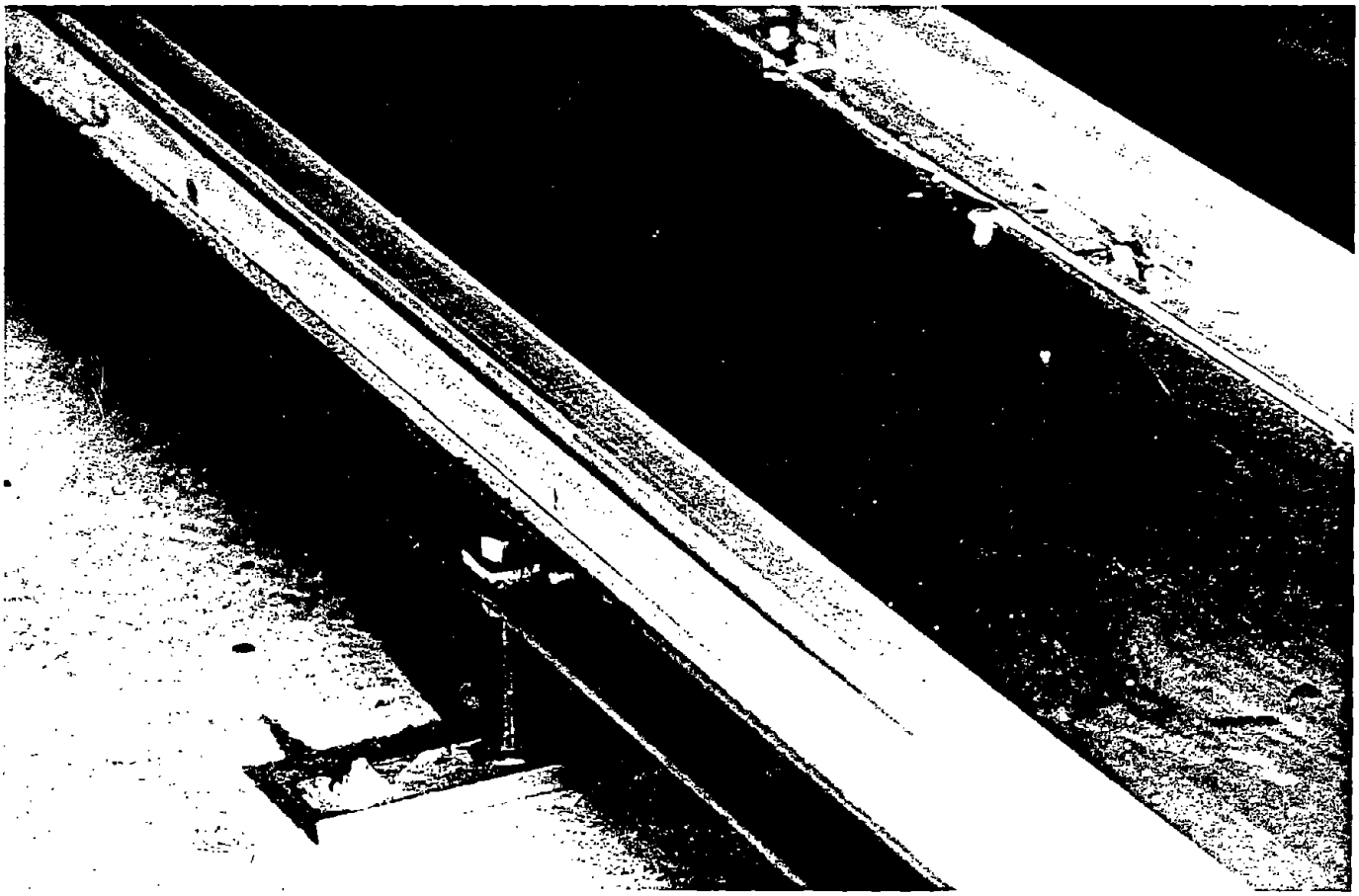

Figure B.13 Installed 213 m Scale Model Test Track.

the top of the channel beams. These adjustment mechanisms are required due to inevitable concrete floor settlement, temperature gradients, and relaxation of internal stresses in large section members that will tend to distort and misalign the track. Measured stiffness properties of the track structure are given in [29].

Measurements of Model Track Geometry

Track geometry was determined using statistical models in [29]. The resulting spectral densities for vertical and lateral alignment, cross-elevation, and gauge are given in Figure B.14 through B.17 plotted with scaled track geometry data. [31]

Railhead Profile

The rail profile used in the model track is a geometrically scaled reproduction of a new 133 lb CF and I rail. The results presented in this report are specific to the wheel and rail profiles used, and may differ for other geometries. The 1/40 rail cant is built into the model rail profile, so that the gauge edge of the railhead is vertical.

The rail section is shown in Figure B.18. The rails are machined from annealed polycarbonate resin bar stock using special cutting tools with the specified profile. Tool wear was checked to monitor profile uniformity over the rail sections. Sections were numbered in sequence of machining; they were installed in the same sequence to ensure gradual profile changes (if any) over the track length. Two contact profiles, identified as A and B, were machined so that a second surface is available at no extra cost should the first surface be changed by wear or impact damage. Two V-grooves were machined on the sides as seats for mounting spring brackets; a small extra groove is added to identify the contact profile.

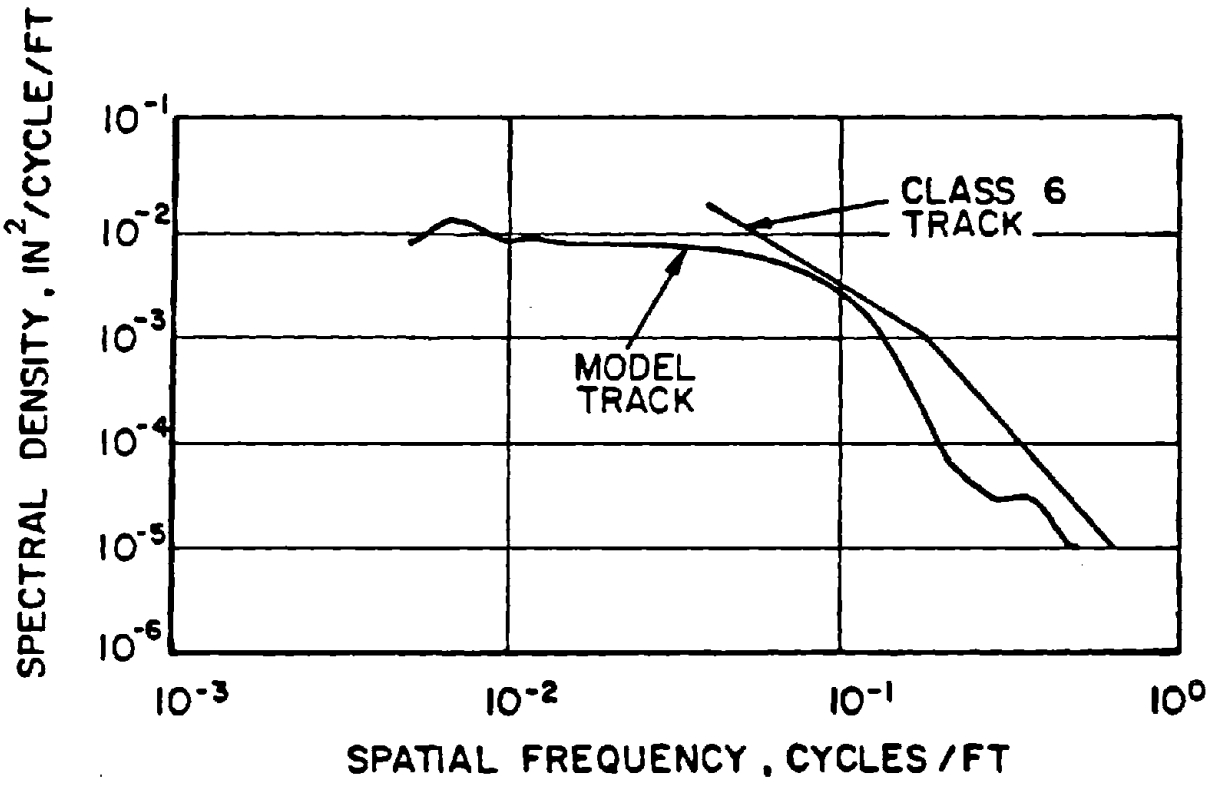

Figure B.14 Spectral Density of Model and Scaled Class 6 Track Profile (Vertical Alignment) [31].

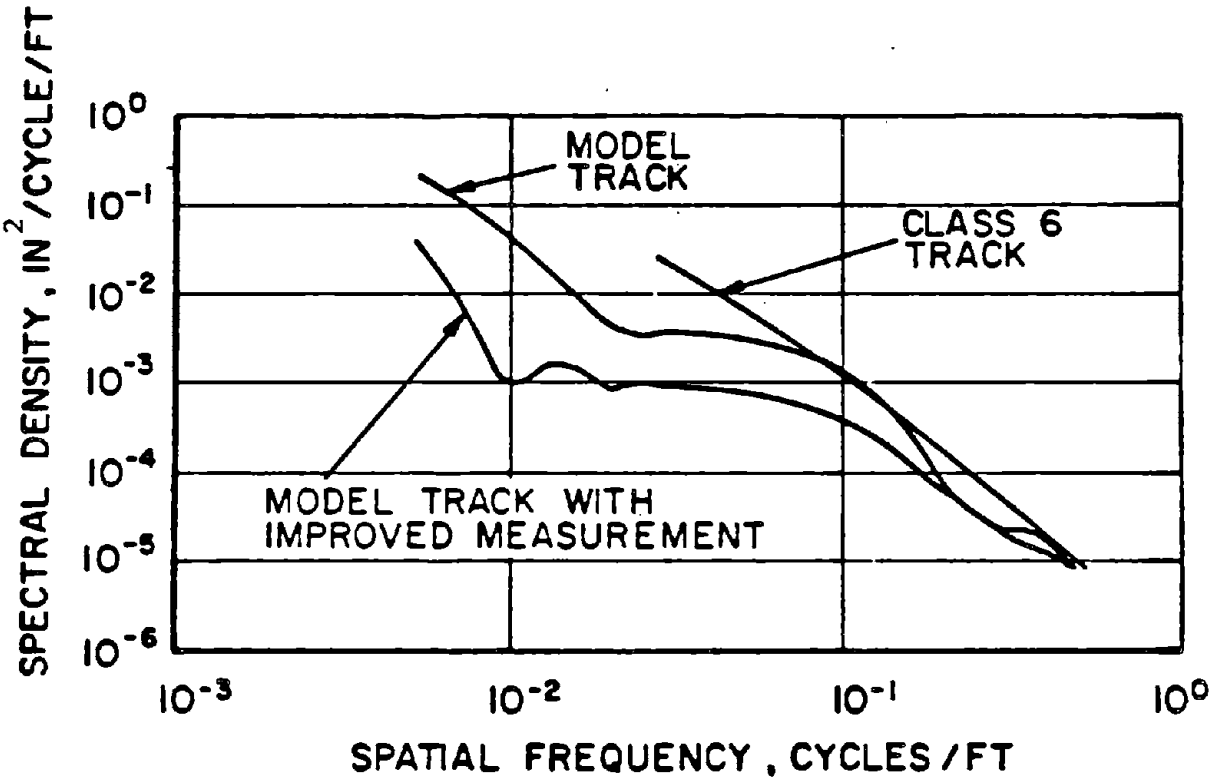

Figure B.15 Spectral Density of Model and Scaled Class 6 Track Alignment (lateral) [31].

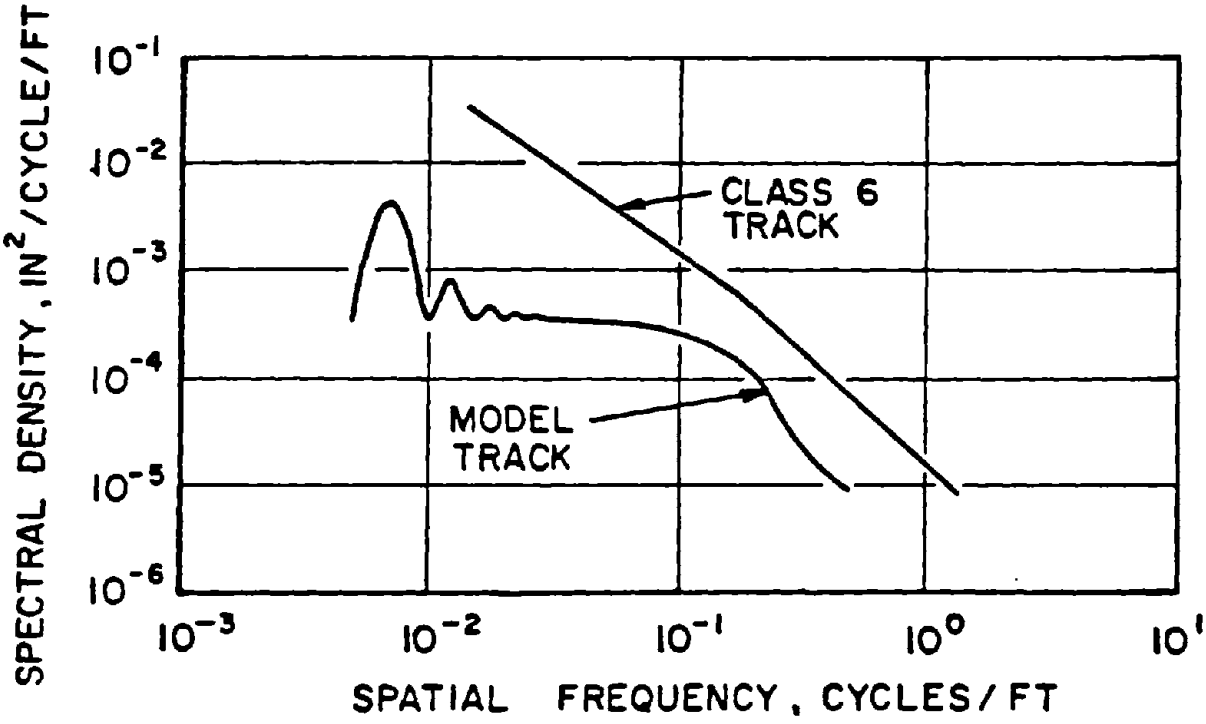

Figure B.16 Spectral Density of Model and Scaled Class 6 Track Cross Level [31].

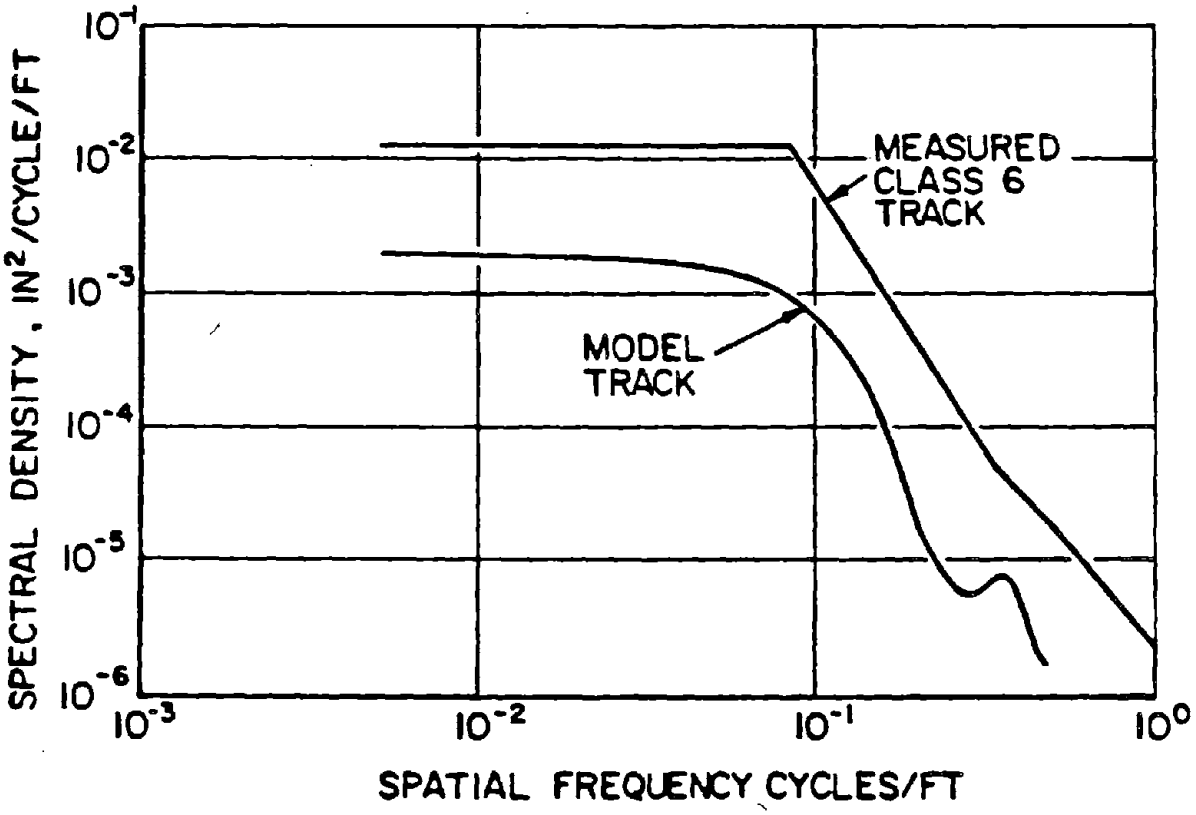

Figure B.17 Spectral Denisty of Model and Scaled Class 6 Track Gauge [31].

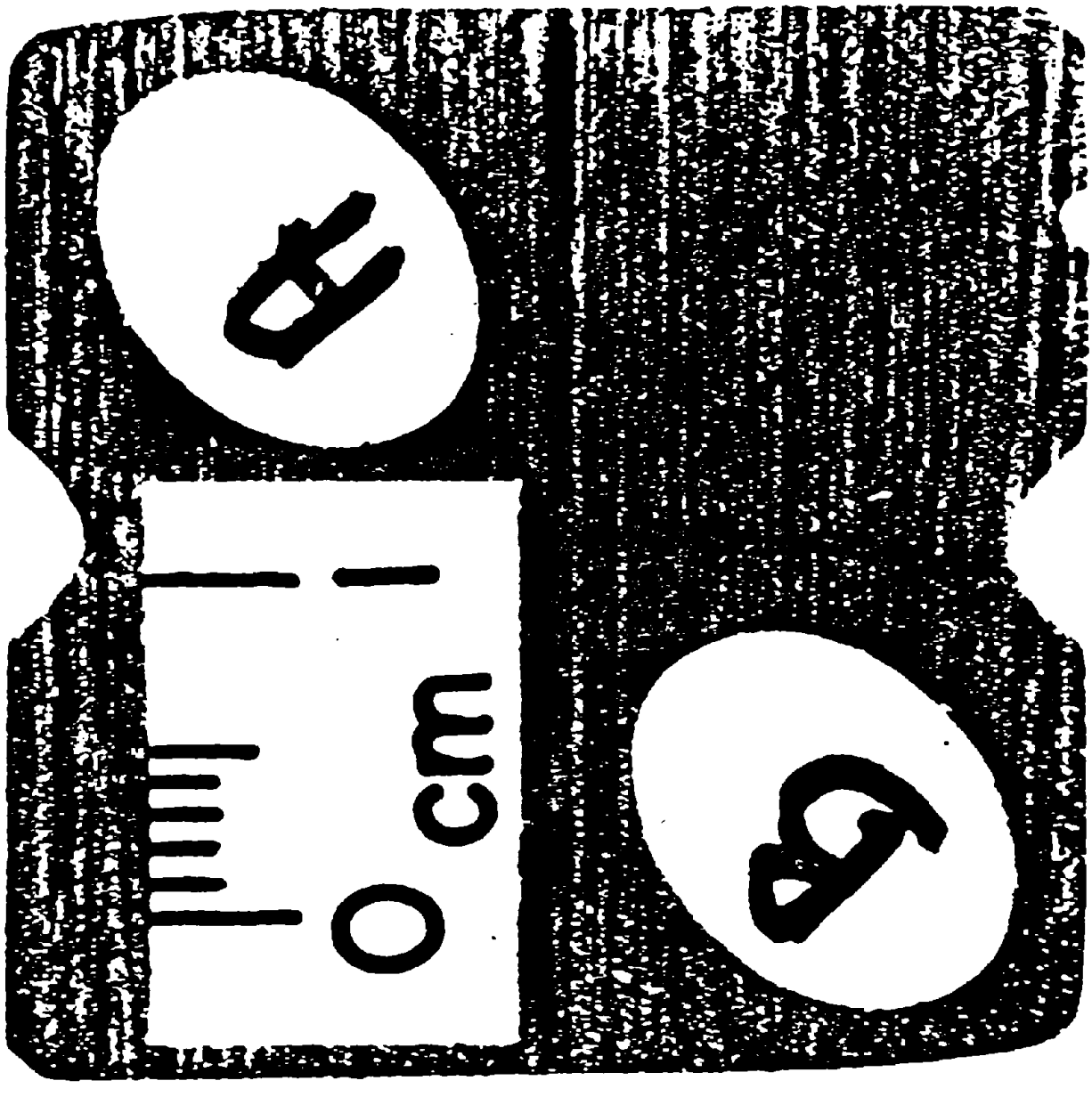

Figure B.18 Cross Section of Model Rails.

The rail is generally square in cross-section, and is considered to be rigid as mounted on the support structure. As described previously, in the present experiments rail flexibility is not included, so as to isolate truck dynamics.

Preparation of Wheel and Rail Contact Surfaces

The establishment of experimental conditions that produce scaled wheelset forces and moments was found to be critically sensitive to the coefficient of friction μ between the wheel and rail surfaces. Considerable effort was required to develop procedures for cleaning and final surface finishing to achieve uniform, realistic adhesion characteristics.

Adhesion limits μ have been measured to range from 0.1 to 0.5 in field tes using full-scale vehicles, the limit being a strong function of surface condition, presence of contaminants, and wetness, and a weak function of forward velocity. It is desirable to design experiments to operate at the upper end of the range, since the effects of all creep forces (which are proportional to μ) are more readily measured. The polycarbonate resin has a friction coefficient of 0.52 (from product literature) to 0.3 (from roller rig measurements). Under ideal conditions, therefore, it is suitable for use as a material for wheel/rail contact surfaces.

For the initial wheelset experiments the wheel profile had a satin finish resulting from the precise machining performed on a numerically-controlled lathe. The rail surface, machined using a specially contoured flycutter, had longitudinal grooves due to imperfections in the cutting tool, and lateral, scalloped markings due to movement of the rail past the cutter. Although these machining marks were less than 25 μm in depth,

they significantly reduced the achievable adhesion limit. Even with extensive chemical cleaning to remove contaminants, the maximum friction coefficient measured (in yaw moment tests in flange contact) was about 0.1.

A procedure was later developed to remove these tool marks using emery paper (grit Nos. 180 and 400) and micromesh diamond cloth (no. 1000) successively, each used in machine sanders held in jigs to preserve the original rail profile. The contact surface is inked with felt markers to highlight the machine marks; the surface is abraded until all tool marks are removed and a smooth finish is achieved. The wheels and track are chemically cleaned with methyl alcohol prior to each run, with a strong industrial solvent used periodically to remove grease accumulated after the track has been unused for extended periods.

B.5 Description of Wheelclimb Experiments

Experiments are conducted at constant forward velocity and axle load, preset at the beginning of each test. Lateral forces are applied to the model as shown in Figure B.19 . Wheel/rail reaction forces are measured by the strain gauge balance which produces signals proportional to the total wheel/rail contact forces acting on the wheelset (axle L/V ratio). Comparisons with theory are made using the axle L/V ratio, since separate wheel force measurements were not made. Quasisteady derailment (Process A) is measured by progressive lateral loading of the model with a ballscrew drive motor, with vertical load, roll moment and forward velocity held constant. During the dynamic experiments (Processes B and C), a pneumatic

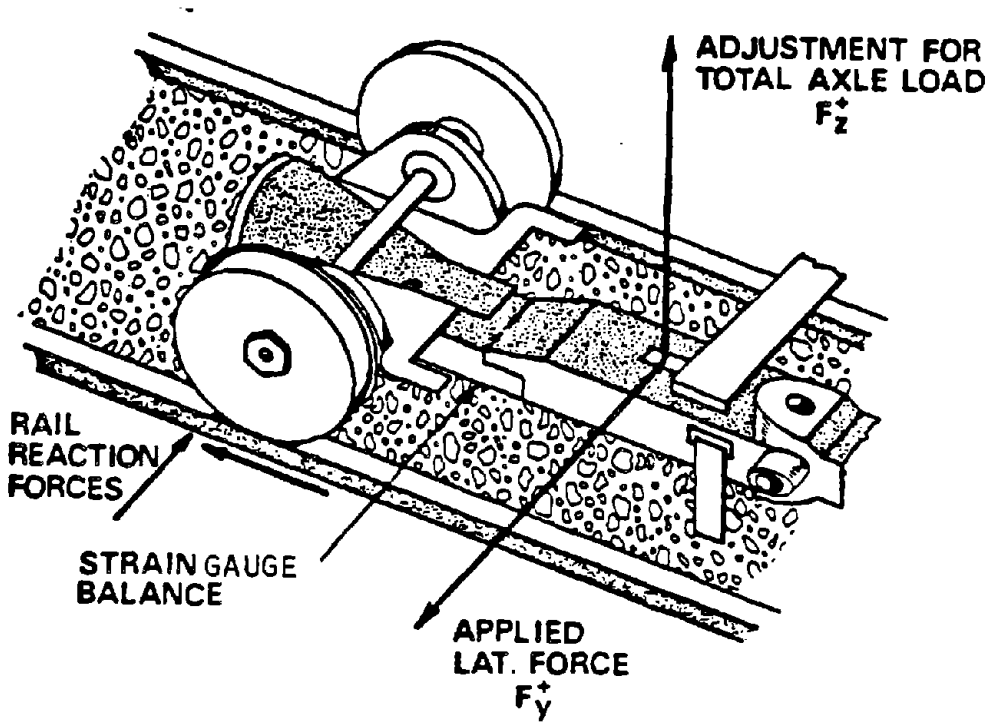

Figure B.19 Application of Forces to Wheelset Model.

servo actuated photoelectrically at specific locations along the 200m test track applies lateral forces to the wheelset model. The magnitude and duration of the applied lateral forces are varied during the series of experiments, as well as vertical axle load and forward velocity. To provide uniform initial conditions for the experiments, the wheelset is held against stops near the opposing rail prior to application of the lateral force. Responses are recorded on an FM tape recorder, and subsequently digitized for detailed analysis off-line.

Experiments on Process A were conducted at yaw angles over the range of -3° to $+3^{\circ}$, for roll moments covering the range possible without wheellift at either wheel. To simulate Process B, a series of experiments was conducted at constant yaw angles of 3° to -3° by locking this degree of freedom. Experiments for Process C were conducted using a yaw spring suspension with low stiffness. Tests were conducted on the wheelset from below critical speed to beyond the onset of hunting. Lateral force pulse inputs were superimposed on the track inputs to simulate dynamic curving.

Experiments were performed to determine the reproducibility of the derailment events. This information is useful in determining the extent to which derailment processes may be described by differential equations in a deterministic manner, without including random variations in parameters or forcing functions. The results of these experiments were highly reproducible at specific track locations, but exhibited variation in results when the same forces were applied to the wheelset at different sites along the track as shown in Figure B.20. Since the rails were

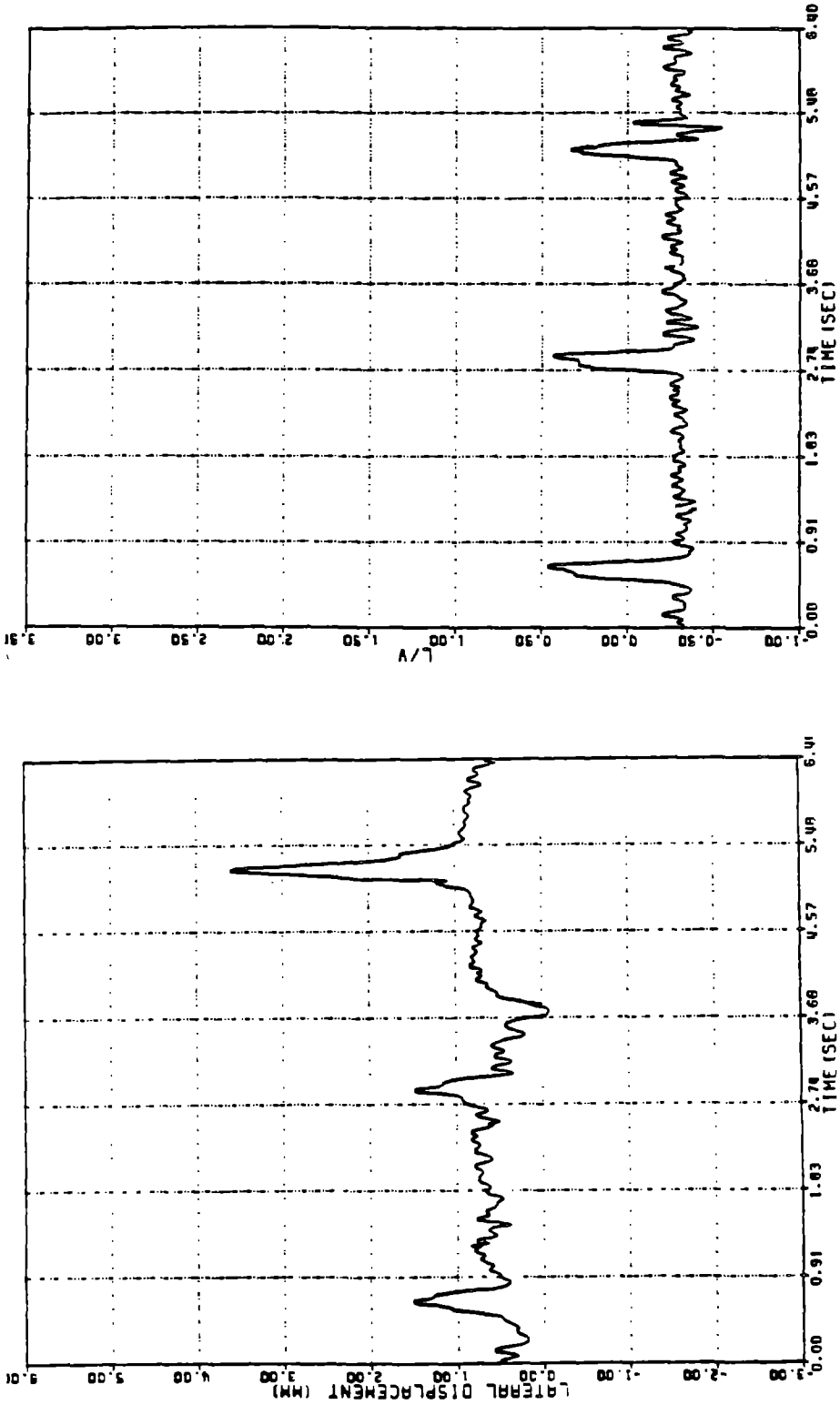

Figure B. 20 Effect of Track Location on Dynamic Wheelclimb Results for Equal Lateral Force Inputs.

machined to a profile that is relatively uniform along the track and the rails cleaned with methyl alcohol prior to each test, the occurence of derailment appears to be sensitive to minor local variations in friction coefficient and railhead profile.

APPENDIX C

DESCRIPTION OF PHASE TWO EXPERIMENTS

C.1 Purpose

The experiments conducted during Phase Two of the research program were designed to help resolve the following issues:

1. The time durations of large lateral forces during derailment events that were measured in the Phase One experiments were significantly larger than those predicted from simulation. The bandwidth of the instrumentation used in Phase One was limited to 25 Hz, which would filter lateral force impulse-like signals. The bandwidth of instrumentation used in Phase Two was extended to 100 Hz, which was determined to be sufficient to pass the predicted lateral force signals.
2. In the Phase One experiments, the strain gauge balance was the only force measuring device employed. This created an ambiguity in resolving dynamic forces acting on the individual wheels, inertial forces, and externally applied loads. Under quasisteady derailment conditions, with inertial forces insignificant, the remaining loads were in equilibrium, so that they could be resolved analytically. Under dynamic loading conditions, it is necessary to have independent measurements of the load signals. In the Phase Two experiments, an instrumented wheelset with plate mounted strain gauges was used to yield lateral and vertical force signals for each wheel. A load cell was used to monitor the external lateral force input, with an accelerometer used to sense inertial forces in the lateral direction.

In the remainder of this Appendix the hardware and experimental procedures used in Phase Two are briefly documented.

C.2 Instrumented Wheelset Design

An instrumented wheelset was designed to provide measurements of lateral and vertical forces acting on each wheel, subject to the following design criteria:

1. Maximum sensitivity of output signal to input load.
2. Minimum sensitivity of output signal to other loads (cross-sensitivity).
3. Minimum sensitivity of output signal to load point location.
4. Minimum sensitivity of output signal to thermal and centrifugal stresses.
5. Minimum ripple in output signal when subjected to continuous load.

To determine the best choice of strain gauge bridge geometry the strain field of the wheel plate surface was mapped, for various combinations of load magnitudes and application points. Using the mapped fields as a data base, a number of bridge designs proposed in the literature were evaluated using computer simulations.

For the lateral bridge, a constant output, two-sided configuration proposed by ASEA/SJ was selected. This configuration, shown in Figure C.1, is described in [32]. The principal advantages of this design were moderately high sensitivity and no need for processing of the signal downstream of the strain gauge bridge amplifier [32]. The principal disadvantages cited in [32], sensitivity to thermal and centrifugal stresses, proved to be insignificant problems for the Lexan scale model wheels used.

For the vertical bridge, an "A+B" triangular output configuration proposed by ASEA/SJ was selected. This configuration, shown in Figure C.2, is also described in [32]. Two bridges of the geometry shown in the figure are required, mounted

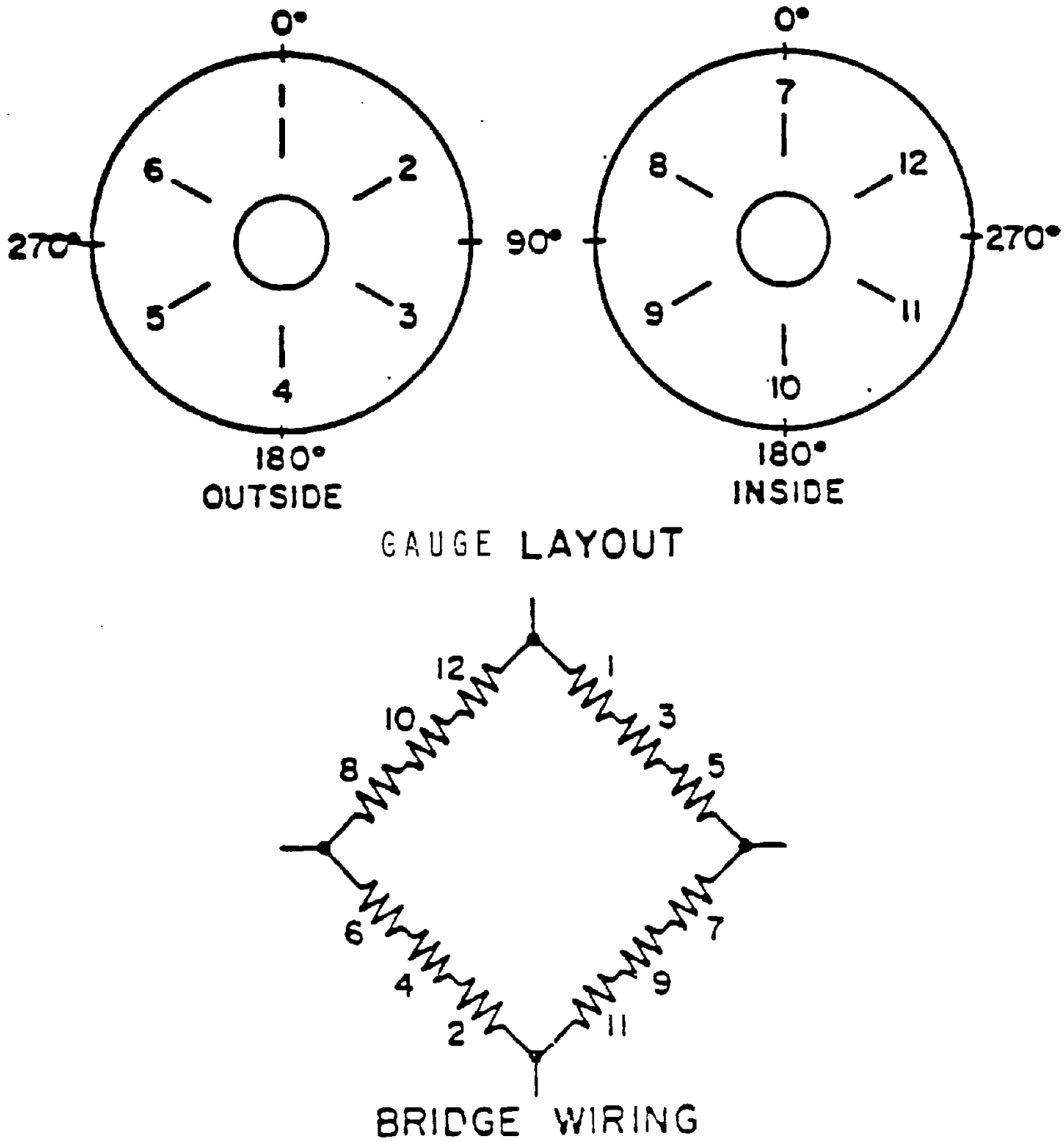

Figure C.1 - Configuration for lateral force strain gauge bridge (from [32]).

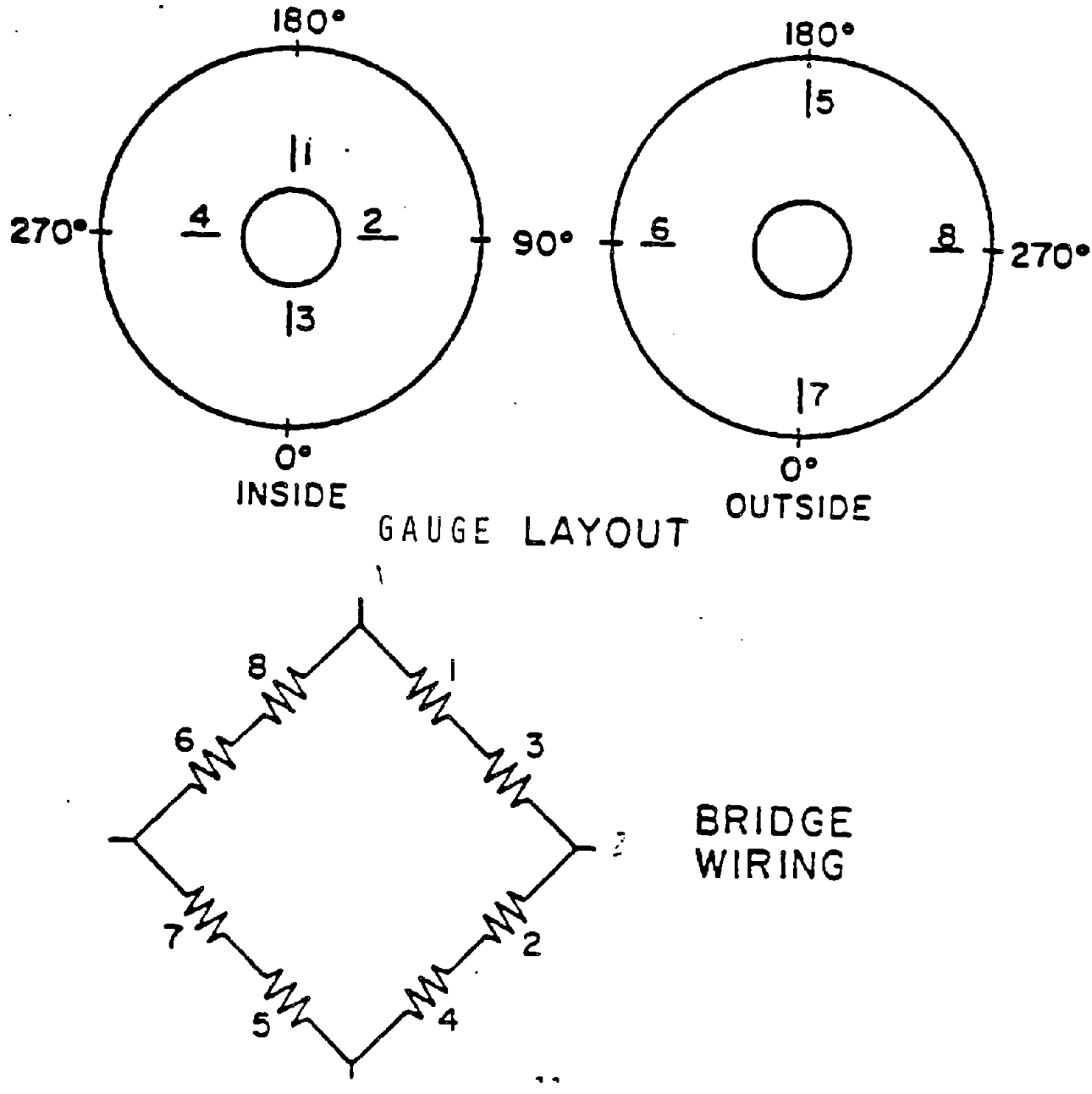

Figure C.2 - Configuration for vertical force strain gauge bridge (from [32]). Two bridges of this type are mounted at 45 deg. spacing.

45 deg out of phase with each other. The outputs of the two strain gauge bridge amplifiers are added together using the following equation,

$$\text{Output} = \text{Max}\ (|A|,\ |B|,\ K(|A| + |B|)) \qquad (C.1)$$

where K is a constant selected to minimize ripple. In the experiments reported here, bridge signals A and B were recorded directed, with the operations specified by Eq. C.1 performed by digital computer during post-experiment data reduction.

The final wheel designs required application of twenty-eight strain gauges, fourteen to each side of the wheel. Gauges selected were Micro-Measurements EA-41-062DN-350, selected for their small size, convenience of mounting, and compatibility with the Lexan wheel material. The strain gauge signal bridges were connected to their external excitation and amplifiers via slip rings mounted at each axle end. The completed assembly is shown in Figure C.3.

C.2 Instrumented Wheelset Instrumentation and Calibration

The strain gauge bridges were excited and sensed using Analog Devices Model 2B31 strain gauge conditioners. Three-pole, Bessel type active lowpass filters were used, with a cutoff frequency of 100 Hz.

The completed wheelset and signal conditioning subsystem was calibrated by mounting the wheels in a machining lathe fitted with a specially-designed rolling wheel fixture. The fixture was equipped with a wheel machined to the same cross-section profile as the rail used in the track experiments. The fixture provided variable vertical and lateral loads, over a range of load application points. Using the lathe/fixture apparatus, the wheelset could be calibrated under running conditions similar to those encountered during derailment tests.

The calibration experiments consisted of applications of vertical loads in the range 0 to 34 n (derailment tests at 22 n nominal load), lateral loads in the

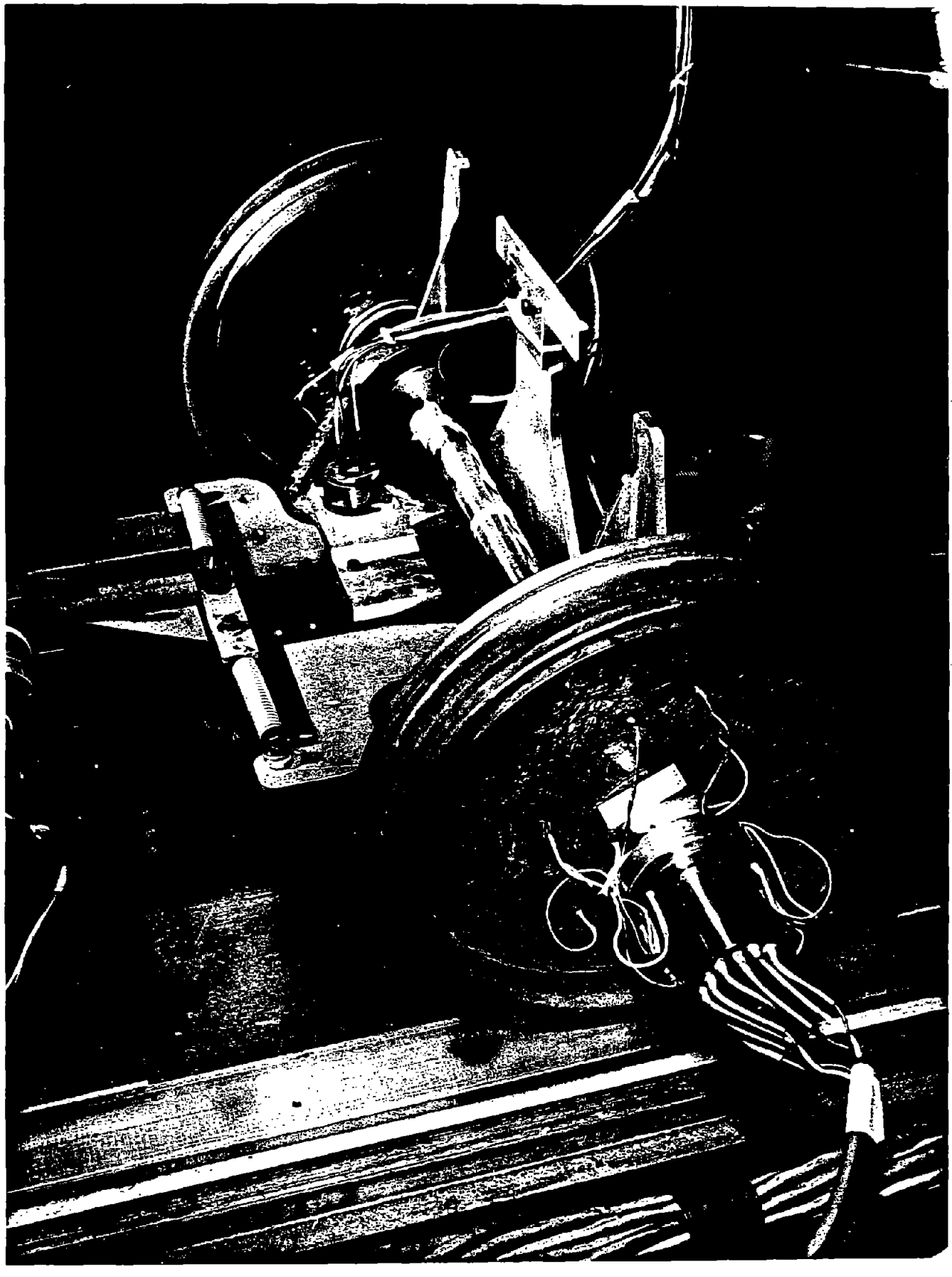

Figure C.3 - Assembled single wheelset apparatus, including plate instrumented wheelset.

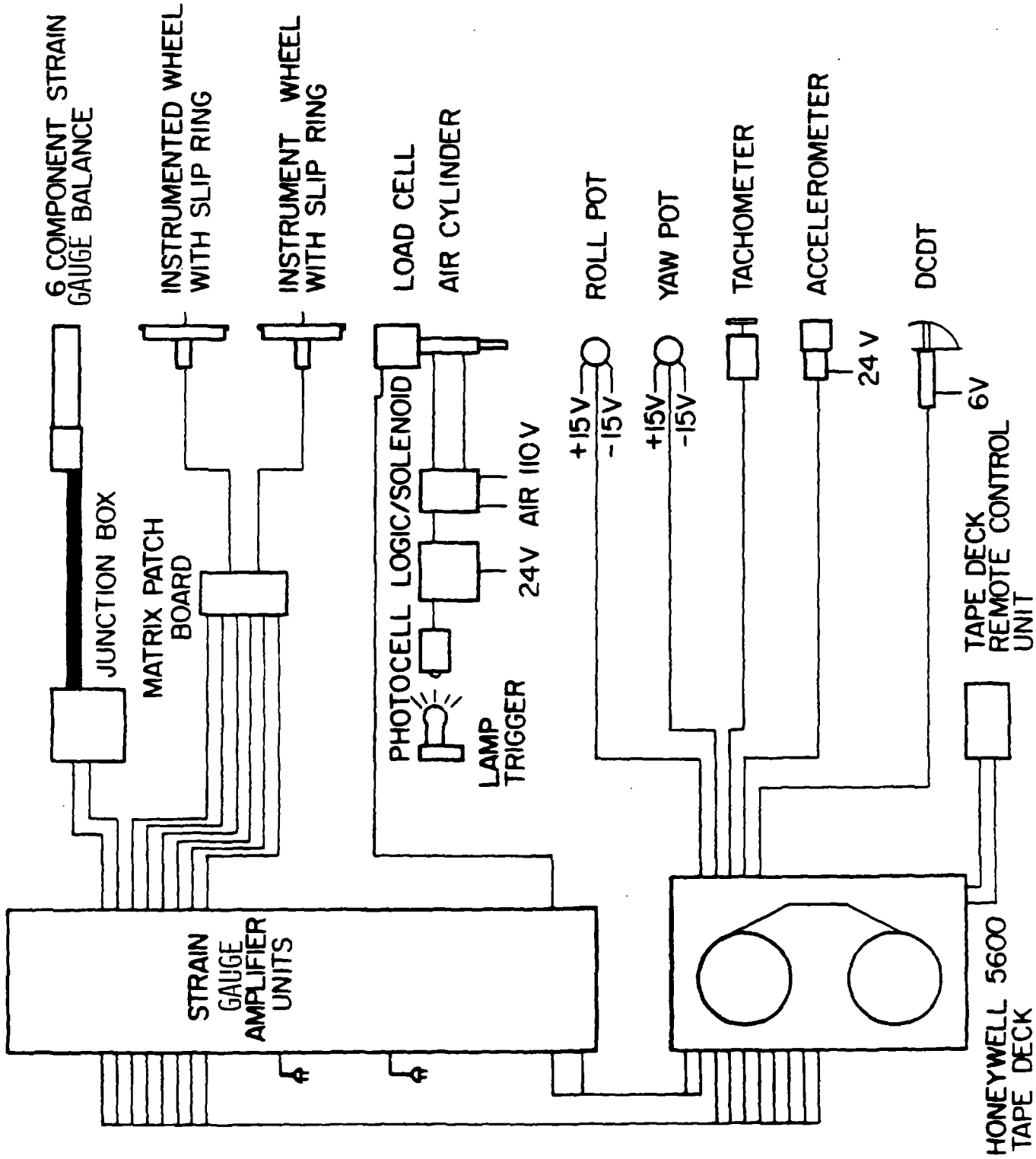

Figure C-4 - Instrumentation System for Phase Two Experiments

range 0 to 18 n (maximum lateral impulse load subsequently measured was 90 n), for contact point locations from the flange to the outside edge of the wheel. From these calibration tests, the sensitivities of the output signals to applied loads were determined. The sensitivities were found to be independent of contact point location and cross-load to within $\pm$ 10%, as desired.

C.3 Instrumentation and Data Acquisition Systems

The complete instrumentation system for the Phase Two experiments is shown in Figure C.4. The system is similar to that used in Phase One, with the exceptions of the instrumented wheelsets, higher bandwidth strain gauge amplifiers, and load cell for measurement of external applied lateral force. Data was recorded on a fourteen track Honeywell 5600 FM tape recorder. The availability of more tracks eliminated the need for multiplexing (as in Phase One), permitting higher bandwidth for all signals. Subsequent to the track experiments, the data was processed by lowpass anti-aliasing filters (100 Hz bandwidth), and digitized at 400 Hz on a Preston Scientific GMAD-1 analog-to-digital converter. Data storage and reduction were performed on a Hewlett-Packard 21MXE Series 1000 minicomputer system located at the Princeton University Gas Dynamics Laboratory.

Appendix D

LISTING OF DYNAMIC WHEELCLIMB SIMULATION

PROGRAM "WHSET"

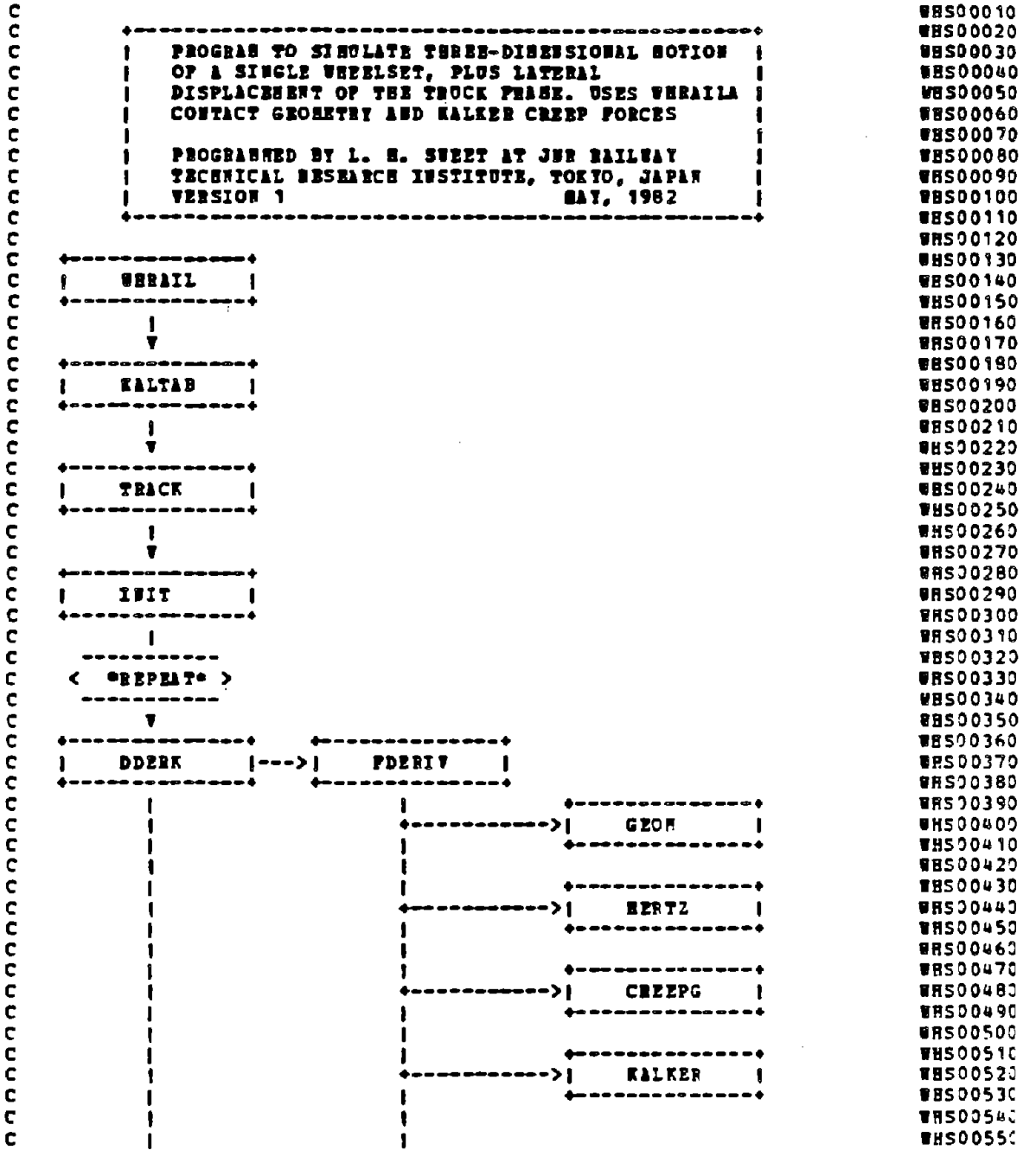
PROGRAM TO SIMULATE THREE-DIMENSIONAL MOTION
OF A SINGLE WHEELSET, PLUS LATERAL
DISPLACEMENT OF THE TRUCK FRAME. USES WRAILA
CONTACT GEOMETRY AND KALKER CREEP FORCES
PROGRAMMED BY L. H. SWEET AT JNR RAILWAY
TECHNICAL RESEARCH INSTITUTE, TOKYO, JAPAN
VERSION 1 MAY, 1982
WRAIL
KALTAB
TRACK
INIT
REPEAT
DDERK
FDERIV
GEOM
HERTZ
CREEPG
KALKER

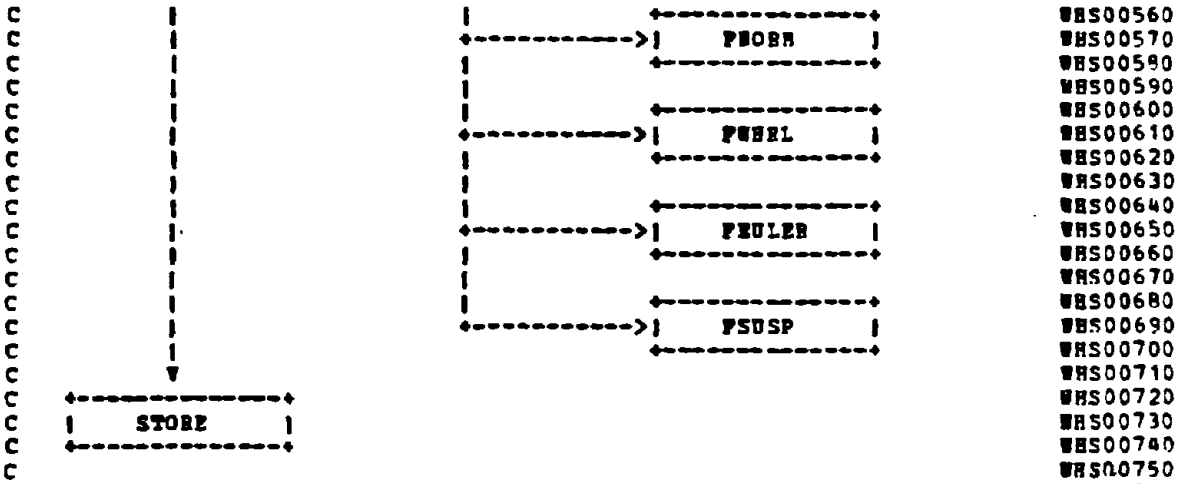


```
C                                                                       WHS00560
C                                                                       WHS00570
C                                                                       WHS00580
C                                                                       WHS00590
C                                                                       WHS00600
C                                                                       WHS00610
C                                                                       WHS00620
C                                                                       WHS00630
C                                                                       WHS00640
C                                                                       WHS00650
C                                                                       WHS00660
C                                                                       WHS00670
C                                                                       WHS00680
C                                                                       WHS00690
C                                                                       WHS00700
C                                                                       WHS00710
C                                                                       WHS00720
C                                                                       WHS00730
C                                                                       WHS00740
C                                                                       WHS00750
C<<<<<<<<<<<<<<<<<<<<<<<<<<<<<<<<<<<<<<<<<<<<<<<<<<<<<<<<<<<<<<<<<<<<<< WHS00760
C<<<<<<<<<<<<<<<<<<<<<<<<<<<<<<<<<<<<<<<<<<<<<<<<<<<<<<<<<<<<<<<<<<<<<< WHS00770
C                                                                       WHS00780
C                                                                       WHS00790
C                                                                       WHS00800
C                                                                       WHS00810
      REAL MIX,MZZ0                                                     WHS00820
      DIMENSION FX(21,13,13),FY(21,13,13),Y(7),F3(2),DY(7),AUX(40),     WHS00830
     1       F1(2),F2(2),IFLAG(3),PS(7)                                 WHS00840
      EXTERNAL FDERIV                                                   WHS00850
      COMMON /KALK/ FX,FY                                               WHS00860
      COMMON /VPROD/ VEL,VOR                                            WHS00870
      COMMON /LOAD/ FZ,MIX,FY0,MZZ0                                     WHS00880
      COMMON /FORCES/ F1,F2,F3                                          WHS00890
      COMMON /ACCEL/ YDDOT,PSDDOT                                       WHS00900
      COMMON /TRUCK/ PS,PSIT                                            WHS00910
      DATA EPS1,DEL,T,H /1.0E-02,0.0,0.0,1.0E-03/                       WHS00920
      DATA TMAX,NMAX /.20,4000/                                         WHS00930
      DATA IPLOT /4/                                                    WHS00940
      DATA EMAX /5.0E-08/                                               WHS00950
      DATA IFLAG /3*0/                                                  WHS00960
      CALL WHRAIL                                                       WHS00970
      CALL KALTAB                                                       WHS00980
      CALL TRACK                                                        WHS00990
      CALL INIT(Y)                                                      WHS01000
      CALL FBODE(Y)                                                     WHS01010
      DO 45 I=1,2                                                       WHS01020
45    IF (F3(I) .LE. 0.0) IFLAG(I)=1                                    WHS01030
      IF (IFLAG(1) .EQ. 1 .OR. IFLAG(2) .EQ. 1) GO TO 30                WHS01040
      CALL FDERIV(T,Y,DY)                                               WHS01050
      T=0.0                                                             WHS01060
      CALL STORE(T,Y)                                                   WHS01070
      NPT=0                                                             WHS01080
      WRITE (6,104)                                                     WHS01090
104   FORMAT (' ENTER DISPLAY INTERVAL')                                WHS01100
```

```
      READ (5,*) INT                                                    WHS01110
      WRITE (6,101)                                                     WHS01120
101   FORMAT (' SIMULATION BEGINS')                                     WHS01130
20    CALL PROBE(T)                                                     WHS01140
      DO 25 I=1,2                                                       WHS01150
25    IF (F3(I) .LE. 0.0) IFLAG(I)=1                                    WHS01160
C     IF (IFLAG(1) .NE. 1 .AND. IFLAG(2) .NE. 1) GO TO 26               WHS01170
C     CALL STORE(TMAX,Y)                                                WHS01180
C     GO TO 30                                                          WHS01190
26    IER=-12345                                                        WHS01200
      H=AMIN1(H,HMAX)                                                   WHS01210
      CALL DERK(FDERIV,T,Y,DY,7,EPS1,H,AUX,IER)                         WHS01220
      IF (IER .EQ. 100) GO TO 20                                        WHS01230
      YDDOT=DY(2)                                                       WHS01240
      PSDDOT=DY(5)                                                      WHS01250
      IF (MOD(NPT,IPLOT) .EQ. 0) CALL STORE(T,Y)                        WHS01260
      IF (T .GT. TMAX) GO TO 30                                         WHS01270
      IF (ABS(Y(1)) .LT. 0.0200) GO TO 35                               WHS01280
      IFLAG(3)=1                                                        WHS01290
      CALL STORE (T,Y)                                                  WHS01300
      GO TO 30                                                          WHS01310
35    NPT=NPT+1                                                         WHS01320
      IF (NPT .GE. NMAX) GO TO 30                                       WHS01330
      IF (MOD(NPT,INT) .NE. 0) GO TO 20                                 WHS01340
      WRITE (6,100) NPT,T,H,Y(1),Y(2),Y(4),Y(6),Y(7)                    WHS01350
100   FORMAT (I4,2E9.2,4X,5E10.2)                                       WHS01360
      GO TO 20                                                          WHS01370
30    CONTINUE                                                          WHS01380
      WRITE (6,102) IFLAG                                               WHS01390
102   FORMAT(' FLAGS = ',3I10)                                          WHS01400
      STOP                                                              WHS01410
      END                                                               WHS01420
C                                                                       WHS01430
C                        +--------------+                               WHS01440
C                        |    INIT      |                               WHS01450
C                        +--------------+                               WHS01460
C                                                                       WHS01470
      SUBROUTINE INIT(T)                                                WHS01480
C                                                                       WHS01490
C READS IN SIMULATION CONTROL PARAMETERS FROM TERMINAL                  WHS01500
C SETS PROGRAM PARAMETERS FROM DATA STATEMENTS                          WHS01510
C                                                                       WHS01520
      REAL IYY,IZZ,IXX,MW,MU,MD,MXX,MZZD,KY,KPHI,KZ,KPSI,MT             WHS01530
      DIMENSION Y(7),F3(2),ALPHA(2),L(2),RHO(2),RV(2),ATH(2),BTH(2),    WHS01540
     1       CHI(2),F1(2),F2(2),PS(7)                                   WHS01550
      COMMON /MPARAM/ MW,IYY,IZZ,IXX,MT                                 WHS01560
      COMMON /SPARAM/ BY,KY,BZ,KZ,KPSI,BPSI,OMEGA,KPHI,BPHI            WHS01570
      COMMON /VFREQ/ VEL,VOR                                            WHS01580
      COMMON /MATERL/ MU,EN                                             WHS01590
      COMMON /LOAD/ FZ,MXX,FYO,MZZO                                     WHS01600
      COMMON /GZO/ Z,DZ,DDZ,PHI,DPHI,DDPHI,ALPHA,L,RHO,RV,ATH,BTH,CHI   WHS01610
      COMMON /FORCES/ F1,F2,F3                                          WHS01620
      COMMON /ACCEL/ YDDOT,PSDDOT                                       WHS01630
      COMMON /TRUCK/ PS,PSIT                                            WHS01640
      READ (1,*) MW,MT                                                  WHS01650
```

```
      READ (1,*) IXX,IYY,IZZ                                          WHS01660
      READ (1,*) BY,KY                                                WHS01670
      READ (1,*) BZ,KZ                                                WHS01680
      READ (1,*) BPSI,KPSI                                            WHS01690
      READ (1,*) BPHI,KPHI                                            WHS01700
      READ (1,*) BOMEGA                                               WHS01710
      READ (1,*) MU,MU,E                                              WHS01720
      READ (1,*) VEL                                                  WHS01730
      READ (1,*) PZ,HXI                                               WHS01740
      READ (1,*) PIO,HZZO                                             WHS01750
      READ (1,*) PSIT                                                 WHS01760
      EN=4.0*E/(3.0*(1.0-MU**2))                                      WHS01770
      CALL GEOM(0.0)                                                  WHS01780
      RO=RY(2)                                                        WHS01790
      Y(1)=0.0                                                        WHS01800
      Y(2)=0.0                                                        WHS01810
      VOR=VEL/RO                                                      WHS01820
      Y(3)=VOR                                                        WHS01830
      Y(4)=PSIT                                                       WHS01840
      Y(5)=0.0                                                        WHS01850
      Y(6)=0.0                                                        WHS01860
      Y(7)=0.0                                                        WHS01870
      YDDOT=0.0                                                       WHS01880
      PS(2)=0.0                                                       WHS01890
      CALL GEOM(Y(1))                                                 WHS01900
      RETURN                                                          WHS01910
      END                                                             WHS01920
C                                                                     WHS01930
C                        +--------------+                             WHS01940
C                        |    TRACK     |                             WHS01950
C                        +--------------+                             WHS01960
C                                                                     WHS01970
      SUBROUTINE TRACK                                                WHS01980
C                                                                     WHS01990
C READS SIMULATED OR MEASURED TRACK GEOMETRY INPUTS FROM CMS FILES    WHS02000
C                                                                     WHS02010
      RETURN                                                          WHS02020
      END                                                             WHS02030
C                                                                     WHS02040
C                        +--------------+                             WHS02050
C                        |    FDERIV    |                             WHS02060
C                        +--------------+                             WHS02070
C                                                                     WHS02080
      SUBROUTINE FDERIV(T,Y,DY)                                       WHS02090
C                                                                     WHS02100
C SUBROUTINE CALLED BY DDERK TO EVALUATE FIRST DERIVATIVES OF ALL     WHS02110
C STATE VARIABLES AT EACH TIME STEP.  EQUATIONS ARE IN THE FORM:      WHS02120
C       DY(I) = (FWR(I) +FEUL(I) + FS(I) + FEXT(I)) / MASS(I)        WHS02130
C WHERE                                                               WHS02140
C              FWR = WHEEL/RAIL INTERACTION FORCES                    WHS02150
C             FEUL = EULER FORCES                                     WHS02160
C               FS = SUSPENSION FORCES                                WHS02170
C             FEXT = EXTERNAL FORCES                                  WHS02180
C             MASS = GENERALIZED INERTIA FOR EACH STATE VARIABLE      WHS02190
C                                                                     WHS02200
```

```
      REAL L(2),IYY,IZZ,IXX,MASS,MW,MT,MXX,MZZ0                          WHS02210
      DIMENSION Y(7),DY(7),P3(2),AAXIS(2),BAXIS(2),VWU(2),ANGLE(2),      WHS02220
     1        P1(2),P2(2),CHI(2),FWR(7),FEUL(7),FS(7),FEXT(7),            WHS02230
     2        ALPHA(2),RHO(2),RV(2),ATH(2),BTH(2),MASS(7),SIGN(2)        WHS02240
      COMMON /GEO/ Z,DZ,DDZ,PHI,DPHI,DDPHI,ALPHA,L,RHO,RV,ATH,BTH,CHI    WHS02250
      COMMON /MPARAM/ MW,IYY,IZZ,IXX,MT                                  WHS02260
      COMMON /CNTROL/ RANGE,STEP,M,N,EPS,PI                              WHS02270
      COMMON /VFEED/ VEL,VOR                                             WHS02280
      COMMON /LOAD/ FZ,MXX,FY0,MZZ0                                      WHS02290
      COMMON /FORCES/ F1,F2,F3                                           WHS02300
      COMMON /ACCEL/ YDDOT,PSDDOT                                        WHS02310
      COMMON /TRUCK/ FS,PSIT                                             WHS02320
      CALL GEOM(Y(1)-TRK)                                                WHS02330
      CALL HERTZ(AAXIS,BAXIS)                                            WHS02340
      CALL CREEPG(Y,AAXIS,BAXIS,VWU,ANGLE,SIGN)                          WHS02350
      CALL KALKER(AAXIS,BAXIS,VWU,ANGLE,CHI,Y,SIGN)                      WHS02360
      CALL FWHEL(FWR)                                                    WHS02370
      CALL FEULER(Y,FEUL)                                                WHS02380
      CALL FSUSP(Y)                                                      WHS02390
C                                                                        WHS02400
      MASS(1)=1.0                                                        WHS02410
      MASS(2)=MW                                                         WHS02420
      MASS(3)=IYY                                                        WHS02430
      MASS(4)=1.0                                                        WHS02440
      MASS(5)=IZZ                                                        WHS02450
      MASS(6)=1.0                                                        WHS02460
      MASS(7)=MT                                                         WHS02470
      DO 5 I=1,7                                                         WHS02480
5     FEXT(I)=0.0                                                        WHS02490
      FEXT(7)=FY0                                                        WHS02500
      FEXT(5)=MZZ0                                                       WHS02510
      DO 10 I=1,7                                                        WHS02520
10    DY(I)=(FWR(I)+FEUL(I)+FS(I)+FEXT(I))/MASS(I)                       WHS02530
C                                                                        WHS02540
      DY(1)=Y(2)                                                         WHS02550
      DY(4)=Y(5)                                                         WHS02560
      DY(6)=Y(7)                                                         WHS02570
C                                                                        WHS02580
C REDUCED-ORDER MODEL                                                    WHS02590
C     DY(3)=0.0                                                          WHS02600
C     DY(4)=0.0                                                          WHS02610
C     DY(5)=0.0                                                          WHS02620
      RETURN                                                             WHS02630
      END                                                                WHS02640
C                                                                        WHS02650
C                        +--------------+                                WHS02660
C                        |    SAMPLE    |                                WHS02670
C                        +--------------+                                WHS02680
C                                                                        WHS02690
      SUBROUTINE SAMPLE                                                  WHS02700
C                                                                        WHS02710
C SAMPLES TIME SIMULATION AT UNIFORM TIME INTERVALS SET BY INIT          WHS02720
C                                                                        WHS02730
      RETURN                                                             WHS02740
      END                                                                WHS02750
```

```
C                                                                       WRS02760
C                        +--------------+                               WRS02770
C                        |    STORE     |                               WRS02780
C                        +--------------+                               WRS02790
C                                                                       WRS02800
      SUBROUTINE STORE(T,Y)                                             WRS02810
C                                                                       WRS02820
C STORES SAMPLED SIMULATION DATA IN CSD FILES FOR FUTURE PROCESSING      WRS02830
C                                                                       WRS02840
      REAL MU,L                                                         WRS02850
      DIMENSION Y(7),F3(2),ALPHA(2),L(2),RHO(2),RV(2),ATH(2),BTH(2),    WRS02860
     1        CHI(2),F1(2),F2(2),QP(2)                                  WRS02870
      COMMON /VPROD/ VEL,VOR                                            WRS02880
      COMMON /RATERL/ MU,ZM                                             WRS02890
      COMMON /GEO/ Z,DZ,DDZ,PHI,DPHI,DDPHI,ALPHA,L,RHO,RV,ATH,BTH,CHI   WRS02900
      COMMON /FORCES/ F1,F2,F3                                          WRS02910
      WRDISP=Y(1)*1000.                                                 WRS02920
      OMEGA=Y(3)/VOR                                                    WRS02930
      YAW=Y(4)*1000.                                                    WRS02940
      TRDISP=Y(6)*1000.                                                 WRS02950
      DO 10 I=1,2                                                       WRS02960
      C1=COS(ALPHA(I))                                                  WRS02970
      S1=SIN(ALPHA(I))                                                  WRS02980
10    QP(I)=-(-1)**I*(MU*F2(I)*C1+S1)/(MU*F2(I)*S1-C1)                  WRS02990
C     IF (F3(I) .LE. 0.0) QP(I)=0.0                                     WRS03000
      WRITE (2,*) T,WRDISP,TRDISP,OMEGA,YAW,QP,F3                       WRS03010
      RETURN                                                            WRS03020
      END                                                               WRS03030
C                                                                       WRS03040
C                        +--------------+                               WRS03050
C                        |    WRRAIL    |                               WRS03060
C                        +--------------+                               WRS03070
C                                                                       WRS03080
      SUBROUTINE WRRAIL                                                 WRS03090
C                                                                       WRS03100
C READ STORED WRRAILA DATA                                              WRS03110
C                                                                       WRS03120
      DIMENSION TZ(161),TDZ(161),TDDZ(161),TPHI(161),TDPHI(161),        WRS03130
     1    TDDPHI(161),TALPHA(161,2),TL(161,2),TRHO(161,2),TRV(161,2),   WRS03140
     2    TATH(161,2),TBTH(161,2),TCHI(161,2)                           WRS03150
      COMMON /TGEOM/ TZ,TDZ,TDDZ,TPHI,TDPHI,TDDPHI,TALPHA,TL,TRHO,TRV,  WRS03160
     1    TATH,TBTH,TCHI                                                WRS03170
      COMMON /CNTROL/ RANGE,STEP,N,M,EPS,PI                             WRS03180
      NAMELIST /WRRL/ TZ,TDZ,TDDZ,TPHI,TDPHI,TDDPHI,TALPHA,TL,TRHO,TRV, WRS03190
     1    TATH,TBTH,TCHI                                                WRS03200
      READ(3,WRRL)                                                      WRS03210
      DO 10 J=1,161                                                     WRS03220
      TPHI(J)=-TPHI(J)                                                  WRS03230
      TDPHI(J)=-TDPHI(J)                                                WRS03240
10    TDDPHI(J)=-TDDPHI(J)                                              WRS03250
      RETURN                                                            WRS03260
      END                                                               WRS03270
C                                                                       WRS03280
C                        +--------------+                               WRS03290
C                        |    KALTAB    |                               WRS03300
```

```
C                        +-------------+                                  WHS03310
C                                                                         WHS03320
      SUBROUTINE KALTAB                                                   WHS03330
      DIMENSION FX(21,13,13),FY(21,13,13),FXTEMP(13,13),FYTEMP(13,13)     WHS03340
      COMMON /KALK/ FX,FY                                                 WHS03350
C                                                                         WHS03360
C READ KALKER TABLES FROM CDC FILES (FILE NOS. 51 THROUGH 71)             WHS03370
C                                                                         WHS03380
      DO 10 I=1,21                                                        WHS03390
      NNN=50+I                                                            WHS03400
      READ (NNN,200) ((FXTEMP(K,N),N=1,13),K=1,13),                       WHS03410
     1               ((FYTEMP(K,N),N=1,13),K=1,13)                        WHS03420
200   FORMAT(//////,13(/,5X,13(F9.3)),//////,13(/,5X,13(F9.3)))           WHS03430
      DO 20 N=1,13                                                        WHS03440
      DO 20 K=1,13                                                        WHS03450
      FX(I,K,N)=FXTEMP(K,N)                                               WHS03460
20    FY(I,K,N)=FYTEMP(K,N)                                               WHS03470
10    CONTINUE                                                            WHS03480
      RETURN                                                              WHS03490
      END                                                                 WHS03500
C                                                                         WHS03510
C                        +-------------+                                  WHS03520
C                        |     GEOM    |                                  WHS03530
C                        +-------------+                                  WHS03540
C                                                                         WHS03550
      SUBROUTINE GEOM(Y)                                                  WHS03560
C                                                                         WHS03570
C COMPUTES CONTACT GEOMETRY PARAMETERS AS FUNCTION OF LATERAL             WHS03580
C POSTION OF WHEELSET.  DATA IS STORED IN TABULAR FORM, WITH POSITIVE      WHS03590
C DISPLACEMENT DATA AT THE TOP OF THE TABLE.                              WHS03600
C                                                                         WHS03610
C         Y = WHEELSET LATERAL POSITION                                   WHS03620
C       PHI = WHEELSET ROLL ANGLE                                         WHS03630
C      DPHI = D(PHI) / DY                                                 WHS03640
C     DDPHI = D2(PHI) / DY2                                               WHS03650
C         Z = WHEELSET C.M. VERTICAL DISPLACEMENT                         WHS03660
C        DZ = D(Z) / DY                                                   WHS03670
C       DDZ = D2(Z) / DY                                                  WHS03680
C      L(I) = HORIZONTAL DISTANCE FROM C.M. TO CONTACT POINTS             WHS03690
C  ALPHA(I) = CONTACT ANGLE                                               WHS03700
C     RV(I) = ROLLING RADIUS                                              WHS03710
C    RHO(I) = GEOMETRIC MEAN OF HERTZ CONTACT ELLIPSE                     WHS03720
C    ATH(I) = A(THETA)                                                    WHS03730
C    BTH(I) = B(THETA)                                                    WHS03740
C    CHI(I) = NORMALIZED KALKER SPIN PARAMETER                            WHS03750
C                 I=1 FOR RIGHT WHEEL                                     WHS03760
C                 I=2 FOR LEFT WHEEL                                      WHS03770
C                                                                         WHS03780
      REAL L                                                              WHS03790
      DIMENSION TZ(161),TDZ(161),TDDZ(161),TPHI(161),TDPHI(161),          WHS03800
     1    TDDPHI(161),TALPHA(161,2),TL(161,2),TRHO(161,2),TRV(161,2),     WHS03810
     2    TATH(161,2),TBTH(161,2),TCHI(161,2),ALPHA(2),L(2),RHO(2),       WHS03820
     3    RV(2),ATH(2),BTH(2),CHI(2),AUX(100),TALPH1(161),TALPH2(161),     WHS03830
     4    TL1(161),TL2(161),TRHO1(161),TRHO2(161),TRV1(161),TRV2(161),     WHS03840
     5    TATH1(161),TATH2(161),TBTH1(161),TBTH2(161),TCHI1(161),          WHS03850
```

```
     6    TCHI2(161)                                                        WHS03860
      COMMON /TGBOH/ TZ,TDZ,TDDZ,TPHI,TDPHI,TDDPHI,TALPHA,TL,TRHO,TRV,     WHS03870
     1    TATH,TBTH,TCHI                                                   WHS03880
      COMMON /GEO/ Z,DZ,DDZ,PHI,DPHI,DDPHI,ALPHA,L,RHO,RV,ATH,BTH,CHI      WHS03890
      COMMON /CNTROL/ RANGE,STEP,N,H,EPS                                   WHS03900
      EQUIVALENCE (TALPHA(1),TALPH1(1)),(TALPHA(162),TALPH2(1)),           WHS03910
     1            (TL(1),TL1(1)),(TL(162),TL2(1)),                         WHS03920
     2            (TRHO(1),TRHO1(1)),(TRHO(162),TRHO2(1)),                 WHS03930
     3            (TRV(1),TRV1(1)),(TRV(162),TRV2(1)),                     WHS03940
     4            (TATH(1),TATH1(1)),(TATH(162),TATH2(1)),                 WHS03950
     5            (TBTH(1),TBTH1(1)),(TBTH(162),TBTH2(1)),                 WHS03960
     6            (TCHI(1),TCHI1(1)),(TCHI(162),TCHI2(1))                  WHS03970
C                                                                           WHS03980
C  INTERPOLATION IS PERFORMED BY SUBROUTINE "IVP" FROM IBM SL-MATH          WHS03990
C  LIBRARY, WHICH IS BASED ON AITKEN'S ITERATIVE METHOD                     WHS04000
C                                                                           WHS04010
      YTABLE=Y                                                              WHS04020
      R=RANGE                                                               WHS04030
      ST=-STEP                                                              WHS04040
      IF (Y .GT. RANGE) YTABLE=RANGE                                        WHS04050
      IF (Y .LT. -RANGE) YTABLE=-RANGE                                      WHS04060
      CALL IVP (R,ST,TPHI,N,YTABLE,H,EPS,PHI,AUX,IER)                       WHS04070
      CALL IVP (R,ST,TDPHI,N,YTABLE,H,EPS,DPHI,AUX,IER)                     WHS04080
      CALL IVP (R,ST,TDDPHI,N,YTABLE,H,EPS,DDPHI,AUX,IER)                   WHS04090
      CALL IVP (R,ST,TZ,N,YTABLE,H,EPS,Z,AUX,IER)                           WHS04100
      CALL IVP (R,ST,TDZ,N,YTABLE,H,EPS,DZ,AUX,IER)                         WHS04110
      CALL IVP (R,ST,TDDZ,N,YTABLE,H,EPS,DDZ,AUX,IER)                       WHS04120
      CALL IVP (R,ST,TALPH1,N,YTABLE,H,EPS,AL1,AUX,IER)                     WHS04130
      CALL IVP (R,ST,TALPH2,N,YTABLE,H,EPS,AL2,AUX,IER)                     WHS04140
      ALPHA(1)=-AL1+PHI                                                     WHS04150
      ALPHA(2)=AL2+PHI                                                      WHS04160
      CALL IVP (R,ST,TL1,N,YTABLE,H,EPS,L(1),AUX,IER)                       WHS04170
      CALL IVP (R,ST,TL2,N,YTABLE,H,EPS,L(2),AUX,IER)                       WHS04180
      CALL IVP (R,ST,TRHO1,N,YTABLE,H,EPS,RHO(1),AUX,IER)                   WHS04190
      CALL IVP (R,ST,TRHO2,N,YTABLE,H,EPS,RHO(2),AUX,IER)                   WHS04200
      CALL IVP (R,ST,TRV1,N,YTABLE,H,EPS,RV(1),AUX,IER)                     WHS04210
      CALL IVP (R,ST,TRV2,N,YTABLE,H,EPS,RV(2),AUX,IER)                     WHS04220
      CALL IVP (R,ST,TATH1,N,YTABLE,H,EPS,ATH(1),AUX,IER)                   WHS04230
      CALL IVP (R,ST,TATH2,N,YTABLE,H,EPS,ATH(2),AUX,IER)                   WHS04240
      CALL IVP (R,ST,TBTH1,N,YTABLE,H,EPS,BTH(1),AUX,IER)                   WHS04250
      CALL IVP (R,ST,TBTH2,N,YTABLE,H,EPS,BTH(2),AUX,IER)                   WHS04260
      CALL IVP (R,ST,TCHI1,N,YTABLE,H,EPS,CHI(1),AUX,IER)                   WHS04270
      CALL IVP (R,ST,TCHI2,N,YTABLE,H,EPS,CHI(2),AUX,IER)                   WHS04280
C                                                                           WHS04290
      RETURN                                                                WHS04300
      END                                                                   WHS04310
C                                                                           WHS04320
C                        +--------------+                                   WHS04330
C                        |    HERTZ     |                                   WHS04340
C                        +--------------+                                   WHS04350
C                                                                           WHS04360
      SUBROUTINE HERTZ(AAXIS,BAXIS)                                         WHS04370
C                                                                           WHS04380
C COMPUTE DIMENSIONS OF HERTZ CONTACT ELLIPSE                               WHS04390
C                                                                           WHS04400
```

```
      REAL L,MU                                                          WHS04410
      DIMENSION P3(2),AAXIS(2),BAXIS(2),RHO(2),ATH(2),BTH(2),CHI(2),     WHS04420
     1          ALPHA(2),L(2),RV(2),P1(2),P2(2)                          WHS04430
      COMMON /GEO/ Z,DZ,DDZ,PHI,DPHI,DDPHI,ALPHA,L,RHO,RV,ATH,BTH,CHI    WHS04440
      COMMON /MATERL/ MU,EN                                              WHS04450
      COMMON /VPBND/ VEL,VOR                                             WHS04460
      COMMON /FORCES/ P1,P2,P3                                           WHS04470
      DO 10 I=1,2                                                        WHS04480
      IF (P3(I) .LE. 0.0) GO TO 10                                       WHS04490
      PEN=(P3(I)*RHO(I)/EN)**(1./3.)                                     WHS04500
      AAXIS(I)=ATH(I)*PEN                                                WHS04510
      BAXIS(I)=BTH(I)*PEN                                                WHS04520
10    CONTINUE                                                           WHS04530
      RETURN                                                             WHS04540
      END                                                                WHS04550
C                                                                        WHS04560
C                        +--------------+                                WHS04570
C                        |    CREEPG    |                                WHS04580
C                        +--------------+                                WHS04590
C                                                                        WHS04600
      SUBROUTINE CREEPG(Y,AAXIS,BAXIS,VBU,ANGLE,SIGN)                    WHS04610
C                                                                        WHS04620
C COMPUTE NON-DIMENSIONAL CREEPAGES IN POLAR FORM                        WHS04630
C                                                                        WHS04640
      REAL L,MU                                                          WHS04650
      DIMENSION VBU(2),ANGLE(2),AAXIS(2),BAXIS(2),Y(7),CHI(2),           WHS04660
     1          RV(2),ALPHA(2),L(2),RHO(2),ATH(2),BTH(2),SIGN(2)         WHS04670
      COMMON /GEO/ Z,DZ,DDZ,PHI,DPHI,DDPHI,ALPHA,L,RHO,RV,ATH,BTH,CHI    WHS04680
      COMMON /MATERL/ MU,EN                                              WHS04690
      COMMON /VPBND/ VEL,VOR                                             WHS04700
      COMMON /CNTROL/ RANGE,ST,H,E,EPS,PI                                WHS04710
C                                                                        WHS04720
C DEFINE STATE VARIABLES                                                 WHS04730
C                                                                        WHS04740
      YDOT=Y(2)                                                          WHS04750
      OMEGA=Y(3)                                                         WHS04760
      PSI=Y(4)                                                           WHS04770
      PSIDOT=Y(5)                                                        WHS04780
C                                                                        WHS04790
C COMPUTE NONDIMENSIONAL CREEPAGES                                       WHS04800
C                                                                        WHS04810
      DO 10 I=1,2                                                        WHS04820
      GAMA1=(VEL-COS(PSI)*OMEGA*RV(I)+(-1)**I*PSIDOT*L(I))/VEL           WHS04830
      IF (I .EQ. 1) II=2                                                 WHS04840
      IF (I .EQ. 2) II=1                                                 WHS04850
      V2=-(L(1)+L(2))*COS(ALPHA(II))*DPHI*YDOT/SIN(ABS(ALPHA(1))         WHS04860
     1       +ALPHA(2))                                                  WHS04870
      GAMA2=(-SIN(PSI)*V2/VEL)/COS(ALPHA(I))                             WHS04880
      RHOBC=RHO(I)/(MU*SQRT(AAXIS(I)*BAXIS(I)))                          WHS04890
      XI=ABS(GAMA1*RHOBC)                                                WHS04900
      SIGN(I)=1.                                                         WHS04910
      IF (GAMA1.LT.0.) SIGN(I)=-1.                                       WHS04920
      ETA=GAMA2*RHOBC                                                    WHS04930
      IF (I.EQ.1) ETA=-ETA                                               WHS04940
C                                                                        WHS04950
```

```
C CONVERT TO POLAR FORM USING KALKER'S DEFINITIONS                      WHS04960
C                                                                       WHS04970
      VNU(I)=(XI**2+ETA**2)**0.5                                        WHS04980
      IF ((XI .EQ. 0.) .AND. (ETA .GE. 0.)) ANGLE(I)=90.                WHS04990
      IF ((XI .EQ. 0.) .AND. (ETA .LT. 0.)) ANGLE(I)=-90.               WHS05000
      IF (XI .EQ. 0.) GO TO 200                                         WHS05010
      ANGLE(I)=ATAN(ETA/XI)*180./PI                                     WHS05020
200   CONTINUE                                                          WHS05030
10    CONTINUE                                                          WHS05040
      RETURN                                                            WHS05050
      END                                                               WHS05060
C                                                                       WHS05070
C                        +--------------+                               WHS05080
C                        |    KALKER    |                               WHS05090
C                        +--------------+                               WHS05100
C                                                                       WHS05110
      SUBROUTINE KALKER(AAXIS,BAXIS,VNU,ANGLE,CHI,Y,SIGN)               WHS05120
C                                                                       WHS05130
C SELECTS STORED KALKER TABLE FOR GIVEN A/B AND SPIN CHI                WHS05140
C PERFORMS 2-DIMENSIONAL TABLE INTERPOLATION                            WHS05150
C                                                                       WHS05160
      DIMENSION PX(21,13,13),PY(21,13,13),AOB1(21),AOB2(21),            WHS05170
     1          CHI1(21),CHI2(21),AAXIS(2),BAXIS(2),VNU(2),ANGLE(2),    WHS05180
     2          P1(2),P2(2),CHI(2),Y(13),Y(7),SIGN(2),P3(2)             WHS05190
      COMMON /KALK/ PX,PY                                               WHS05200
      COMMON /FORCES/ P1,P2,P3                                          WHS05210
      LOGICAL COND1,COND2                                               WHS05220
      DATA AOB1/0.0,1.025,3*1.075,2*1.125,2*1.175,4.6,2*9.5,2*11.75,    WHS05230
     1         3*13.,8*13.9/,                                           WHS05240
     2      AOB2/1.025,1.075,3*1.125,2*1.175,2*4.6,9.5,2*11.75,2*13.,   WHS05250
     3         3*13.9,8*20./,                                           WHS05260
     4      CHI1/3*.0,.1925,.255,.0,.2375,.0,.23,2*.0,.183,.0,.1385,.0, WHS05270
     5           .085,.06,.0,.0875,.1125,.1375/,                        WHS05280
     6      CHI2/2*10.,.1925,.255,10.,.2375,10.,.230,10.,10.,.183,10.,  WHS05290
     7           .1385,10.,.085,.06,10.,.0875,.1125,.1375,10./          WHS05300
      DATA V/0.0,0.1,0.2,0.35,0.5,0.65,0.8,1.1,1.4,1.7,2.0,2.5,3.0/     WHS05310
C                                                                       WHS05320
C PERFORM KALKER TABLE INTERPOLATION FOR EACH CONTACT POINT, I=1,2       WHS05330
C                                                                       WHS05340
      DO 100 I=1,2                                                      WHS05350
      IF (P3(I) .GT. 0.0) GO TO 30                                      WHS05360
      P1(I)=0.0                                                         WHS05370
      P2(I)=0.0                                                         WHS05380
      GO TO 100                                                         WHS05390
30    CONTINUE                                                          WHS05400
      AOB=AAXIS(I)/BAXIS(I)                                             WHS05410
      DO 10 J=1,21                                                      WHS05420
      COND1=(AOB .GT. AOB1(J)) .AND. (AOB .LE. AOB2(J))                 WHS05430
      COND2=(CHI(I) .GT. CHI1(J)) .AND. (CHI(I) .LE. CHI2(J))           WHS05440
      IF (COND1 .AND. COND2) GO TO 20                                   WHS05450
   10 CONTINUE                                                          WHS05460
      NFILE=0                                                           WHS05470
      GO TO 999                                                         WHS05480
   20 NFILE=J                                                           WHS05490
C                                                                       WHS05500
```

```
C SETUP INPUT TO INTERPOLATION ROUTINE.  P IS FRACTIONAL INCREMENT IN    WHS05510
C VNU TABLE. II IS THE COORDINATE OF BASE POINT FOR INTERPOLATION        WHS05520
C                                                                        WHS05530
      VN=AMIN1(VNU(I),3.0)                                               WHS05540
      II=12                                                              WHS05550
      DO 25 I1=1,12                                                      WHS05560
25    IF ((VN .GE. V(I1)) .AND. (VN .LT. V(I1+1))) II=I1                 WHS05570
      P=(VN-V(II))/(V(II+1)-V(II))                                       WHS05580
C                                                                        WHS05590
C CALL 2-DIMENSIONAL INTERPOLATION ROUTINE                               WHS05600
C                                                                        WHS05610
      CALL INTP2D(PY,J,II,ANGLE(I),P,1,PP1)                              WHS05620
      CALL INTP2D(PY,J,II,ANGLE(I),P,2,PP2)                              WHS05630
C                                                                        WHS05640
      P1(I)=-SIGN(I)*PP1                                                 WHS05650
      P2(I)=-PP2                                                         WHS05660
      IF (I.EQ.1) P2(I)=-P2(I)                                           WHS05670
100   CONTINUE                                                           WHS05680
C                                                                        WHS05690
C END OF WALKER TABLE INTERPOLATION LOOP                                 WHS05700
C                                                                        WHS05710
      RETURN                                                             WHS05720
C                                                                        WHS05730
C ABORT END - NO WALKER FILE FOUND                                       WHS05740
C                                                                        WHS05750
999   DISP=1000.*Y(1)                                                    WHS05760
      WRITE(2,1000)DISP,NTSTEP                                           WHS05770
      WRITE(6,1000)DISP,NTSTEP                                           WHS05780
 1000 FORMAT('  NO DATA FILE FOUND--PROGRAM TERMINATED AT ',F7.2,        WHS05790
     1' DISPLACEMENT (MM)',/,T42,'IN THE ',I4,'TH TIME STEP')            WHS05800
C                                                                        WHS05810
      RETURN                                                             WHS05820
      END                                                                WHS05830
C                                                                        WHS05840
C                        +--------------+                                WHS05850
C                        |    FNORM     |                                WHS05860
C                        +--------------+                                WHS05870
C                                                                        WHS05880
      SUBROUTINE FNORM(Y)                                                WHS05890
C                                                                        WHS05900
C CALCULATES NORMAL FORCE F3(I) AT EACH CONTACT POINT FROM                WHS05910
C TWO-DIMENSIONAL FORCE AND MOMENT BALANCE ON WHEELSET, INCLUDING        WHS05920
C DYNAMIC TERMS                                                          WHS05930
C                                                                        WHS05940
      REAL L,MW,IYY,IZZ,IXX,MU,MT,L12,KY,KPHI,KZ,KPSI,MXX,MZZ0           WHS05950
      DIMENSION F3(2),Y(7),F2(2),AA(2),BB(2),ALPHA(2),L(2),RV(2),        WHS05960
     1      RHO(2),ATH(2),BTH(2),CHI(2),S1(2),C1(2),F1(2),FS(7)          WHS05970
      COMMON /GEO/ Z,DZ,DDZ,PHI,DPHI,DDPHI,ALPHA,L,RHO,RV,ATH,BTH,CHI    WHS05980
      COMMON /SPARAM/ BY,KY,BZ,KZ,KPSI,BPSI,OMEGA,KPHI,BPHI              WHS05990
      COMMON /MPARAM/ MW,IYY,IZZ,IXX,MT                                  WHS06000
      COMMON /LOAD/ FZ,MXX,FY0,MZZ0                                      WHS06010
      COMMON /FORCES/ F1,F2,F3                                           WHS06020
      COMMON /MATREL/ MU,ZW                                              WHS06030
      COMMON /ACCEL/ YDDOT,PSDDOT                                        WHS06040
      COMMON /TRUCK/ FS,PSIT                                             WHS06050
```

```
      ZDDOT=DZ*YDDOT+DDZ*Y(2)**2                                          WHS06060
      PHDDOT=DPHI*YDDOT+DDPHI*Y(2)**2                                     WHS06070
      A=FZ-HW*ZDDOT-BZ*ZDOT-KZ*Z                                          WHS06080
      B=HXX-IXX*PHDDOT-(IZZ-IYY)*Y(5)**2*PHI-IYY*Y(3)*Y(5)                WHS06090
     1      -KPHI*PHI-BPHI*DPHI*Y(2)                                     WHS06100
      DO 10 I=1,2                                                         WHS06110
      S1(I)=SIN(ALPHA(I))                                                 WHS06120
10    C1(I)=COS(ALPHA(I))                                                 WHS06130
      L12=L(1)+L(2)                                                       WHS06140
      D1=L12*(C1(1)-HU*F2(1)*S1(1))                                       WHS06150
      D2=L12*(C1(2)-HU*F2(2)*S1(2))                                       WHS06160
      RBAR=0.5*(RV(1)+RV(2))                                              WHS06170
      F3(1)=(L(2)*A+B+RBAR*(FS(2)-HW*YDDOT))/D1                           WHS06180
      F3(2)=(L(1)*A-B-RBAR*(FS(2)-HW*YDDOT))/D2                           WHS06190
C                                                                         WHS06200
C CHECK FOR F3(I) > 0. PREVENTS NEGATIVE F3(I) AND GIVES WARNING          WHS06210
C                                                                         WHS06220
      DO 25 I=1,2                                                         WHS06230
25    F3(I)=AMAX1(F3(I),0.0)                                              WHS06240
C                                                                         WHS06250
      RETURN                                                              WHS06260
      END                                                                 WHS06270
C                                                                         WHS06280
C                          +--------------+                               WHS06290
C                          |    FWHRL     |                               WHS06300
C                          +--------------+                               WHS06310
C                                                                         WHS06320
      SUBROUTINE FWHRL(FWR)                                               WHS06330
C                                                                         WHS06340
      REAL L,HU                                                           WHS06350
      DIMENSION F3(2),FWR(7),ALPHA(2),L(2),RV(2),F1(2),F2(2),RHO(2),      WHS06360
     1      ATH(2),STH(2),CHI(2)                                          WHS06370
      COMMON /GEO/ Z,DZ,DDZ,PHI,DPHI,DDPHI,ALPHA,L,RHO,RV,ATH,STH,CHI     WHS06380
      COMMON /MATERL/ HU,ZW                                               WHS06390
      COMMON /FORCES/ F1,F2,F3                                            WHS06400
      DO 10 J=1,7                                                         WHS06410
10    FWR(J)=0.0                                                          WHS06420
      DO 20 I=1,2                                                         WHS06430
      FWR(2)=FWR(2)+F3(I)*(HU*F2(I)*COS(ALPHA(I)) + SIN(ALPHA(I)))        WHS06440
      FWR(3)=FWR(3)-HU*F1(I)*F3(I)*RV(1)                                  WHS06450
20    FWR(5)=FWR(5)+(-1)**I*F1(I)*F3(I)*L(I)                              WHS06460
      RETURN                                                              WHS06470
      END                                                                 WHS06480
C                                                                         WHS06490
C                          +--------------+                               WHS06500
C                          |    FEULER    |                               WHS06510
C                          +--------------+                               WHS06520
C                                                                         WHS06530
      SUBROUTINE FEULER(Y,FEUL)                                           WHS06540
C                                                                         WHS06550
C COMPUTES FORCES RESULTING FROM EULER TERMS IN EQUATIONS OF MOTION       WHS06560
C INVOLVING CROSS PRODUCTS OF ANGULAR DISPLACEMENTS AND VELOCITIES        WHS06570
C                                                                         WHS06580
      REAL L,IXX,IYY,IZZ,HU,HW,HT,KY,KPHI,KZ,KPSI                         WHS06590
      DIMENSION Y(7),FEUL(7),L(2),ALPHA(2),RHO(2),RV(2),ATH(2),STH(2),    WHS06600
```

```
     1     CBI(2)                                                          WHS06610
      COMMON /GEO/ Z,DZ,DDZ,PHI,DPHI,DDPHI,ALPHA,L,RHO,BV,ATB,BTB,CBI     WHS06620
      COMMON /SPARAM/ BY,KY,BZ,KZ,KPSI,BPSI,BOMEGA,KPHI,BPHI              WHS06630
      COMMON /BPARAM/ BW,IYY,IZZ,IXX,BT                                   WHS06640
      COMMON /MATERL/ RU,EW                                               WHS06650
      COMMON /ACCEL/ YDDOT,PSDDOT                                         WHS06660
      PHDOT=DPHI*Y(2)                                                     WHS06670
      DO 10 J=1,7                                                         WHS06680
10    FEUL(J)=0.0                                                         WHS06690
      FEUL(3)=(Y(5)*PHDOT+PHI*PSDDOT)*IYY-Y(5)*PHDOT*(IZZ-IXX)            WHS06700
      FEUL(5)=Y(5)*PHI*PHDOT*IZZ-IYY*Y(3)*PHDOT                           WHS06710
     1                -(IXX-IYY)*PHI*PHDOT*Y(5)                          WHS06720
      RETURN                                                              WHS06730
      END                                                                 WHS06740
C                                                                         WHS06750
C                        +--------------+                                 WHS06760
C                        |    FSUSP     |                                 WHS06770
C                        +--------------+                                 WHS06780
C                                                                         WHS06790
      SUBROUTINE FSUSP(Y)                                                 WHS06800
C                                                                         WHS06810
C COMPUTES FORCES RESULTING FROM DISPLACEMENT OF PRIMARY SUSPENSIONS       WHS06820
C BETWEEN WHEELSET AND BOGIE FRAME, INCLUDING LATERAL, VERTICAL, ROLL,    WHS06830
C AND YAW STIFFNESS AND DAMPING, PLUS DRAG OR BRAKING FORCE ON AXLE       WHS06840
C                                                                         WHS06850
      REAL L,KY,KPHI,KZ,KSPI                                              WHS06860
      DIMENSION Y(7),FS(7)                                                WHS06870
      COMMON /SPARAM/ BY,KY,BZ,KZ,KPSI,BPSI,BOMEGA,KPHI,BPHI              WHS06880
      COMMON /TRUCK/ FS,PSIT                                              WHS06890
      FS(1)=0.0                                                           WHS06900
      FS(2)=KY*(Y(6)-Y(1))+BY*(Y(7)-Y(2))                                 WHS06910
      FS(3)=-BOMEGA*Y(3)                                                  WHS06920
      FS(4)=0.0                                                           WHS06930
      FS(5)=-BPSI*Y(5)+KPSI*(PSIT-Y(4))                                   WHS06940
      FS(6)=0.0                                                           WHS06950
      FS(7)=KY*(Y(1)-Y(6))+BY*(Y(2)-Y(7))                                 WHS06960
      RETURN                                                              WHS06970
      END                                                                 WHS06980
C                                                                         WHS06990
C                        +--------------+                                 WHS07000
C                        |  BLOCK DATA  |                                 WHS07010
C                        +--------------+                                 WHS07020
C                                                                         WHS07030
      BLOCK DATA                                                          WHS07040
C                                                                         WHS07050
C USED TO INITIALIZE PARAMETERS IN BLOCK COMMON /CNTROL/                  WHS07060
C                                                                         WHS07070
      COMMON /CNTROL/ RANGE,STEP,N,M,EPS,PI                               WHS07080
      REAL RANGE/40.68E-03/,STEP/5.08E-04/,EPS/-0.05/,PI/3.14159/         WHS07090
      INTEGER N/161/,M/3/                                                 WHS07100
      END                                                                 WHS07110
C                                                                         WHS07120
C ========================================================================WHS07130
C                          SERVICE ROUTINES                               WHS07140
C ========================================================================WHS07150
```

```
C                                                                       WHS07160
C                        +--------------+                               WHS07170
C                        |    INTP2D    |                               WHS07180
C                        +--------------+                               WHS07190
C                                                                       WHS07200
C SERVICE ROUTINE TO PERFORM TWO-DIMENSIONAL INTERPOLATION              WHS07210
C                                                                       WHS07220
      SUBROUTINE INTP2D(F,J,II,ANGLE,P,IFLAG,VALUE)                     WHS07230
      DIMENSION F(21,13,13),ROW1(15),ROW2(15),AUX(30)                   WHS07240
      DATA EPS/-1.0E-02/                                                WHS07250
      DO 10 I=1,13                                                      WHS07260
      ROW1(I+1)=F(J,II,I)                                               WHS07270
10    ROW2(I+1)=F(J,(II+1),I)                                           WHS07280
      ROW1(1)=F(J,II,2)*(-1)**IFLAG                                     WHS07290
      ROW2(1)=F(J,(II+1),2)*(-1)**IFLAG                                 WHS07300
      ROW1(15)=F(J,II,12)*(-1)**IFLAG                                   WHS07310
      ROW2(15)=F(J,(II+1),12)*(-1)**IFLAG                               WHS07320
      CALL IVP(-105.,15.,ROW1,15,ANGLE,3,EPS,FA,AUX,IER)                WHS07330
      CALL IVP(-105.,15.,ROW2,15,ANGLE,3,EPS,FB,AUX,IER)                WHS07340
      VALUE=(1.0-P)*FA + P*FB                                           WHS07350
      RETURN                                                            WHS07360
      END                                                               WHS07370
```

APPENDIX E
PATENT DISCLOSURE STATEMENT

In accordance with the patents rights course of the terms and conditions of this contract, and after comprehensive review of the work performed, it was found that no new patentable items were produced under this contract. However, significant innovations and advancements to the field of research on derailment safety were achieved.

The following hardware and software items were developed as a result of the sponsorship of research under Contract DOT-TSC-1603:

1) Scale model wheelset experimental apparatus for use in studies of derailment processes.
2) Computer programs for analysis of measured wheel/rail forces for comparison with proposed derailment criteria.
3) Measurement and data reduction methods for on-line diagnostics of impending derailment conditions.
4) Computer programs for simulation of quasisteady and dynamic wheelclimb derailment processes.

The above items are potentially useful to both model scale and full scale experiments and analysis of rail vehicle derailment safety.

114 copies